NASA TR R-100

NATIONAL AERONAUTICS AND SPACE ADMINISTRATION

TECHNICAL REPORT

R-100

COLLECTION OF ZERO-LIFT DRAG DATA ON BODIES OF REVOLUTION FROM FREE-FLIGHT INVESTIGATIONS

By WILLIAM E. STONEY, JR.

1961

For sale by the Superintendent of Documents, U.S. Government Printing Office, Washington 25, D.C. Yearly subscription, $15; foreign, $19; single copy price varies according to size ---------- Price $1.75 cents (this issue)

TECHNICAL REPORT R-100

COLLECTION OF ZERO-LIFT DRAG DATA ON BODIES OF REVOLUTION FROM FREE-FLIGHT INVESTIGATIONS

By WILLIAM E. STONEY, JR.

Langley Research Center
Langley Field, Va.

TECHNICAL REPORT R-100

COLLECTION OF ZERO-LIFT DRAG DATA ON BODIES OF REVOLUTION FROM FREE-FLIGHT INVESTIGATIONS [1]

By WILLIAM E. STONEY, Jr.

SUMMARY

A compilation is made of most of the zero-lift drag results obtained from free-flight measurements made by the Langley Pilotless Aircraft Research Division on fin-stabilized bodies of revolution. The data are arranged on standard forms, which also contain the significant geometrical factors. Supplementary data have been provided to facilitate the determination of the body pressure drags from the measured total drags. Summary plots and discussions have been included to provide a unified and broad picture of the effects of body geometry on zero-lift drag. The Mach number range of the tests extends from 0.6 to approximately 2.0 and the Reynolds numbers based on body length from 2×10^6 *to* 100×10^6.

INTRODUCTION

At the present time, the most accurate method of obtaining the zero-lift drag at transonic and low supersonic Mach numbers of an arbitrarily shaped body of revolution is measurement by means of wind-tunnel or free-flight tests. The importance of accurate knowledge of zero lift has been increased by the usefulness of the "area rule" concept in the design of complete aircraft configurations, since this concept states that the drag of a complete aircraft configuration can be determined from its equivalent body of revolution.

The Langley Pilotless Aircraft Research Division has flown nearly 200 bodies of revolution of different sizes and shapes for the purpose of measuring their drag at zero lift. The results of many of these tests have been published in reports dealing with the systematic variations which they explored (refs. 1 to 16). However, many of these models were designed as equivalent bodies of revolution, and their drags have been published in the widely scattered reports dealing with the airplane configurations they represented. In view of the large amount of data available and of the comparative obscurity of a large part of it, it was believed that a collection of such data presented in a standard form would be of aid to the aircraft and missile designers.

This collection is presented in a form that will be useful in several ways. The large number of shapes presented herein may allow the designer to estimate easily the drag of a desired shape by a simple comparison. Supplementary data and theoretical estimates have been provided to facilitate the determination of the body pressure drags from the measured total drags. Summary plots and discussions have been included to provide the user with a unified and broad picture of the effects of body geometry on drag at zero lift.

SYMBOLS

A	cross-sectional area of body
C_D	drag coefficient
ΔC_D	incremental drag coefficient
$\Delta C_{D,F}$	incremental drag coefficient due to fins
C_f	friction drag coefficient based on wetted area
C_p	pressure coefficient
d	maximum diameter
l	length
M	Mach number
N_{Re}	Reynolds number
p	free-stream static pressure
p_l	local static pressure

[1] Supersedes NACA Technical Note 4201 by William E. Stoney, Jr., 1958.

R	maximum body radius
r	local body radius
r_b	radius at body base
r_N	nose radius
S	surface (wetted) area
U	free-stream velocity
x	axial coordinate
θ_b	body slope at $x/l_T=1$ (slope is always negative but is expressed as positive)
ρ	air density
μ	viscosity
Subscripts:	
A	afterbody
B	body
b	base
C	cylindrical center section
F	fin
f	friction
max	maximum
N	nose
$N+A$	nose plus afterbody
T	total

TESTS

Most data included in this compilation were obtained by methods for which details are included in references 1 to 16. In brief, the procedure was as follows: A fin-stabilized model flying at or near zero lift was tracked with a CW Doppler radar unit as it decelerated through a speed range from supersonic Mach numbers to high subsonic Mach numbers. The resulting velocity time history was arithmetically differentiated to give a deceleration time history. Shortly before or after the flight, a record of the atmospheric properties (density, temperature, and wind velocity) was obtained from the flight of a radiosonde balloon. This record, together with a space-position time record of the flight, permitted the zero-lift drag coefficient to be calculated. The tests differ only in the method of launching the models into free flight and in the method of obtaining the altitude time history. Data are included for 177 models for which the pertinent geometric parameters are listed in tables I and II.

ROCKET MODEL TESTS

The rocket-test method provides for propulsion of the models by rockets located either in the model or behind the model in the form of booster rockets which dropped away after burnout. In these tests the models were also tracked by an NACA modified SCR–584 position radar tracking unit, the data of which were used to obtain the space-position time records used in the data reduction. In general, the rocket models were fairly large: 5 to 8 inches in diameter and up to 12 feet in length. The data were obtained with the models at all altitudes up to over 50,000 feet and to Mach numbers over 4. A few models carried telemetering equipment and from these the total drag was also obtained from decelerometers and the base drag from pressure cells.

HELIUM-GUN TESTS

The second technique, the helium-gun test, provides for launching of small models (roughly 2 inches in diameter and 12 inches long) from a helium gun. The helium gun used to launch these models was a 24-foot smooth-bore barrel 6 inches in diameter attached by valves to a 100-cubic-foot tank of helium under a pressure of 200 pounds per square inch absolute. The models were ejected at Mach numbers up to 1.4. The space time histories of these models were calculated from the velocity-time data, and the data were reduced as before. A satisfactory check of the flight-path calculation method was made by tracking several models with the SCR–584 unit. The models were fired at an angle of 20° to the horizontal and never rose over an altitude of 2,000 feet.

ACCURACY

Inasmuch as the tests were made over a period of several years with continually varying techniques, it is difficult to assign a general figure for their accuracy. The velocimeter record is accurate to within 0.2 percent, and the derived accelerations, although obtained by a short-time averaging process, are accurate to within 1 percent except in the region of the drag rise where it is possible for abrupt changes to be somewhat alleviated by the averaging process.

One means of determining accuracy is by comparison of the drag of identical models, since all the variable factors, inaccuracies in body ordinates, velocity measurement, atmospheric conditions, wind velocity, and data reduction are included. From the variations shown by the models of configurations 8, 22, 27 to 30, 75 to 77, 106 to 109, 128, 139, and 151, reasonable limits of

error for C_D and Mach number appear to be

$$\Delta C_D = \pm 0.01$$

$$\Delta M = \pm 0.01$$

Another check on the accuracy is given by a comparison of the data of model 109 with a wind-tunnel test of an identical configuration. This comparison is shown in figure 1 and is quite good.

A third indication of the accuracy of the tests is given by a comparison of the nose pressure drags obtained from eight helium-gun models with values measured in a wind tunnel and calculated by second-order theory. The comparisons are quite close and indicate accuracy at least to the values quoted. (See the discussion on nose drags in the section "Summary Curves.")

RESULTS AND DISCUSSION

GENERAL ARRANGEMENT

Inasmuch as the important product of these tests is the body pressure drag, the configurations are separated into two types—"smooth" and "bumpy"—and the results are presented in sequence according to increasing fineness ratio. A smooth body is defined as one for which the meridian increases without inflection points to a maximum and stays constant or decreases without inflection points to a minimum. All other bodies are classified as bumpy. Inasmuch as only the nose and afterbody contribute to the pressure drag, the significant fineness ratio of the smooth bodies has been assumed to be based on the sum of the nose and afterbody lengths l_{N+A}. The nose is herein defined as the forward part of the body with increasing radii up to the maximum diameter and the afterbody as that part with decreasing radii from the maximum diameter to the base. Cylindrical sections of maximum diameter are considered as separate units and thus the sum of the values of fineness ratio of the nose and afterbody l_{N+A}/d can be less than the total fineness ratio of the body l_T/d. (See table I.) Grouping in this manner is justified on the assumption that the effects of the nose on the afterbody drag are of second order. Since such a simple geometrical division cannot, in general, be made for the bumpy bodies, results for these configurations are presented in sequence according to increases in their total fineness ratios (table II). This classification by fineness ratio has the advantage of simplicity, and its usefulness is based on the general fact that this parameter is the most important single factor affecting body pressure drag.

The shape of the parts of the body is another variable and since the assumption that the effect of shape is independent of fineness ratio appears to be useful, the body ordinates have been nondimensionalized and are presented in the appendix in graphical form for each of the configurations. In order to utilize this assumption strictly, the individual parts should have been presented individually; however, this manner of presentation would have posed great problems for the bumpy bodies and was abandoned in favor of the simpler method used. This method has the advantage of allowing comparisons of bumpy and smooth bodies to be made by matching their nondimensional ordinate curves and their total fineness ratios. Comparisons of the drag curves of such bodies allow estimates of the bumpiness of a bumpy body, that is, insofar as drag is concerned.

Figures containing pertinent information on body shape and type of test for each configuration are presented, together with drag and Reynolds number plots, in the appendix. The figures in this appendix are arranged in sequence according to the configuration numbers given in tables I and II. Many of these data were originally presented in references 1 to 16. Curves of friction, base, step, and fin drag to supplement the basic data are given in figures 2 to 5. Summary curves of data from various systematic investigations are presented in figures 6 to 10. Some curves showing the general effect of body shape on drag appear in figures 11 to 15.

MODEL CHARACTERISTICS

Enough information appears in the sketches and graphical presentation of the ordinates given for each configuration in the appendix to allow reconstruction of the model with reasonable accuracy. Many of the smooth bodies had analytical meridians of parabolic form or mixed parabolic and hemispherical form; this notation has been made in the figures. The following equations were used for parabolic noses and afterbodies:

Nose:

$$\frac{r}{R} = \frac{2x}{l_N} - \left(\frac{x}{l_N}\right)^2$$

TABLE I.—GEOMETRIC CHARACTERISTICS OF SMOOTH CONFIGURATIONS

Configuration	l_{N+A}/d	l_T/d	l_N/d	l_A/d	S_B/A_{max}	S_F/A_{max}	A_b/A_{max}	θ_b, deg	Test	Reference
1–8	0. 50	12. 00	0. 50	0. 00	49. 00	6. 36	1. 00	0. 00	Helium gun	--
9	3. 71	8. 57	1. 38	2. 33	28. 30	11. 00	. 00	12. 20	Helium gun	--
10	4. 62	7. 70	1. 92	2. 70	25. 20	6. 40	. 00	68. 00	Helium gun	--
11	4. 64	11. 20	3. 50	1. 14	39. 30	11. 00	. 45	8. 00	Rocket	1
12	4. 85	7. 15	2. 02	2. 83	22. 40	11. 00	. 00	15. 70	Helium gun	--
13	4. 98	13. 47	2. 98	2. 00	51. 50	24. 60	. 52	4. 02	Helium gun	2
14	4. 98	13. 47	2. 98	2. 00	51. 30	24. 60	. 52	4. 02	Helium gun	2
15	5. 00	5. 00	2. 00	3. 00	13. 60	11. 00	. 00	18. 80	Helium gun	--
16	5. 00	5. 00	2. 00	3. 00	13. 30	11. 00	. 00	11. 90	Helium gun	--
17	5. 00	7. 78	2. 00	3. 00	25. 00	11. 00	. 00	12. 70	Helium gun	--
18	5. 10	5. 10	1. 92	3. 18	14. 60	11. 00	. 00	90. 00	Helium gun	--
19	5. 20	13. 70	3. 20	2. 00	51. 00	24. 60	. 52	4. 02	Rocket	3
20	5. 20	13. 70	3. 20	2. 00	51. 00	24. 60	. 52	4. 02	Helium gun	2
21	5. 34	9. 51	2. 67	2. 67	30. 60	11. 00	. 00	15. 60	Helium gun	--
22	5. 70	5. 70	5. 70	. 00	11. 40	. 00	1. 00	−5. 00	Helium gun	--
23	5. 79	14. 29	3. 79	2. 00	51. 90	24. 60	. 52	4. 02	Helium gun	2
24	5. 84	5. 84	. 50	5. 34	19. 00	11. 00	. 19	7. 00	Rocket	4
25	5. 84	12. 90	3. 10	2. 74	51. 80	12. 40	. 25	18. 60	Rocket	--
26	6. 00	8. 78	3. 00	3. 00	26. 20	11. 00	. 00	12. 90	Helium gun	--
27	6. 04	6. 04	1. 21	4. 83	19. 16	11. 00	. 19	9. 20	Rocket	5
28	6. 04	6. 04	4. 83	1. 21	16. 84	11. 00	. 19	25. 00	Rocket	5
29	6. 04	6. 04	2. 42	3. 62	18. 39	11. 00	. 19	8. 80	Rocket	5
30	6. 04	6. 04	3. 62	2. 42	17. 64	11. 00	. 19	13. 00	Rocket	5
31	6. 04	6. 04	3. 71	2. 33	17. 60	11. 00	. 37	6. 10	Helium gun	--
32	6. 08	9. 60	5. 01	1. 07	31. 60	12. 30	. 69	5. 45	Helium gun	--
33	6. 10	14. 60	4. 10	2. 00	52. 30	24. 60	. 52	4. 02	Helium gun	3
34	6. 10	14. 60	4. 10	2. 00	52. 30	24. 60	. 52	4. 02	Rocket	3
35	6. 42	9. 32	2. 98	3. 44	30. 20	11. 00	. 00	13. 30	Helium gun	--
36	6. 50	15. 00	4. 50	2. 00	52. 60	24. 60	. 52	4. 02	Rocket	3
37	6. 51	10. 87	2. 71	3. 80	35. 60	12. 82	. 00	60. 00	Helium gun	--
38	6. 52	13. 90	3. 80	2. 72	49. 60	12. 40	. 25	17. 40	Rocket	--
39	7. 00	7. 00	2. 80	4. 20	19. 00	11. 00	. 00	12. 90	Helium gun	--
40	7. 16	7. 16	1. 81	5. 35	24. 00	11. 00	. 19	7. 00	Rocket	4
41	7. 30	7. 30	1. 95	5. 35	24. 20	11. 00	. 19	7. 00	Rocket	4
42	7. 33	8. 57	3. 02	4. 31	25. 60	11. 00	. 00	90. 00	Helium gun	--
43	7. 35	7. 35	2. 00	5. 35	22. 70	11. 00	. 19	6. 00	Rocket	4
44	7. 43	7. 43	3. 58	3. 85	20. 90	11. 00	. 00	15. 00	Helium gun	--
45	7. 47	7. 47	2. 12	5. 35	24. 30	11. 00	. 19	6. 00	Rocket	4
46	7. 60	7. 60	2. 25	5. 35	25. 10	11. 00	. 19	7. 00	Rocket	4
47	7. 66	7. 66	2. 33	5. 33	25. 30	11. 00	. 19	7. 00	Rocket	4
48	7. 72	10. 90	6. 00	1. 72	32. 60	11. 00	. 00	2. 90	Helium gun	--
49	7. 78	11. 50	6. 00	1. 78	35. 50	11. 00	. 00	29. 30	Helium gun	6
50	7. 78	11. 50	6. 00	1. 78	35. 50	11. 00	. 00	29. 30	Helium gun	6
51	7. 80	11. 08	3. 42	4. 38	34. 40	11. 00	. 00	9. 80	Helium gun	--
52	7. 90	7. 90	2. 57	5. 33	25. 70	11. 00	. 19	7. 00	Rocket	4
53	8. 00	8. 00	3. 20	4. 80	21. 90	11. 00	. 00	8. 50	Helium gun	--
54	8. 00	8. 00	4. 66	3. 44	23. 16	5. 80	. 17	9. 50	Helium gun	--
55	8. 00	8. 00	4. 00	4. 00	26. 30	4. 43	. 00	14. 00	Helium gun	--
56	8. 00	12. 00	3. 00	5. 00	36. 38	11. 00	. 19	3. 20	Helium gun	7
57	8. 00	12. 00	3. 00	5. 00	37. 05	11. 00	. 19	3. 20	Helium gun	7
58	8. 00	12. 00	3. 00	5. 00	38. 35	11. 00	. 19	3. 20	Helium gun	7
59	8. 00	12. 00	3. 00	5. 00	38. 40	11. 00	. 19	3. 20	Helium gun	7
60	8. 00	12. 00	3. 00	5. 00	38. 78	11. 00	. 19	3. 20	Helium gun	7

TABLE I.—GEOMETRIC CHARACTERISTICS OF SMOOTH CONFIGURATIONS—Concluded

Configuration	l_{N+A}/d	l_T/d	l_N/d	l_A/d	S_B/A_{max}	S_F/A_{max}	A_b/A_{max}	θ_b, deg	Test	Reference
61	8.00	12.00	3.00	5.00	37.24	11.00	0.19	3.20	Helium gun	7
62	8.00	12.00	3.00	5.00	37.58	11.00	.19	3.20	Helium gun	7
63	8.00	12.00	3.00	5.00	38.40	11.00	.19	3.20	Helium gun	7
64	8.10	8.10	2.73	5.37	26.08	11.00	.19	7.00	Rocket	4
65	8.20	10.93	3.38	4.82	34.10	11.00	.00	9.00	Helium gun	--
66	8.30	8.30	2.96	5.34	26.50	11.00	.19	7.00	Rocket	4
67	8.33	9.02	3.27	5.06	26.60	9.20	.0384	23.00	Helium gun	8
68	8.44	8.44	3.20	5.24	24.90	5.45	.26	3.50	Rocket	--
69	8.50	8.50	3.60	4.90	26.30	9.74	.30	5.60	Rocket	9
70	8.50	8.50	3.16	5.34	26.80	11.00	.19	7.00	Rocket	4
71	8.60	8.60	5.59	3.01	25.70	5.20	.36	4.55	Rocket	--
72	8.65	8.65	3.28	5.37	27.30	11.00	.19	7.00	Rocket	4
73	8.81	8.81	4.04	4.77	28.80	11.00	.33	6.90	Helium gun	--
74	8.91	8.91	1.78	7.13	28.26	11.00	.19	6.50	Rocket	5
75	8.91	8.91	7.13	1.78	24.84	11.00	.19	18.30	Rocket	5
76	8.91	8.91	3.56	5.35	27.00	11.00	.19	6.00	Rocket	4 5
77	8.91	8.91	5.35	3.56	26.02	11.00	.19	10.20	Rocket	5
78	8.91	8.91	7.13	1.78	26.10	11.00	1.00	.00	Helium gun	6
79	8.91	8.91	7.13	1.78	23.70	11.00	.00	29.30	Helium gun	6
80	8.91	8.91	7.13	1.78	24.80	11.00	.19	17.50	Helium gun	6
81	8.91	8.91	7.13	1.78	25.40	11.00	.49	9.60	Helium gun	6
82	8.91	8.91	7.13	1.78	24.20	11.00	.19	9.00	Helium gun	6
83	8.91	8.91	7.13	1.78	25.10	11.00	.49	4.87	Helium gun	6
84	8.91	8.91	4.66	4.25	24.50	11.00	.09	9.70	Helium gun	--
85	8.91	12.50	4.66	4.25	38.80	11.00	.09	10.70	Helium gun	--
86	9.13	9.13	3.28	5.85	28.00	8.30	.008	30.00	Helium gun	8
87	9.38	9.38	3.63	5.75	28.00	6.40	.11	7.00	Rocket	10
88	9.54	9.54	4.20	5.34	28.60	6.40	.17	8.75	Rocket	10
89	10.00	10.00	4.00	6.00	30.88	11.40	.25	4.47	Rocket	--
90	10.00	10.00	4.73	5.27	29.60	17.76	.15	6.45	Rocket	11
91	10.54	10.54	5.38	5.16	34.40	11.00	.19	7.00	Rocket	4
92	10.63	10.63	7.13	3.50	33.00	11.00	1.00	.00	Helium gun	6
93	10.63	10.63	7.13	3.50	31.60	11.00	.49	5.40	Helium gun	6
94	10.63	10.63	7.13	3.50	30.06	11.00	.19	14.80	Helium gun	6
95	10.63	10.63	7.13	3.50	28.30	11.00	.00	15.80	Helium gun	6
96	11.19	21.20	7.16	4.03	62.50	11.00	.19	4.00	Rocket	12
97	11.19	17.20	7.16	4.03	48.80	11.00	.19	4.00	Rocket	12
98	12.13	12.13	7.13	5.00	38.90	11.00	1.00	.00	Helium gun	6
99	12.13	12.13	7.13	5.00	36.90	11.00	.49	3.42	Helium gun	6
100	12.13	12.13	7.13	5.00	35.80	11.00	.49	1.70	Helium gun	6
101	12.13	12.13	7.13	5.00	33.30	11.00	.19	3.20	Helium gun	6
102	12.13	12.13	7.13	5.00	35.20	11.00	.19	6.40	Helium gun	6
103	12.13	12.13	7.13	5.00	32.20	11.00	.00	11.70	Helium gun	6
104	12.20	12.20	7.50	4.70	36.30	30.80	.364	7.60	Rocket	--
105	12.20	12.20	7.50	4.70	36.30	30.80	.364	7.60	Rocket	--
106	12.50	12.50	2.50	10.00	39.65	11.00	.19	3.20	Rocket	5
107	12.50	12.50	10.00	2.50	34.85	11.00	.19	12.60	Rocket	5
108	12.50	12.50	5.00	7.50	38.10	11.00	.19	4.30	Rocket	5
109	12.50	12.50	7.50	5.00	36.50	11.00	.19	6.40	Rocket	5
110	12.50	12.50	6.25	6.25	33.40	11.00	.00	90.00	Helium gun	--
111	17.78	17.78	10.65	7.10	52.00	11.00	.19	4.60	Rocket	12
112	24.50	24.50	14.70	9.80	71.60	11.00	.19	3.30	Rocket	12

TABLE II.—GEOMETRIC CHARACTERISTICS OF BUMPY CONFIGURATIONS

Configuration	l_T/d	S_B/A_{max}	S_F/A_{max}	A_b/A_{max}	θ_b, deg	Test	Reference
113							
114	3. 67	12. 40	0. 00	1. 00	—7. 60	Helium gun	------
115							
116	5. 23	13. 10	5. 80	. 04	5. 50	Helium gun	-------
117	5. 26	24. 79	11. 64	. 14	23. 90	Helium gun	-------
118	5. 29	16. 00	11. 64	. 23	17. 30	Helium gun	-------
119	5. 36	15. 60	11. 28	. 09	24. 20	Helium gun	-------
120	5. 45	14. 10	6. 28	. 04	5. 50	Helium gun	-------
121	5. 68	16. 60	11. 60	. 17	20. 20	Helium gun	-------
122	6. 00	17. 50	12. 00	. 00	13. 60	Helium gun	-------
123	6. 66	17. 19	9. 22	. 06	16. 70	Helium gun	-------
124	6. 82	15. 70	5. 43	. 0652	5. 00	Helium gun	-------
125	6. 84	18. 20	10. 76	. 00	90. 00	Helium gun	-------
126	6. 86	21. 15	12. 20	. 18	18. 00	Helium gun	-------
127	6. 95	19. 90	11. 64	. 20	8. 80	Helium gun	-------
128	6. 98	21. 16	11. 80	. 26	10. 30	Helium gun	-------
129	6. 98	21. 27	11. 80	. 29	9. 70	Helium gun	-------
130	7. 08	19. 40	13. 00	. 00	90. 00	Helium gun	14
131	7. 08	21. 35	11. 86	. 20	11. 30	Helium gun	-------
132	7. 08	19. 60	3. 56	. 12	6. 50	Helium gun	-------
133	7. 14	20. 26	9. 90	. 00	90. 00	Helium gun	-------
134	7. 33	21. 70	11. 70	. 19	. 00	Helium gun	-------
135	7. 42	19. 00	11. 50	. 05	15. 40	Helium gun	-------
136	7. 55	18. 70	6. 63	. 08	5. 00	Helium gun	-------
137	7. 70	18. 80	11. 95	. 006	90. 00	Helium gun	-------
138	7. 75	20. 90	5. 78	. 20	26. 50	Helium gun	-------
139	7. 76	21. 54	11. 00	. 00	9. 40	Helium gun	-------
140	8. 00	24. 80	13. 20	. 18	33. 20	Helium gun	-------
141	8. 03	20. 70	9. 00	. 09	7. 90	Helium gun	-------
142	8. 04	24. 04	13. 00	. 23	12. 60	Helium gun	-------
143	8. 07	23. 75	4. 12	. 15	4. 30	Helium gun	-------
144	8. 10	25. 11	13. 20	. 18	21. 50	Helium gun	-------
145	8. 10	25. 08	13. 20	. 18	17. 10	Helium gun	-------
146	8. 11	21. 00	7. 67	. 09	5. 00	Helium gun	-------

Afterbody:

$$\frac{r}{R}=1-\left(1-\frac{r_b}{R}\right)\left(\frac{x}{l_A}\right)^2$$

Pertinent fineness ratios, area ratios, and angles are given for each configuration to facilitate comparisons of configurations. The type of test (rocket or helium gun) is also noted.

PRESENTATION OF DATA

Total zero-lift drag coefficients based on body frontal area and Reynolds number based on body length are presented for each configuration. The total-drag curves are curves faired through the original data points for the present report and thus may in some cases differ slightly from fairings previously made in references 1 to 16. For those configurations for which more than one model was flown the individual curves are labeled a, b, and so forth. (See, for example, the drag plot for configuration 8 in the appendix.) For the models on which base pressures were measured, the base pressures are also presented.

For convenience, the friction drag calculated by the method of Van Driest (ref. 17) has been presented for each model. For cases in which the Reynolds numbers and the data appeared to be such that the flow over both the body and fins was turbulent, the points calculated were indicated by a square symbol and connected with a dashed line. If the data appeared to be in the range in which the fin boundary layer may have been either laminar or turbulent, calculations were made for both conditions, and the points for both conditions were presented and left unconnected. (See appendix, configuration 10.) The

TABLE II—GEOMETRIC CHARACTERISTICS OF BUMPY CONFIGURATIONS—Concluded

Configuration	l_T/d	S_B/A_{max}	S_F/A_{max}	A_b/A_{max}	θ_b, deg	Test	Reference
147	8.12	25.40	13.20	0.18	17.90	Helium gun	-------
148	8.23	20.80	11.72	.00	16.80	Helium gun	-------
149	8.27	24.00	10.90	.29	2.80	Helium gun	-------
150	8.28	20.70	11.80	.06	15.00	Helium gun	-------
151	8.40	23.00	7.88	.17	6.10	Helium gun	-------
152	8.43	23.10	6.00	.17	6.80	Helium gun	-------
153	8.48	23.76	12.62	.30	2.40	Helium gun	-------
154	8.49	23.12	11.00	.00	7.40	Helium gun	-------
155	8.52	23.40	11.50	.08	2.50	Helium gun	-------
156	8.57	25.70	9.70	.00	90.00	Rocket	-------
157	8.70	24.54	13.12	.20	12.10	Helium gun	-------
158	8.84	25.64	6.64	.18	4.60	Helium gun	-------
159	8.85	25.75	13.14	.21	12.30	Helium gun	-------
160	8.91	25.00	11.00	.19	7.00	Rocket	15
161	8.92	24.10	11.50	.07	12.60	Helium gun	-------
162	9.08	26.26	14.40	.16	9.10	Helium gun	-------
163	9.09	24.40	11.60	.03	8.50	Helium gun	-------
164	9.10	25.55	11.64	.04	10.00	Helium gun	-------
165	9.22	26.17	7.14	.20	4.35	Helium gun	-------
166	9.28	26.91	7.28	.20	4.06	Helium gun	-------
167	9.31	28.19	10.00	.21	4.60	Helium gun	16
168	9.31	28.19	10.00	.21	4.60	Rocket	16
169	10.00	20.35	11.50	.00	90.00	Helium gun	-------
170	10.00	27.40	11.00	.00	6.80	Helium gun	-------
171	10.00	28.40	16.50	.25	4.15	Rocket	-------
172	10.04	30.40	11.00	.00	90.00	Helium gun	-------
173	10.46	27.40	15.35	.02	4.00	Helium gun	-------
174	10.70	29.80	11.00	.00	6.80	Helium gun	-------
175	11.02	32.40	17.04	.19	7.05	Helium gun	-------
176	11.39	29.20	11.00	.00	18.90	Helium gun	-------
177	12.05	31.90	15.00	.04	5.00	Helium gun	-------

circular symbols represent the calculation for turbulent body flow plus laminar fin flow.

A word of warning is in order at this point: In the figures in which both the circular and square symbols appear at the subsonic end of the Mach number scale and only the fully turbulent (square) symbol appears at the supersonic value (for example, configuration 158), the Reynolds numbers are such that it is possible that transition from laminar to turbulent flow has occurred at some Mach number between the two extremes. This possibility means that any pressure or wave drags derived by subtracting base, fin, and friction drag from the total drag can be in error by the amount of the difference between the turbulent and laminar fin friction drags. Configuration 158 presents a case in point, although for this model the transition appears rather dramatically in the total-drag curve. This type of drag variation is unusual, and the change would not be at all apparent if the transition had occurred in the rapidly rising section of the drag curve.

This compilation in the appendix represents a collection of total-drag curves for various bodies of revolution stabilized by fins. The usefulness of the data is largely determined by the information which can be obtained from these total drags concerning the values of the pressure or wave drags of the bodies alone (i.e., not influenced by the fins), since it is the value of this component of the supersonic drag that is always difficult and often impossible to calculate from theoretical considerations in the low supersonic speed ranges considered. In order to obtain the wave drag of the body alone from the test results, the friction, base, and fin pressure drags must be known or assumed.

The friction drag can be calculated accurately for most bodies. For many bodies, the base drag is

591396—61——2

negligible and the base drag for most of the remaining bodies can be estimated accurately from empirical curves. The fin affects the drag in three ways: fin pressure drag due to fin induced pressures, pressure drag of the fin due to the body, and pressure drag on the body due to the fins. The value of the first component has been either measured or calculated for most of the fins used. Values of the interference terms are, in general, not calculable. For the models of the present report, it appears reasonable to assume that the interference terms are negligible for most cases since the fins are extremely thin. The interference has been shown to be essentially zero by wind-tunnel tests of configuration 109 (see fig. 1) since the fin drag obtained by subtracting results for finned and unfinned models agreed exactly (except at $M=1$) with fin drags obtained on special free-flight models on which the interference drag was zero by virtue of the cylindrical shape of the body. Since configuration 109 is of high fineness ratio, this result cannot be applied generally. An attempt to measure fin interference was made with configurations 48 and 49. Although these bodies had low-fineness-ratio afterbodies on which the fin interference was expected to be large, the measured differences were small and in the opposite sense to that expected.

The following sections provide the data necessary in the breakdown of the total-drag curves into their component parts.

FRICTION DRAG

Figure 2 presents average flat-plate friction coefficients based on wetted area as functions of total Reynolds number for various Mach numbers. All values are for an insulated wall (no heat flow), which is correct for the wooden-surface models and is nearly correct for the models with metal surfaces and Mach numbers near 1. These values were used in the calculation of the friction drags shown in the appendix for configurations 1 to 177. The use of flat-plate values for bodies of revolution is not exactly correct because of at least two factors—first, the difference between two- and three-dimensional flow, and, second, the existence of velocities higher than free-stream velocity on the surface of the bodies. Both effects are functions of body fineness ratio, the effects being most in evidence at lower values of l_T/d. Reference 18 gives an approximate correction factor for the higher average velocities existing on bodies of revolution as

$$\frac{(C_{D,f})_{\text{body of rev}}}{(C_{D,f})_{\text{flat plate}}}=1+\frac{0.5}{l_T/d}$$

which is supposedly valid at Mach numbers as high as 1. Both effects are apparently small for the bodies included in this compilation. The ratio of $C_{D,f}$ to C_f is given in the tables as S_B/A_{max} (the

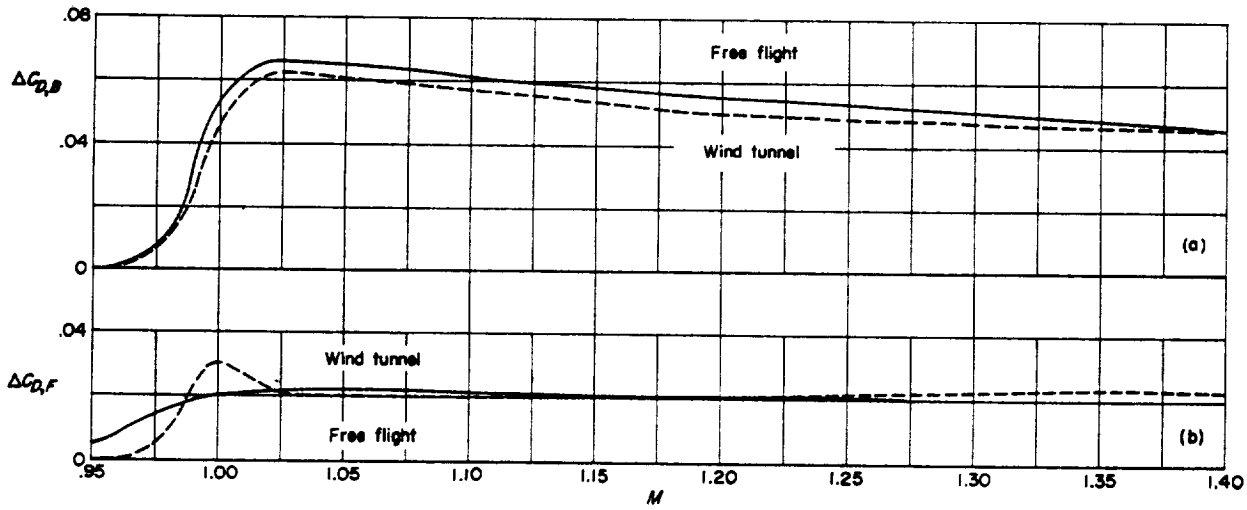

(a) Comparison of drag rise.
(b) Drag rise of fins and fin-body interference.

FIGURE 1.—Comparisons of data for configuration 109 obtained from wind-tunnel and free-flight tests.

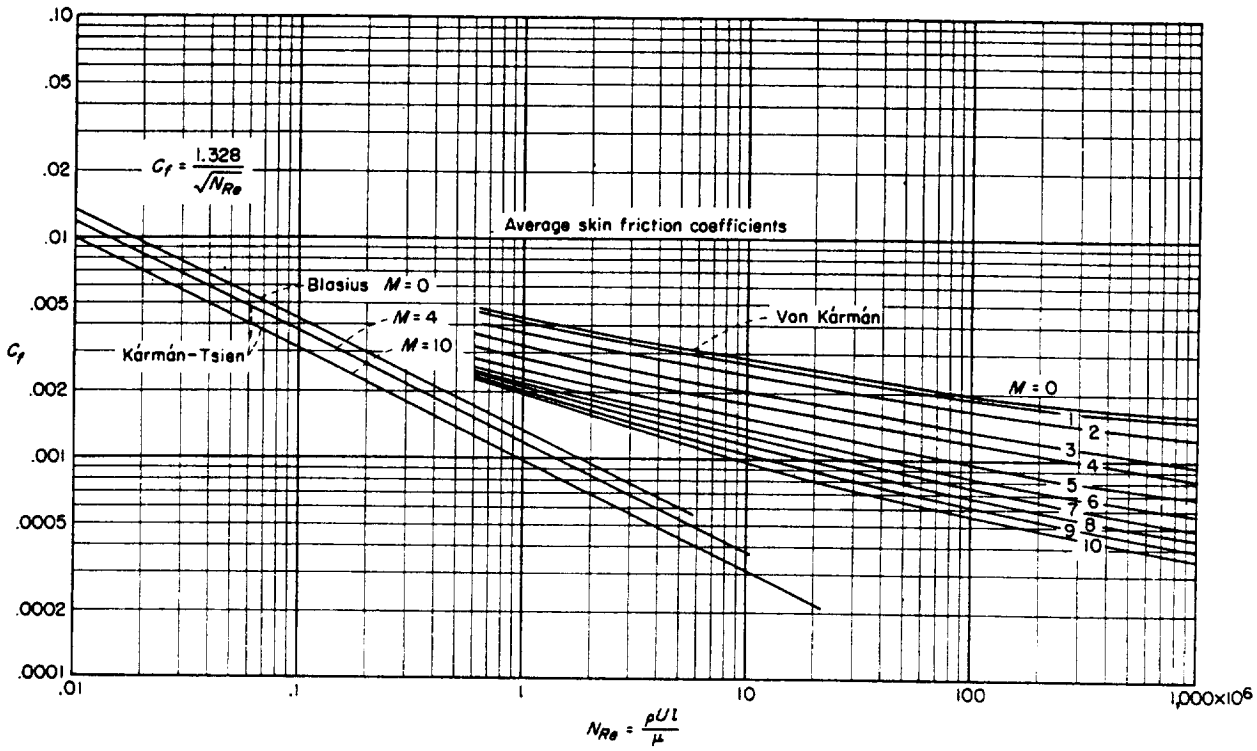

FIGURE 2.—Average skin-friction coefficients for flat plates based on wetted area.

ratio of body wetted area to body frontal area), so that changes from C_f to $C_{D,f}$ may be quickly estimated. The values were calculated from the relationship

$$\frac{C_{D,f}}{C_f} = 4\frac{l}{d}\int \frac{r}{R}\, d\frac{x}{l}$$

Another assumption has been made in the calculation of the friction drag; namely, the bodies have been assumed to have either completely laminar or completely turbulent flow on the body and fins. This assumption may be erroneous for some of the models flown at Reynolds numbers from 1×10^6 to 5×10^6 and this possibility should be kept in mind in the analysis of such data. The only models for which this assumption is obviously wrong are configurations 104 and 105 (see appendix), even though they flew at extremely high Reynolds numbers. These configurations are both models of the NACA RM–10 body, which has been extensively tested in wind tunnels. (See refs. 13, 19, and 20.) These models are more carefully finished than the majority tested and long runs of laminar flow (Reynolds numbers up to 40×10^6) have been detected on the body on some flights. Even more likely are long runs of laminar flow on the fins and since the fins of these models contribute nearly as much friction-drag area as the body, their presence would cause a large error in the calculations as made. With these considerations, if the pressure drag of this configuration is desired, it would be best to obtain it from theory or from the wind-tunnel results presented in references 13, 19, and 20. Note, however, that the base drags obtained from flight measurements should be the most accurate, since the tunnel measurements contain sting-interference effects. References 13, 19, and 20 also give examples of the effects of Reynolds number, transition, and heat transfer on friction drag.

BASE PRESSURE AND BASE DRAG

Reference 21 contains an excellent analysis and data on base pressure behind both two- and three-dimensional bodies when the boundary layer is turbulent ahead of the base and the Mach numbers are in the range considered in this report. The following discussion follows this reference.

Three-dimensional base drag.—Figure 3 presents the base pressure coefficients as a function of Mach number for a cylindrical afterbody of infinite length (refs. 21 to 23). As mentioned in reference 21, the base pressure behind a cylindrical base can be influenced by flow conditions such as

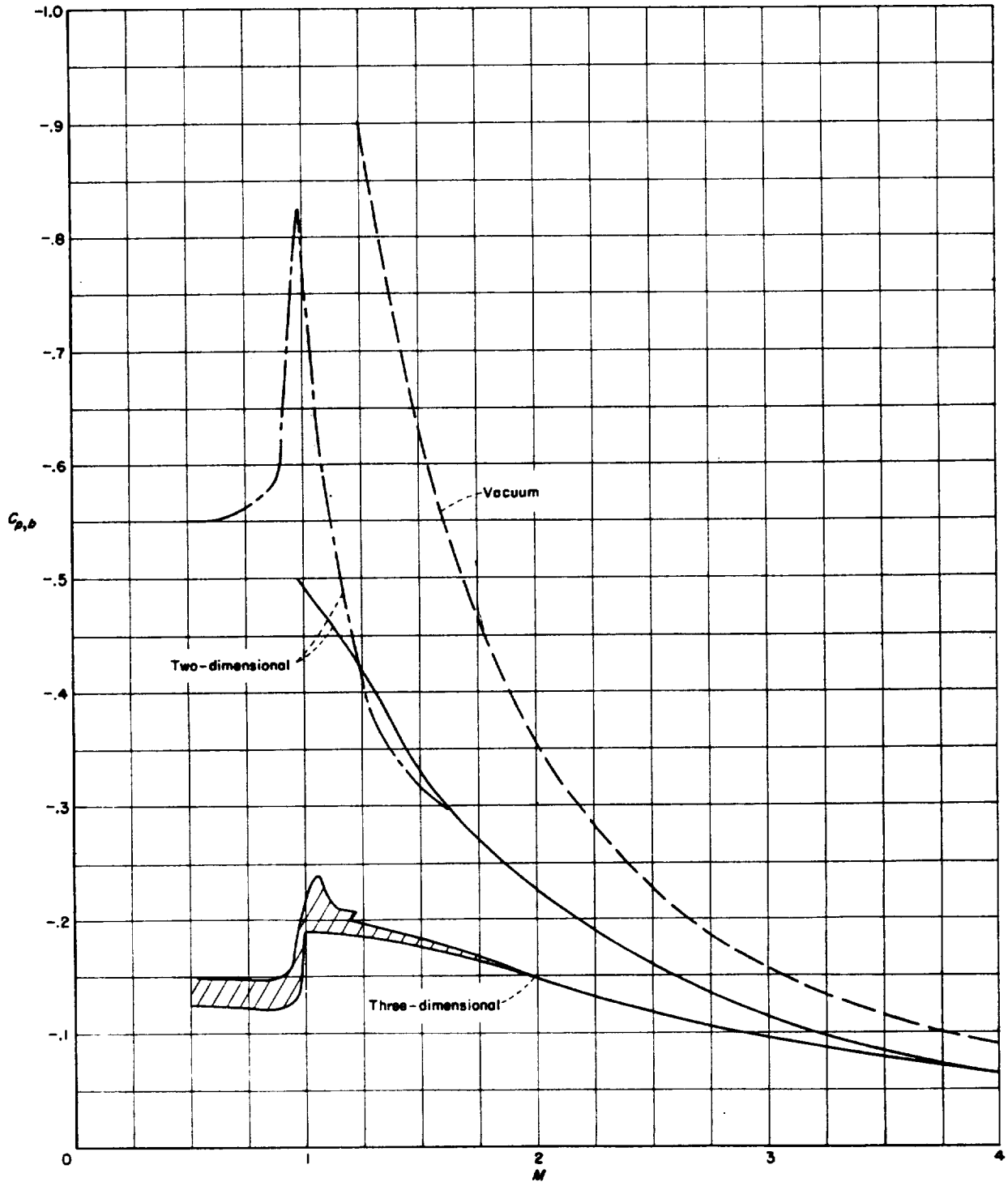

FIGURE 3.—Base-pressure coefficients behind two- and three-dimensional bodies for which flow is turbulent ahead of base.

fin and nose pressure fields ahead of the base even when the boundary layer is turbulent well ahead of the base. For the bodies studied in the present report, such differences are believed to be small enough to allow the curve shown in figure 3 to be used, the possibility of such an error being always kept in mind, however, especially for subsonic speeds. (See ref. 18, pp. 30 to 34.)

Most of the bodies included herein have afterbodies, that is, a base diameter which is smaller than the maximum diameter. The base drag of such bodies is discussed in reference 21; however, the method of evaluating such base pressures discussed therein is overcomplicated for the purposes of the present paper, since the value of the base drag is seldom a very large percentage of the total drag for boattailed bodies. Some published wind-tunnel data on the base drag of conical afterbodies suggest the empirical expression

$$C_{D,b}=C_{D,\,cylinder\ base}\left(\frac{r_b}{R}\right)^3$$

Care must be taken in applying this equation at subsonic Mach numbers since it does not account for the possibility of negative base drags which can exist (ref. 24).

Two-dimensional base pressures.—Figure 3 also presents base-pressure coefficients for a two-dimensional base from references 21 and 25. The data represent the base pressures behind slab wings. They are presented herein as an estimate of the pressures behind a rearward facing step on a body of revolution.

PRESSURES ON A FORWARD FACING STEP

Figure 4 presents the pressure coefficients required to separate the turbulent boundary layer in front of a step of several times the boundary-layer thickness. (See ref. 26.) It appears from page 52 of reference 18 that a pressure coefficient of $C_p=0.41$ is valid at subsonic speeds as well as Mach number 1. Again these essentially two-dimensional values are presented as estimates for the pressures ahead of forward facing steps on bodies of revolution.

FIN PRESSURE DRAG

Figure 5 presents the pressure-drag coefficients based on the exposed plan-form area of the fin (note that this is one-half the value of S_p/A_{max}

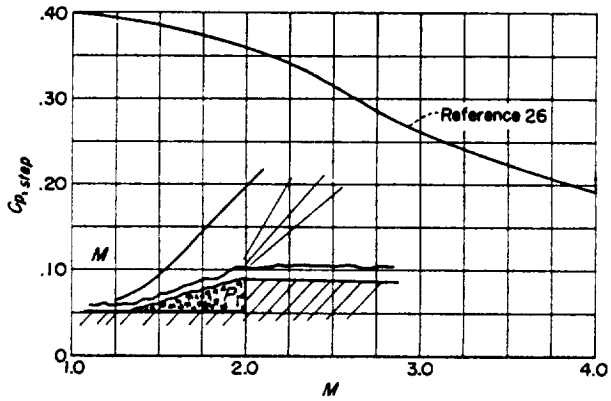

FIGURE 4.—Pressure coefficients on forward facing step for flow with turbulent boundary layer.

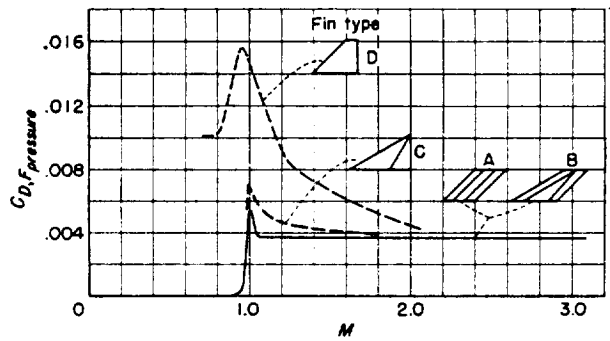

FIGURE 5.—Fin pressure drag coefficients (including base pressure) based on exposed fin area.

tabulated in the basic data sheets of the appendix) for most of the fins used in this report. Extreme accuracy has not been striven for or obtained, since in most cases the fin pressure drag is such a small part of the total drag that a 50-percent error in fin drag is of the order of the test accuracy.

The pressure drag of fin type A (fig. 5), which is used on most of the models, was measured by means of special helium-gun models. The drag of fin type B was measured by special rocket models, the data for which are presented in reference 27. The supersonic pressure drag thus obtained is so similar to that measured on fin type A that they have been shown as one curve. The pressure drag of fin type C was estimated by reducing the drag rise of a 6-percent-thick delta wing of reference 27 (p. 47) by the square of the thickness ratios. The pressure drag of fin type D is simply the two-dimensional base pressure of figure 3 referred now to the fin plan-form area.

SUMMARY CURVES

SYSTEMATIC INVESTIGATIONS

Most of the smooth bodies (table I) were flown in programs designed to investigate the results of systematic geometrical changes in the body shapes on zero-lift drag. Figures 6 to 10 present summary plots of total-drag coefficients for the most important of these investigations. These figures give a broad picture of the effect of the most important variables on the total body drag; that is, fineness ratio and maximum-diameter location (fig. 6), nose shape and fineness ratio (figs. 7 to 9; also configurations 1 to 8 in the appendix), and afterbody fineness ratio and shape (fig. 10). Various other methods of correlating the data will be immediately apparent to the reader, but it is suggested that the original references (see tables I and II) be consulted before too elaborate an analysis is attempted, since the various data have been handled in more detail in these reports than in the present report.

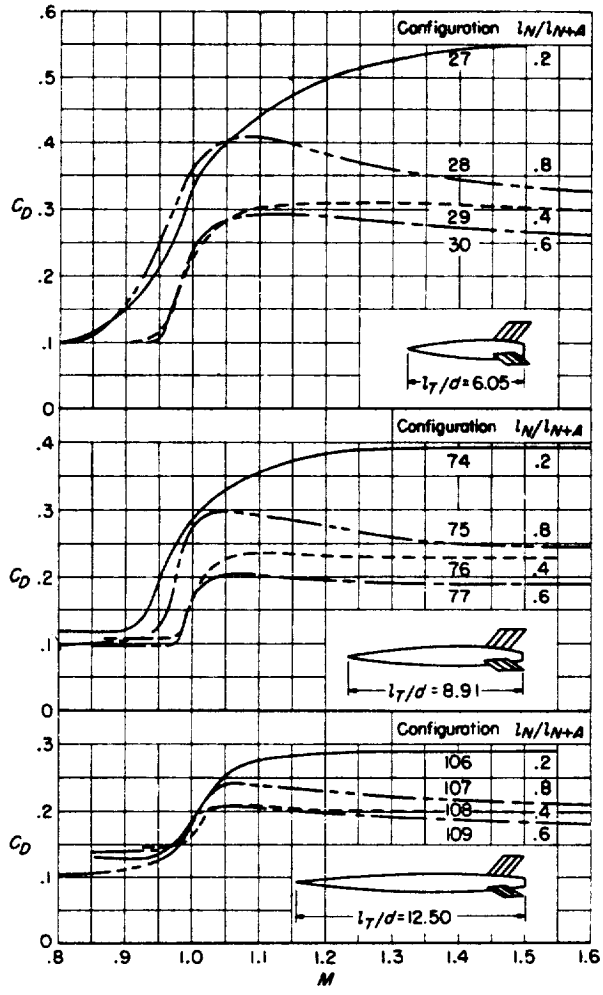

FIGURE 6.—Drag coefficients of parabolic bodies showing effects of fineness ratio and position of maximum diameter.

DRAG ANALYSIS

The data presented herein, together with data from wind-tunnel tests and theoretical results, allow some general conclusions useful to designers to be drawn. The effects of nose and afterbody shape are discussed separately, after which a brief discussion is given of the effects of the shapes of complete bodies.

Nose drag.—In the analysis of nose drag it is helpful to use one of the basic premises of this report, that is, that the effects of shape and fineness ratio may usefully be considered separately. The variation at $M=1.4$ of the nose pressure drag with l_N/d is presented in figure 11. The lower curve represents near minimum nose pressure drags. At low values of l_N/d, the minimum-drag curve was obtained by fairing through the flat-face value ($C_D=0.8C_{p,T}$) and hemisphere values (ref. 28). Above $l_N/d=1.4$ it was determined from second-order calculations (by the method of Van Dyke, ref. 29) of bodies defined by $\frac{r}{R}=\left(\frac{x}{l_N}\right)^{3/4}$ (labeled A in fig. 11) and $\frac{r}{R}=\frac{\frac{2x}{l_N}-\frac{3}{4}\left(\frac{x}{l_N}\right)^2}{1\frac{1}{4}}$ (labeled B in fig. 11). Note that neither of these bodies has zero slope at its maximum diameter. Since the calculations and experiment agree well for noses having $l_N/d=3$ (see fig. 12), a fair amount of confidence may be placed in the values shown. Second-order calculations are also shown for the parabolic nose $\frac{r}{R}=\frac{l_T}{l_N}-\left(\frac{x}{l_N}\right)^2$ used on so many of the models in this report. Taylor-Maccoll cone values are also shown for comparison.

Although l_N/d is shown to be a powerful parameter, the effects of shape can be important, as can be seen in figure 12. The results shown in this figure are particularly gratifying in that the values from free-flight and wind-tunnel tests and several theories are in marked agreement. As can be seen from this figure, there is no one minimum-drag

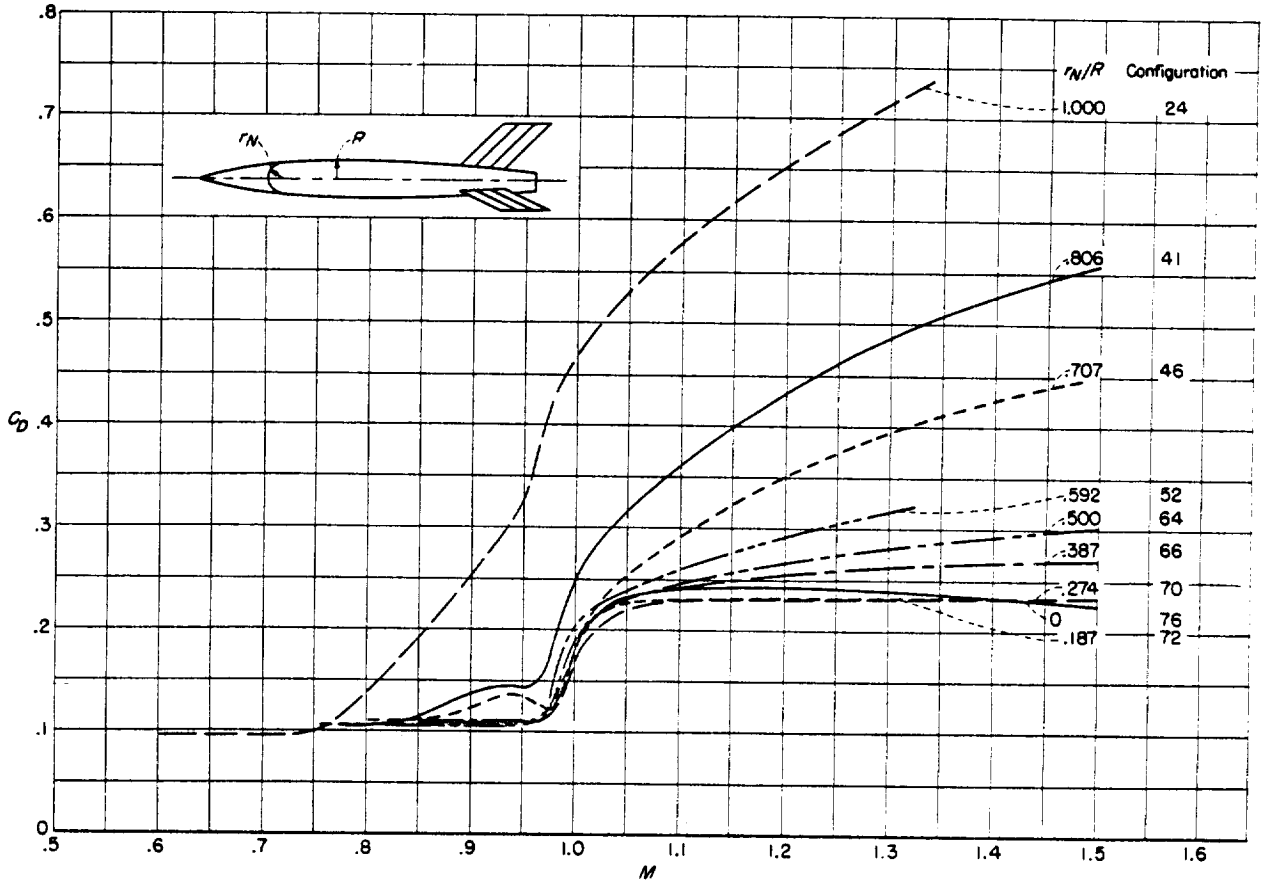

FIGURE 7.—Drag coefficient plotted against Mach number for configurations obtained by rounding off nose of parabolic body of fineness ratio 8.91.

shape for the entire Mach number range but several do well over the entire range. (Refs. 30 and 31 present the drags of many shapes not shown here.) Note that these results are for $l_N/d=3$ and the relative drags may change with l_N/d. Data from reference 30 have been combined with the data of this report in part (b) of figure 12 to illustrate some general statements about the effect of nose geometry on drag. The drags of the $x^{1/4}$ and the ellipsoid nose show the high-peak-drag level and the late-peak-drag Mach numbers characteristic of blunt nose bodies. The $x^{1/4}$ nose though not absolutely sharp (the cone could also have been used) shows the early drag rise and early sharp peak drag and the rapid decrease of drag with Mach number to be expected on sharp-nose bodies of revolution. The Von Kármán nose which has the $x^{3/4}$ profile at its apex but which is blunter immediately behind the apex produces a drag variation with Mach number which incorporates the desirable features of both types of nose, that is, late drag rise, "soft" peak and low peak-drag level, and decreasing supersonic drag. This result is perhaps not so surprising since this nose was designed (from linearized theory) for minimum drag for a given l_N/d at low supersonic Mach numbers.

When these results are applied to the design of a complete body, it must be remembered that the interference drag of the nose on the afterbody is also a function of nose shape. There are indications that the lowest drag shapes which do not have zero slope at their maximum diameter have higher interference drag potential than the more smoothly faired shapes. (See subsequent section, "Total body drag.")

Afterbody drag.—The data of figure 10 have been analyzed to give the drags of the afterbodies caused by the pressures acting over the afterbodies and bases. (For details of the drag breakdowns, see ref. 6.) The results are presented for $M=1.2$

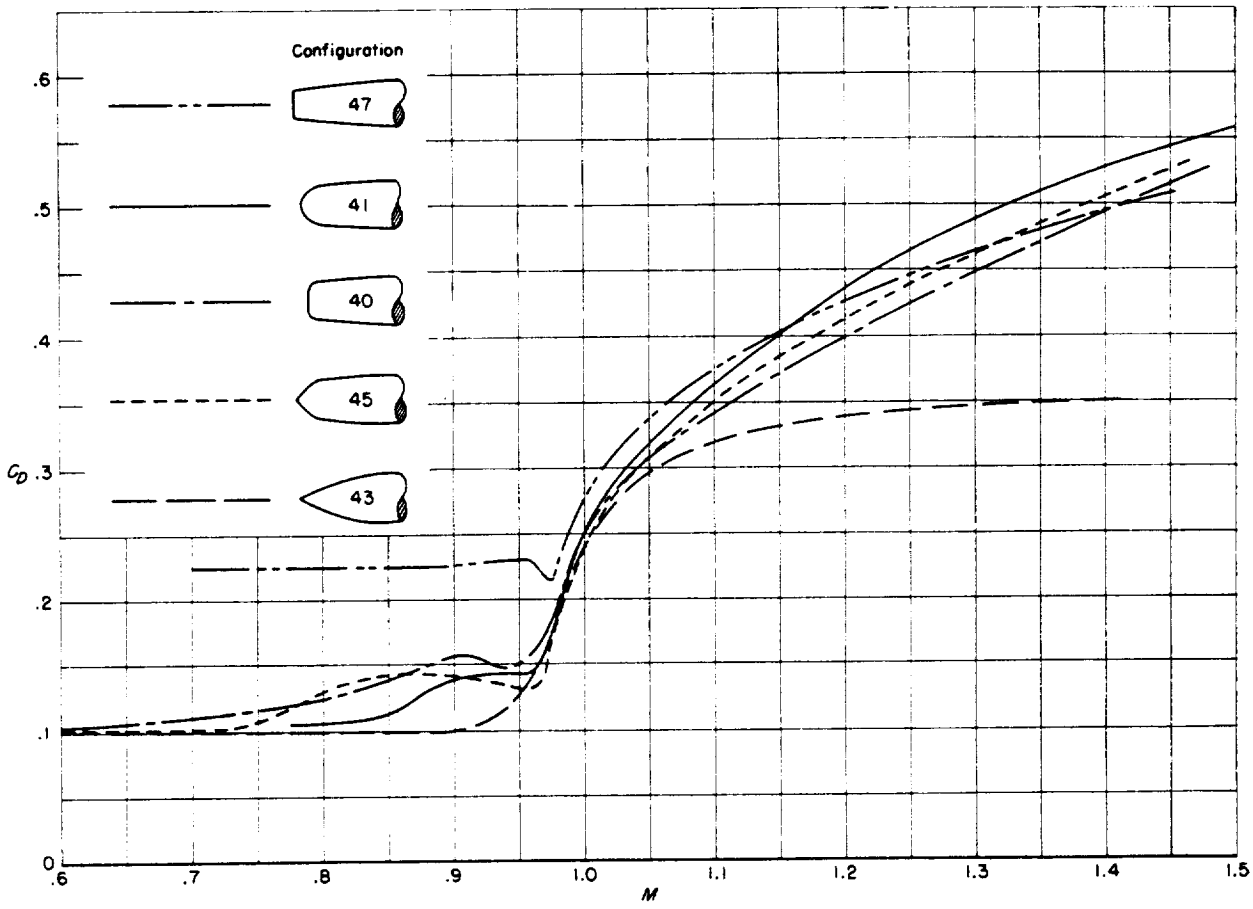

FIGURE 8.—Comparison of drag coefficients for five configurations having nose fineness ratios of about 2.

in figure 13. The data for the conical afterbodies are compared with the following semiempirical equation:

$$C_{D,A}=\frac{0.001\theta_b+0.00071\theta_b^2}{M}\left[1-\left(\frac{r_b}{R}\right)^n\right]+C_{D,b}\left(\frac{r_b}{R}\right)^3 \tag{1}$$

where

$$n=4 \qquad (M<3.5)$$

$$n=3 \qquad (M>3.5)$$

θ_b is the slope of the afterbody in degrees (used as positive, although actually always negative; not applicable for positive values of θ_b), and $C_{D,b}$ is the base pressure drag of the cylinder (fig. 3). The first term of the equation approximates the second-order theoretical values calculated by Jack (ref. 32), whereas the second term is a purely empirical approximation for the effect of base diameter ratio on the base pressure. In view of the inaccuracies inherent in both the experimental and the theoretical values (the theory, for instance, was calculated only for $M>1.5$), the nearly exact agreement of the two shown in figure 13(a) can only be regarded as somewhat fortuitous. However, it is apparent, from the comparisons of this report with the second-order theory of reference 32 and from the comparisons of reference 6 with other theoretical calculations, that afterbody drags can be calculated reasonably accurately for afterbodies having maximum slopes of less than about 15°. At or above this degree of convergence large discrepancies may be expected (see ref. 6), with theoretical calculations tending to overestimate the drag.

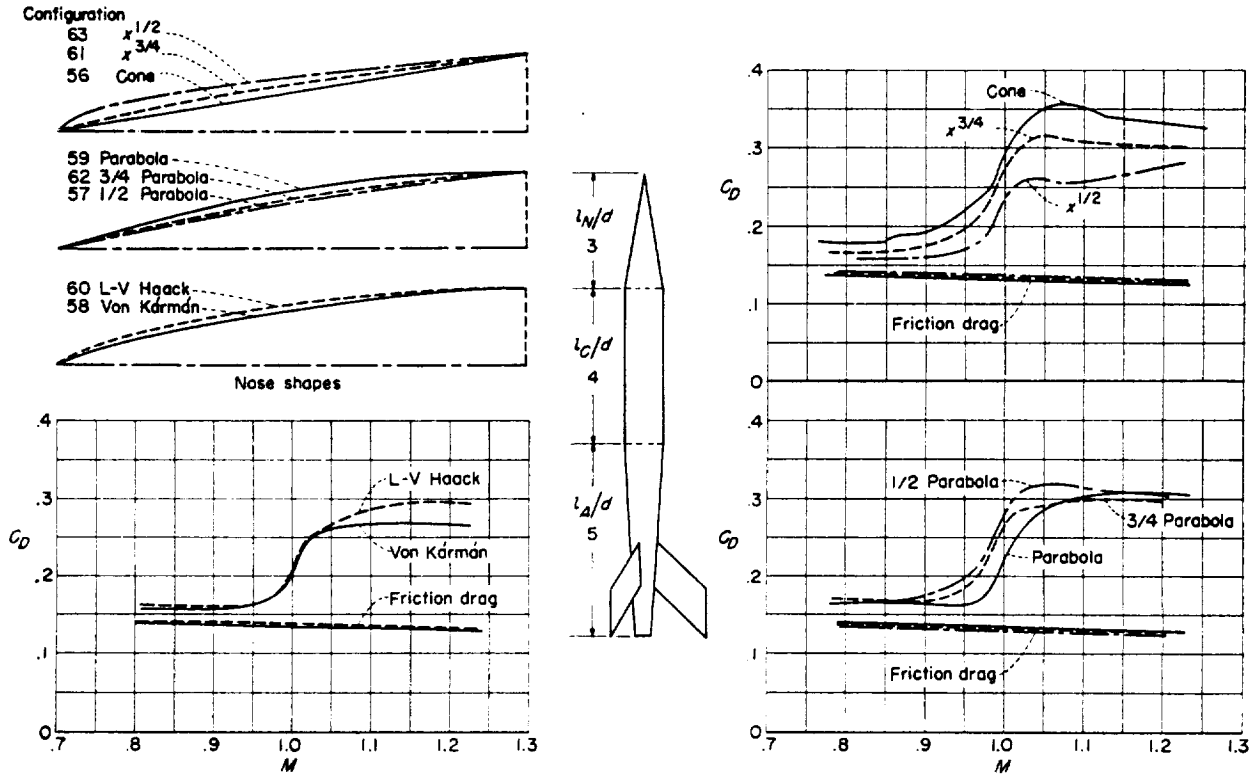

FIGURE 9.—Drag coefficients for eight bodies having fineness-ratio-3 noses of various shapes

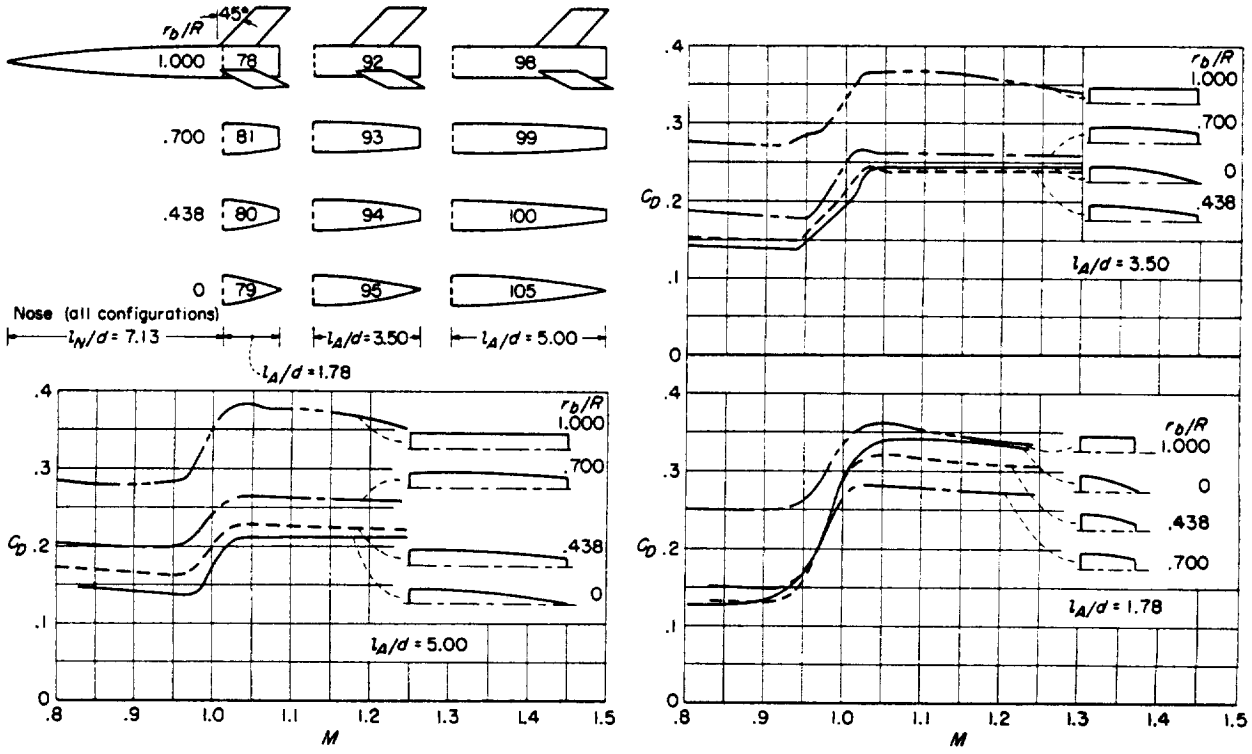

FIGURE 10.—Drag coefficients for 12 bodies having identical noses and different afterbodies.

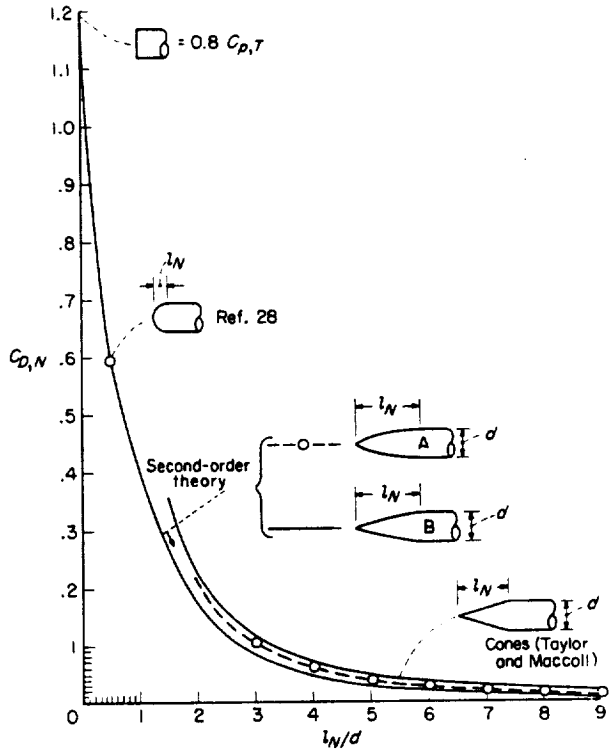

FIGURE 11.—Drag coefficients due to pressures on noses at $M=1.4$.

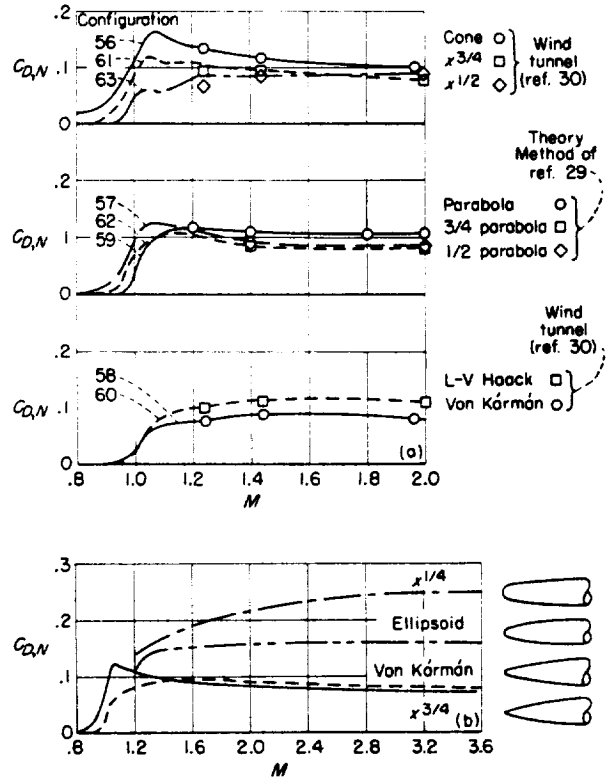

(a) Nose pressure drags of flight models compared with wind-tunnel results and theory.

(b) Nose pressure drags from reference 30 showing general effects of nose shape on drag.

FIGURE 12.—Pressure drag of noses of fineness ratio 3.

All the test results of both parabolic and conical afterbodies and the theoretical calculations lead to an extremely simple rule for selecting minimum drag afterbodies if a required value of l_A/d is given. The center curve in figure 13(b) represents conical afterbodies with a slope of 4.5° (or parabolic meridians with a base slope of 9°). The circular data points represent the parabolic afterbodies of figure 10; note also that the tangent to the parabolic base angle is always exactly twice that of the inscribed conical body. The minimum drag bodies all fall on this line. The fact that for a given value of l_A/d the required ratio of base diameter to maximum diameter is much less important at the higher values of l_A/d can be noted in figure 13(a) and is shown more graphically by the shaded area on the lower figure which shows the limits of configurations for which the drag coefficients lie within about 10 percent of the minimum. The range of optimum conical angles indicated (3.5° to 6.5°) is of the same order (5° to 7°) as that used for some time in ballistics for the drag reduction of bullets.

Total body drag.—If the minimum afterbody drags at each value of l_A/d are taken, the resulting plot (fig. 14) may be said to represent a near minimum possible afterbody pressure drag for $M=1.2$. A similar curve is presented for the nose drag and was obtained by fairing through the blunt nose values from configurations 1 to 7, through the minimum ($l_N/d=3$) nose drag (½ parabola, fig. 12) and through the $M=1.4$ values for the higher values of l_N/d (fig. 11). These curves are presented to give some practical boundaries, admittedly empirical and rough, to the minimum drag problem.

If the nose and afterbody minimum drag coefficients are added for bodies with their maximum diameters at their midpoints, the solid-line curve in figure 15 is obtained. If the same drag coefficients are added, with care taken to place the maximum diameter at the most favorable position, the dashed curve is obtained. (This

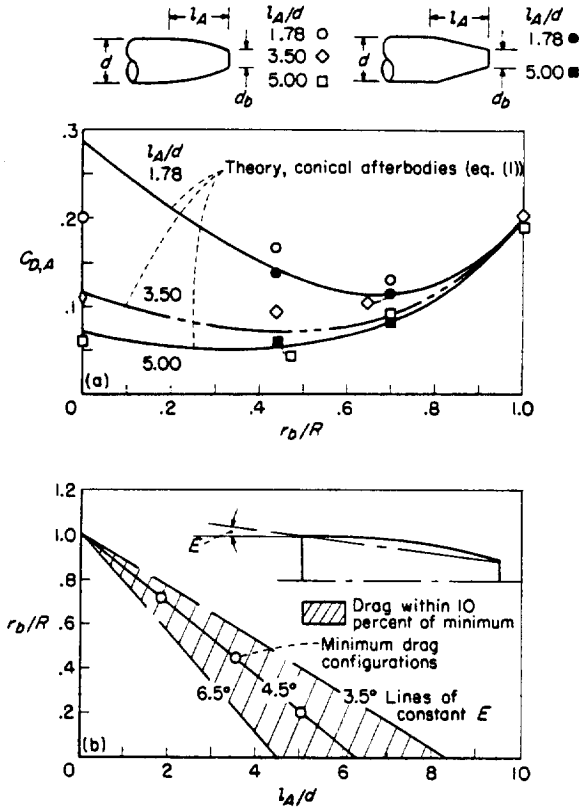

(a) Experimental and theoretical afterbody pressure drag + base drag at $M=1.2$.
(b) Configurations for minimum afterbody drag at $M=1.2$.

FIGURE 13.—Afterbody pressure drag at $M=1.2$.

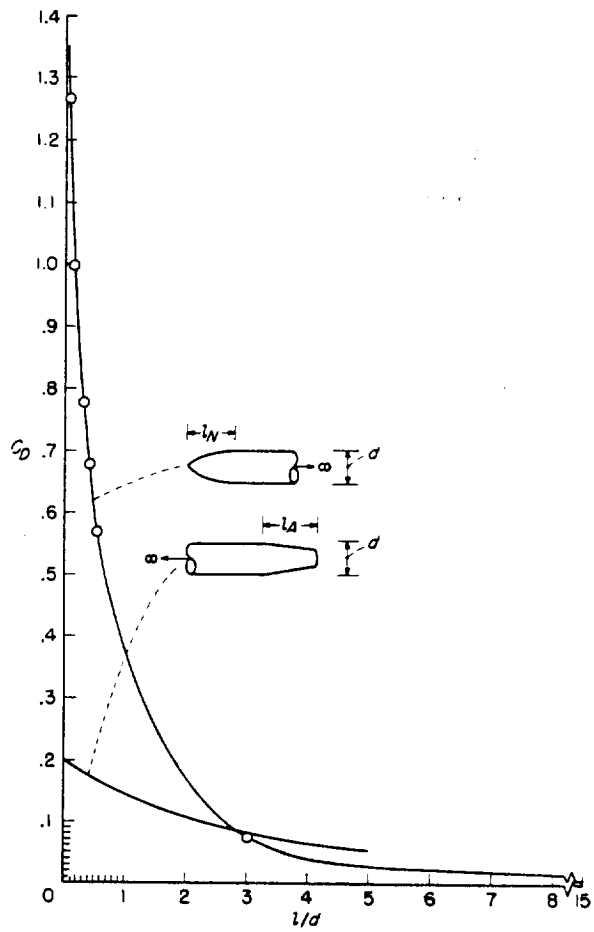

FIGURE 14.—Near-minimum pressure-drag coefficients at $M=1.2$ for noses and afterbodies without interference.

position moves rapidly rearward from $x/l_T=0.55$ for $l_T/d=7$ to $x/l_T=1$ for $l_T/d=3$ for the near minimum curves of figure 14; however, such values are extremely susceptible to small changes in the level of either the nose- or afterbody-drag curves and must only be considered as indicative of the trend.) Also, the drag rises ($\Delta C_D=C_{D,T}-C_{D,f}-C_{D,F}$) for the smooth bodies of this report are plotted at the fineness ratio representing the sum of their nose and afterbody fineness ratios. Most of the bodies at low values of l_T/d actually had cylindrical center sections and thus their interference drag coefficients were low. This fact must be considered when the use of either of the empirical curves as minimum-drag boundaries is contemplated. As an instance of this need, compare the pressure drag coefficients of configurations 84 and 85 in the appendix, which are identical in shape but have the same fineness ratio of nose and afterbody and differ only in the cylindrical center section of configuration 85. The higher pressure drag of configuration 84 must be attributed to interference of the nose on the afterbody. This interference drag seems high in comparison with the drag produced by the interaction of nose and afterbodies of the parabolic bodies of figure 6 which are indicated to be of the order of that for configuration 85 (and essentially zero) by a breakdown of their drag coefficients into component parts and a comparison of the pressure components with second-order theoretical calculations (ref. 29). It seems reasonable to assume that at total fineness ratios below 6, the effect of nose induced pressures on afterbody drag and perhaps more significantly on base pressure (note large base diameter ratios of minimum drag afterbodies of fineness ratios less than 3 (fig. 13(b)), and see ref. 21 for some examples of such effects on base pressures) will be the important and

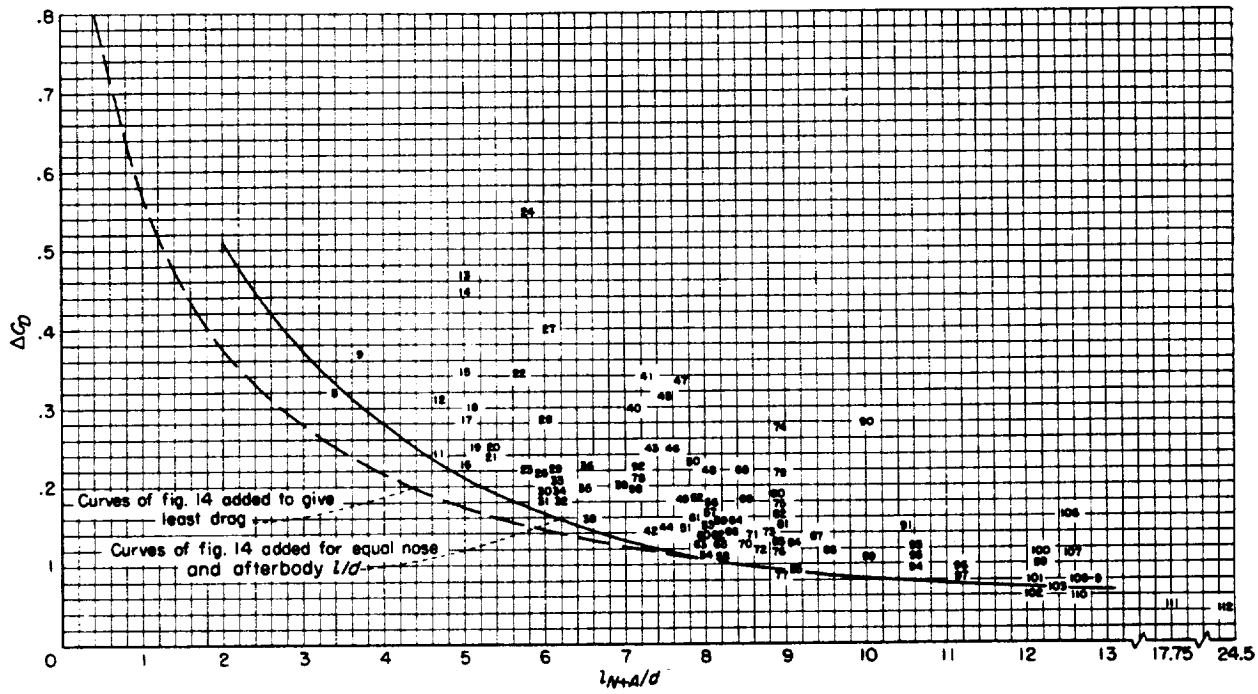

FIGURE 15.—Pressure-drag coefficients at $M=1.2$. $\Delta C_D = C_{D,T} - C_{D,f} - C_{D,F}$.

perhaps the determining factors affecting both the shape of the body and the value of the drag of minimum drag designs.

While it is not a factor considered in the discussions of this report it must always be remembered that the dependence of drag on l/d is also a function of the friction coefficient, and that it is the increase of friction drag with l/d that limits the drag reduction due to increasing l/d.

CONCLUDING REMARKS

A compilation has been presented of data on the zero-lift drag from free-flight measurements on fin-stabilized bodies of revolution. Included are data for 177 configurations from which a designer may easily estimate the drag of a desired shape through simple comparisons. Supplementary plots and theoretical estimates have been included to facilitate the determination of body pressure drags from the measured total drags.

LANGLEY RESEARCH CENTER,
NATIONAL AERONAUTICS AND SPACE ADMINISTRATION,
LANGLEY FIELD, VA., *September 3, 1957.*

REFERENCES

1. Hopko, Russell N.: The Effect of Some Surface Roughness Elements on the Drag of a Body of Revolution at Supersonic Speeds. NACA RM L54I21, 1954.
2. Piland, Robert O., and Putland, Leonard W.: Zero-Lift Drag of Several Conical and Blunt Nose Shapes Obtained in Free Flight at Mach Numbers of 0.7 to 1.3. NACA RM L54A27, 1954.
3. Piland, Robert O.: Preliminary Free-Flight Investigation of the Zero-Lift Drag Penalties of Several Missile Nose Shapes for Infrared Seeking Devices. NACA RM L52F23, 1952.
4. Wallskog, Harvey A., and Hart, Roger G.: Investigation of the Drag of Blunt-Nosed Bodies of Revolution in Free Flight at Mach Numbers From 0.6 to 2.3. NACA RM L53D14a, 1953.
5. Hart, Roger G., and Katz, Ellis R.: Flight Investigations at High-Subsonic, Transonic, and Supersonic Speeds To Determine Zero-Lift Drag of Fin-Stabilized Bodies of Revolution Having Fineness Ratios of 12.5, 8.91, and 6.04 and Varying Positions of Maximum Diameter. NACA RM L9I30, 1949.
6. Stoney, William E., Jr.: Some Experimental Effects of Afterbody Shape on the Zero-Lift Drag of Bodies

for Mach Numbers Between 0.8 and 1.3. NACA RM L53I01, 1953.

7. Stoney, William E., Jr.: Transonic Drag Measurements of Eight Body-Nose Shapes. NACA RM L53K17, 1954.
8. Walters, Richard E.: Application of Transonic Area Rule to a Sharp-Lipped Ducted Nacelle. NACA RM L53J09b, 1954.
9. Sears, R. I., and Merlet, C. F.: Flight Determination of the Drag and Pressure Recovery of an NACA 1-40-250 Nose Inlet at Mach Numbers From 0.9 to 1.8. NACA TN 3218, 1955. (Supersedes NACA RM L50L18.)
10. Sears, R. I., Merlet, C. F., and Putland, L. W.: Flight Determination of Drag of Normal-Shock Nose Inlets With Various Cowling Profiles at Mach Numbers From 0.9 to 1.5. NACA Rep. 1281, 1956. (Supersedes NACA RM L53I25a.)
11. Mason, Homer P., and Gardner, William N.: An Application of the Rocket-Propelled-Model Technique to the Investigation of Low-Lift Buffeting and the Results of Preliminary Tests. NACA RM L52C27, 1952.
12. Welsh, Clement J., and DeMoraes, Carlos A.: Results of Flight Tests To Determine Drag of Parabolic and Cone-Cylinder Bodies of Very Large Fineness Ratios at Supersonic Speeds. NACA RM L51E18, 1951.
13. Jackson, H. Herbert, Rumsey, Charles B., and Chauvin, Leo T.: Flight Measurements of Drag and Base Pressure of a Fin-Stabilized Parabolic Body of Revolution (NACA-RM 10) at Different Reynolds Numbers and at Mach Numbers From 0.9 to 3.3. NACA TN 3320, 1954. (Supersedes NACA RM L50G24.)
14. Hall, James Rudyard: Effect of Wing Size and Amount of Indentation on Applicability of Transonic Area Rule to Swept-Wing Configurations. NACA RM L55F03, 1956.
15. Stoney, William E., Jr., and Putland, Leonard W.: Some Effects of Body Cross-Sectional Shape, Including a Sunken-Canopy Design on Drag As Shown by Rocket-Powered-Model Tests at Mach Numbers From 0.8 to 1.5. NACA RM L52D07, 1952.
16. Hoffman, Sherwood: A Flight Investigation of the Transonic Area Rule for a 52.5° Sweptback Wing-Body Configuration at Mach Numbers Between 0.8 and 1.6. NACA RM L54H13a, 1954.
17. Van Driest, E. R.: The Turbulent Boundary Layer for Compressible Fluids on a Flat Plate With Heat Transfer. Rep. No. AL-997, North American Aviation, Inc., Jan. 27, 1950.
18. Hoerner, Sighard F.: Aerodynamic Drag. Publ. by the author (148 Busteed, Midland Park, N.J.), 1951.
19. Evans, Albert J.: The Zero-Lift Drag of a Slender Body of Revolution (NACA RM-10 Research Model) As Determined From Tests in Several Wind Tunnels and in Flight at Supersonic Speeds. NACA Rep. 1160, 1954. (Supersedes NACA TN 2944.)
20. Carros, Robert J., and James, Carlton S.: Some New Drag Data on the NACA RM-10 Missile and a Correlation of the Existing Drag Measurements at $M=1.6$ and 3.0. NACA TN 3171, 1954.
21. Love, Eugene S.: Base Pressure at Supersonic Speeds on Two-Dimensional Airfoils and on Bodies of Revolution With and Without Fins Having Turbulent Boundary Layers. NACA TN 3819, 1957. (Supersedes NACA RM L53C02.)
22. Hart, Roger G.: Effects of Stabilizing Fins and a Rear-Support Sting on the Base Pressures of a Body of Revolution in Free Flight at Mach Numbers From 0.7 to 1.3. NACA RM L52E06, 1952.
23. Peck, Robert F.: Flight Measurements of Base Pressure on Bodies of Revolution With and Without Simulated Rocket Chambers. NACA TN 3372, 1955. (Supersedes NACA RM L50I28a.)
24. Katz, Ellis, and Stoney, William E., Jr.: Base Pressures Measured on Several Parabolic-Arc Bodies of Revolution in Free Flight at Mach Numbers From 0.8 to 1.4 and at Large Reynolds Numbers. NACA RM L51F29, 1951.
25. Morrow, John D., and Katz, Ellis: Flight Investigation at Mach Numbers From 0.6 to 1.7 To Determine Drag and Base Pressures on a Blunt-Trailing-Edge Airfoil and Drag of Diamond and Circular-Arc Airfoils at Zero Lift. NACA TN 3548, 1955. (Supersedes NACA RM L50E19a.)
26. Love, Eugene S.: Pressure Rise Associated With Shock-Induced Boundary-Layer Separation. NACA TN 3601, 1955.
27. Morrow, John D., and Nelson, Robert L.: Large-Scale Flight Measurements of Zero-Lift Drag of 10 Wing-Body Configurations at Mach Numbers From 0.8 to 1.6. NACA RM L52D18a, 1953.
28. Sommer, Simon C., and Stark, James A.: The Effect of Bluntness on the Drag of Spherical-Tipped Truncated Cones of Fineness Ratio 3 at Mach Numbers 1.2 to 7.4. NACA RM A52B13, 1952.
29. Van Dyke, Milton D.: Practical Calculation of Second-Order Supersonic Flow Past Non-Lifting Bodies of Revolution. NACA TN 2744, 1952.
30. Perkins, Edward W., and Jorgensen, Leland H.: Investigation of the Drag of Various Axially Symmetric Nose Shapes of Fineness Ratio 3 for Mach Numbers From 1.24 to 3.67. NACA RM A52H28, 1952.
31. Eggers, A. J., Resnikoff, Meyer M., and Dennis, David H.: Bodies of Revolution Having Minimum Drag at High Supersonic Airspeeds. NACA Rep. 1306, 1957. (Supersedes NACA TN 3666.)
32. Jack, John R.: Theoretical Pressure Distributions and Wave Drags for Conical Boattails. NACA TN 2972, 1953.

APPENDIX

BASIC DATA FOR CONFIGURATIONS 1 TO 177

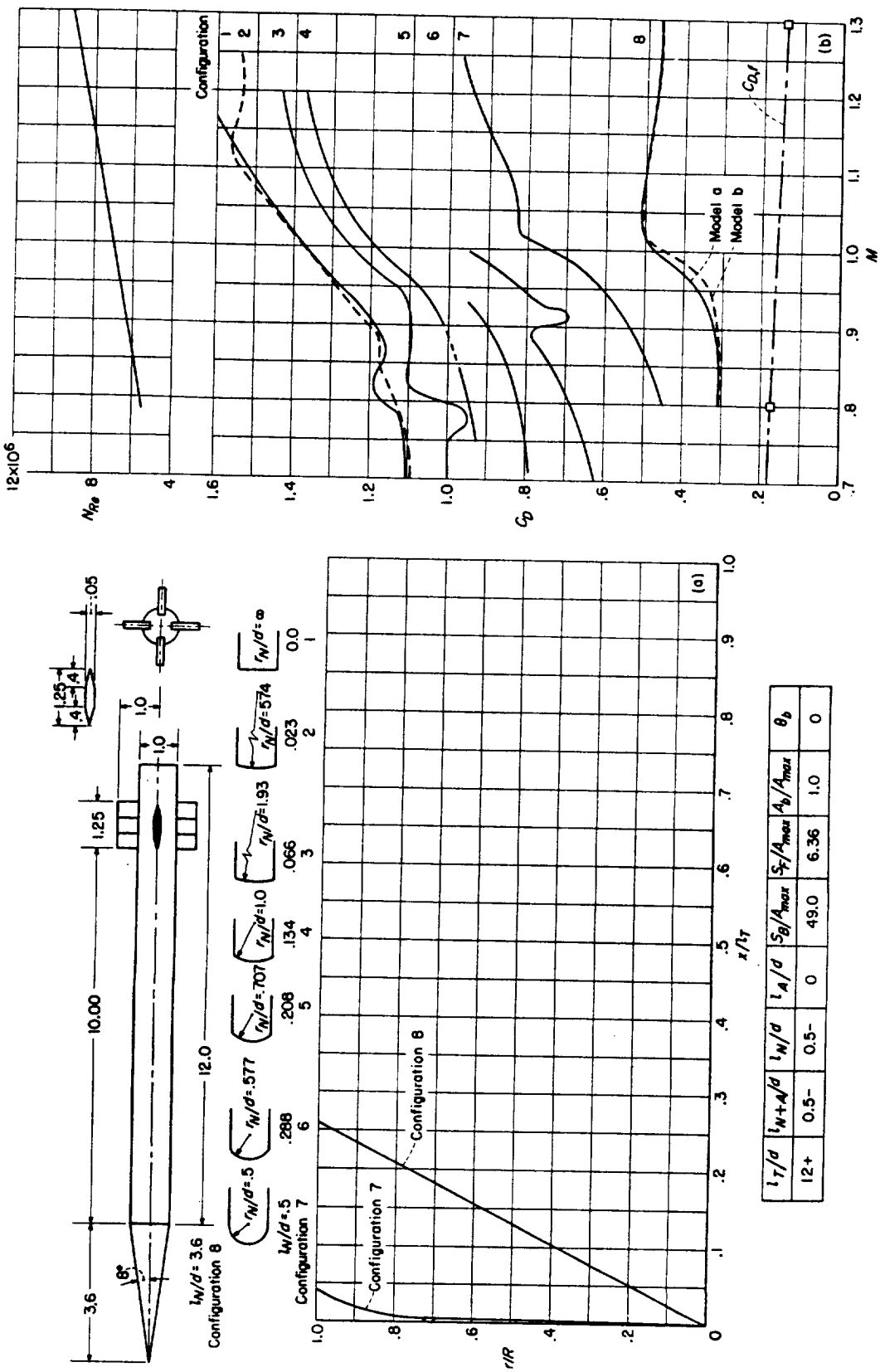

l_T/d	l_{N+A}/d	l_N/d	l_A/d	S_B/A_{max}	S_T/A_{max}	A_b/A_{max}	θ_b
12+	0.5-	0.5-	0	49.0	6.36	1.0	0

(a) Body shape. (Dimensions given are in inches.) (b) N_R, and C_D curves.

CONFIGURATIONS 1 to 8; helium-gun tests. (The abrupt drag variations at subsonic speeds are undoubtedly somewhat distorted by the data-reduction process; however, they are real as evidenced by similar phenomena noted in reference 18 (pp. 200 and 210).)

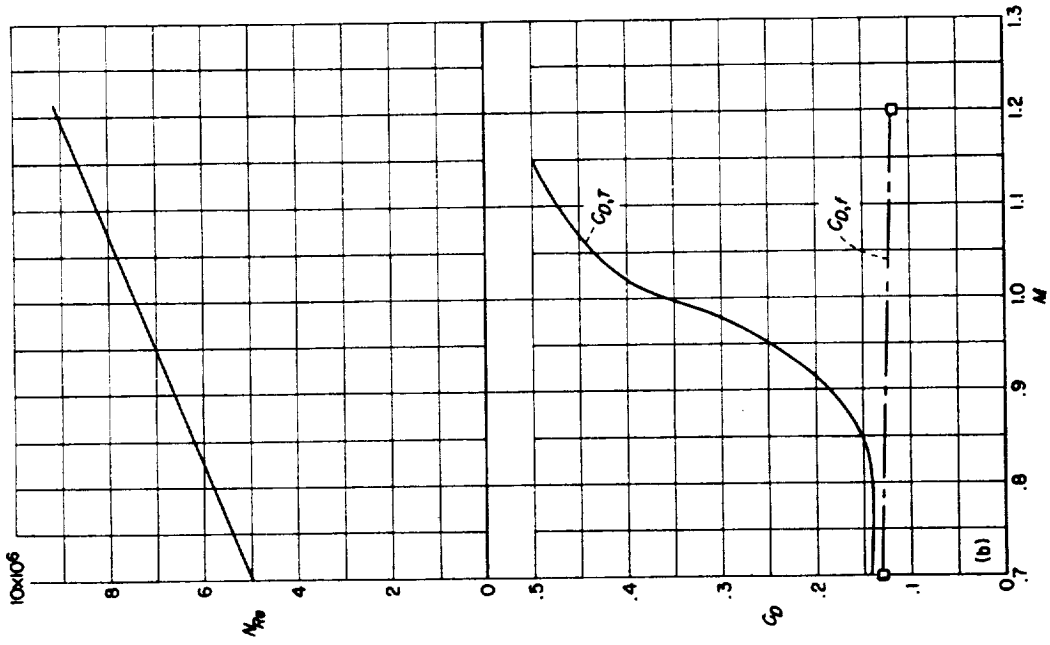

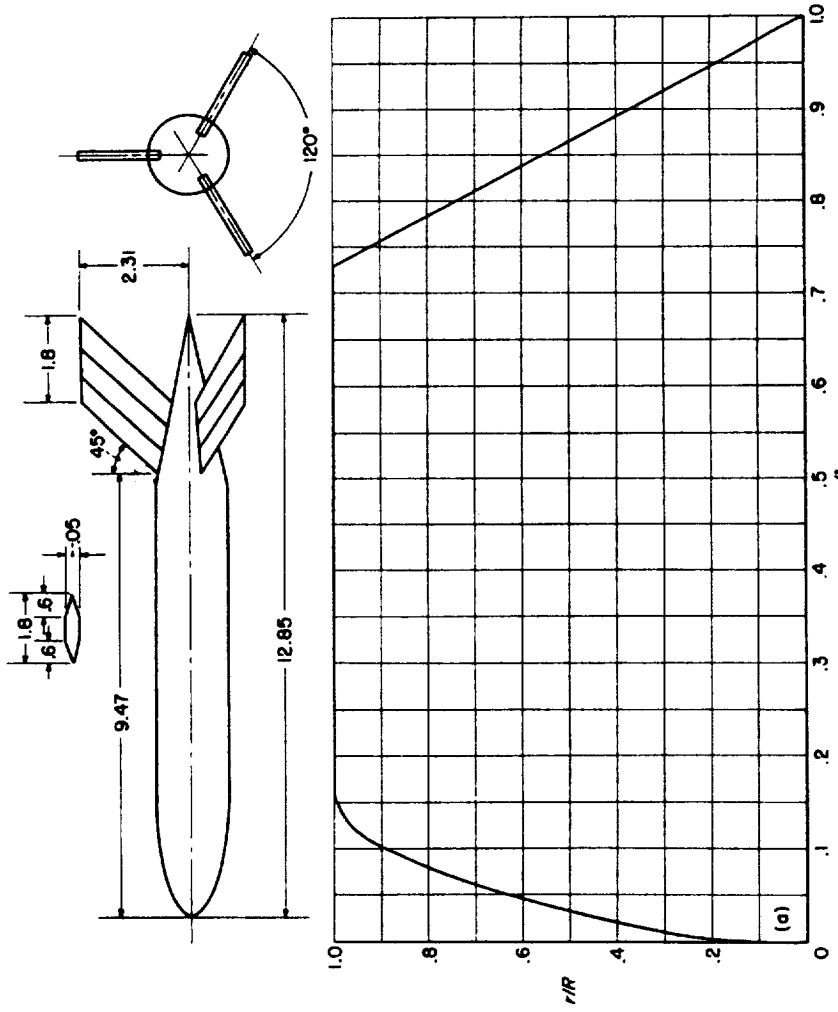

l_T/d	l_{N+A}/d	l_N/d	l_A/d	S_B/A_{max}	S_f/A_{max}	A_b/A_{max}	θ_b
8.57	3.71	1.38	2.33	28.30	11.0	0	12.2°

(a) Body shape. (Dimensions given are in inches.) (b) N_{R_θ} and C_D curves.

CONFIGURATION 9; helium-gun test.

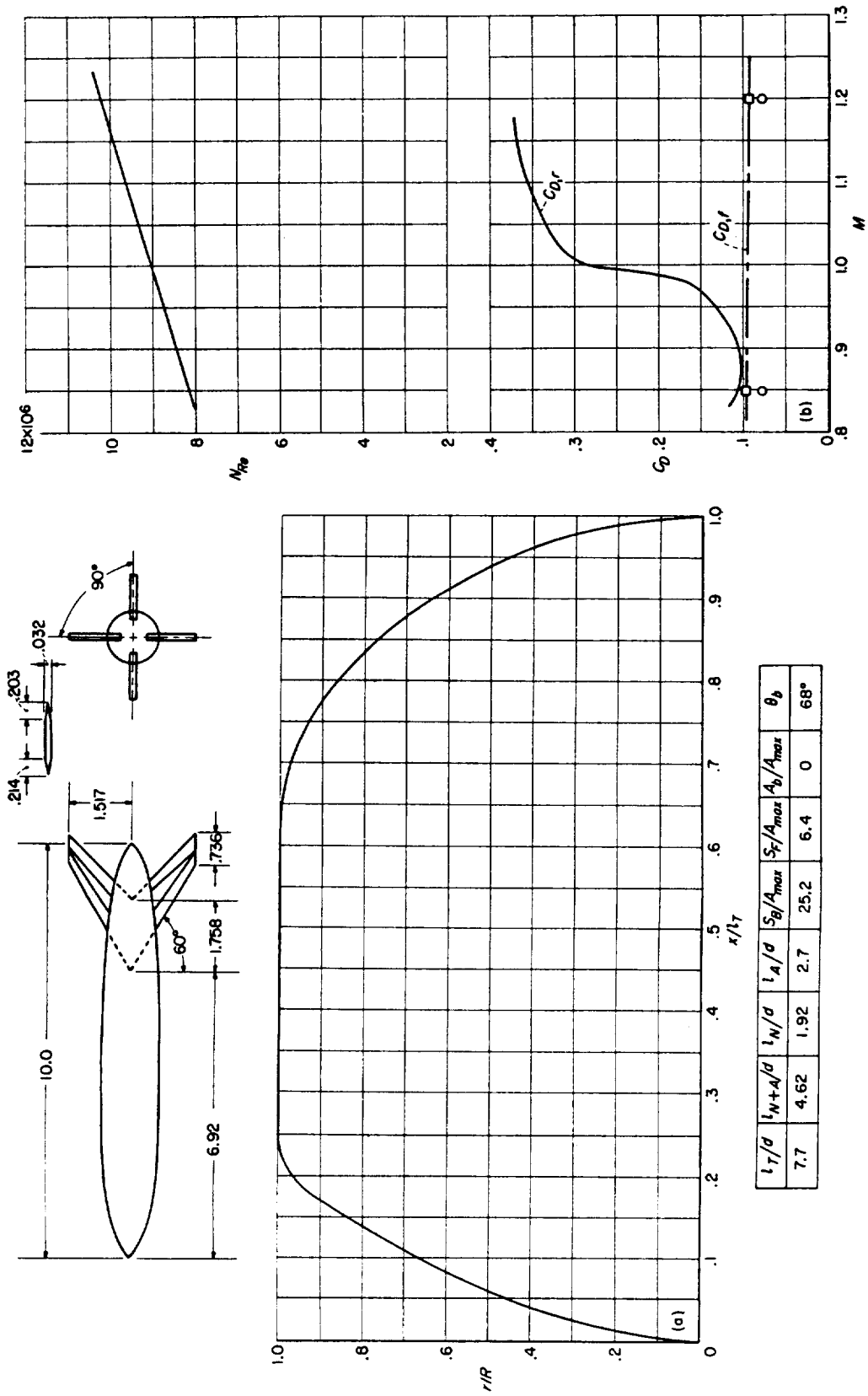

l_T/d	l_{N+A}/d	l_N/d	l_A/d	S_B/A_{max}	S_F/A_{max}	A_b/A_{max}	θ_b
7.7	4.62	1.92	2.7	25.2	6.4	0	68°

(a) Body shape. (Dimensions given are in inches.) (b) N_R, and C_D curves.

CONFIGURATION 10; helium-gun test. (Nondimensional ordinates same as configuration 37.)

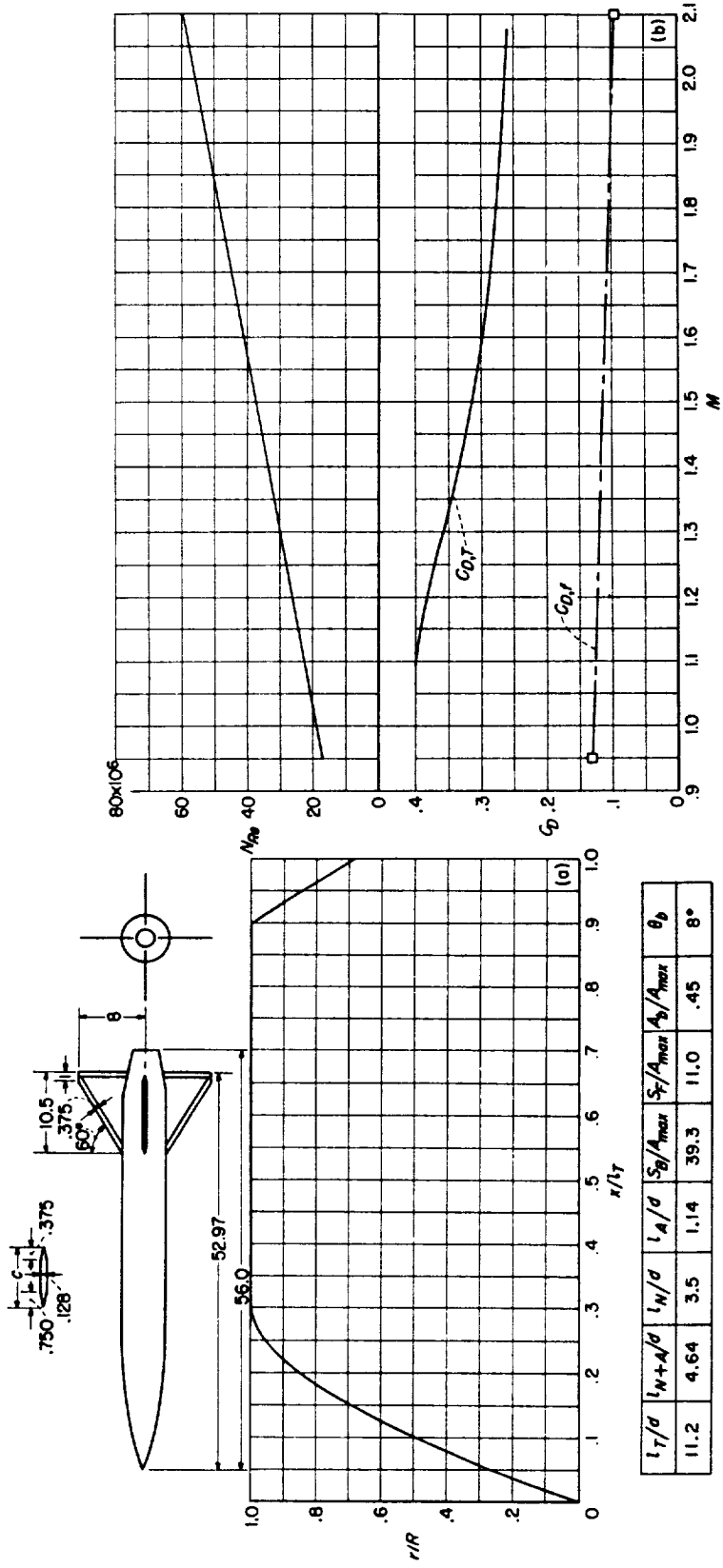

l_T/d	l_{N+A}/d	l_N/d	l_A/d	S_B/A_{max}	S_F/A_{max}	A_b/A_{max}	θ_b
11.2	4.64	3.5	1.14	39.3	11.0	.45	8°

(a) Body shape. (Dimensions given are in inches.) (b) N_{R_∞} and C_D curves.

CONFIGURATION 11; rocket test.

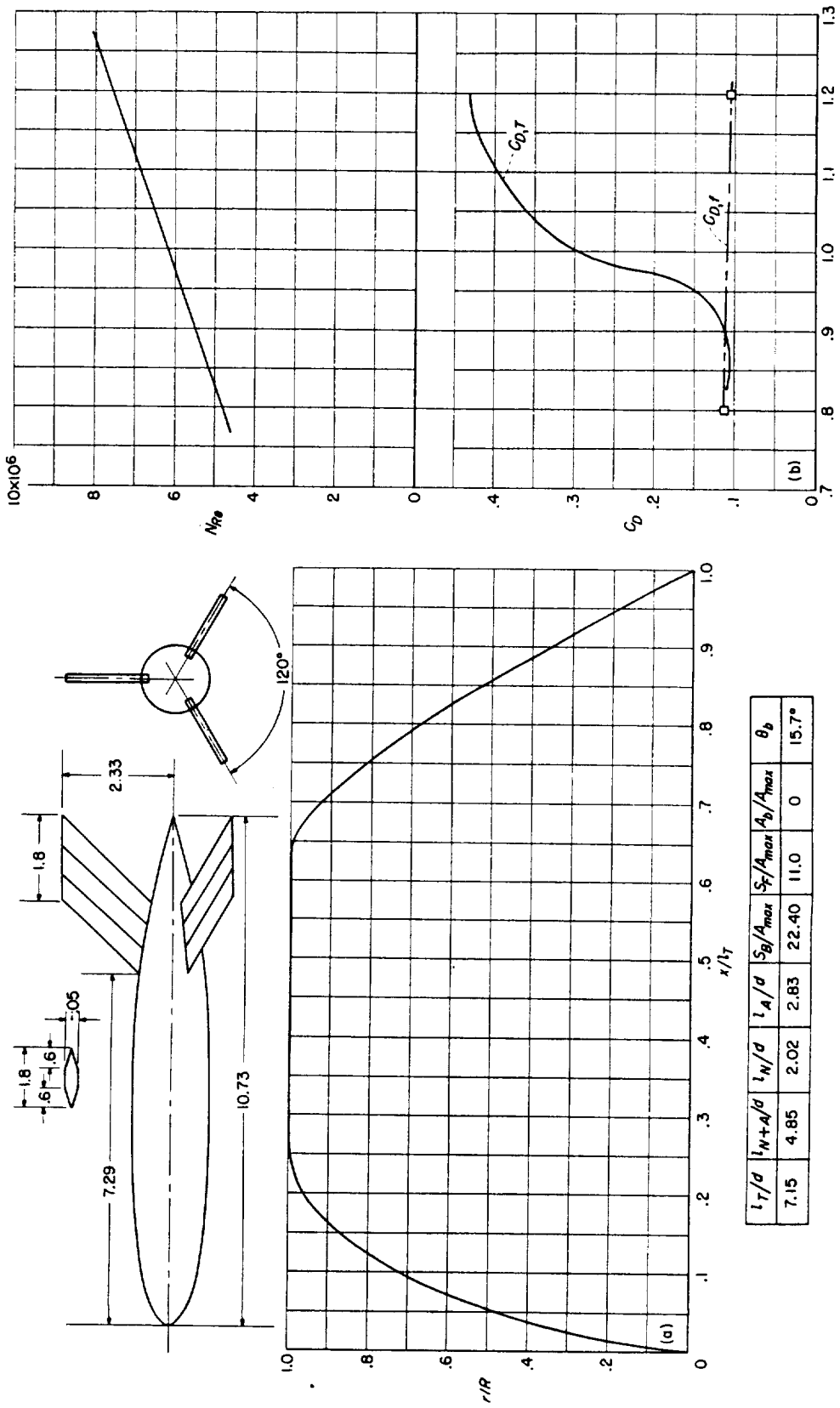

l_T/d	l_{N+A}/d	l_N/d	l_A/d	S_B/A_{max}	S_F/A_{max}	A_b/A_{max}	θ_b
7.15	4.85	2.02	2.83	22.40	11.0	0	15.7°

(a) Body shape. (Dimensions given are in inches.) (b) N_{Re} and C_D curves.

CONFIGURATION 12; helium-gun test.

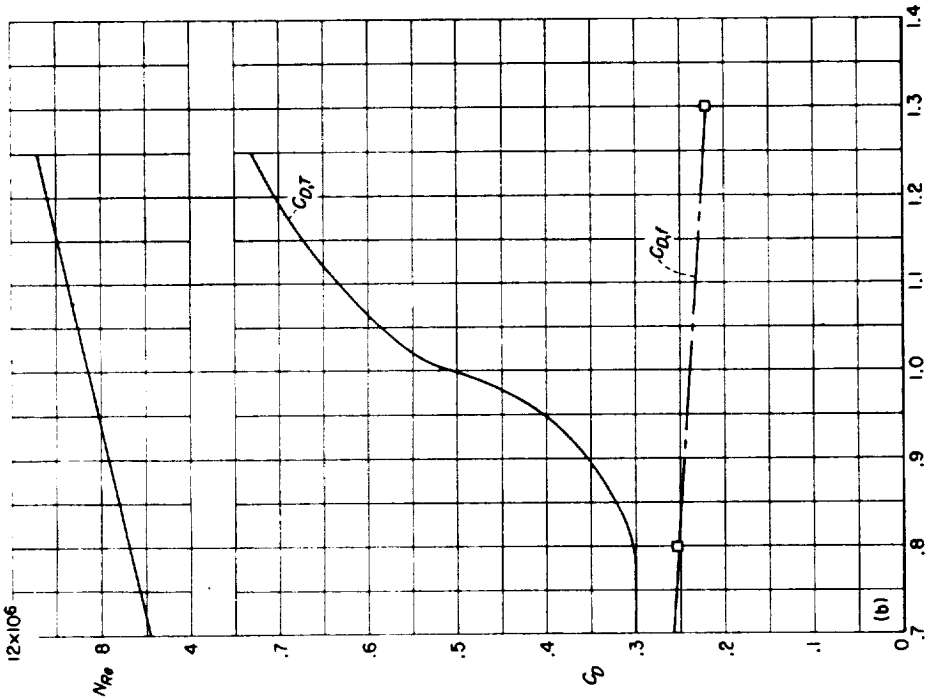

(b) N_R, and C_D curves.

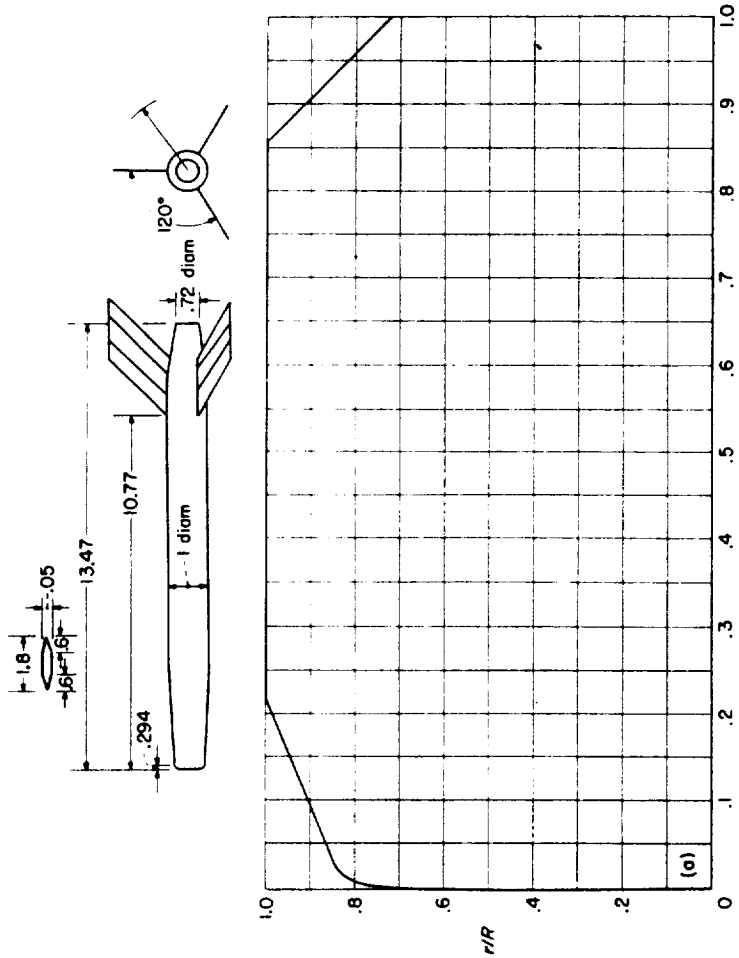

l_T/σ	l_{N+A}/σ	l_N/σ	l_A/σ	S_B/A_{max}	S_F/A_{max}	A_b/A_{max}	θ_b
13.47	4.98	2.98	2.00	51.5	24.6	.52	4.02°

(a) Body shape. (Dimensions given are in inches.)

CONFIGURATION 13; helium-gun test.

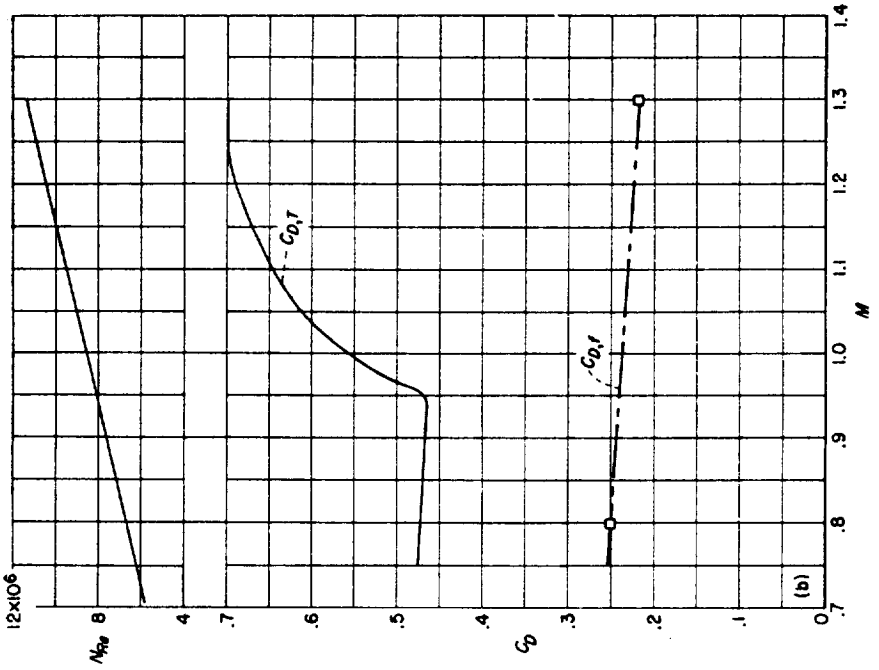

(b) N_{Re} and C_D curves.

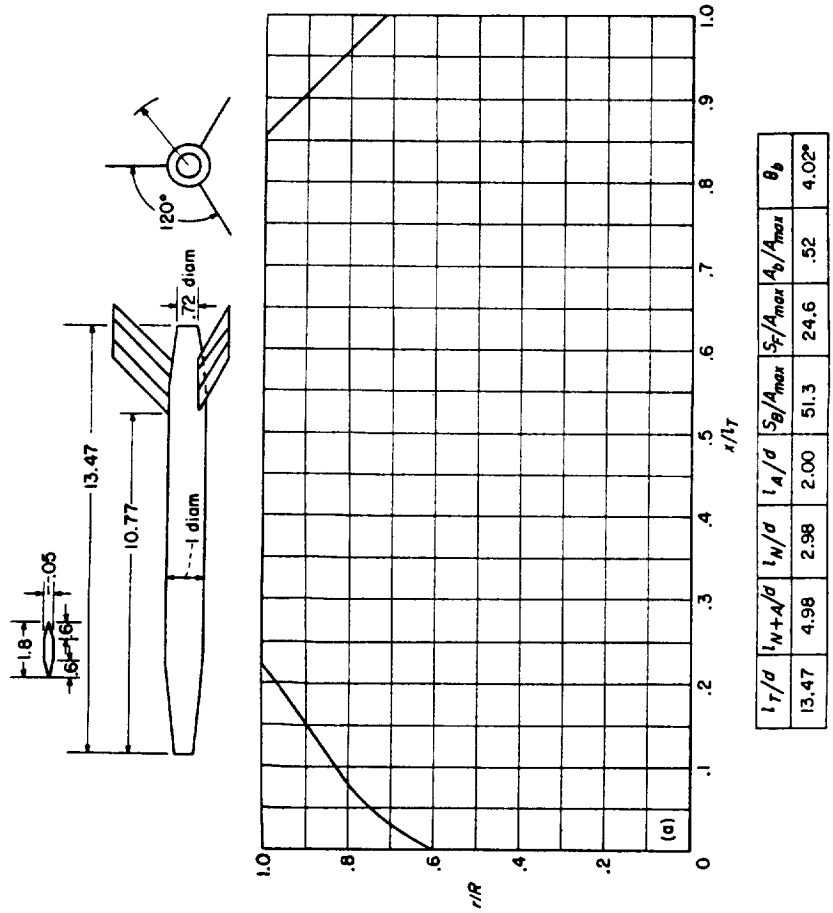

l_T/d	l_{N+A}/d	l_N/d	l_A/d	S_B/A_{max}	S_T/A_{max}	A_b/A_{max}	θ_b
13.47	4.98	2.98	2.00	51.3	24.6	.52	4.02°

(a) Body shape. (Dimensions given are in inches.)

CONFIGURATION 14; helium-gun test.

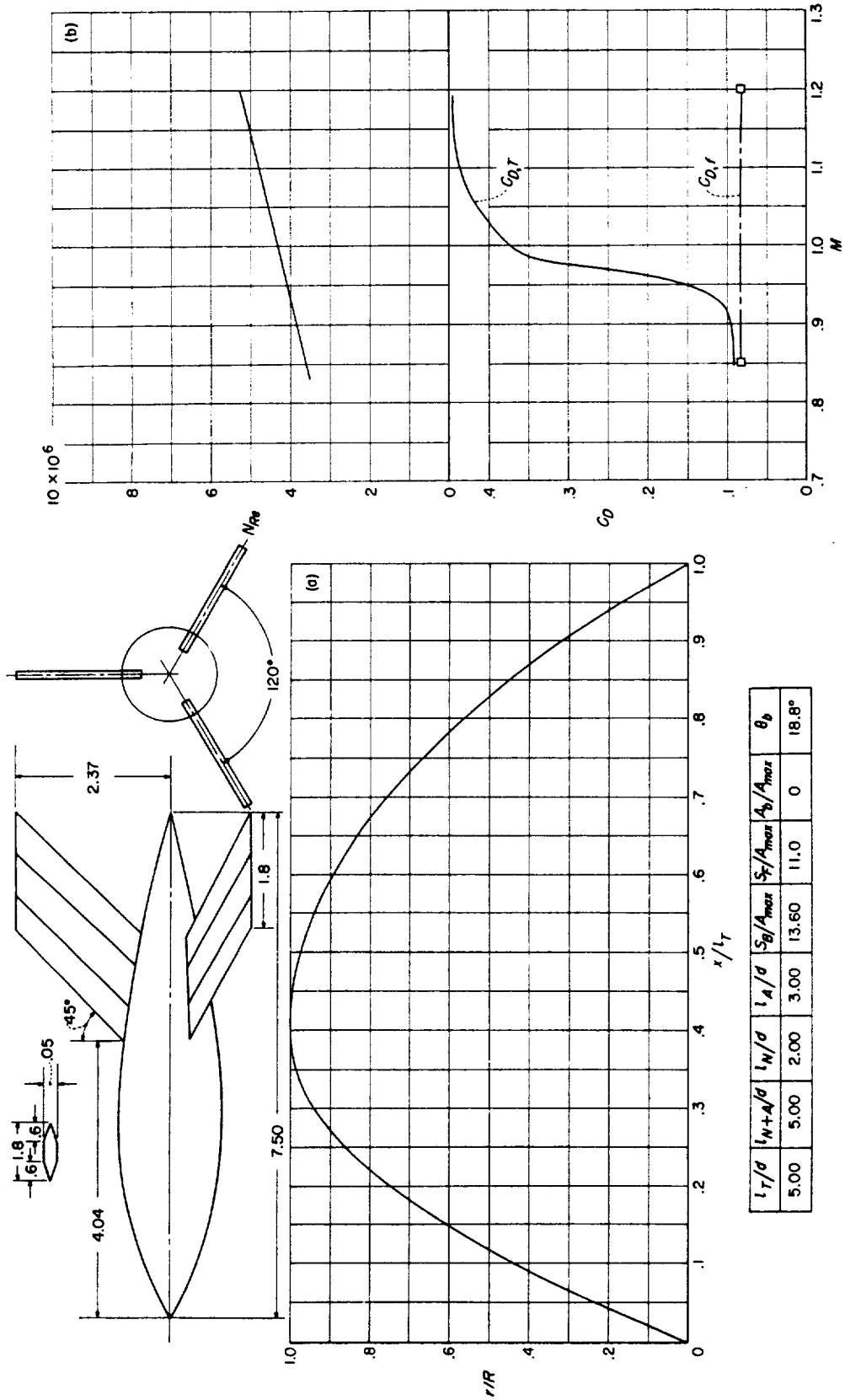

l_T/d	l_{N+A}/d	l_N/d	l_A/d	S_B/A_{max}	S_f/A_{max}	A_b/A_{max}	θ_b
5.00	5.00	2.00	3.00	13.60	11.0	0	18.8°

(a) Body shape. (Dimensions given are in inches.) (b) N_{R_θ} and C_D curves.

CONFIGURATION 15; helium-gun test.

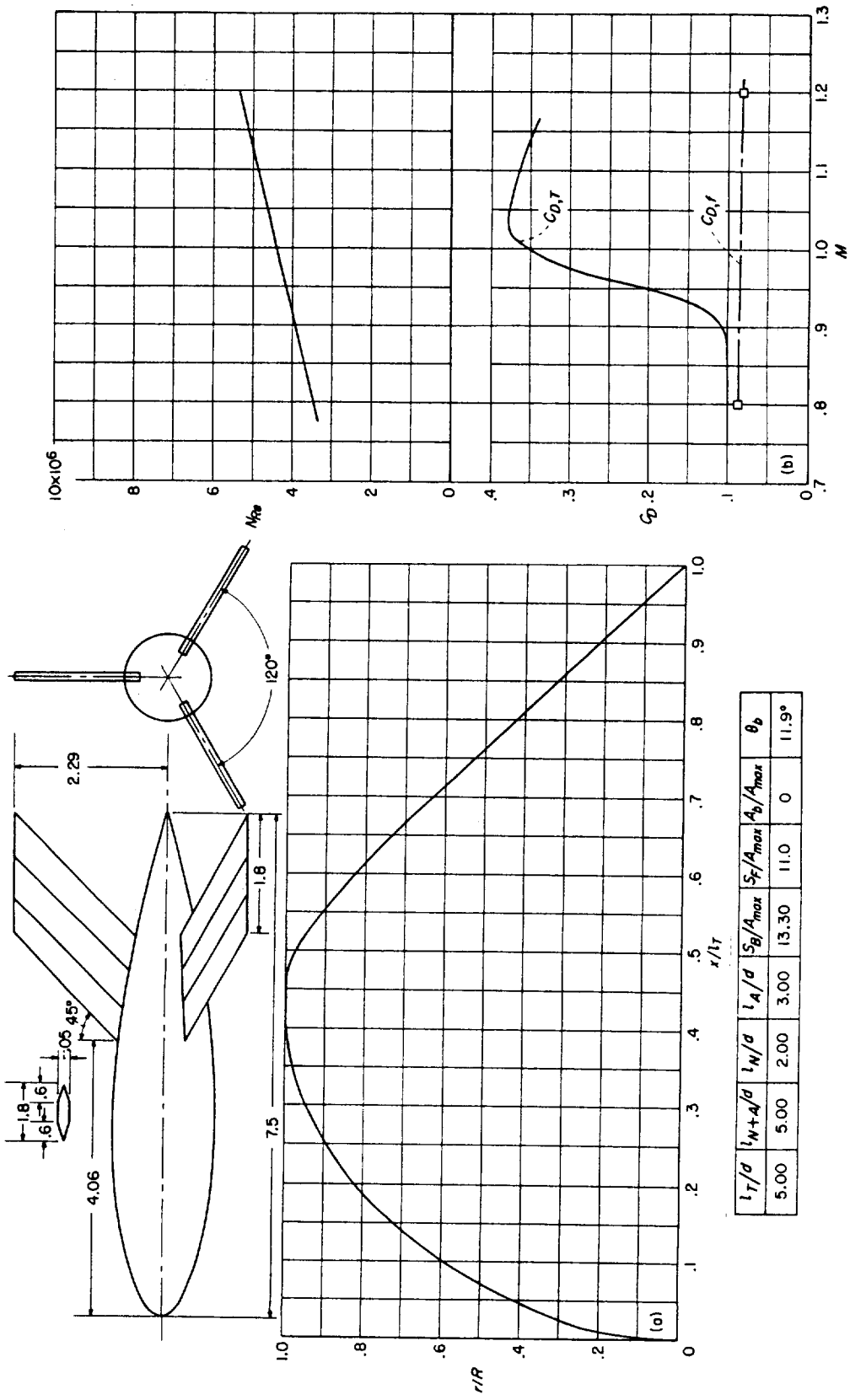

l_T/d	l_{N+A}/d	l_N/d	l_A/d	S_B/A_{max}	S_F/A_{max}	A_b/A_{max}	θ_b
5.00	5.00	2.00	3.00	13.30	11.0	0	11.9°

(a) Body shape. (Dimensions given are in inches.) (b) N_{Re} and C_D curves.

CONFIGURATION 16; helium-gun test.

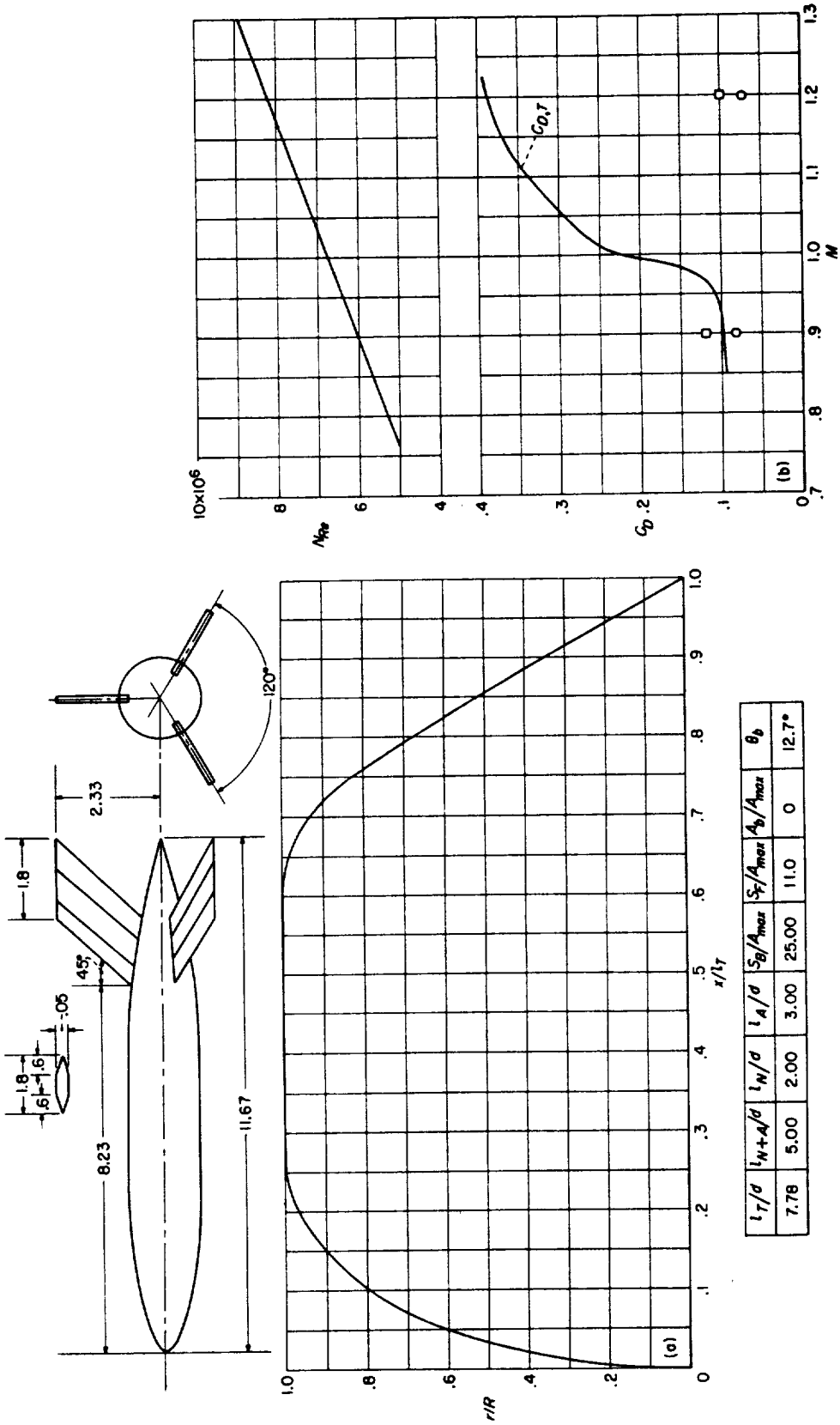

l_T/d	l_{N+A}/d	l_N/d	l_A/d	S_B/A_{max}	S_F/A_{max}	A_b/A_{max}	θ_b
7.78	5.00	2.00	3.00	25.00	11.0	0	12.7°

(a) Body shape. (Dimensions given are in inches.) (b) N_{Re} and C_D curves.

CONFIGURATION 17; helium-gun test.

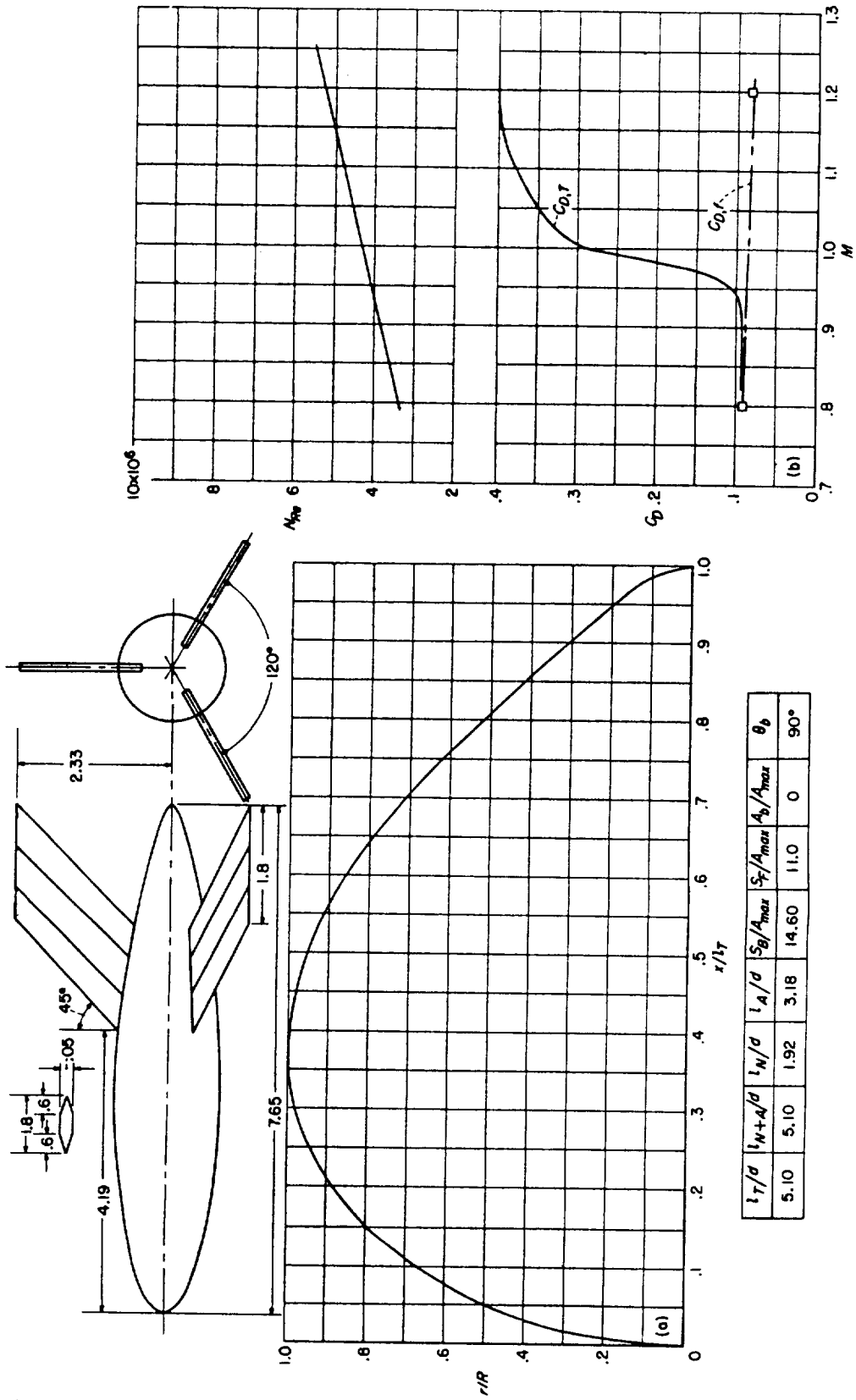

l_T/d	l_{N+A}/d	l_N/d	l_A/d	S_B/A_{max}	S_F/A_{max}	A_b/A_{max}	θ_b
5.10	5.10	1.92	3.18	14.60	11.0	0	90°

(a) Body shape. (Dimensions given are in inches.) (b) N_{R_e} and C_D curves.

CONFIGURATION 18; helium-gun test.

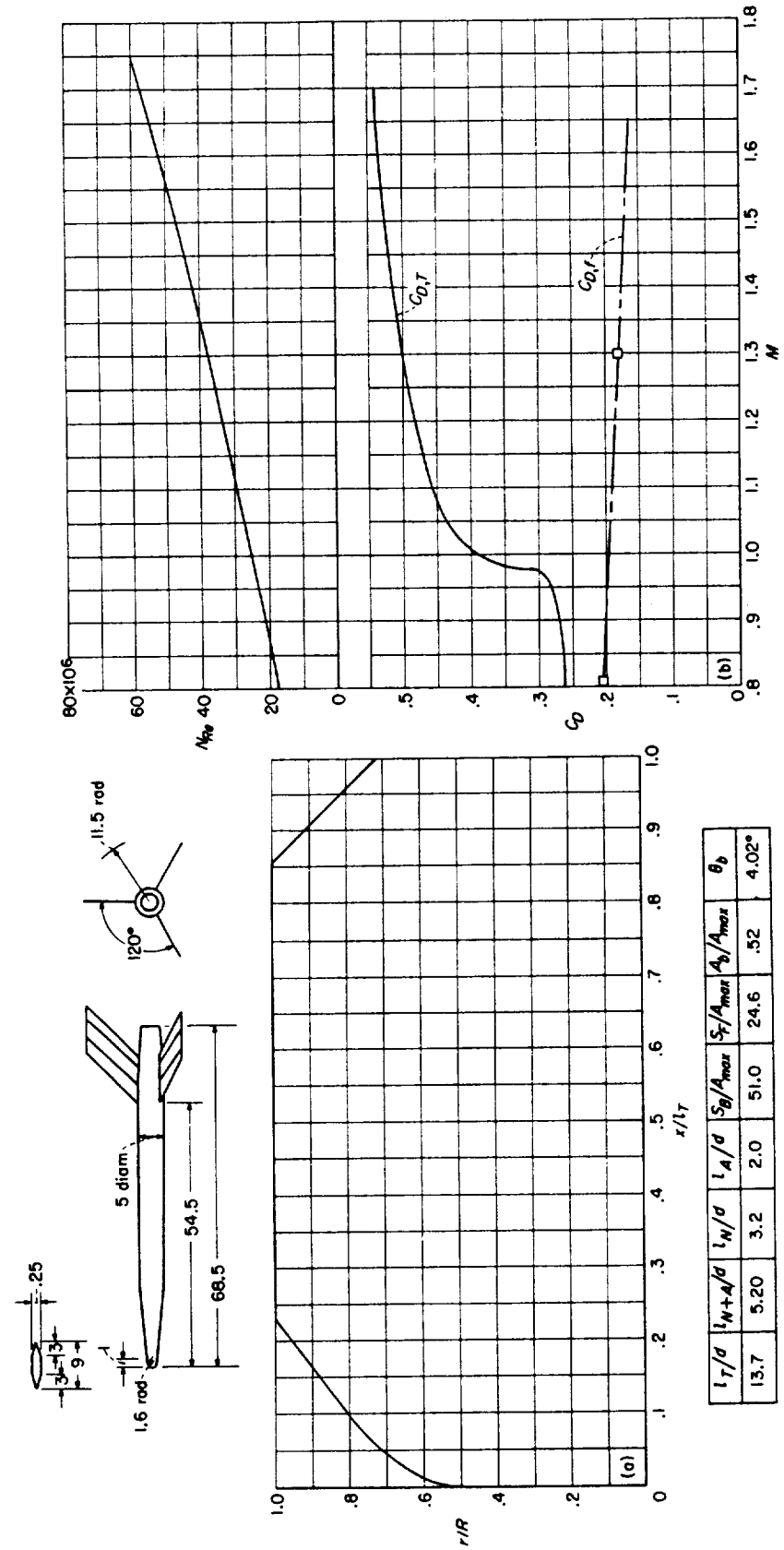

l_T/d	l_{N+A}/d	l_N/d	l_A/d	S_B/A_{max}	S_F/A_{max}	A_b/A_{max}	θ_b
13.7	5.20	3.2	2.0	51.0	24.6	.52	4.02°

(a) Body shape. (Dimensions given are in inches.) (b) N_{Re} and C_D curves.

CONFIGURATION 19 (5 times scale of configuration 20); rocket test.

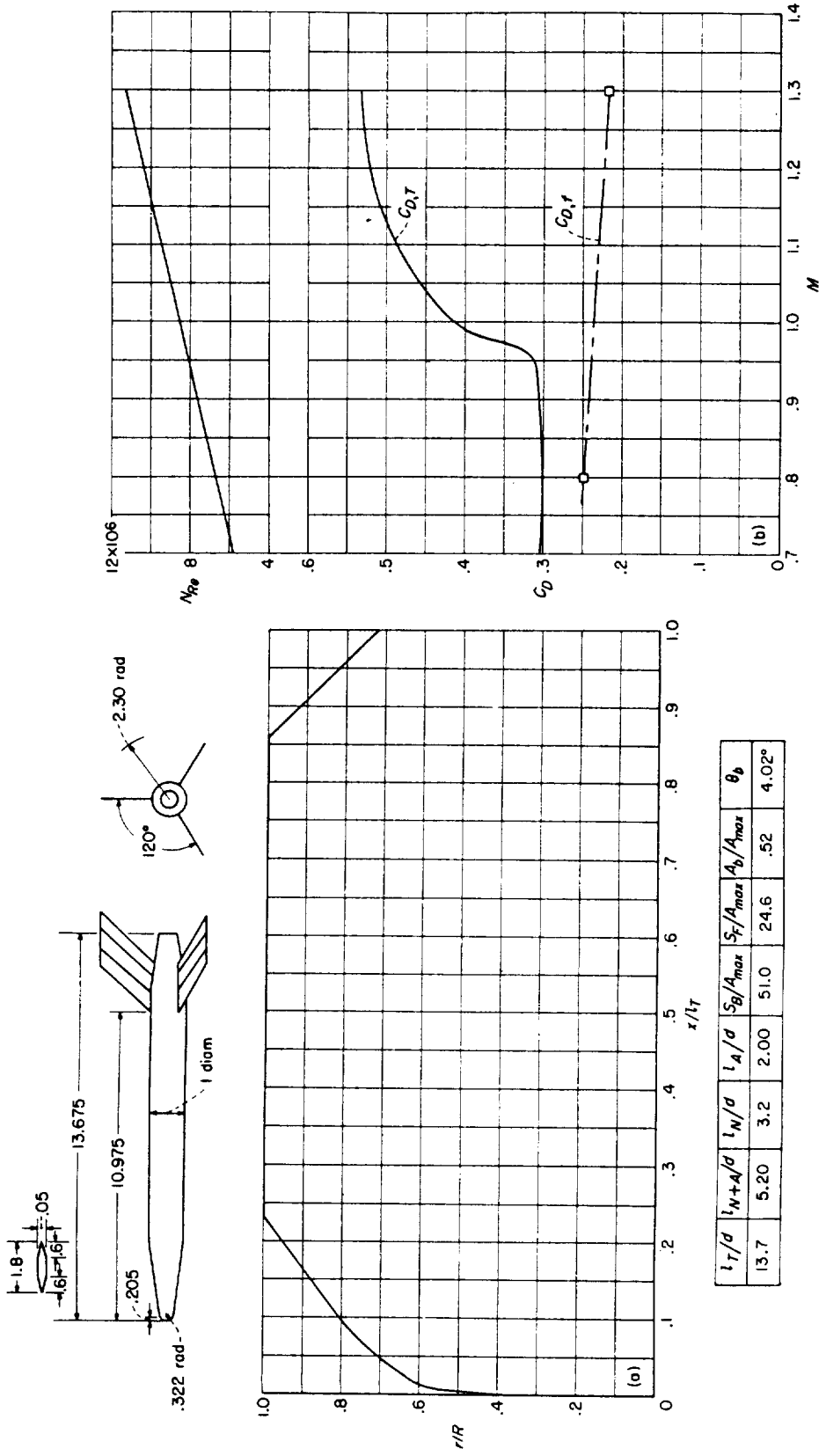

l_T/d	l_{N+A}/d	l_N/d	l_A/d	S_B/A_{max}	S_F/A_{max}	A_b/A_{max}	θ_b
13.7	5.20	3.2	2.00	51.0	24.6	.52	4.02°

(a) Body shape. (Dimensions given are in inches.) (b) N_{Re} and C_D curves.

CONFIGURATION 20 $\left(\frac{1}{5}\text{ scale of configuration 19}\right)$; helium-gun test.

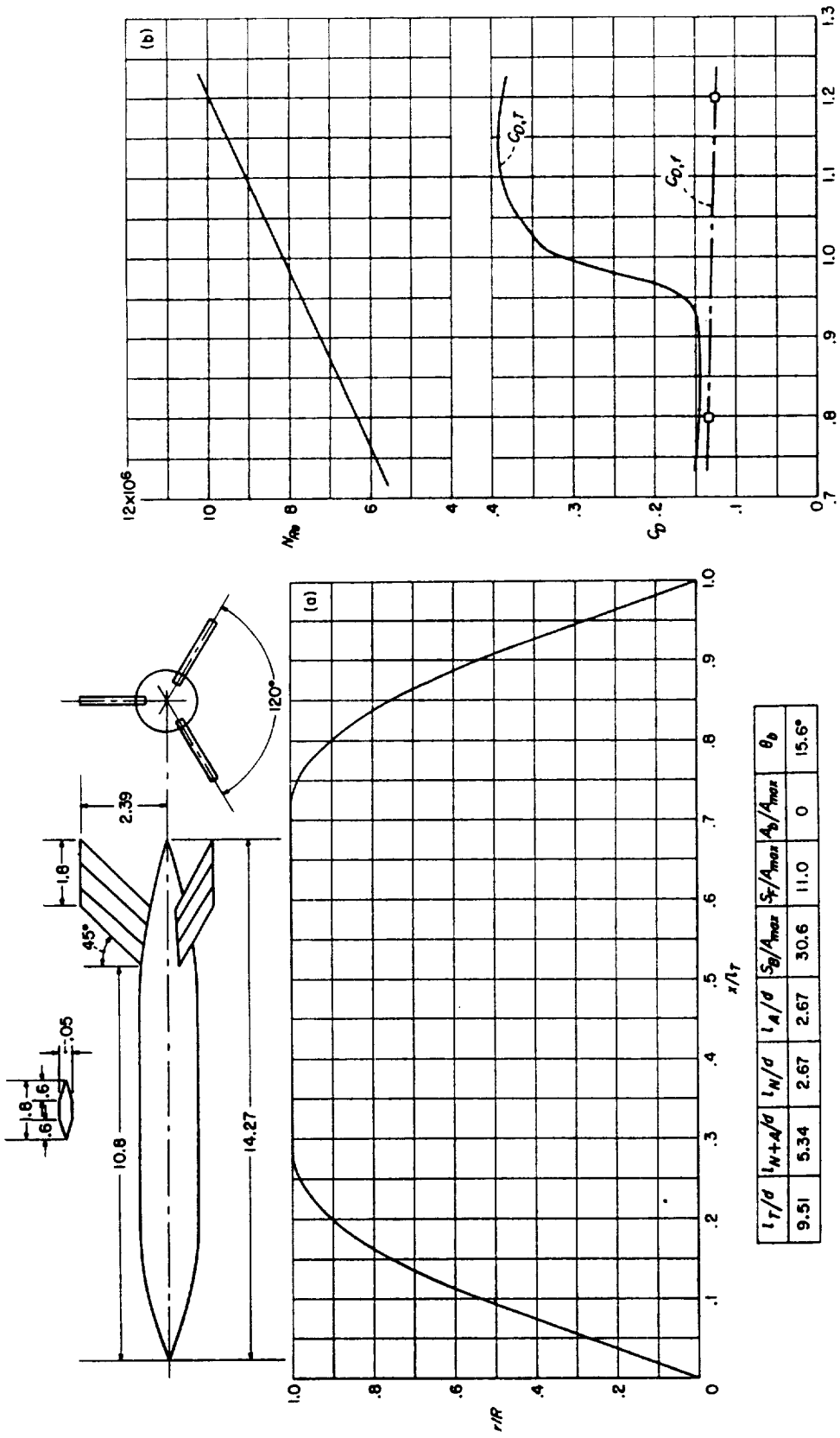

l_T/d	l_{N+A}/d	l_N/d	l_A/d	S_B/A_{max}	S_F/A_{max}	A_b/A_{max}	θ_b
9.51	5.34	2.67	2.67	30.6	11.0	0	15.6°

(a) Body shape. (Dimensions given are in inches.) (b) N_{R_e} and C_D curves.

CONFIGURATION 21; helium-gun test.

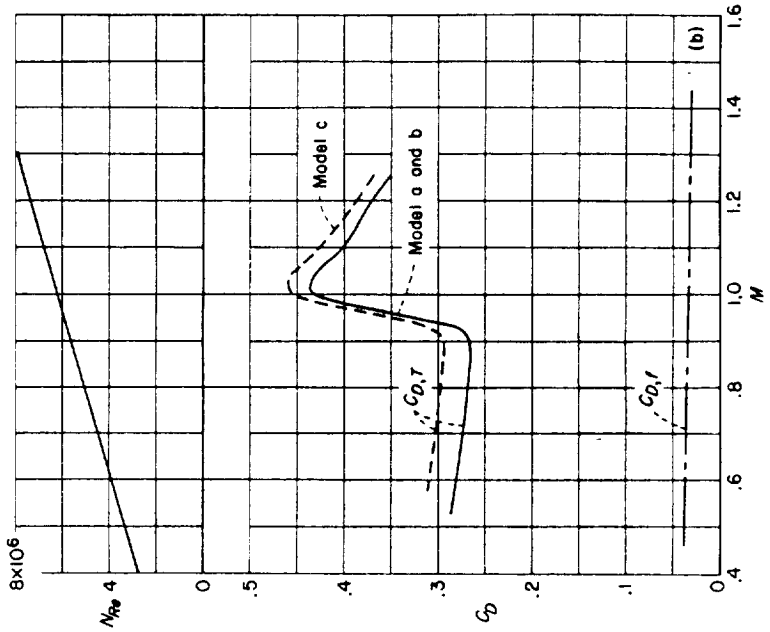

(b) N_{Re} and C_D curves.

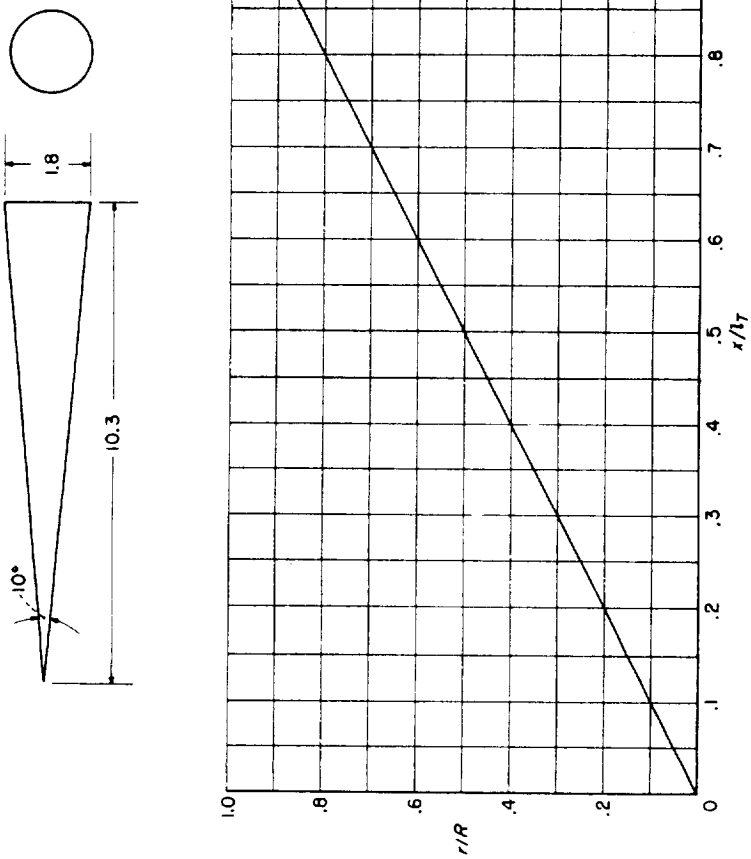

l_T/d	l_{N+A}/d	l_N/d	l_A/d	S_B/A_{max}	S_F/A_{max}	A_b/A_{max}	θ_b
5.7	5.7	5.7		11.40	0	1.0	-5.0°

(a) Body shape. (Dimensions given are in inches.)

CONFIGURATION 22; helium-gun test.

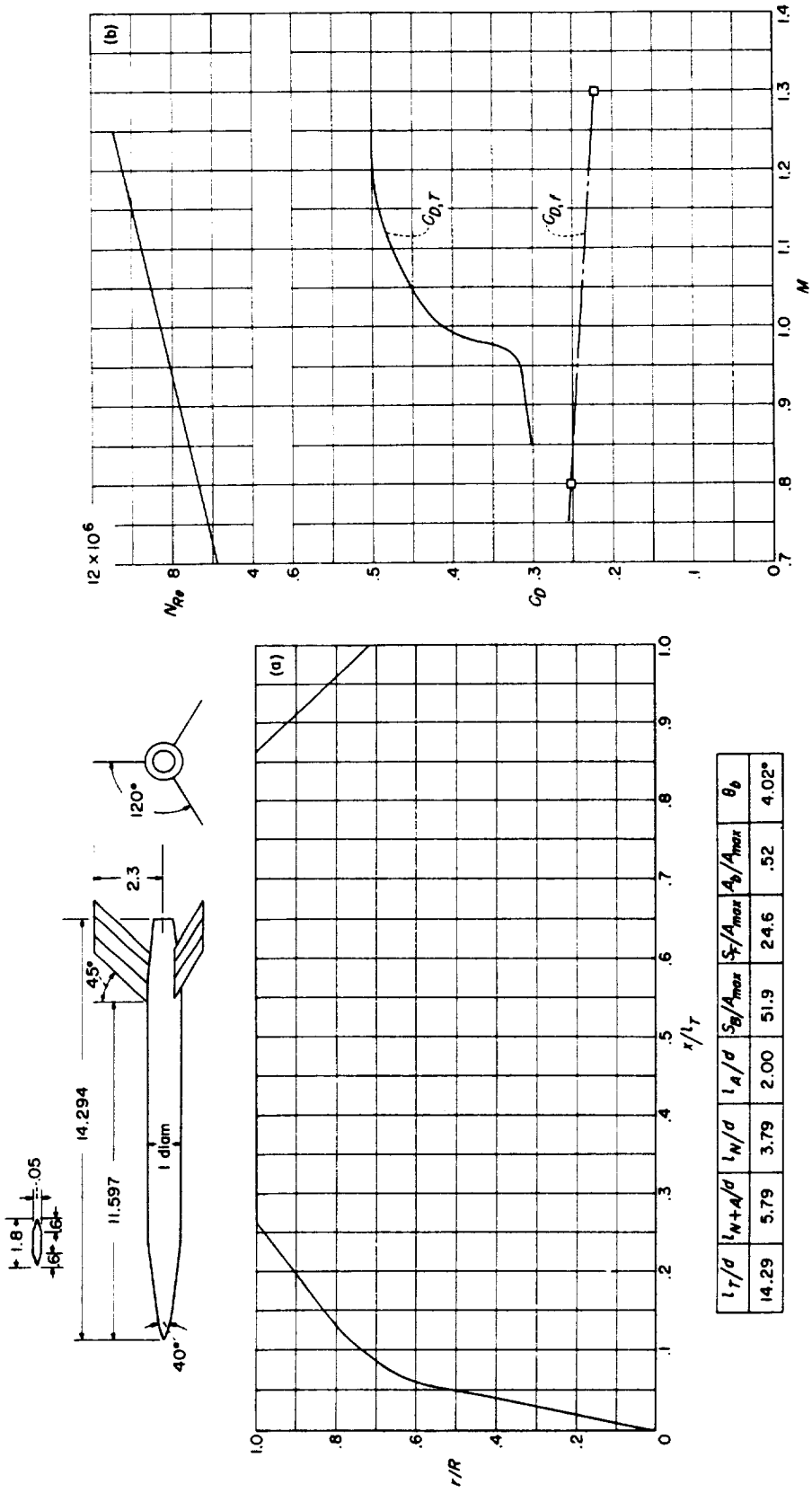

l_T/d	l_{N+A}/d	l_N/d	l_A/d	S_B/A_{max}	S_F/A_{max}	A_b/A_{max}	θ_b
14.29	5.79	3.79	2.00	51.9	24.6	.52	4.02°

(a) Body shape. (Dimensions given are in inches.) (b) N_{Re} and C_D curves.

CONFIGURATION 23; helium-gun test.

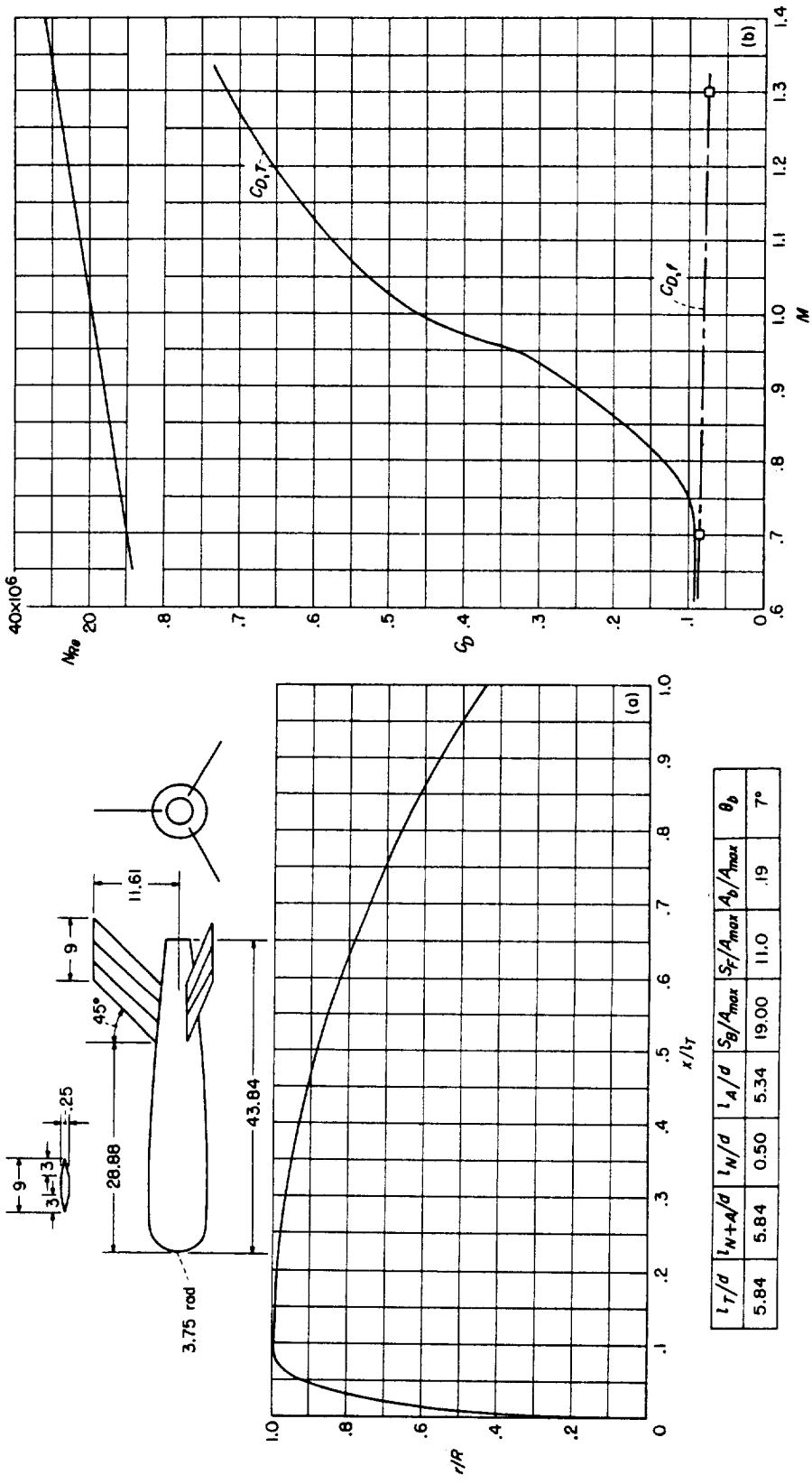

l_T/d	l_{N+A}/d	l_N/d	l_A/d	S_B/A_{max}	S_F/A_{max}	A_b/A_{max}	θ_b
5.84	5.84	0.50	5.34	19.00	11.0	.19	7°

(a) Body shape. (Dimensions given are in inches.) (b) N_{Re} and C_D curves.

CONFIGURATION 24 (hemispherical nose and parabolic afterbody); rocket test.

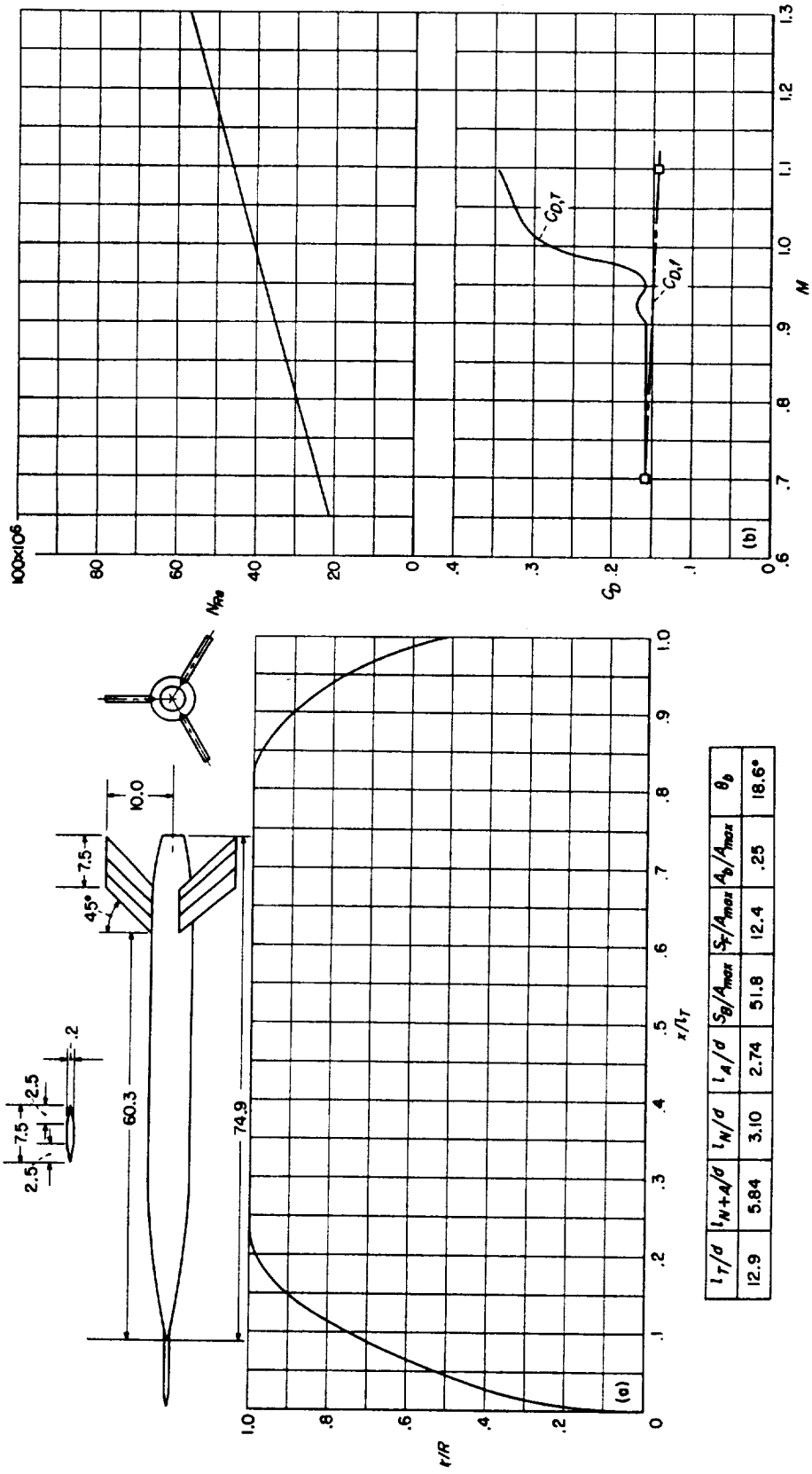

l_T/d	l_{N+A}/d	l_N/d	l_A/d	S_B/A_{max}	S_F/A_{max}	A_b/A_{max}	θ_b
12.9	5.84	3.10	2.74	51.8	12.4	.25	18.6°

(a) Body shape. (Dimensions given are in inches.) (b) N_{Re} and C_D curves.

CONFIGURATION 25; rocket test. (Sting may have some effect on friction drag but hardly any on pressure drag.)

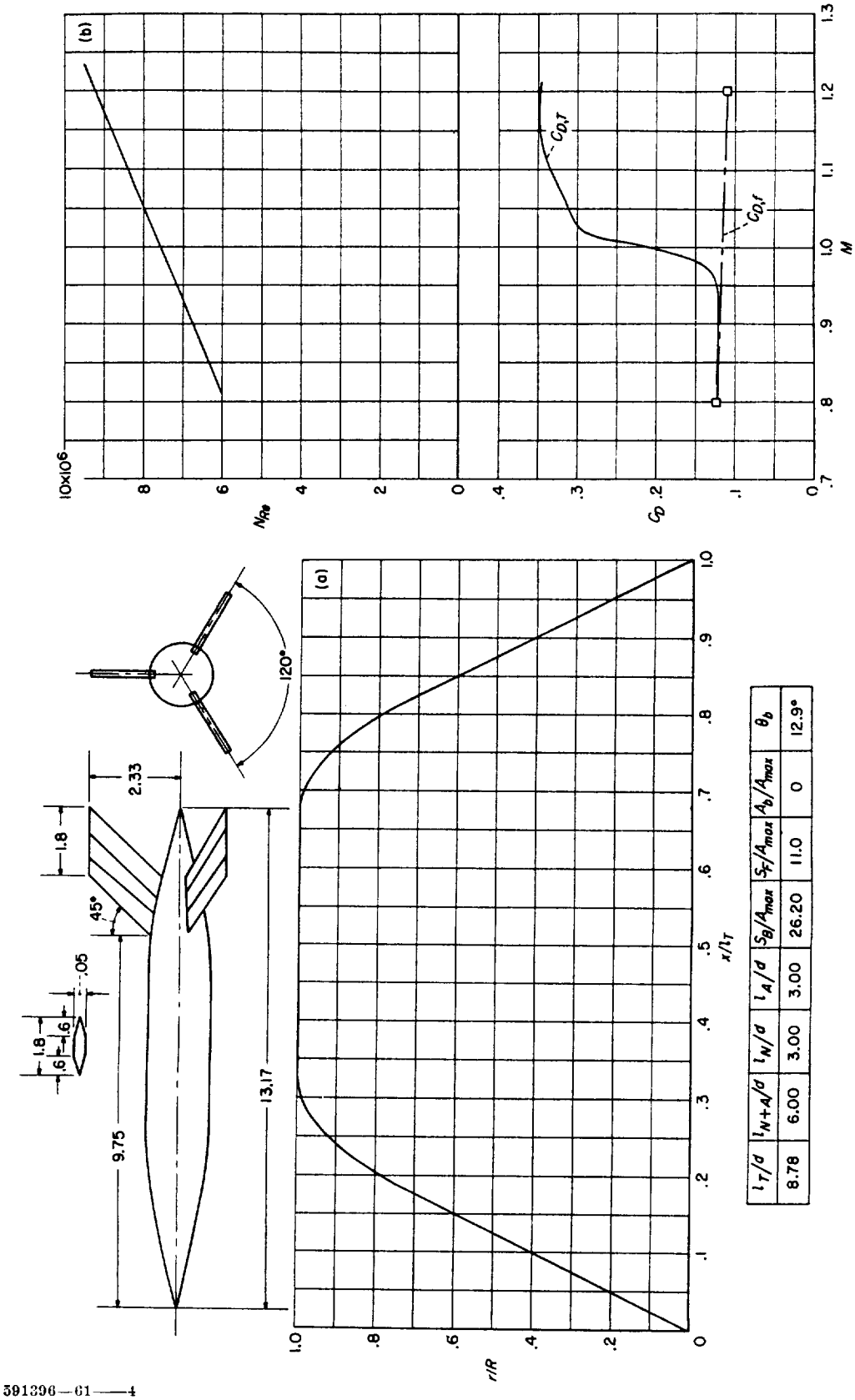

l_T/d	l_{N+A}/d	l_N/d	l_A/d	S_B/A_{max}	S_f/A_{max}	A_b/A_{max}	θ_b
8.78	6.00	3.00	3.00	26.20	11.0	0	12.9°

(a) Body shape. (Dimensions given are in inches.) (b) N_{Re} and C_D curves.

CONFIGURATION 26; helium-gun test.

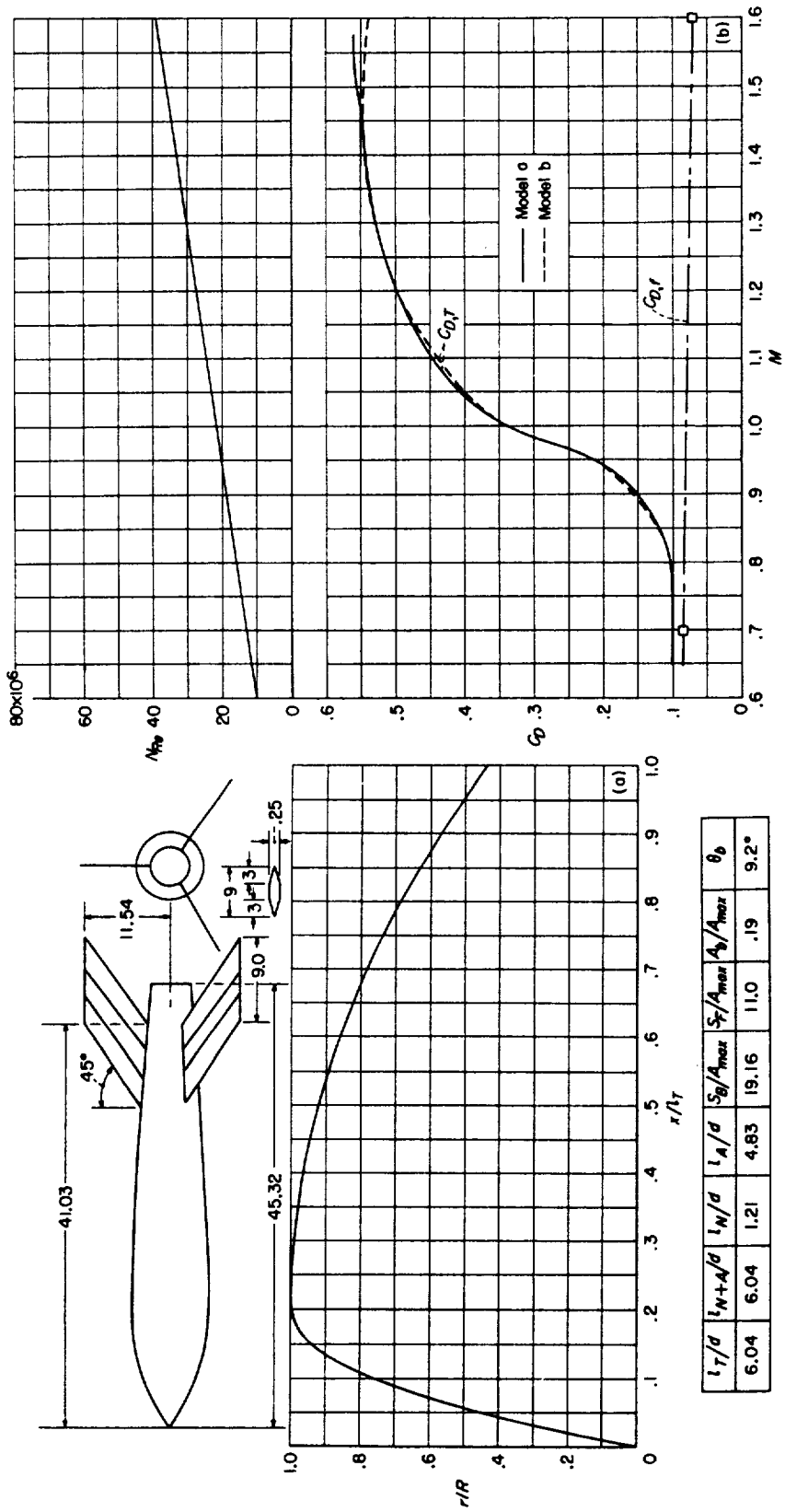

l_T/d	l_{N+A}/d	l_N/d	l_A/d	S_B/A_{max}	S_F/A_{max}	A_b/A_{max}	θ_b
6.04	6.04	1.21	4.83	19.16	11.0	.19	9.2°

(a) Body shape. (Dimensions given are in inches.) (b) N_{Re} and C_D curves.

CONFIGURATION 27 (parabolic nose and afterbody); rocket test.

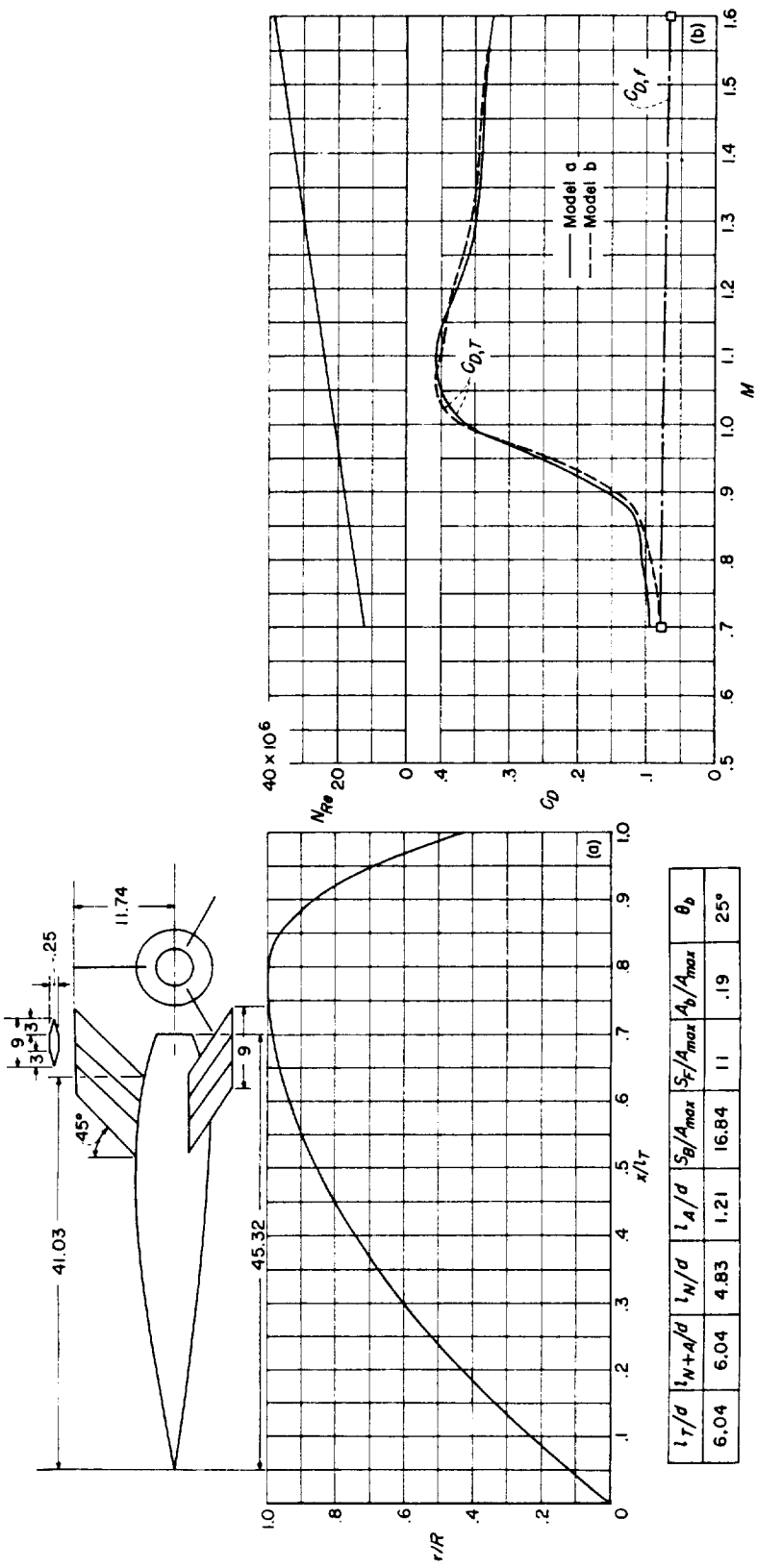

l_T/d	l_{N+A}/d	l_N/d	l_A/d	S_B/A_{max}	S_F/A_{max}	A_b/A_{max}	θ_b
6.04	6.04	4.83	1.21	16.84	11	.19	25°

(a) Body shape. (Dimensions given are in inches.) (b) N_{Re} and C_D curves.

CONFIGURATION 28 (parabolic nose and afterbody); rocket test.

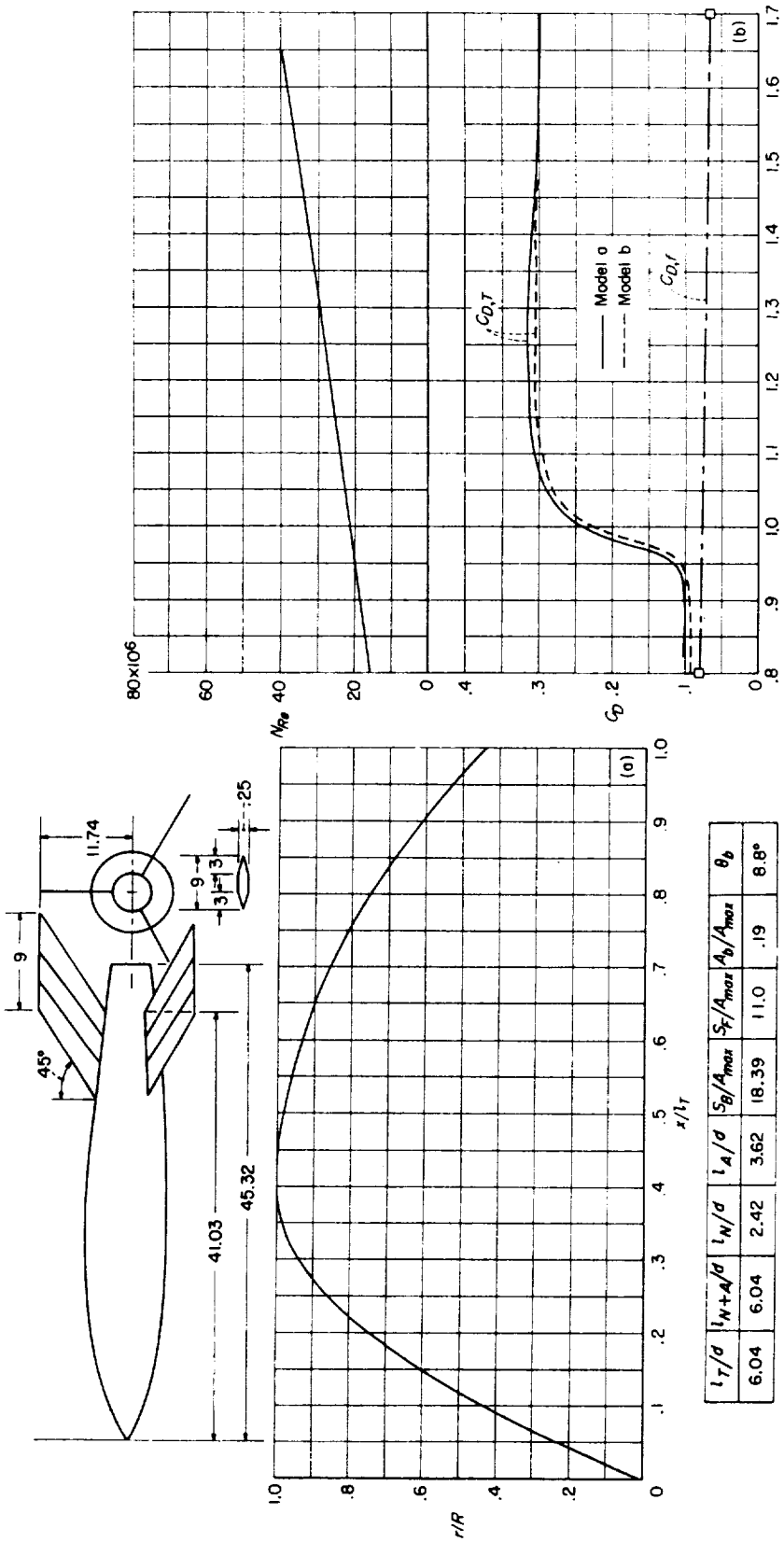

l_T/d	l_{N+A}/d	l_N/d	l_A/d	S_B/A_{max}	S_F/A_{max}	A_b/A_{max}	θ_b
6.04	6.04	2.42	3.62	18.39	11.0	.19	8.8°

(a) Body shape. (Dimensions given are in inches.) (b) N_{Re} and C_D curves.

CONFIGURATION 29 (parabolic nose and afterbody); rocket test.

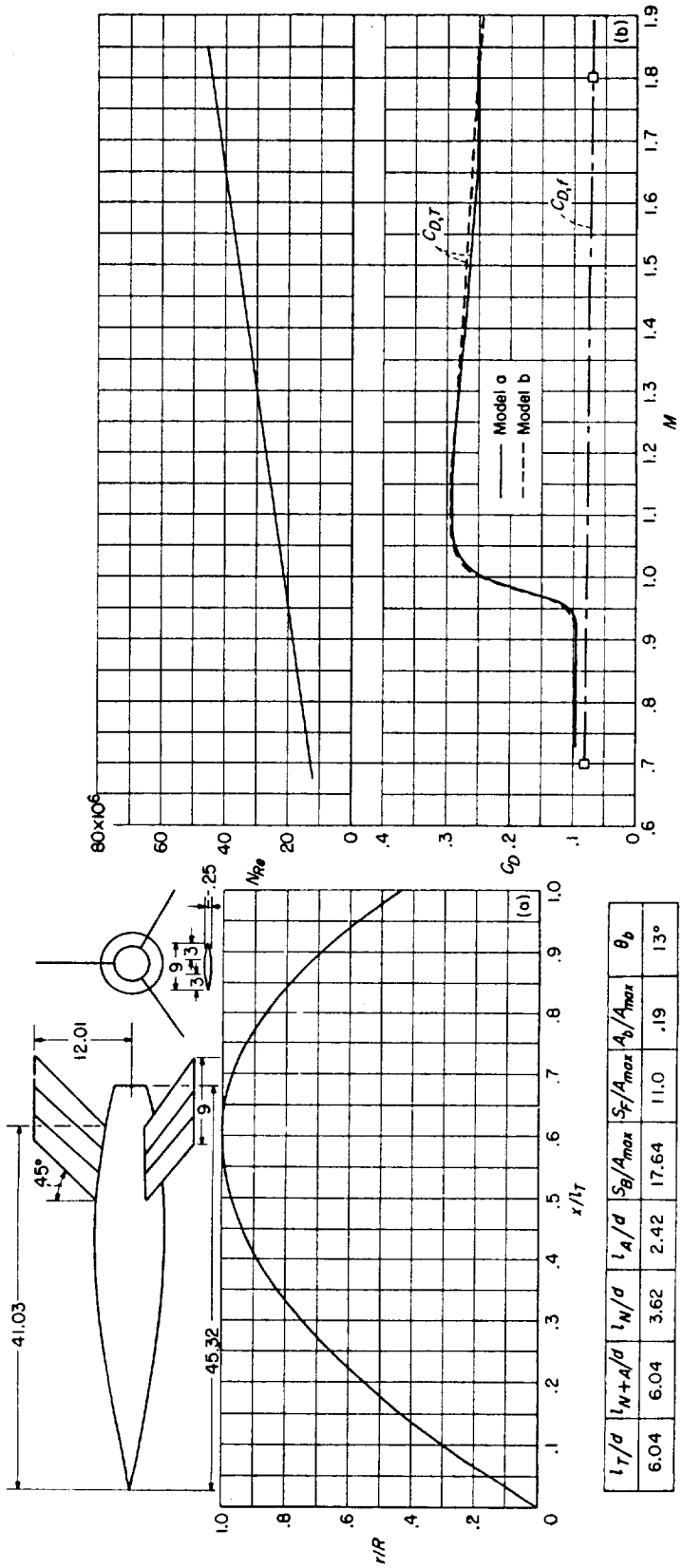

l_T/d	l_{N+A}/d	l_N/d	l_A/d	S_B/A_{max}	S_F/A_{max}	A_b/A_{max}	θ_b
6.04	6.04	3.62	2.42	17.64	11.0	.19	13°

(a) Body shape. (Dimensions given are in inches.) (b) N_{Re} and C_D curves.

CONFIGURATION 30 (parabolic nose and afterbody); rocket test.

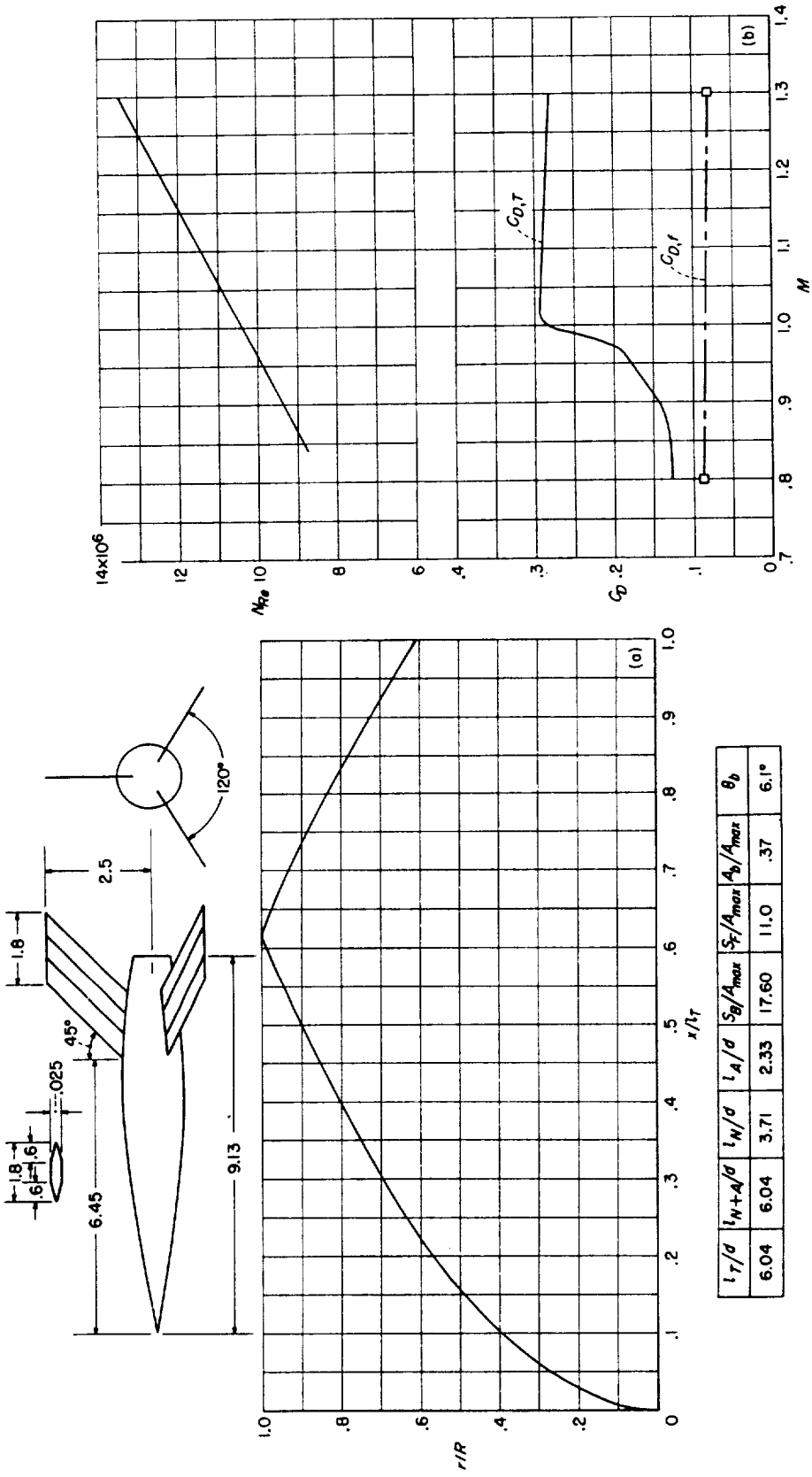

l_T/d	l_{N+A}/d	l_N/d	l_A/d	S_B/A_{max}	S_F/A_{max}	A_b/A_{max}	θ_b
6.04	6.04	3.71	2.33	17.60	11.0	.37	6.1°

(a) Body shape. (Dimensions given are in inches.) (b) N_{Re} and C_D curves.

CONFIGURATION 31; helium-gun test.

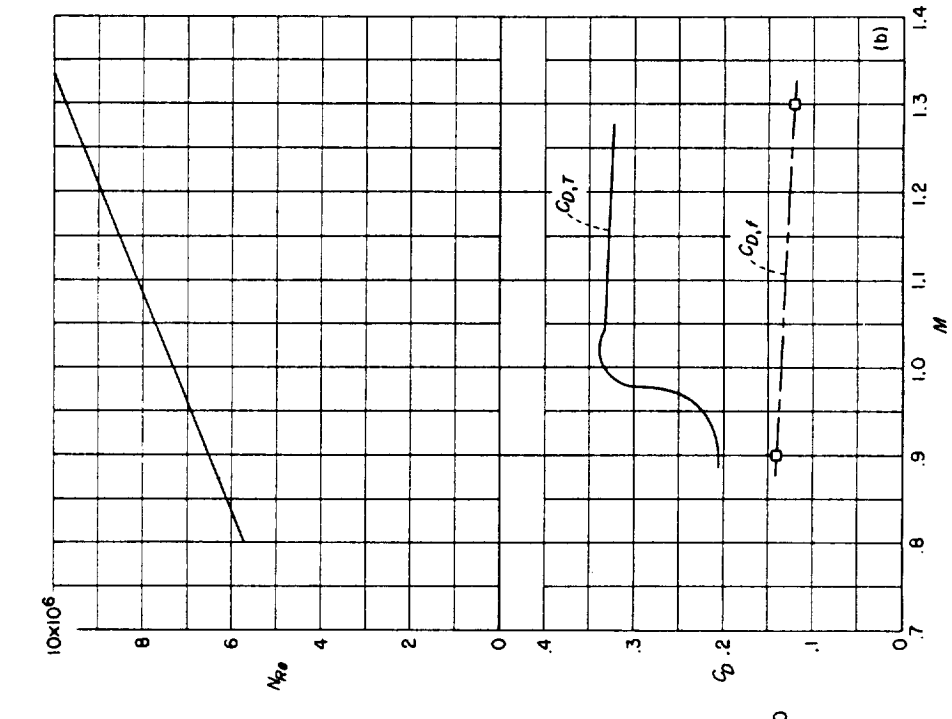

(b) N_{Re} and C_D curves.

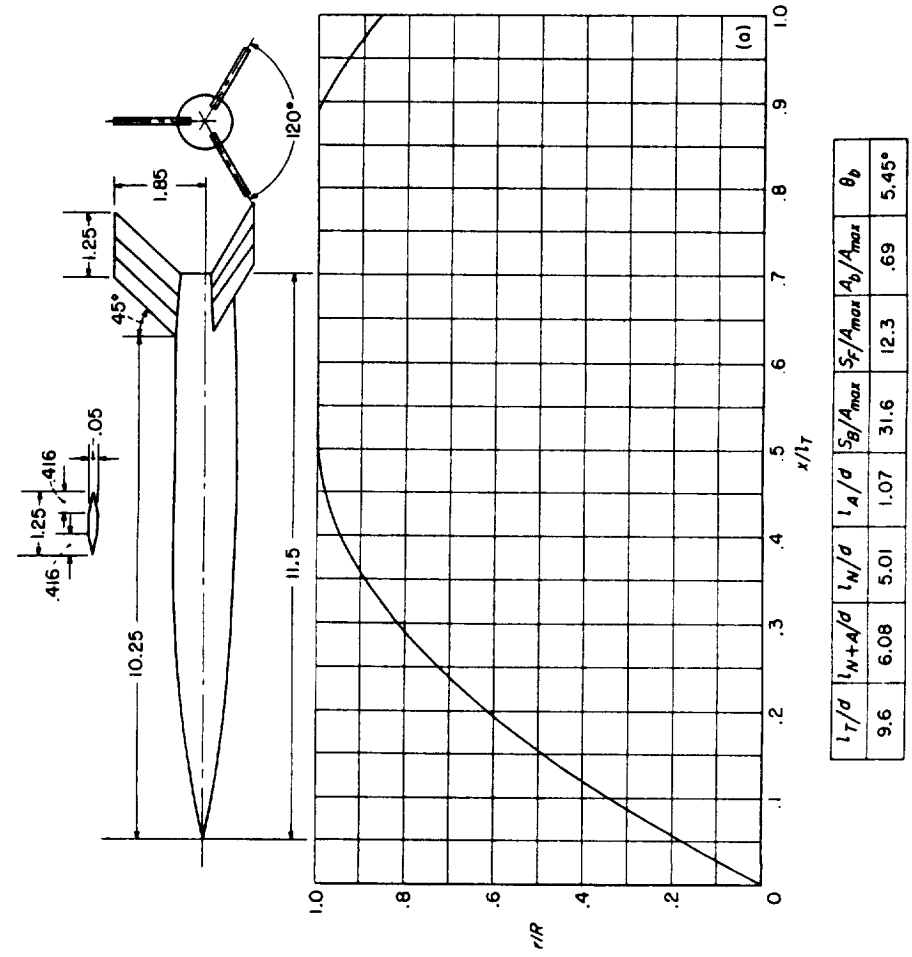

(a) Body shape. (Dimensions given are in inches.)

l_T/d	l_{N+A}/d	l_N/d	l_A/d	S_B/A_{max}	S_F/A_{max}	A_b/A_{max}	θ_b
9.6	6.08	5.01	1.07	31.6	12.3	.69	5.45°

CONFIGURATION 32; helium-gun test.

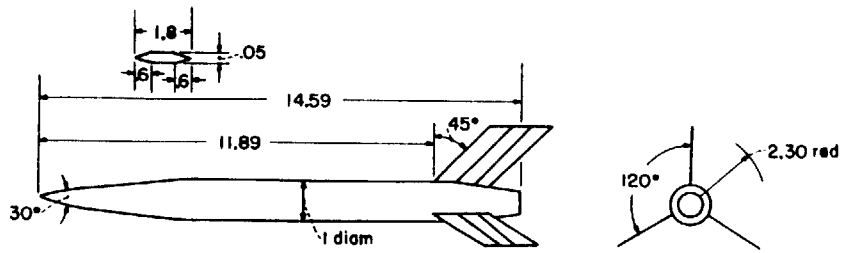

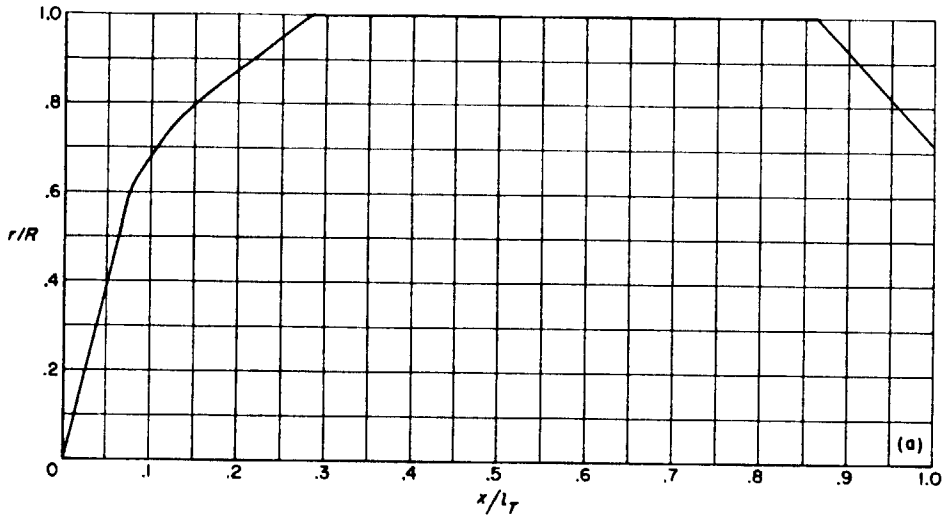

l_T/d	l_{N+A}/d	l_N/d	l_A/d	S_B/A_{max}	S_F/A_{max}	A_b/A_{max}	θ_b
14.6	6.10	4.10	2.0	52.3	24.6	.52	4.02°

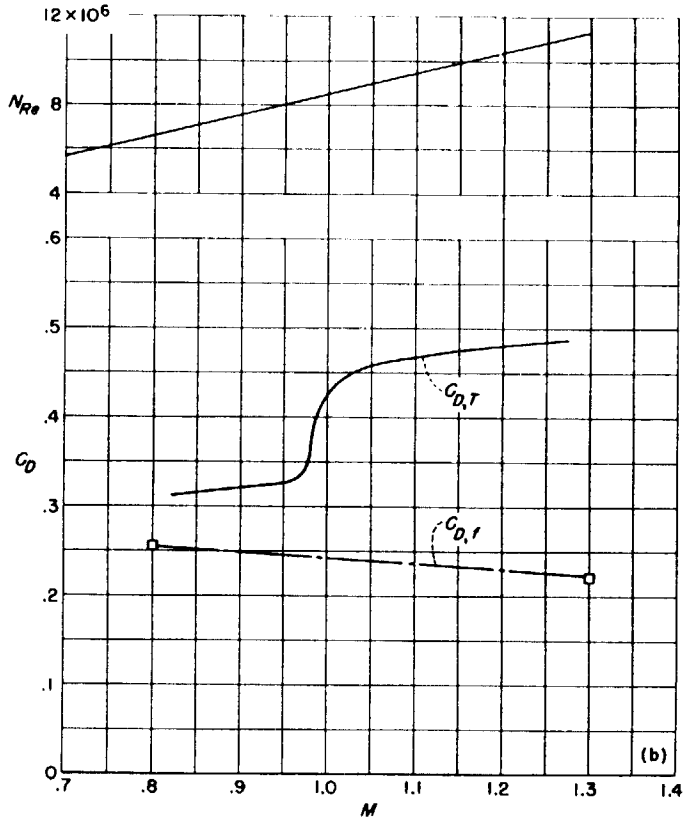

(a) Body shape. (Dimensions given are in inches.) (b) N_{Re} and C_D curves.

CONFIGURATION 33; helium-gun test. (This model ⅛ scale of configuration 34; thus pressure drags of these two configurations should be the same. That they are not the same is obvious, however, if it is assumed that data of configuration 34 are in error in M about $M=0.05$; then the subsonic levels and the early drag rises are compatible. This seems to be justified since the late drag rise of configuration 34 would be quite unusual if it really occurred. Configuration 36 is similar to 34 and showed the more usual earlier rise. The continued increase in drag coefficient of configuration 33 above $M=1.1$ is also peculiar and is probably in error.)

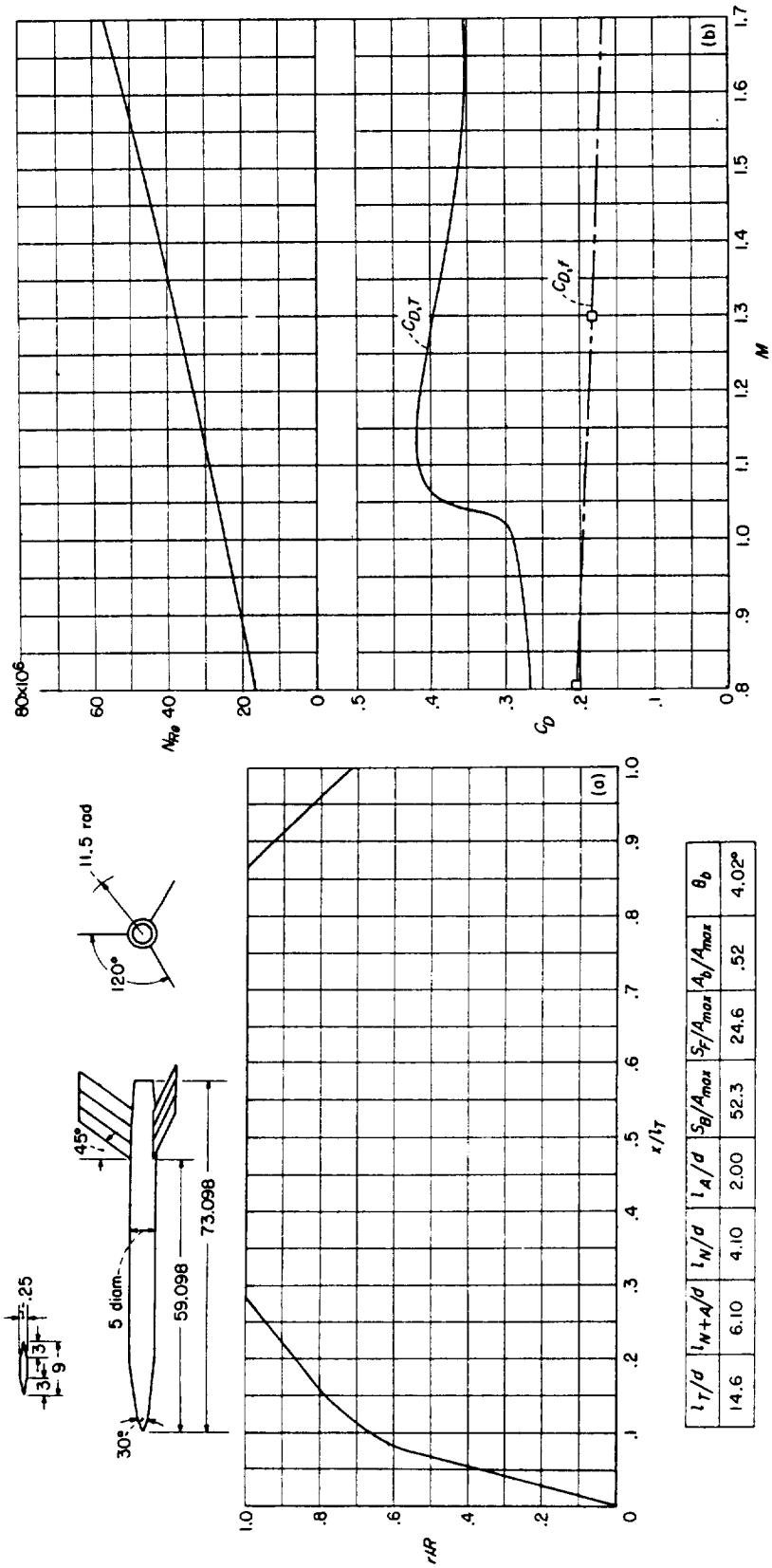

l_T/d	l_{N+A}/d	l_N/d	l_A/d	S_B/A_{max}	S_F/A_{max}	A_b/A_{max}	θ_b
14.6	6.10	4.10	2.00	52.3	24.6	.52	4.02°

(a) Body shape. (Dimensions given are in inches.) (b) N_{Re} and C_D curves.

CONFIGURATION 34; rocket test. (See fig. 41.)

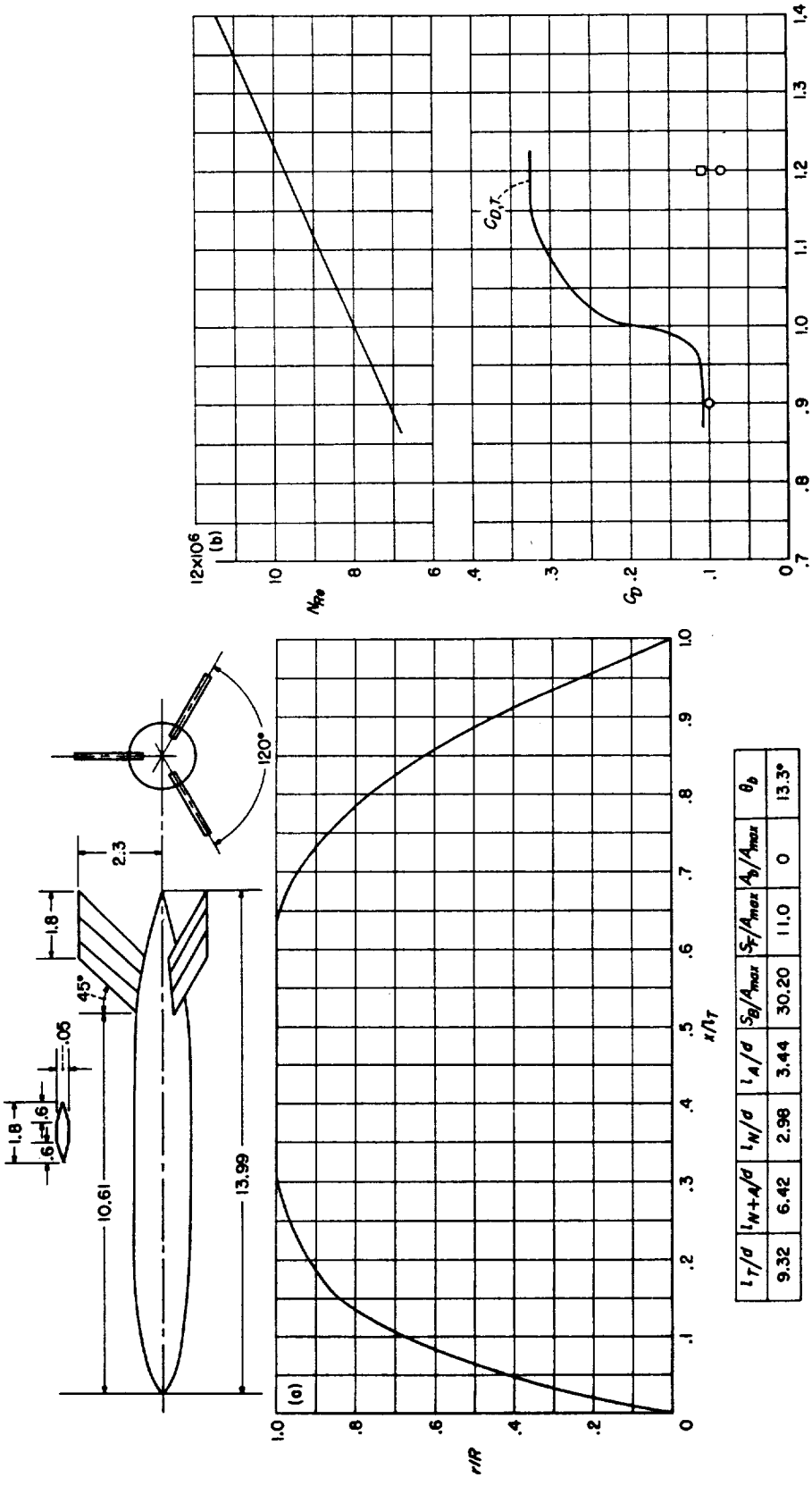

l_T/d	l_{N+A}/d	l_N/d	l_A/d	S_B/A_{max}	S_F/A_{max}	A_b/A_{max}	θ_b
9.32	6.42	2.98	3.44	30.20	11.0	0	13.3°

(a) Body shape. (Dimensions given are in inches.) (b) N_{Re} and C_D curves.

CONFIGURATION 35; helium-gun test.

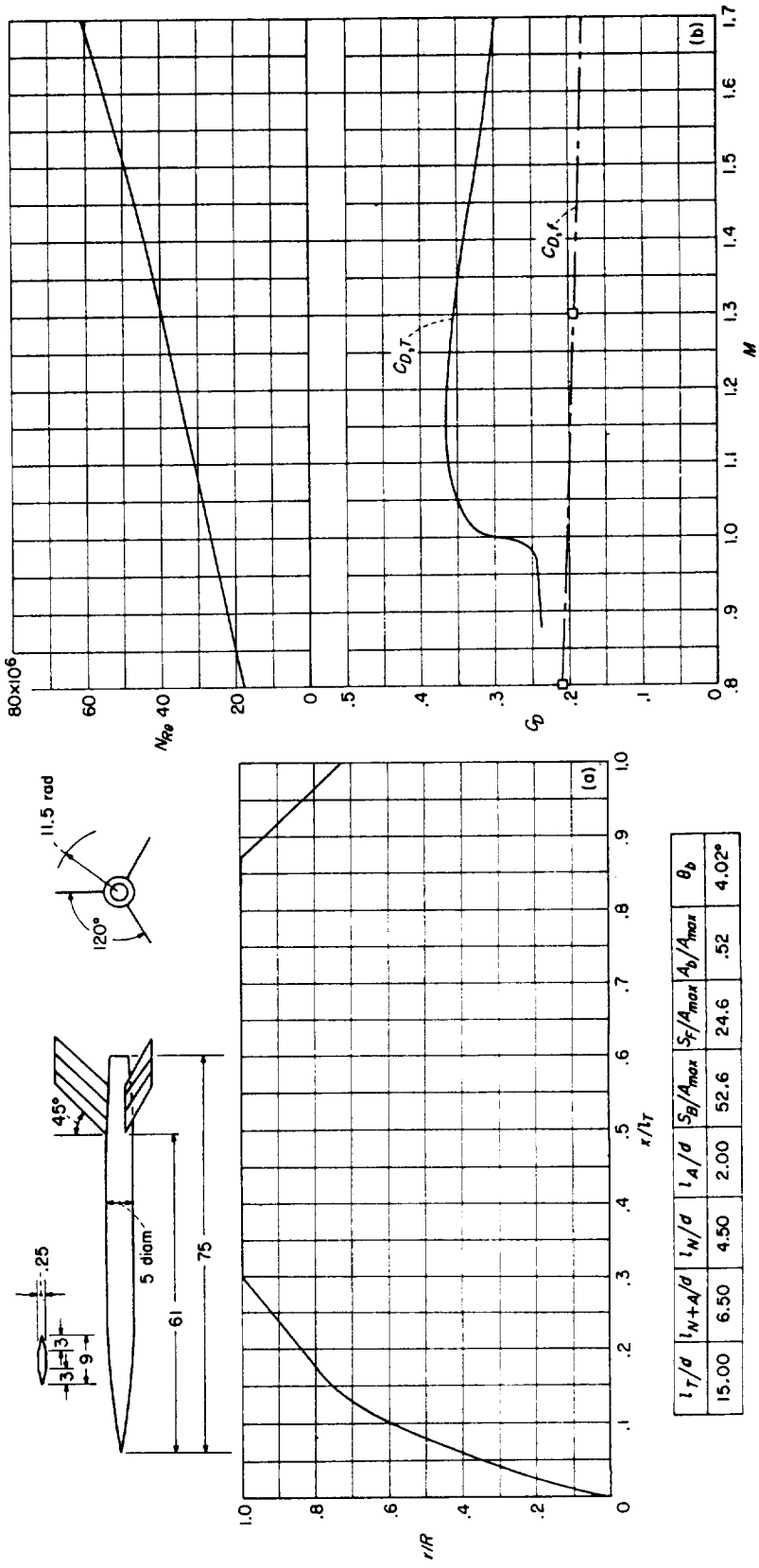

l_T/d	l_{N+A}/d	l_N/d	l_A/d	S_B/A_{max}	S_F/A_{max}	A_b/A_{max}	θ_b
15.00	6.50	4.50	2.00	52.6	24.6	.52	4.02°

(a) Body shape. (Dimensions given are in inches.) (b) N_{Re} and C_D curves.

CONFIGURATION 36; rocket test. (See fig. 41.)

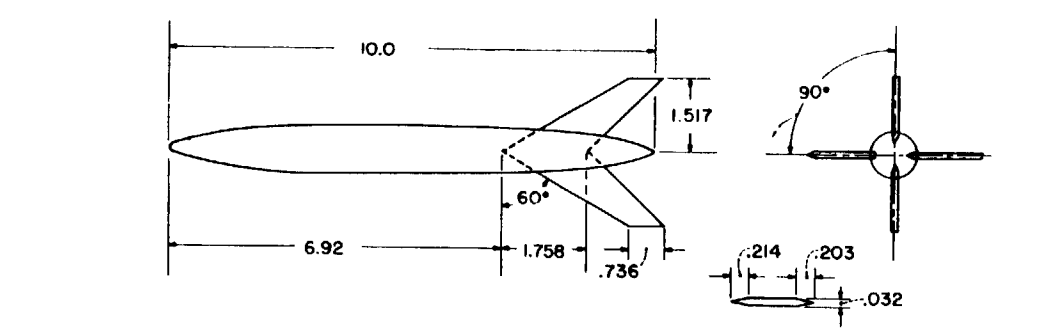

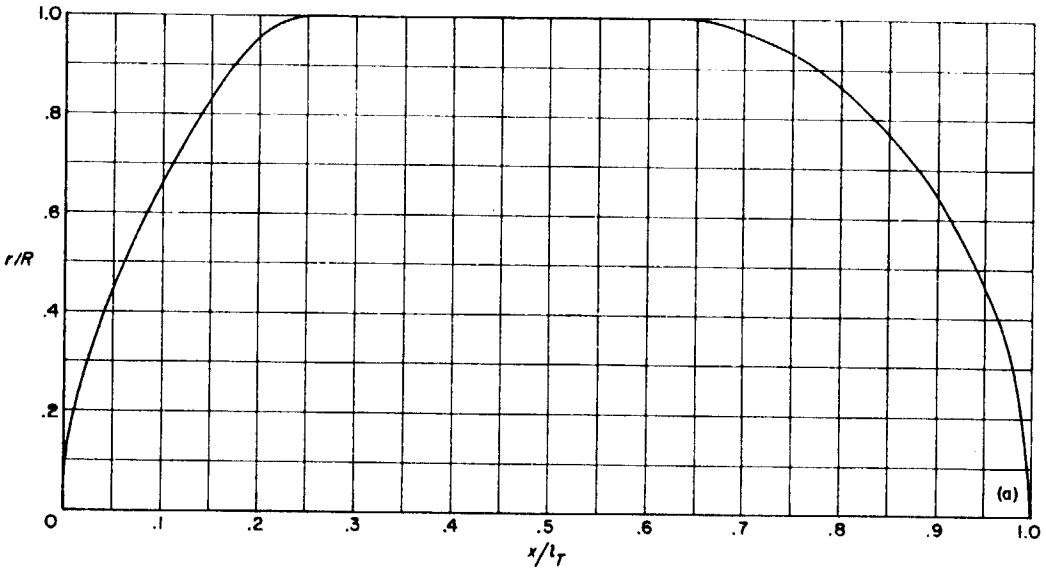

l_T/d	l_{N+A}/d	l_N/d	l_A/d	S_B/A_{max}	S_F/A_{max}	A_b/A_{max}	θ_b
10.87	6.51	2.71	3.8	35.6	12.82	0	60°

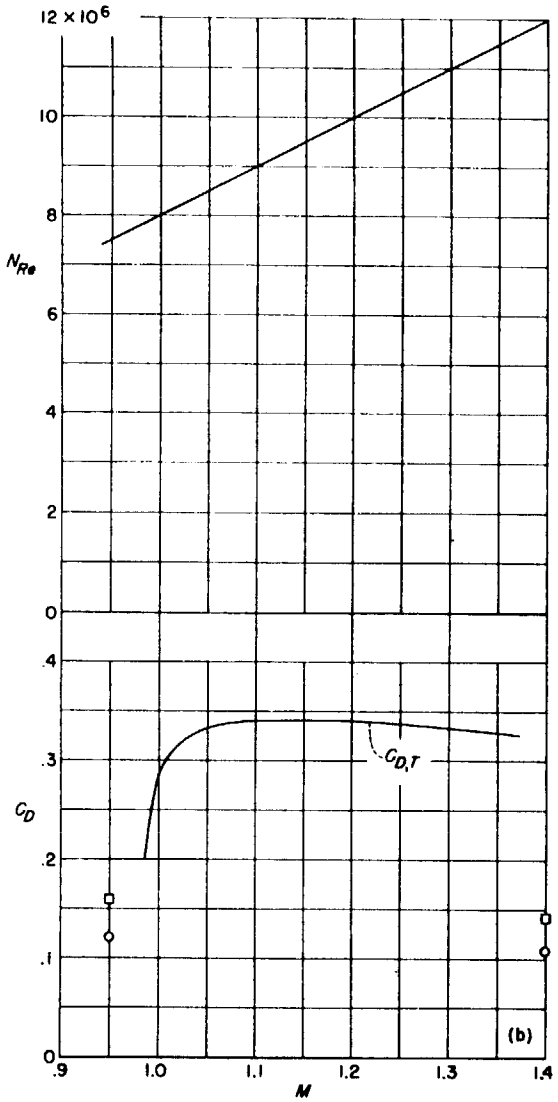

(a) Body shape. (Dimensions given are in inches.) (b) N_{R_e} and C_D curves.

CONFIGURATION 37 (nondimensional ordinates identical to configuration 10); helium-gun test.

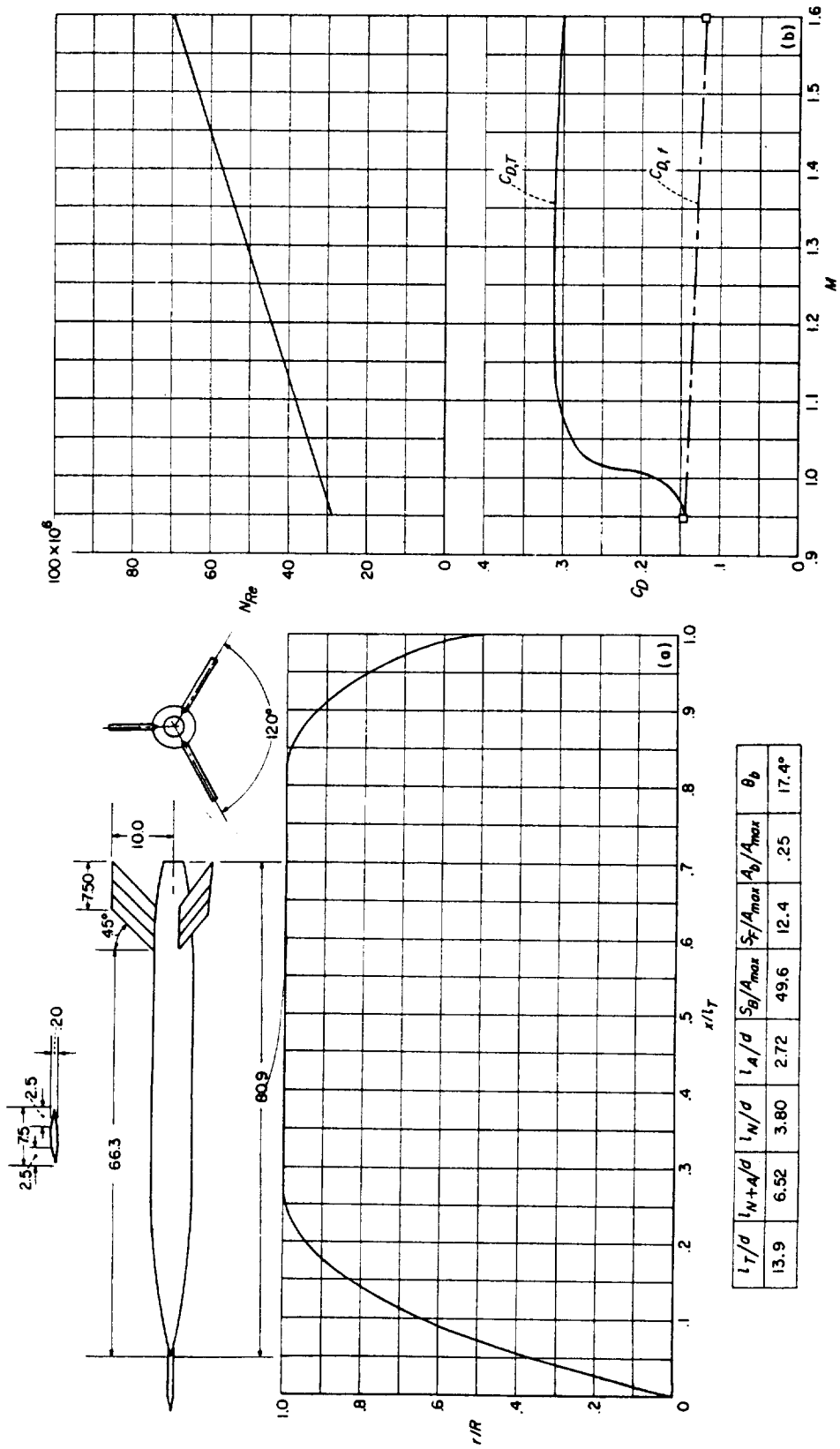

l_T/d	l_{N+A}/d	l_N/d	l_A/d	S_B/A_{max}	S_F/A_{max}	A_b/A_{max}	θ_b
13.9	6.52	3.80	2.72	49.6	12.4	.25	17.4°

(a) Body shape. (Dimensions given are in inches.) (b) N_R, and C_D curves.

CONFIGURATION 38; rocket test. (Spike can affect friction drag but is not likely to affect pressure drag.)

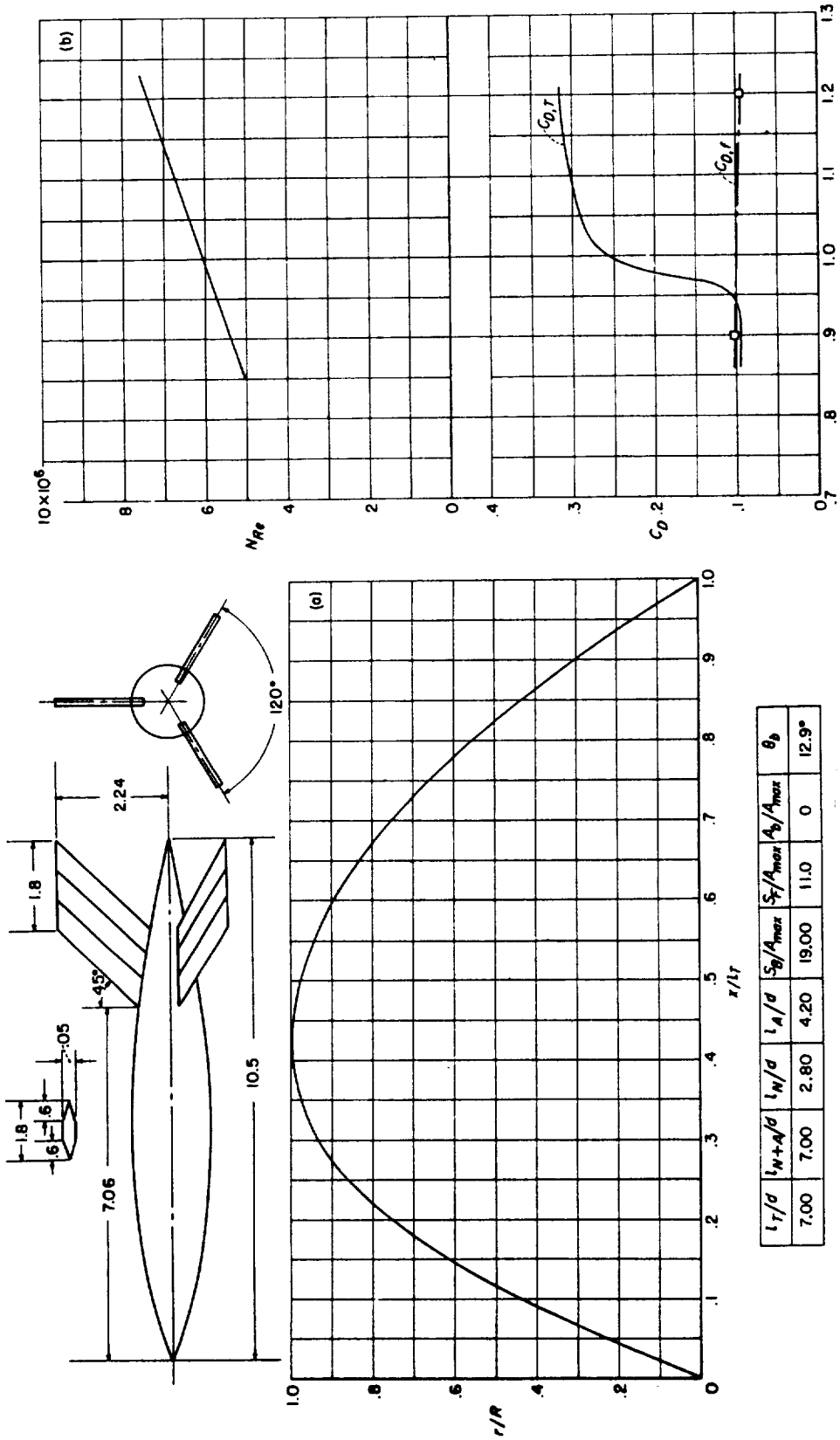

l_T/d	l_{N+A}/d	l_N/d	l_A/d	S_B/A_{max}	S_F/A_{max}	A_b/A_{max}	θ_b
7.00	7.00	2.80	4.20	19.00	11.0	0	12.9°

(a) Body shape. (Dimensions given are in inches.) (b) N_{Re} and C_D curves.

CONFIGURATION 39; helium-gun test.

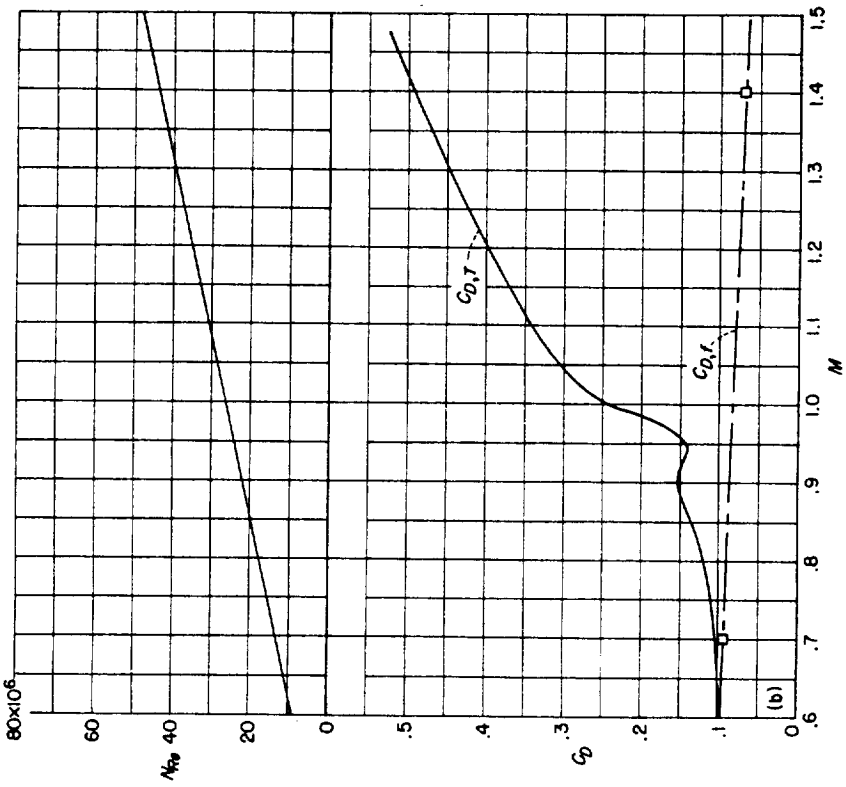

(b) N_{Re} and C_D curves.

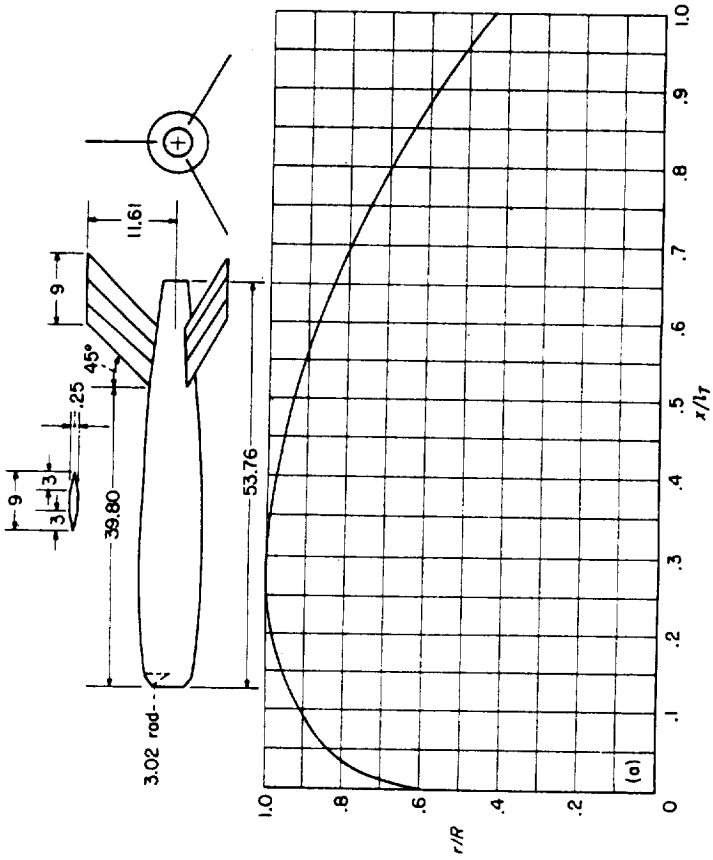

l_T/d	l_{N+A}/d	l_N/d	l_A/d	S_B/A_{max}	S_F/A_{max}	A_b/A_{max}	θ_b
7.16	7.16	1.81	5.35	24.00	11.0	.19	7°

(a) Body shape. (Dimensions given are in inches.)

CONFIGURATION 40 (flat nose having $r/R = 0.57$ flared into parabolic segment by 3.02 radius; parabolic afterbody); rocket test.

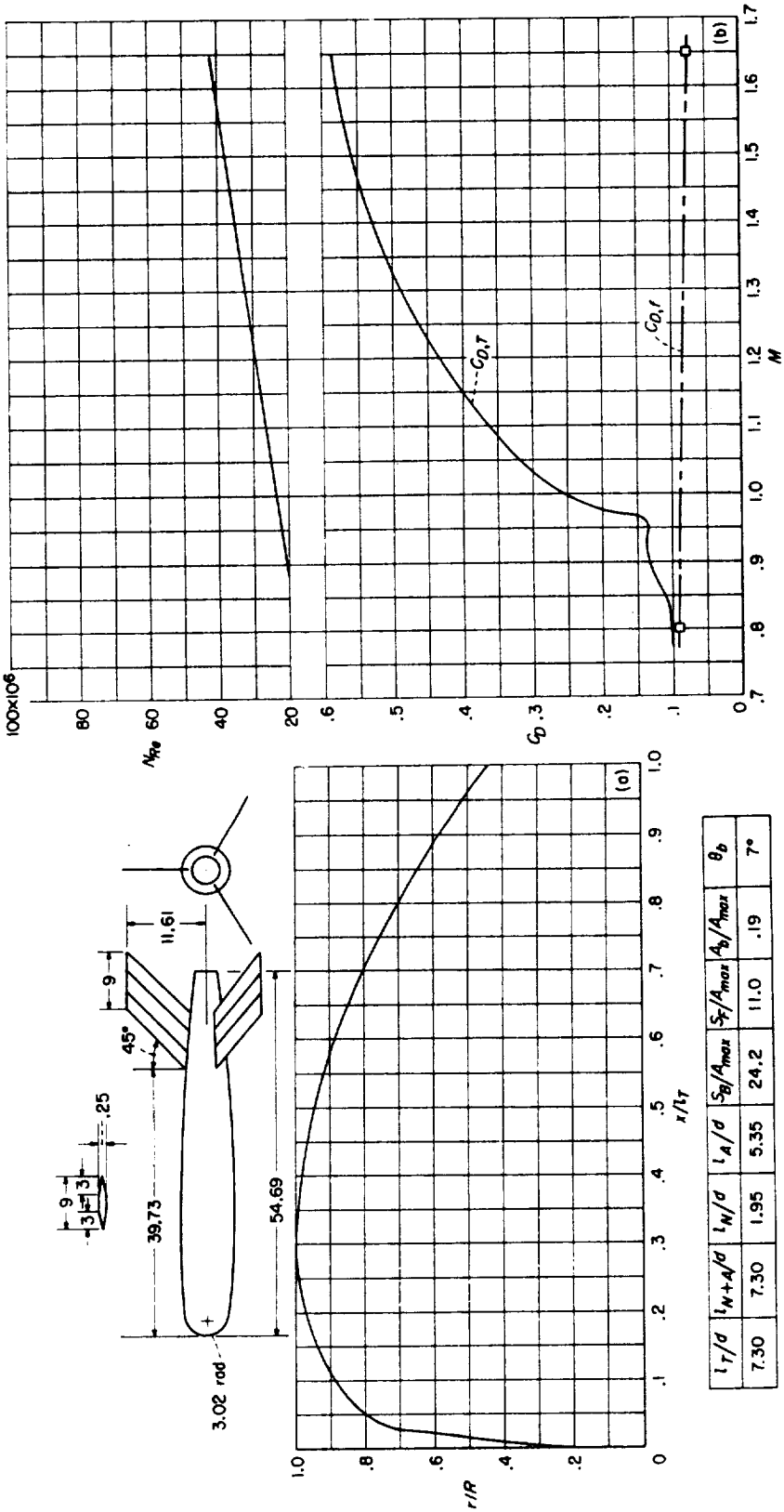

l_T/d	l_{W+A}/d	l_N/d	l_A/d	S_B/A_{max}	S_F/A_{max}	A_b/A_{max}	θ_b
7.30	7.30	1.95	5.35	24.2	11.0	.19	7°

(a) Body shape. (Dimensions given are in inches.) (b) N_{Re} and C_D curves.

CONFIGURATION 41 (nose consists of hemispherical segment plus parabolic segment; parabolic afterbody); rocket test.

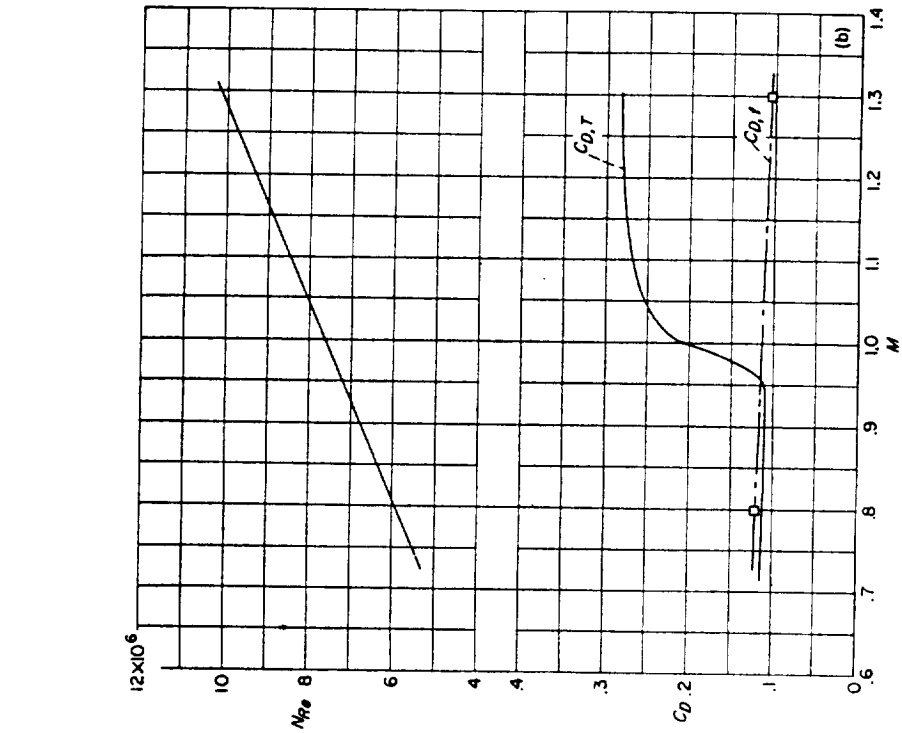

(b) N_{Re} and C_D curves.

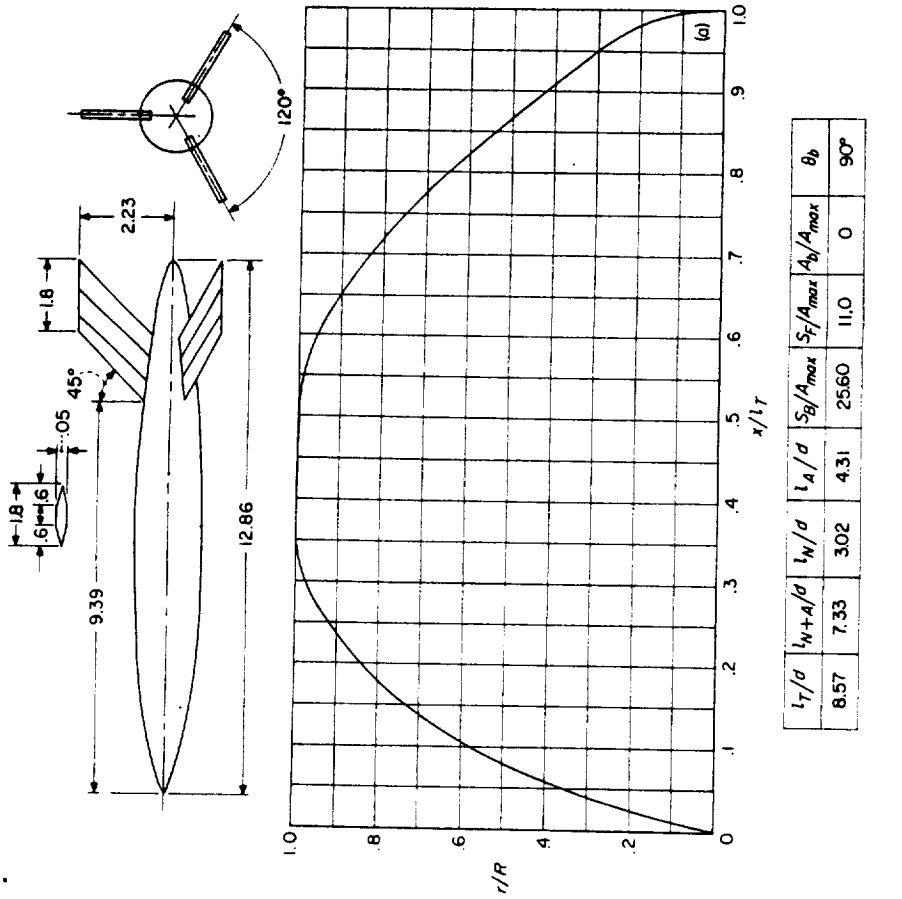

l_T/d	l_{N+A}/d	l_N/d	l_A/d	S_B/A_{max}	S_F/A_{max}	A_b/A_{max}	θ_b
8.57	7.33	3.02	4.31	2560	11.0	0	90°

(a) Body shape. (Dimensions given are in inches.)

CONFIGURATION 42; helium-gun test

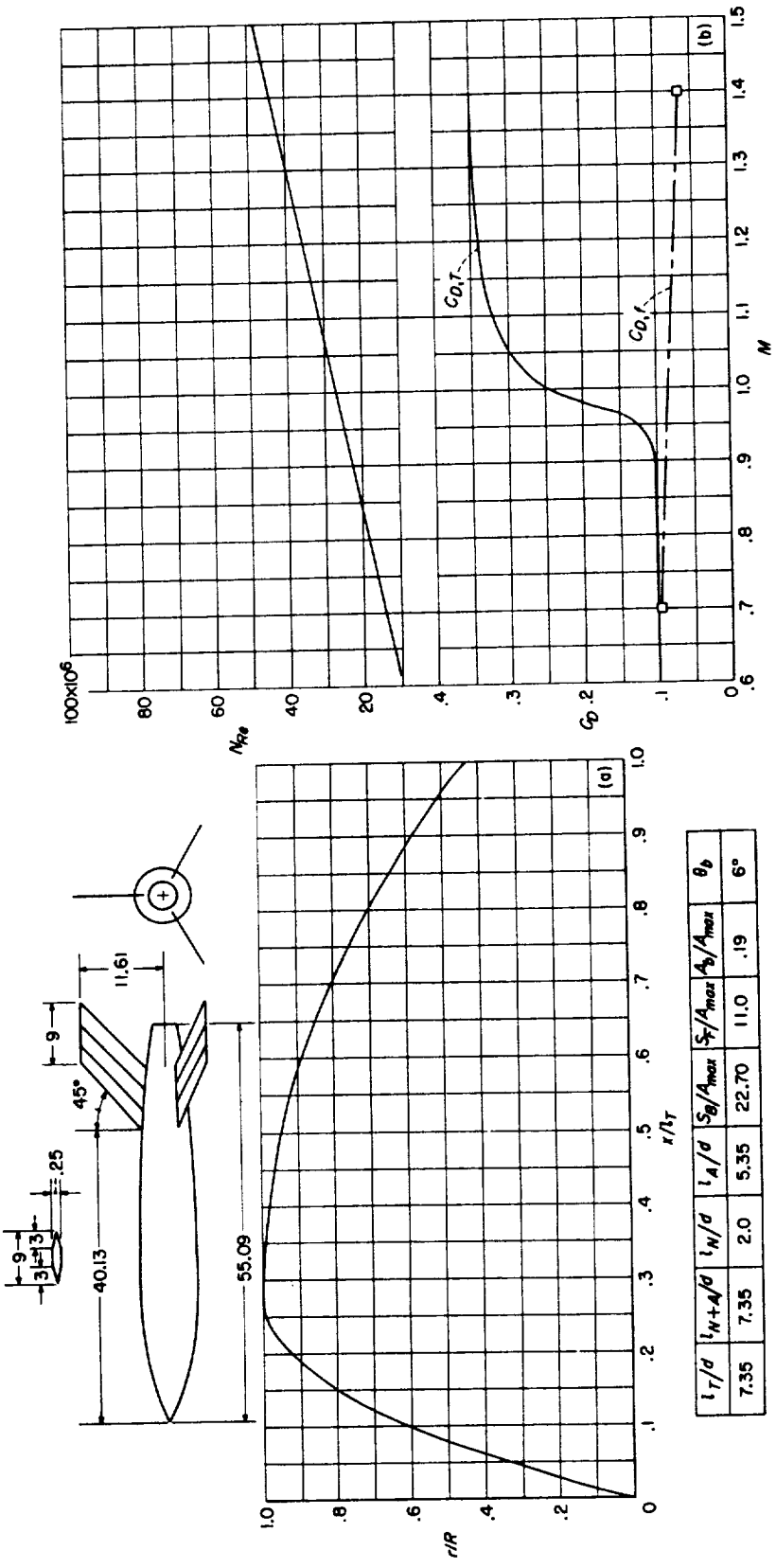

l_T/d	l_{N+A}/d	l_N/d	l_A/d	S_B/A_{max}	S_F/A_{max}	A_b/A_{max}	θ_b
7.35	7.35	2.0	5.35	22.70	11.0	.19	6°

(a) Body shape. (Dimensions given are in inches.) (b) N_{Re} and C_D curves.

CONFIGURATION 43 (parabolic nose and afterbody); rocket test.

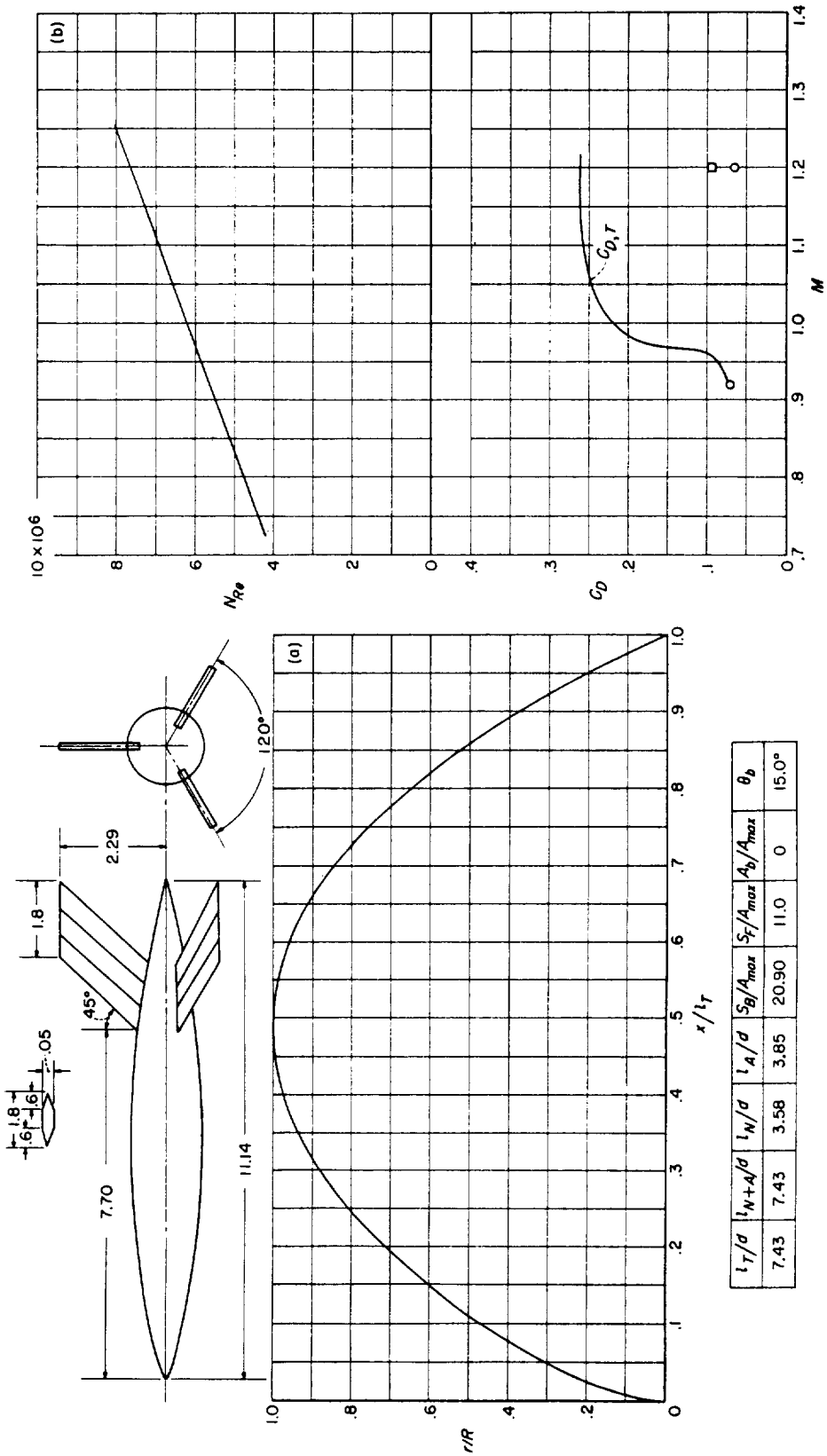

l_T/d	l_{N+A}/d	l_N/d	l_A/d	S_B/A_{max}	S_F/A_{max}	A_b/A_{max}	θ_b
7.43	7.43	3.58	3.85	20.90	11.0	0	15.0°

(a) Body shape. (Dimensions given are in inches.) (b) N_{Re} and C_D curves.

CONFIGURATION 44; helium-gun test.

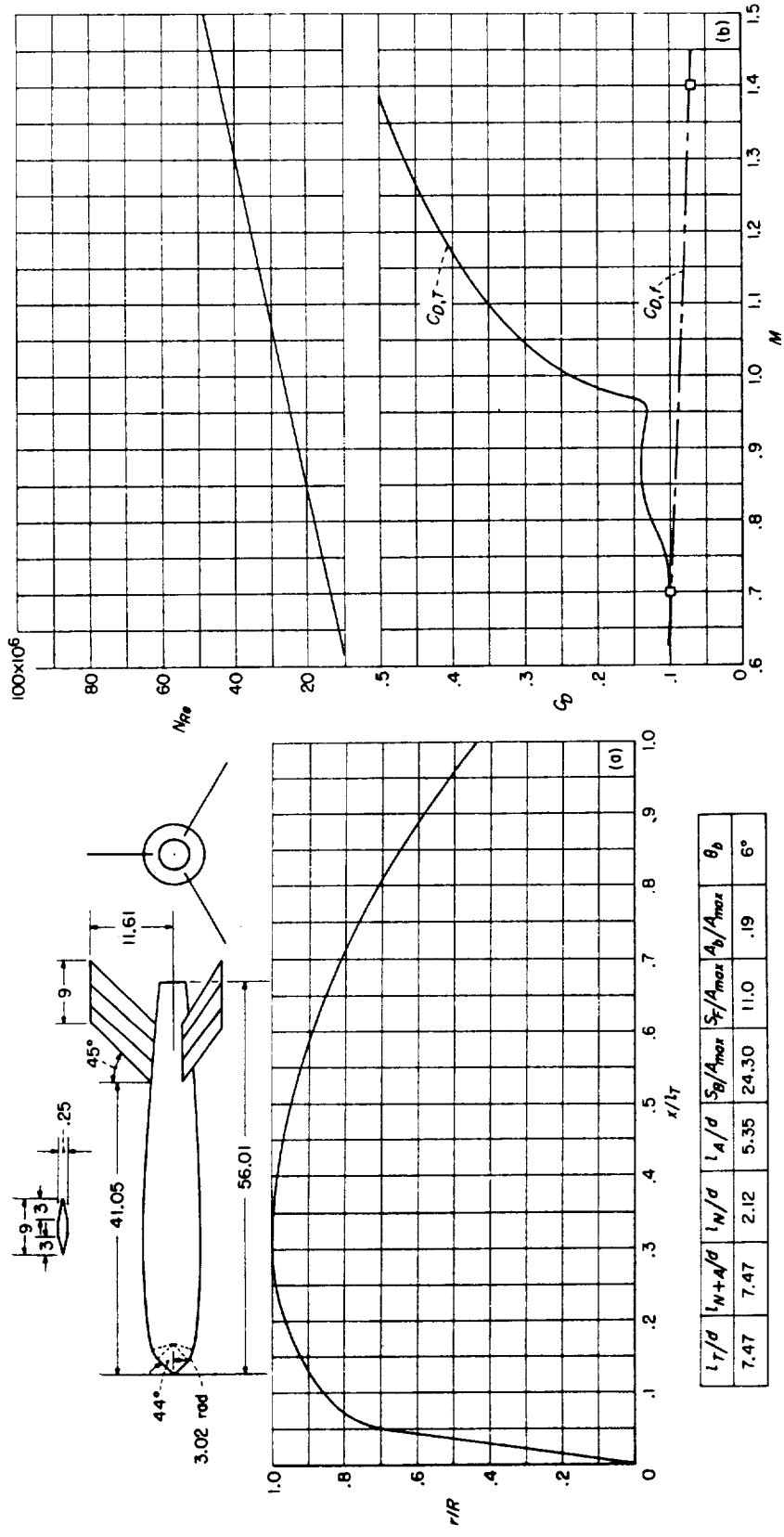

l_T/d	l_{N+A}/d	l_N/d	l_A/d	S_B/A_{max}	S_F/A_{max}	A_b/A_{max}	θ_b
7.47	7.47	2.12	5.35	24.30	11.0	.19	6°

(a) Body shape. (Dimensions given are in inches.) (b) N_{Re} and C_D curves.

CONFIGURATION 45 (conical nose with hemispherical and parabolic segments; parabolic afterbody); rocket test.

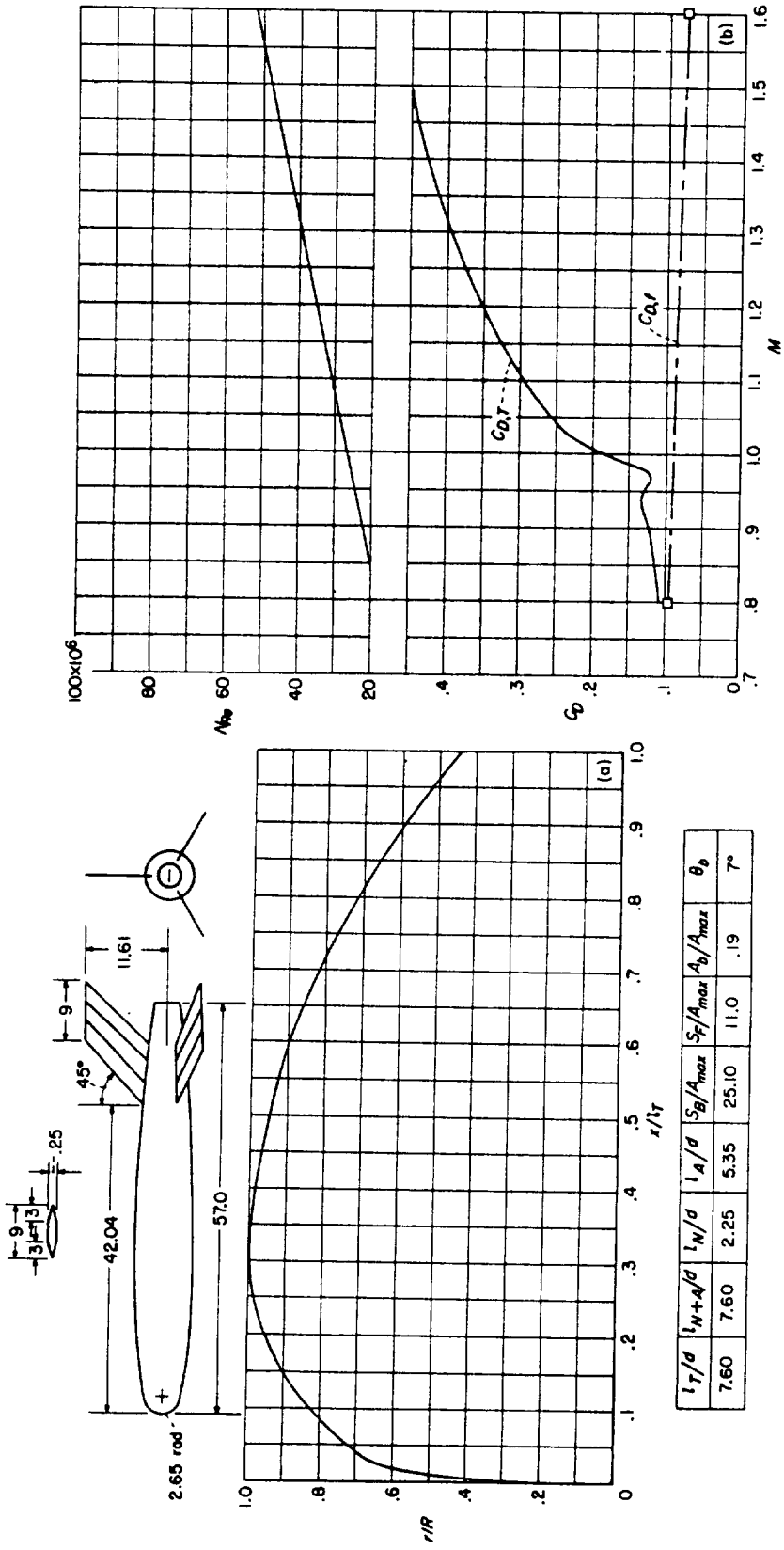

l_T/d	l_{N+A}/d	l_N/d	l_A/d	S_B/A_{max}	S_F/A_{max}	A_b/A_{max}	θ_b
7.60	7.60	2.25	5.35	25.10	11.0	.19	7°

(a) Body shape. (Dimensions given are in inches.) (b) N_{Re} and C_D curves.

CONFIGURATION 46 (nose with hemispherical and parabolic segments; parabolic afterbody); rocket test.

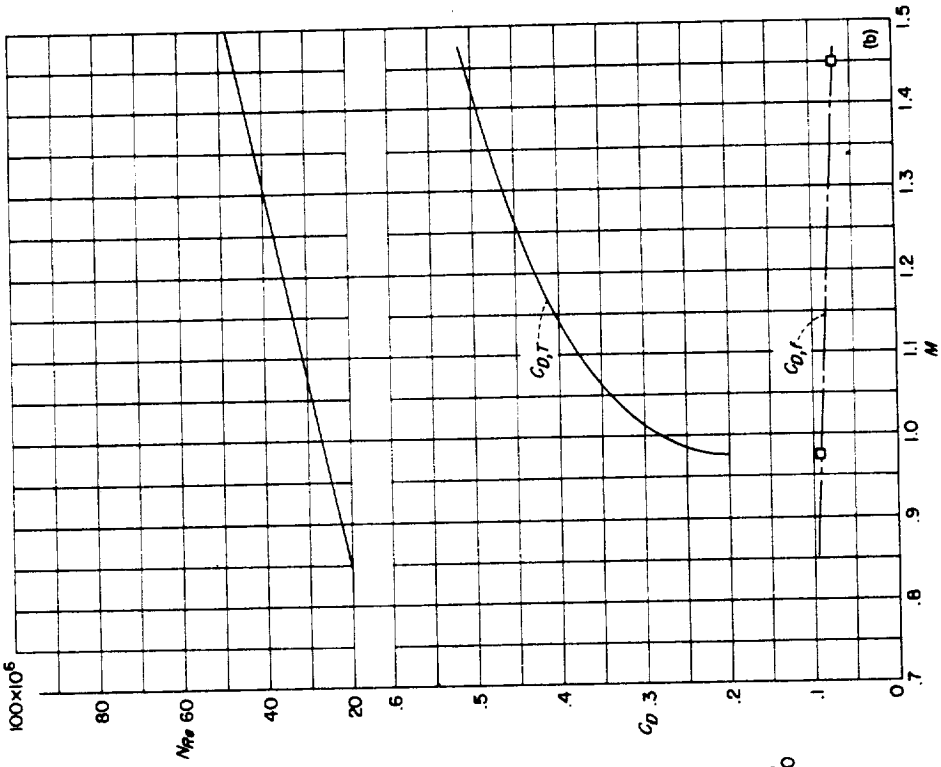

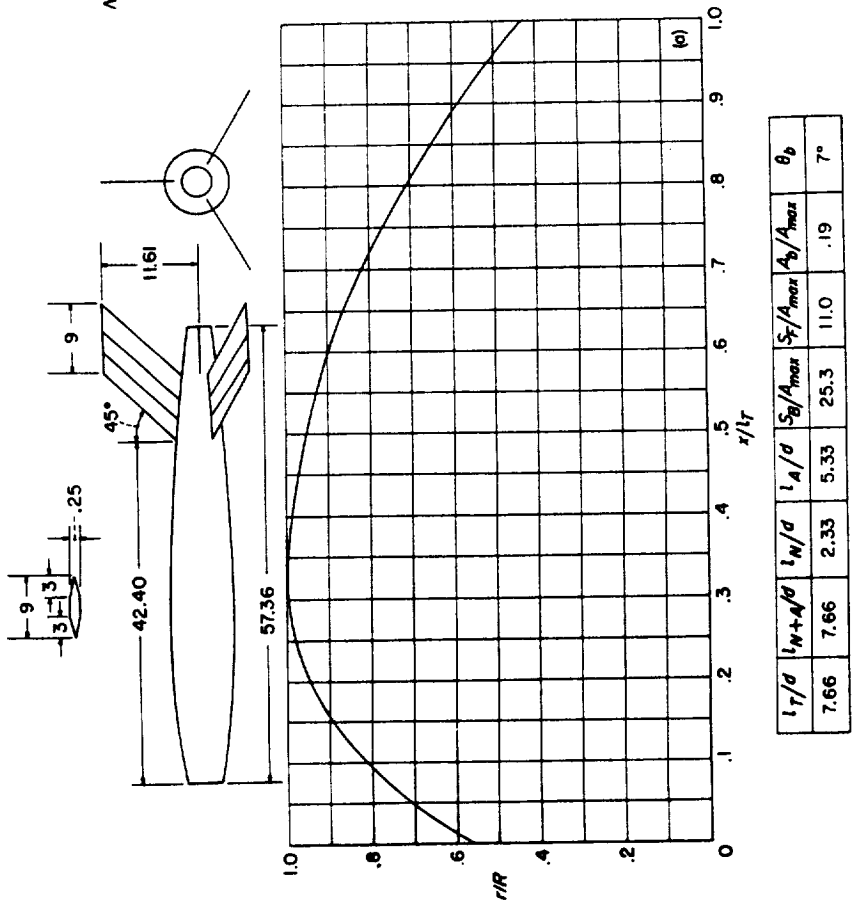

l_T/d	l_{N+A}/d	l_N/d	l_A/d	S_B/A_{max}	S_F/A_{max}	A_b/A_{max}	θ_b
7.66	7.66	2.33	5.33	25.3	11.0	.19	7°

(a) Body shape. (Dimensions given are in inches.) (b) N_{R_e} and C_D curves.

CONFIGURATION 47 (nose consists of parabolic segment; parabolic afterbody); rocket test.

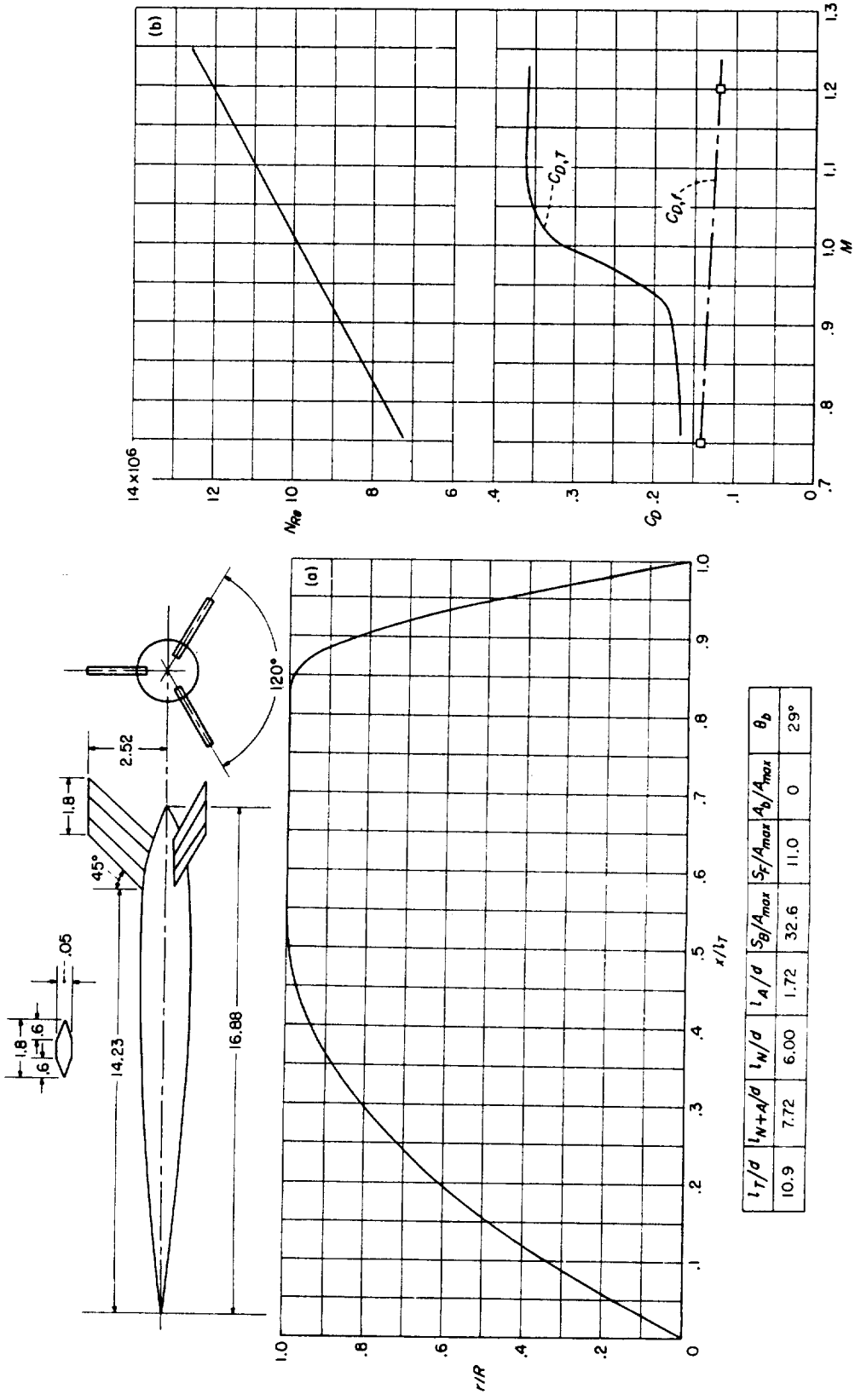

l_T/d	l_{N+A}/d	l_N/d	l_A/d	S_B/A_{max}	S_F/A_{max}	A_b/A_{max}	θ_b
10.9	7.72	6.00	1.72	32.6	11.0	0	29°

(a) Body shape. (Dimensions given are in inches.) (b) N_{Re} and C_D curves.

CONFIGURATION 48 (body differs from configurations 49 and 50 only in removal of Mach 1 area distribution of fins from afterbodies of these models); helium-gun test.

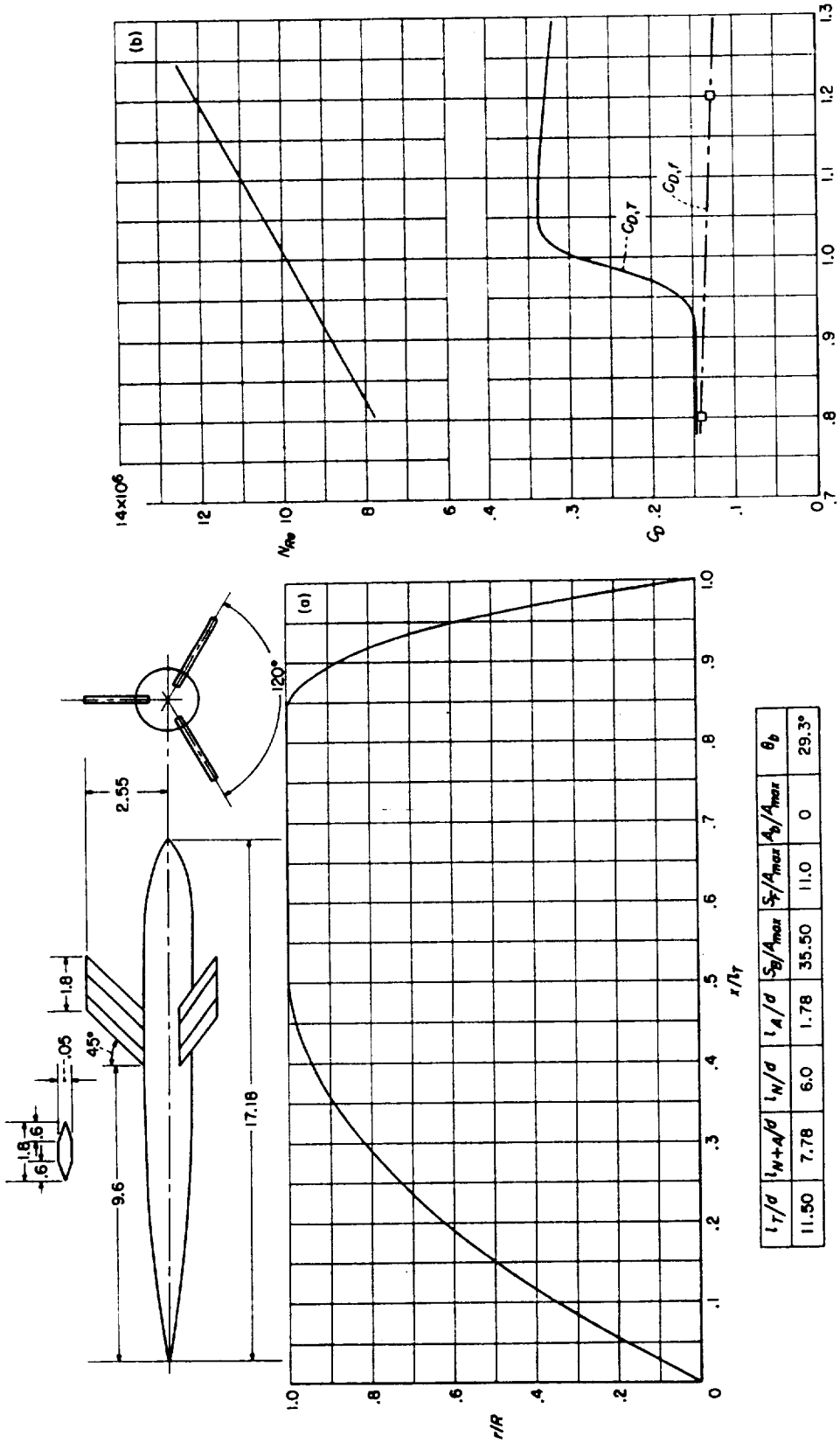

l_T/d	l_{N+A}/d	l_N/d	l_A/d	S_B/A_{max}	S_f/A_{max}	A_b/A_{max}	θ_b
11.50	7.78	6.0	1.78	35.50	11.0	0	29.3°

(a) Body shape. (Dimensions given are in inches.) (b) N_{Re} and C_D curves.

CONFIGURATION 49 (parabolic nose and afterbody with body identical to configuration 50 (see note for configuration 48)); helium-gun test.

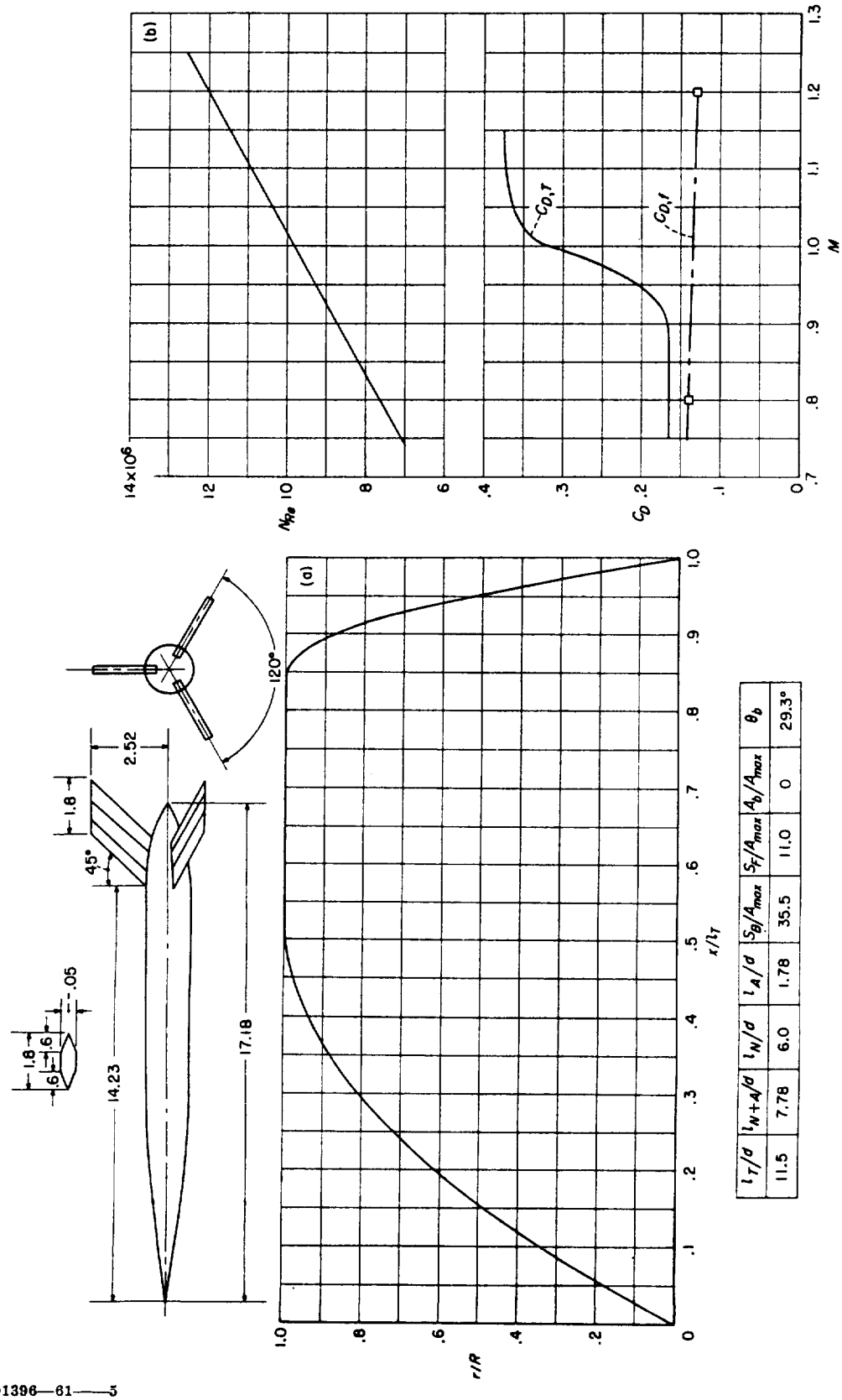

l_T/d	l_{N+A}/d	l_N/d	l_A/d	S_B/A_{max}	S_F/A_{max}	A_b/A_{max}	θ_b
11.5	7.78	6.0	1.78	35.5	11.0	0	29.3°

(a) Body shape. (Dimensions given are in inches.) (b) N_{Re} and C_D curves.

CONFIGURATION 50 (parabolic nose and afterbody with body identical to configuration 49 (see note for configuration 48)); helium-gun test.

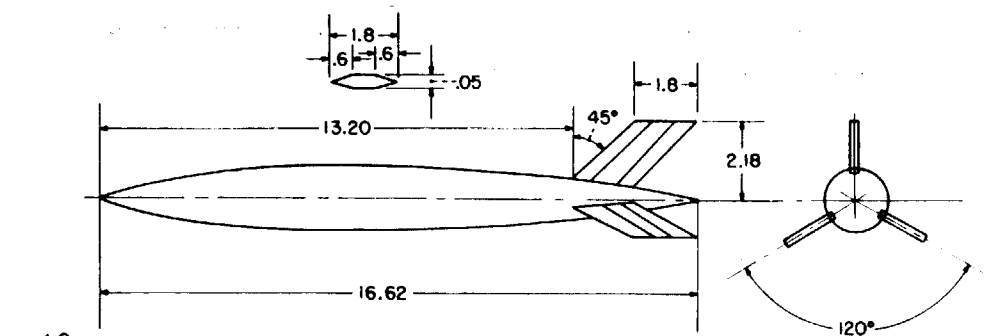

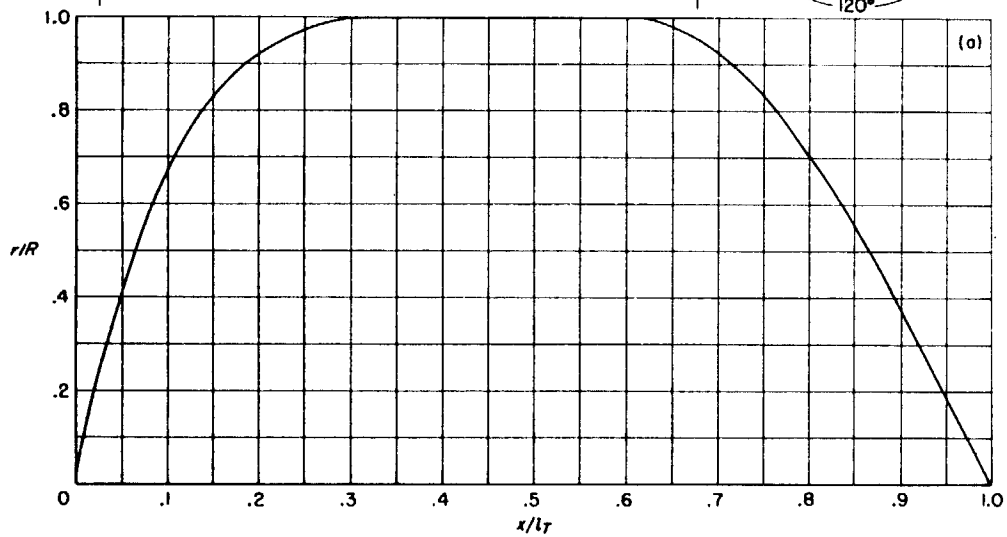

l_T/d	l_{N+A}/d	l_N/d	l_A/d	S_B/A_{max}	S_F/A_{max}	A_b/A_{max}	θ_b
11.08	7.80	3.42	4.38	34.40	11.0	0	9.8°

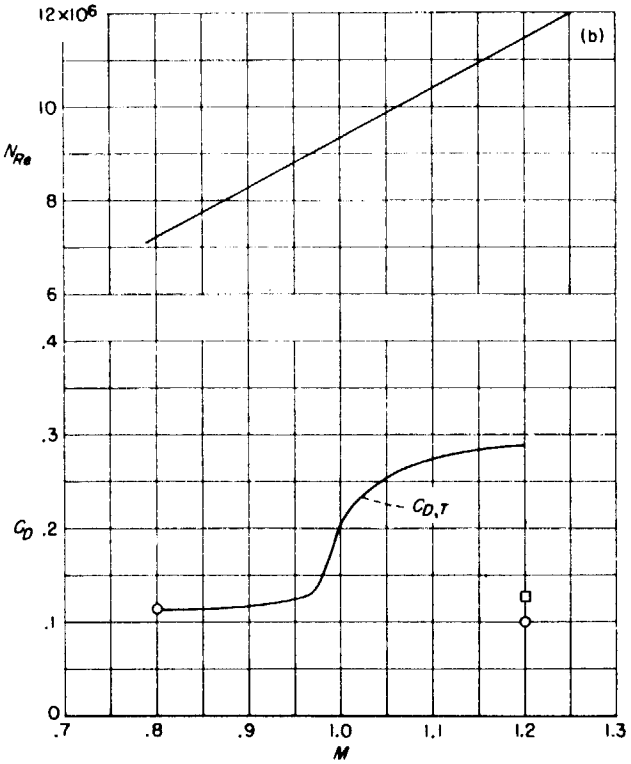

(a) Body shape. (Dimensions given are in inches.) (b) N_{R_θ} and C_D curves.

CONFIGURATION 51; helium-gun test.

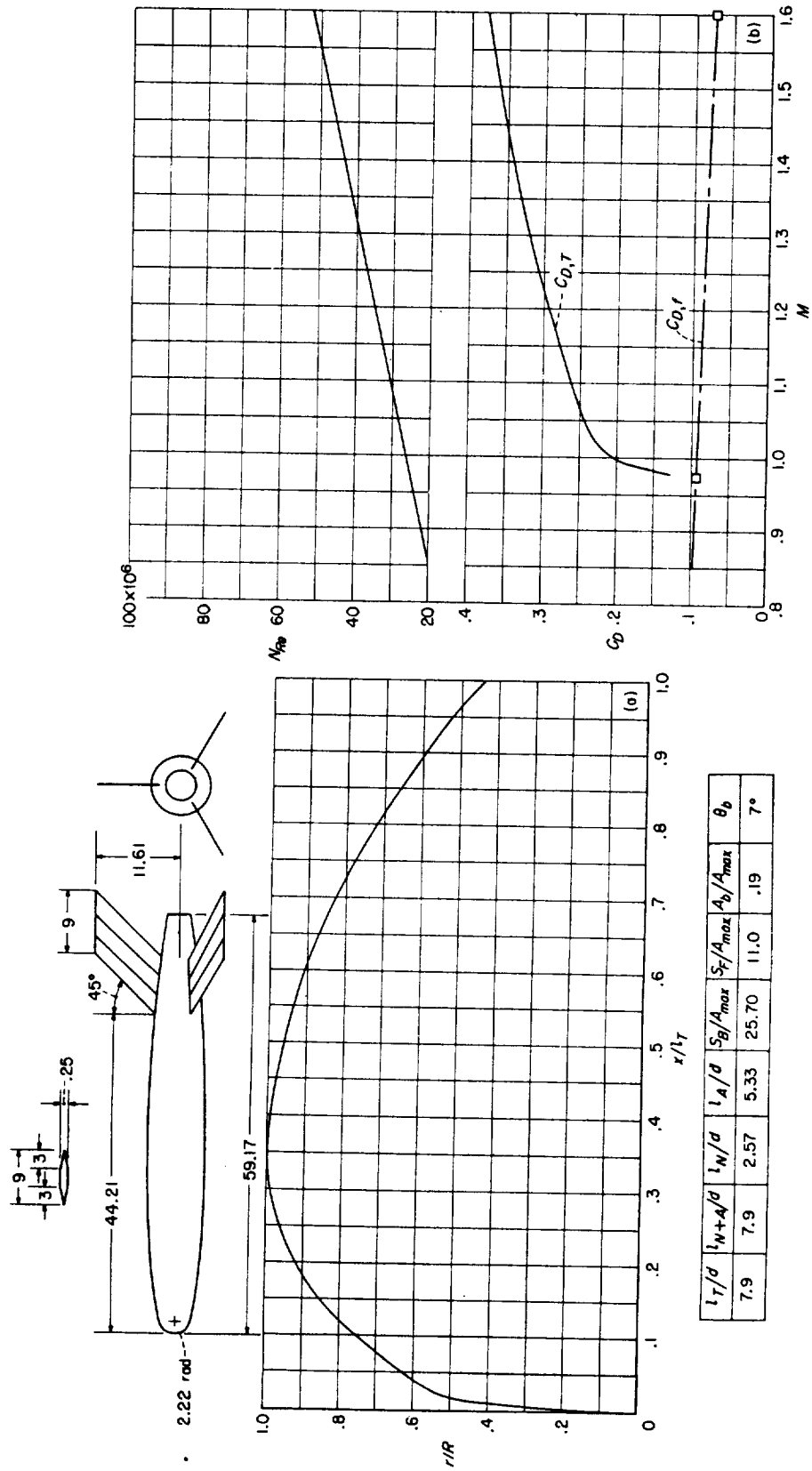

l_T/d	l_{N+A}/d	l_N/d	l_A/d	S_B/A_{max}	S_F/A_{max}	A_b/A_{max}	θ_b
7.9	7.9	2.57	5.33	25.70	11.0	.19	7°

(a) Body shape. (Dimensions given are in inches.) (b) N_{Re} and C_D curves.

CONFIGURATION 52 (nose consists of hemispherical and parabolic segments; parabolic afterbody); rocket test.

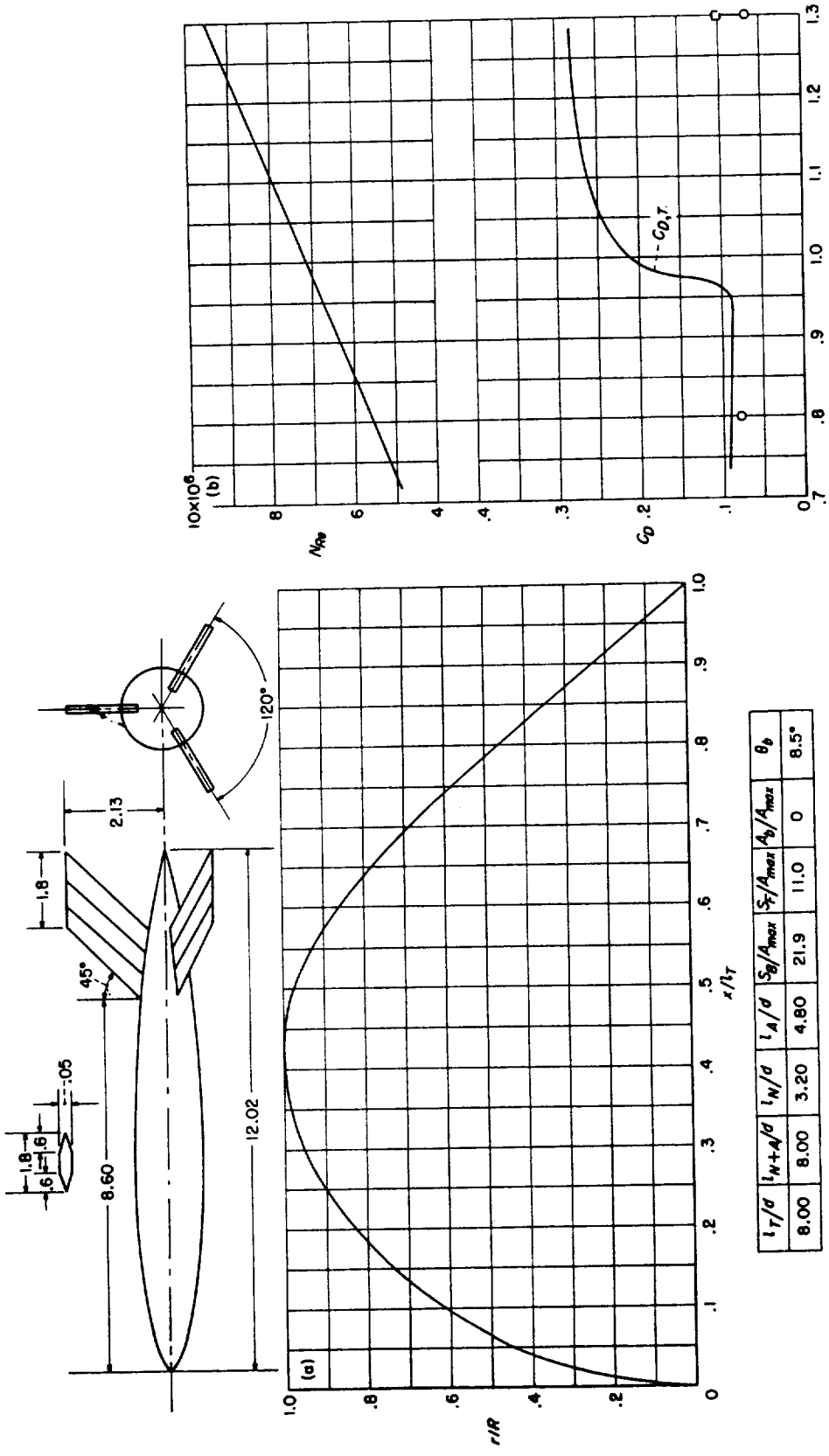

l_T/d	l_{N+A}/d	l_N/d	l_A/d	S_B/A_{max}	S_T/A_{max}	A_b/A_{max}	θ_b
8.00	8.00	3.20	4.80	21.9	11.0	0	8.5°

(a) Body shape. (Dimensions given are in inches.) (b) N_{Re} and C_D curves.

CONFIGURATION 53; helium-gun test.

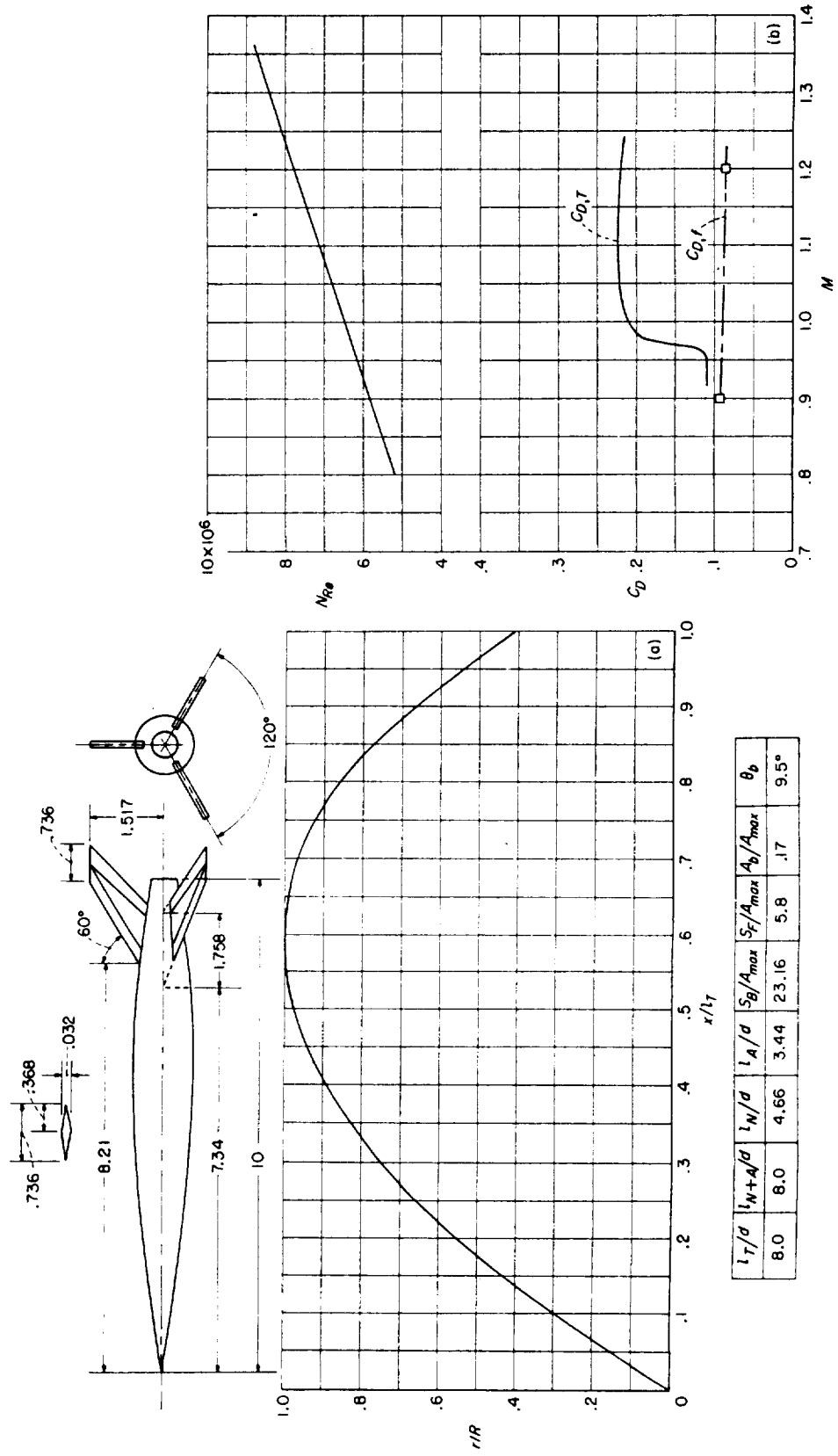

l_T/d	l_{N+A}/d	l_N/d	l_A/d	S_B/A_{max}	S_F/A_{max}	A_b/A_{max}	θ_b
8.0	8.0	4.66	3.44	23.16	5.8	.17	9.5°

(a) Body shape. (Dimensions given are in inches.) (b) N_{Re} and C_D curves.

CONFIGURATION 54; helium-gun test.

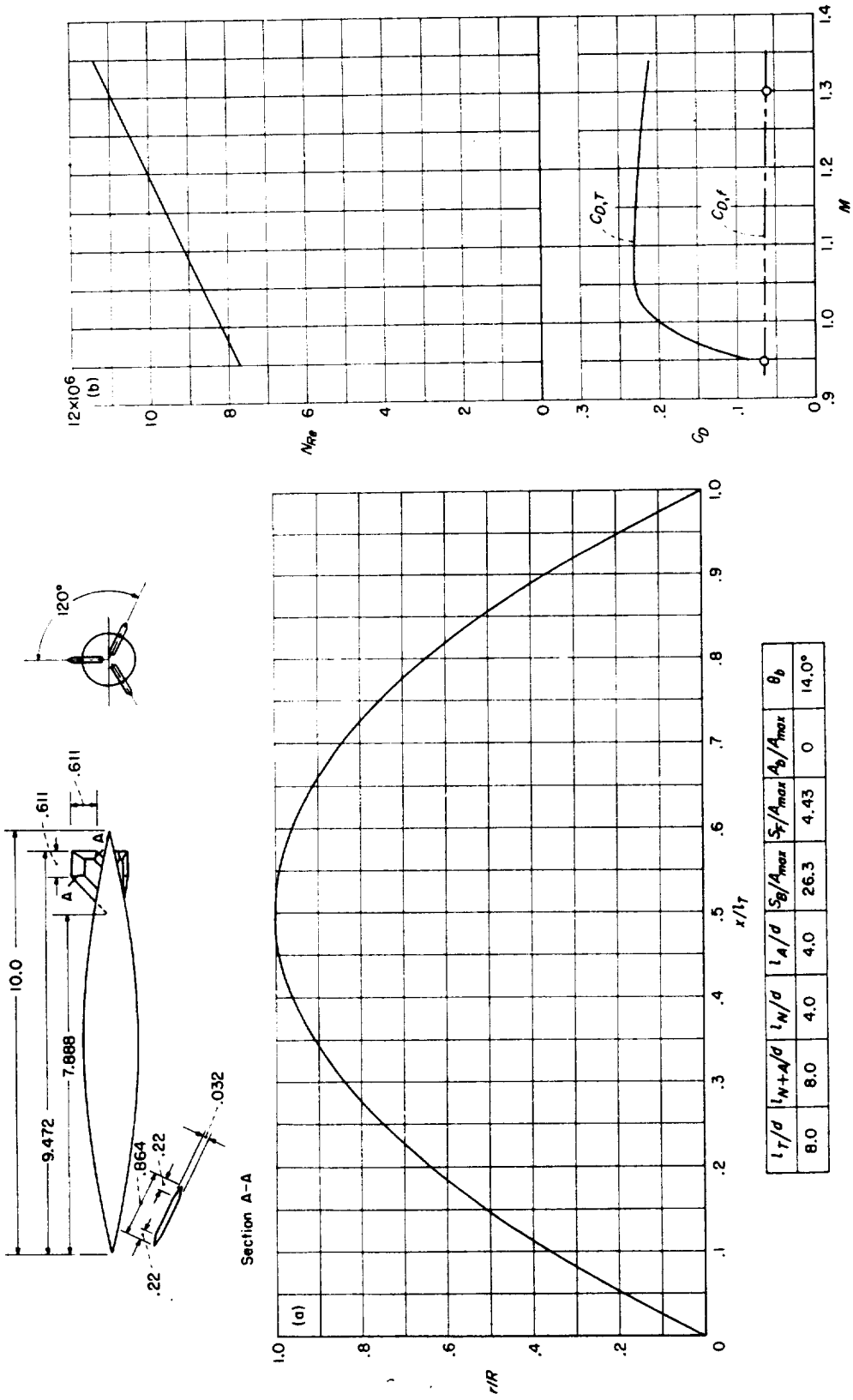

l_T/d	l_{N+A}/d	l_N/d	l_A/d	S_B/A_{max}	S_F/A_{max}	A_b/A_{max}	θ_b
8.0	8.0	4.0	4.0	26.3	4.43	0	14.0°

(a) Body shape. (Dimensions given are in inches.) (b) N_{Re} and C_D curves.

CONFIGURATION 55; helium-gun test.

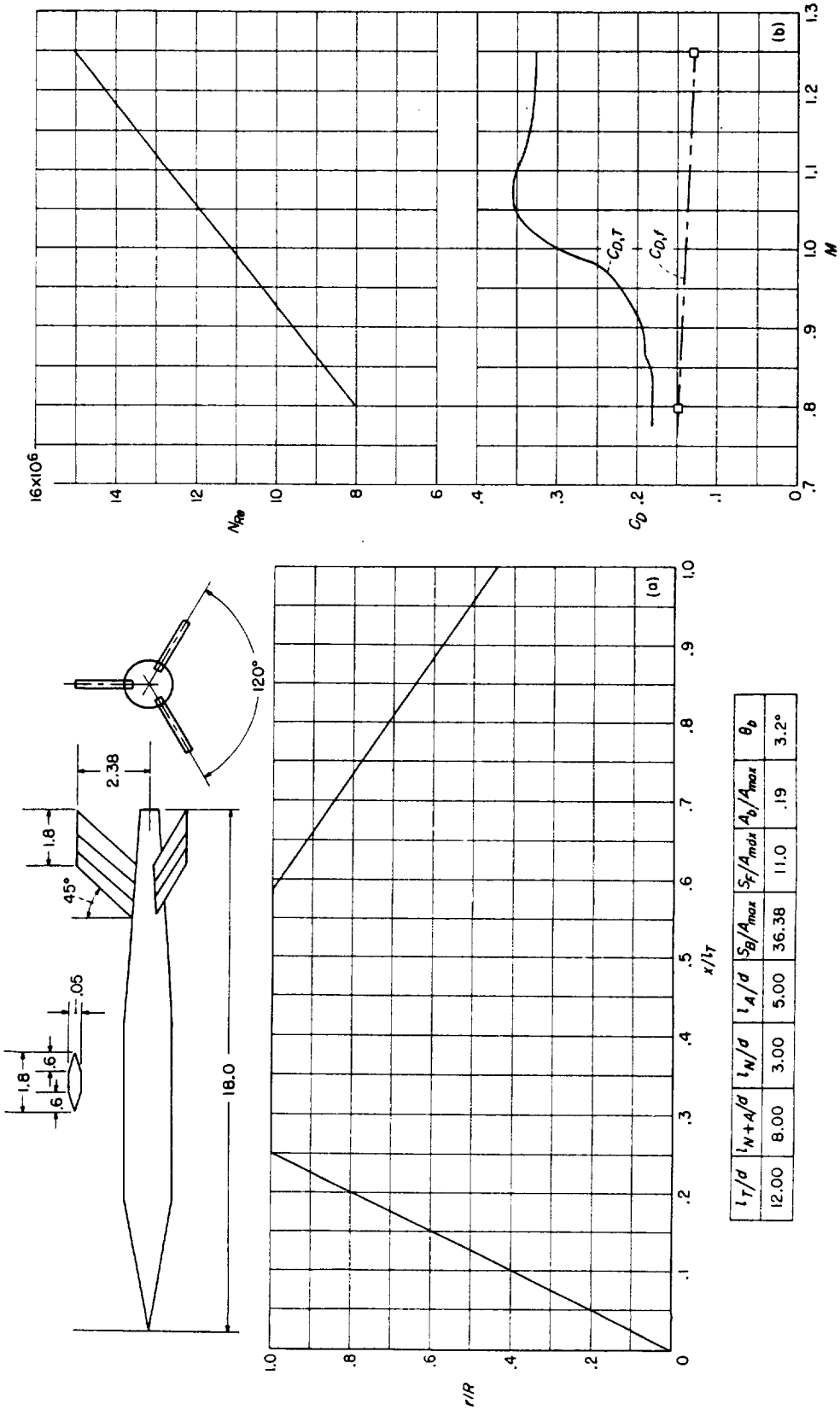

l_T/d	l_{N+A}/d	l_N/d	l_A/d	S_B/A_{max}	S_F/A_{max}	A_b/A_{max}	θ_b
12.00	8.00	3.00	5.00	36.38	11.0	.19	3.2°

(a) Body shape. (Dimensions given are in inches.) (b) N_R, and C_D curves.

CONFIGURATION 56 (conical nose and afterbody); helium-gun test.

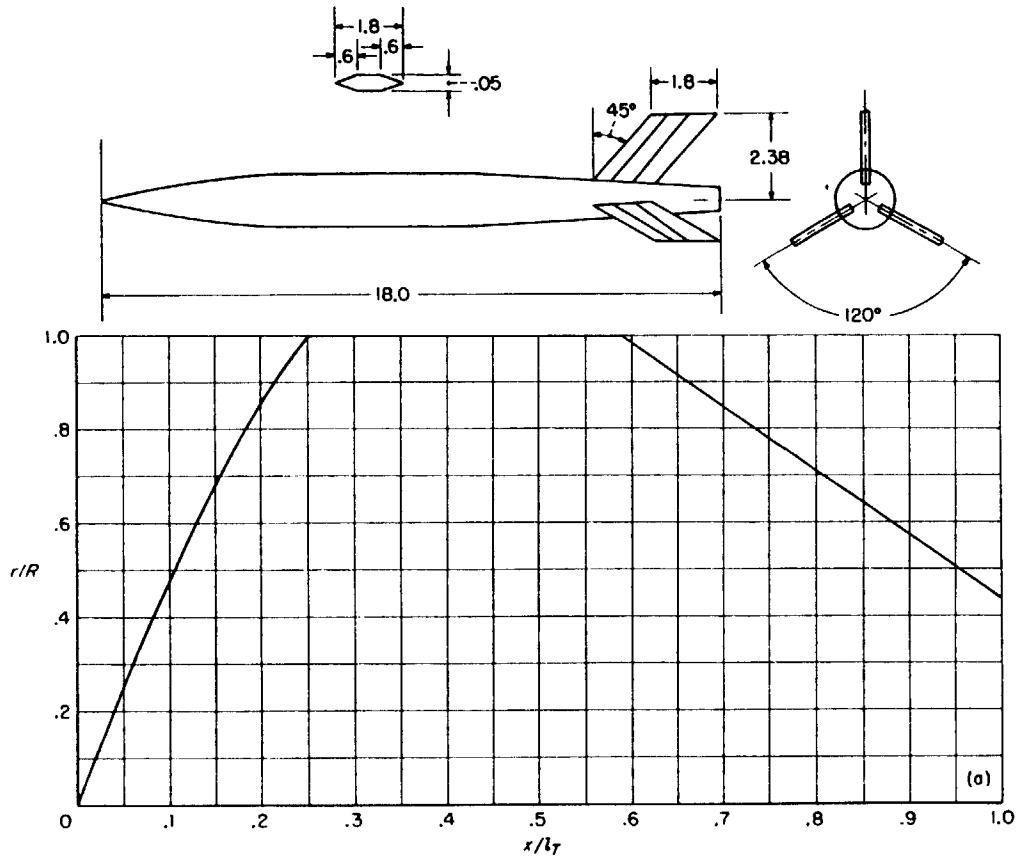

l_T/d	l_{N+A}/d	l_N/d	l_A/d	S_B/A_{max}	S_T/A_{max}	A_b/A_{max}	θ_b
12.0	8.0	3.0	5.0	37.05	11.0	.19	3.2°

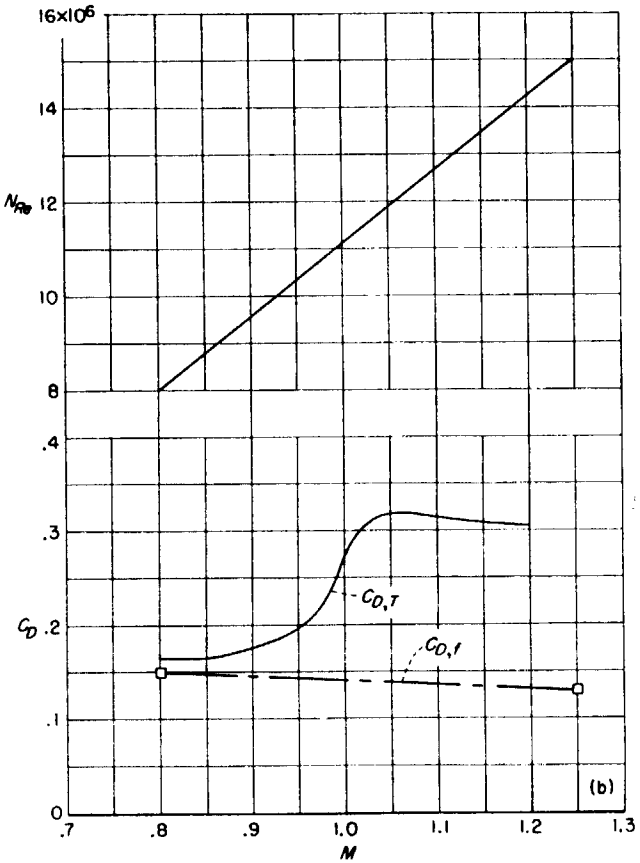

(a) Body shape. (Dimensions given are in inches.) (b) N_{R_θ} and C_D curves.

CONFIGURATION 57 $\left(\text{nose, } \frac{r}{R}=\frac{\frac{2x}{l_N}-\frac{1}{2}\left(\frac{x}{l_N}\right)^2}{1\frac{1}{2}}\text{; conical afterbody}\right)$; helium-gun test.

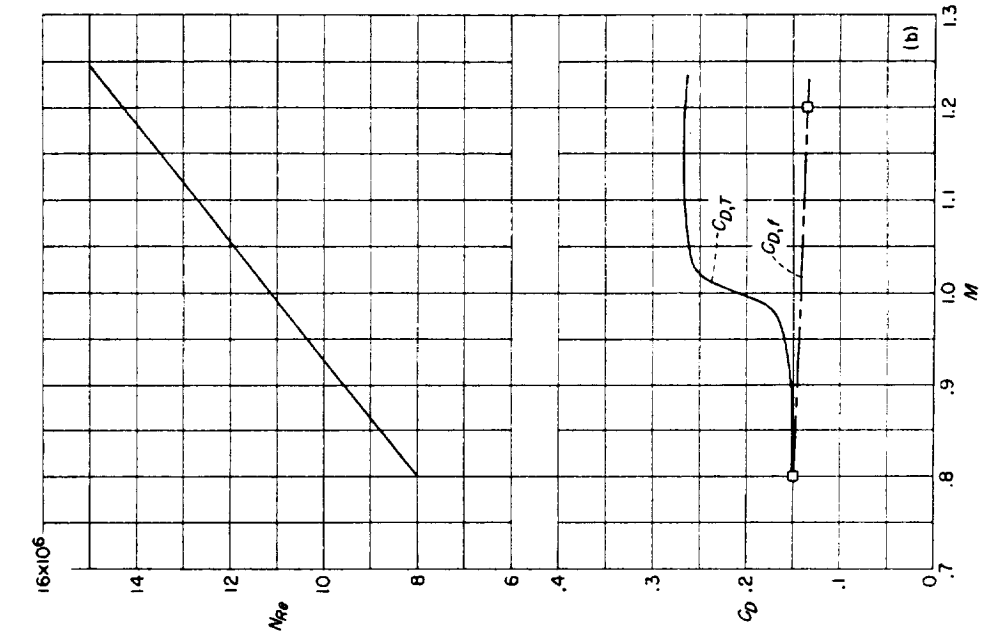

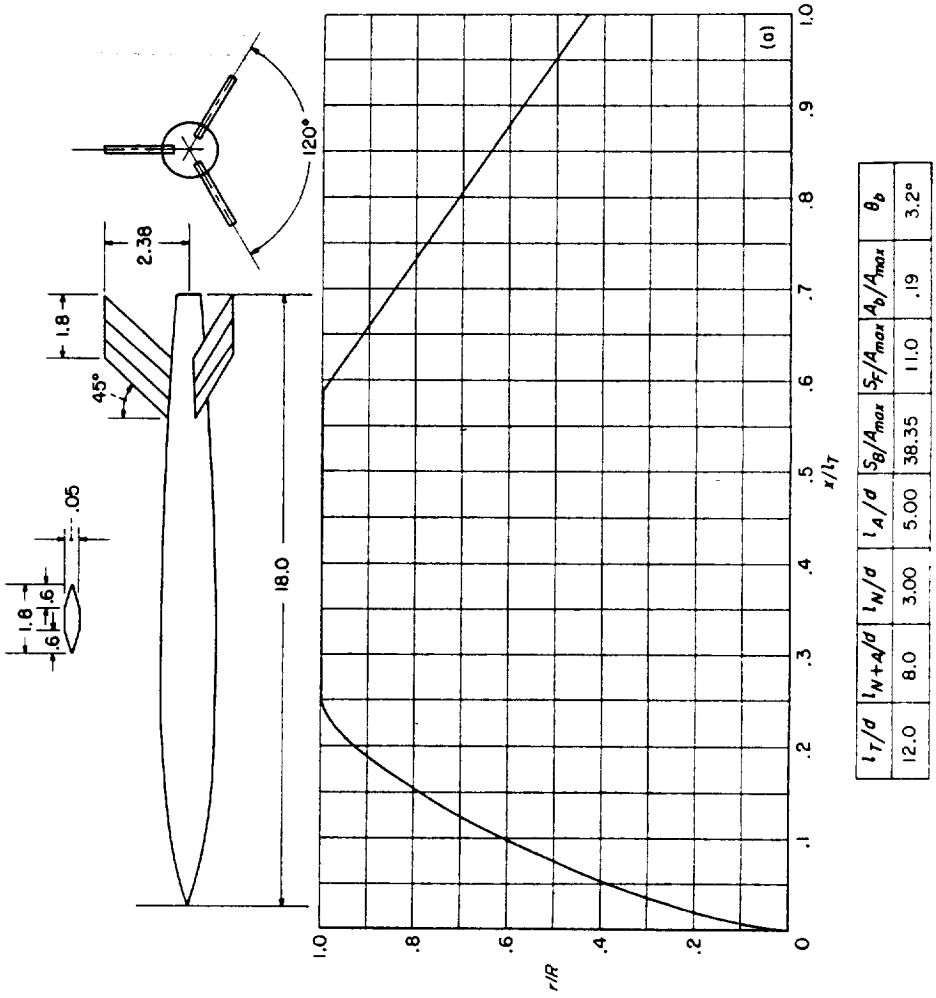

l_T/d	l_{N+A}/d	l_N/d	l_A/d	S_B/A_{max}	S_F/A_{max}	A_b/A_{max}	θ_b
12.0	8.0	3.00	5.00	38.35	11.0	.19	3.2°

(a) Body shape. (Dimensions given are in inches.) (b) N_{Re} and C_D curves.

CONFIGURATION 58 $\left(\text{nose, Von Kármán, } \frac{r}{R}=\frac{1}{\sqrt{\pi}}\sqrt{\phi-1/2\sin 2\phi} \text{ where } \phi=\cos^{-1}\left(1-\frac{2x}{l_N}\right)\right)$; conical afterbody); helium-gun test.

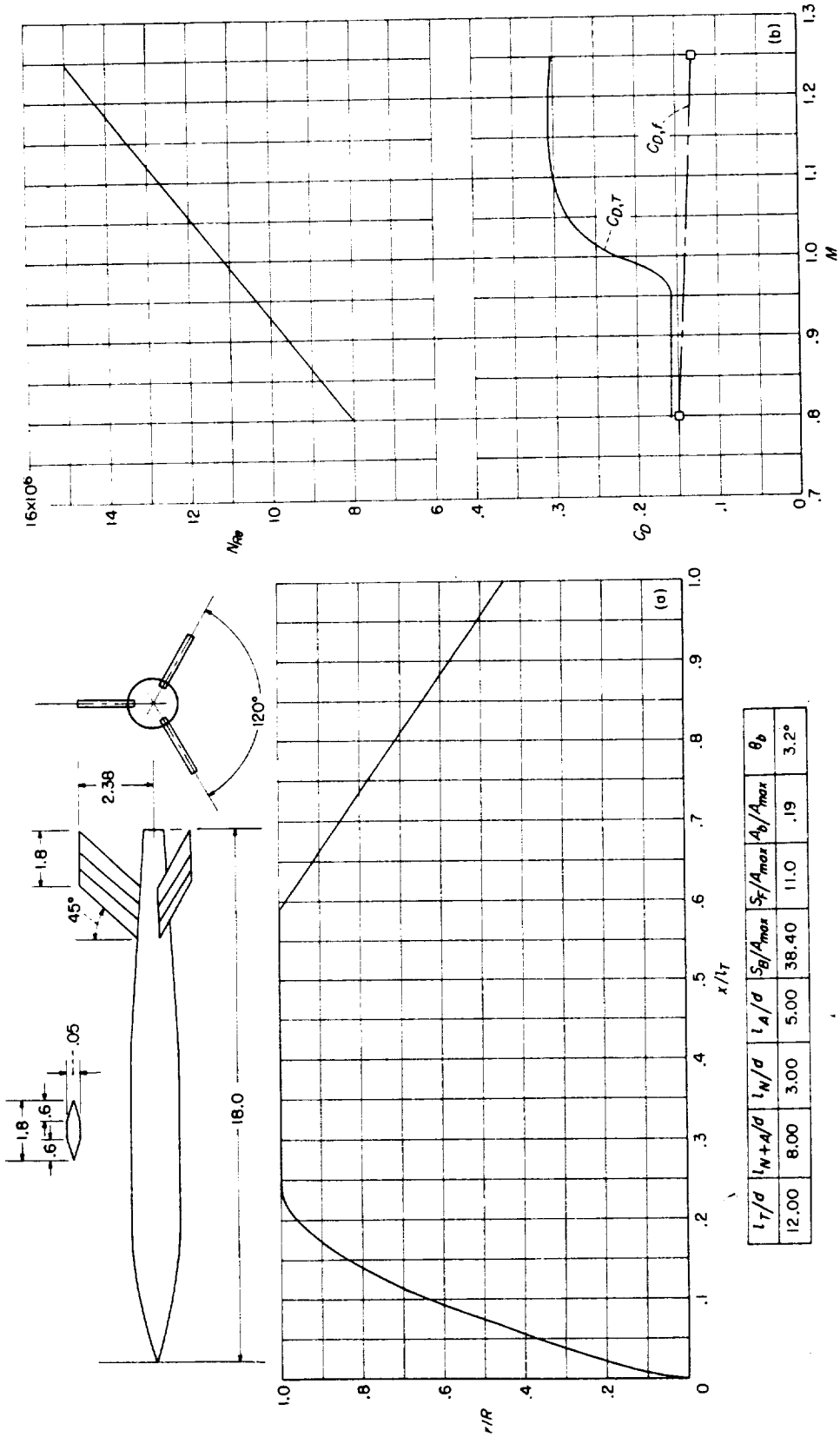

l_T/d	l_{N+A}/d	l_N/d	l_A/d	S_B/A_{max}	S_F/A_{max}	A_b/A_{max}	θ_b
12.00	8.00	3.00	5.00	38.40	11.0	.19	3.2°

(a) Body shape. (Dimensions given are in inches.) (b) N_{R_e} and C_D curves.

CONFIGURATION 50 (parabolic nose; conical afterbody); helium-gun test.

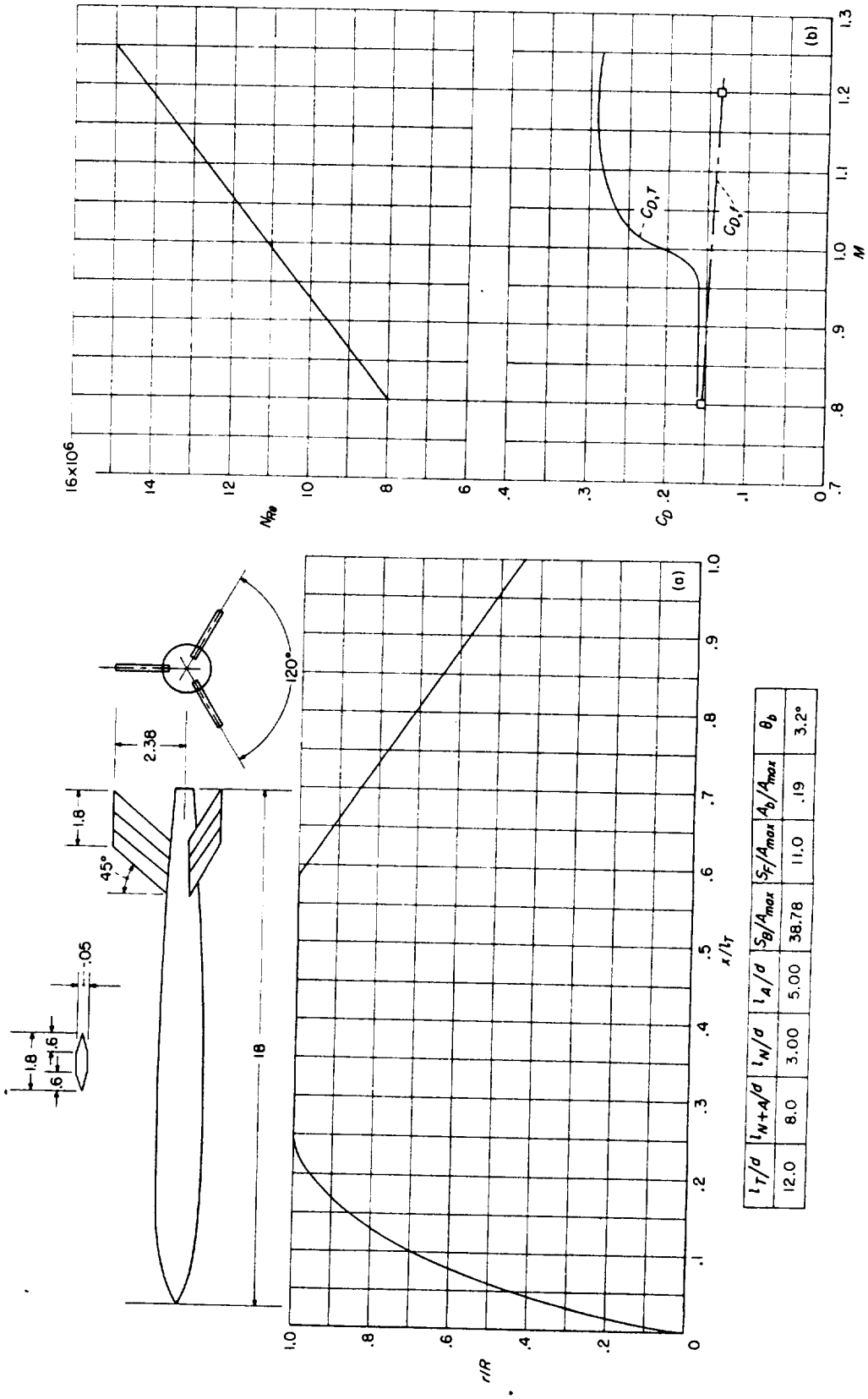

l_T/d	l_{N+A}/d	l_N/d	l_A/d	S_B/A_{max}	S_F/A_{max}	A_b/A_{max}	θ_b
12.0	8.0	3.00	5.00	38.78	11.0	.19	3.2°

(a) Body shape. (Dimensions given are in inches.) (b) N_{Re} and C_D curves.

CONFIGURATION 60 (nose, L-V Haack, $\frac{r}{R}=\frac{1}{\sqrt{\pi}}\sqrt{\phi-1/2\sin 2\phi+1/3\sin^3\phi}$ where $\phi=\cos^{-1}\left(1-\frac{2x}{l_N}\right)$); helium-gun test.

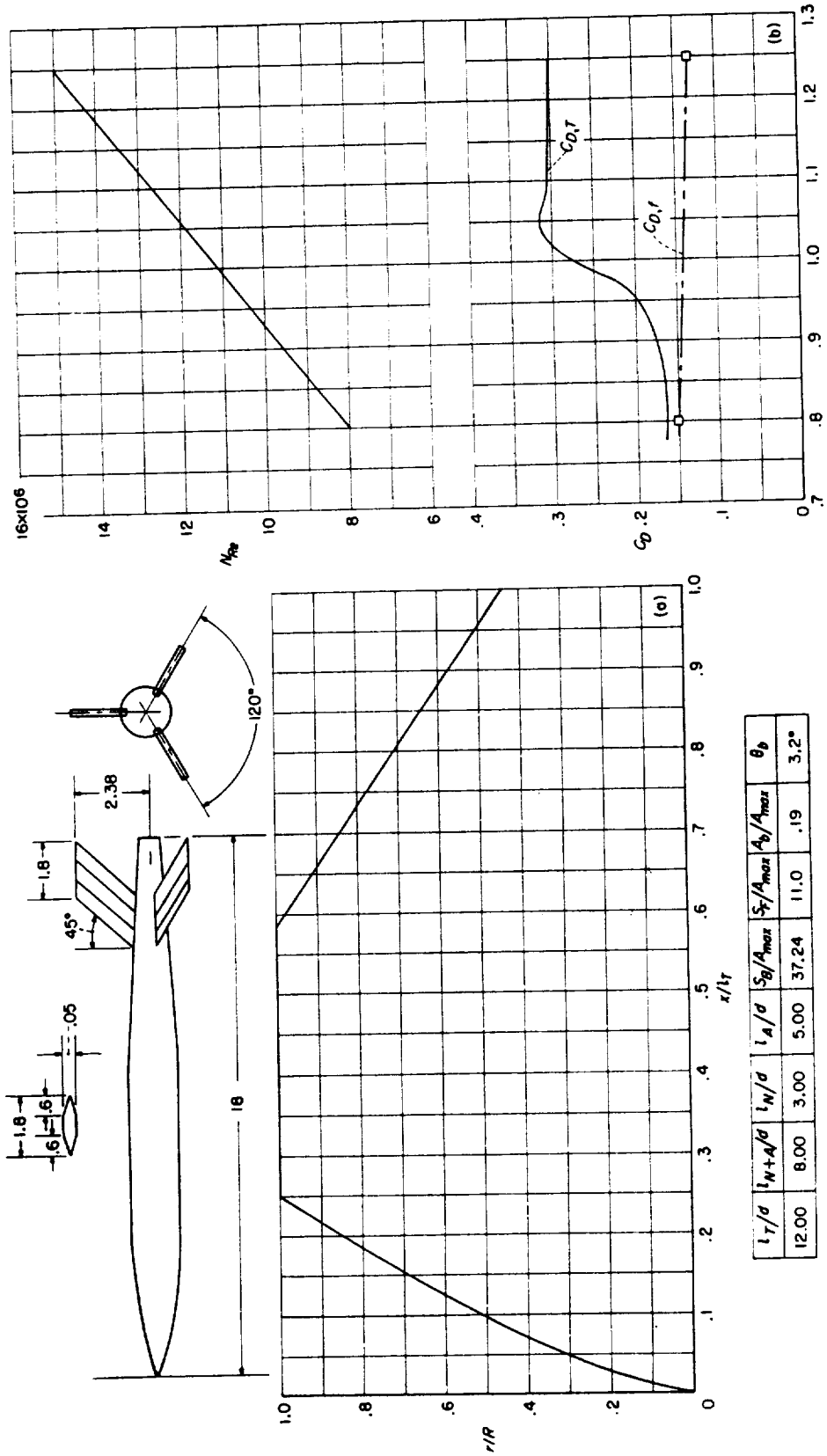

l_T/d	l_{N+A}/d	l_N/d	l_A/d	S_B/A_{max}	S_T/A_{max}	A_b/A_{max}	θ_b
12.00	8.00	3.00	5.00	37.24	11.0	.19	3.2°

(a) Body shape. (Dimensions given are in inches.) (b) N_{Re} and C_D curves.

CONFIGURATION 61 $\left(\text{nose, } \frac{r}{R}=\left(\frac{x}{l_N}\right)^{3/4}\right)$; helium-gun test.

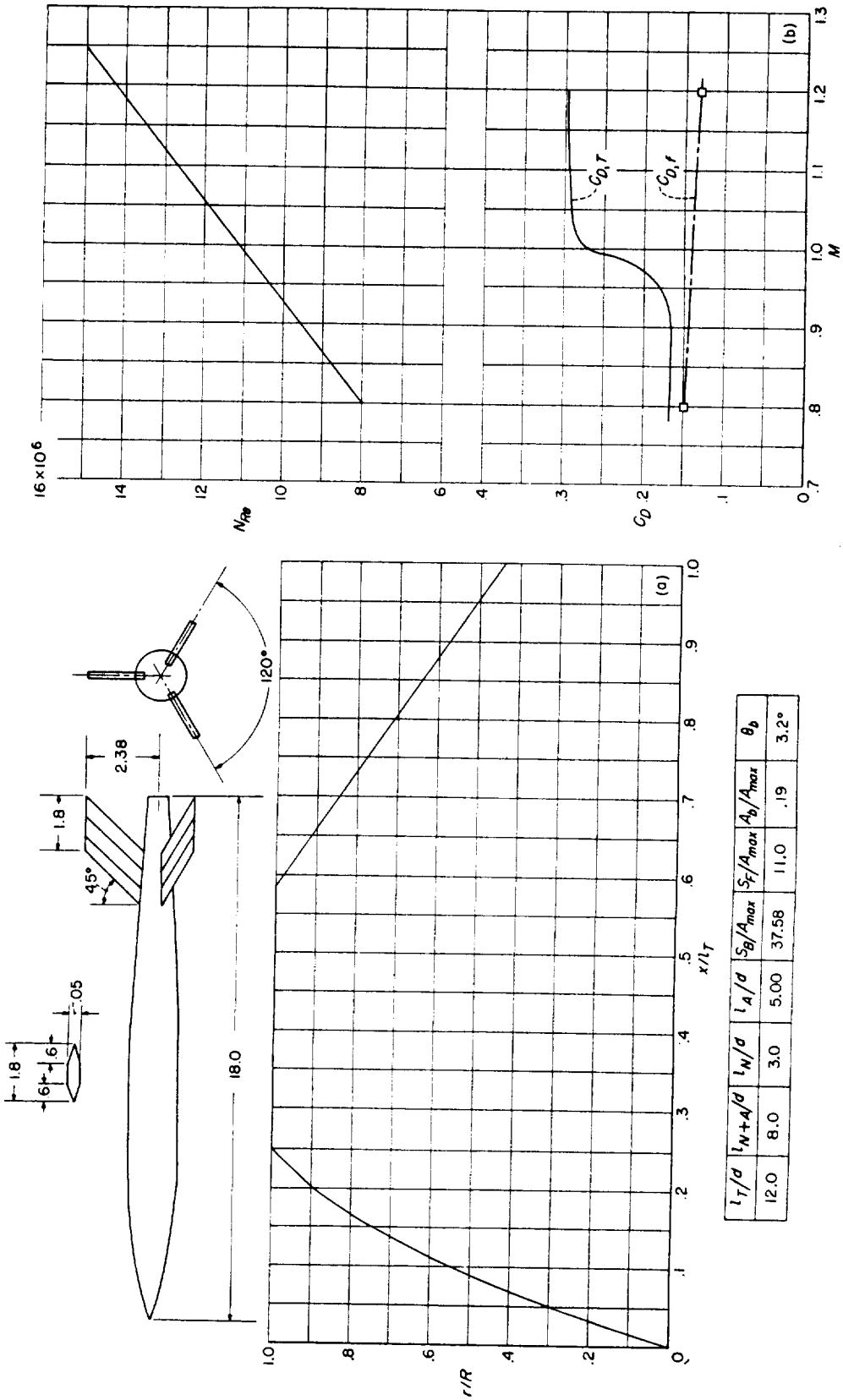

l_T/d	l_{N+A}/d	l_N/d	l_A/d	S_B/A_{max}	S_F/A_{max}	A_b/A_{max}	θ_b
12.0	8.0	3.0	5.00	37.58	11.0	.19	3.2°

(a) Body shape. (Dimensions given are in inches.) (b) N_{Re} and C_D curves.

CONFIGURATION 62 (nose, $\frac{r}{R}=\frac{\frac{2x}{l_N}-\frac{3}{4}\left(\frac{x}{l_N}\right)^2}{1.25}$); helium-gun test.

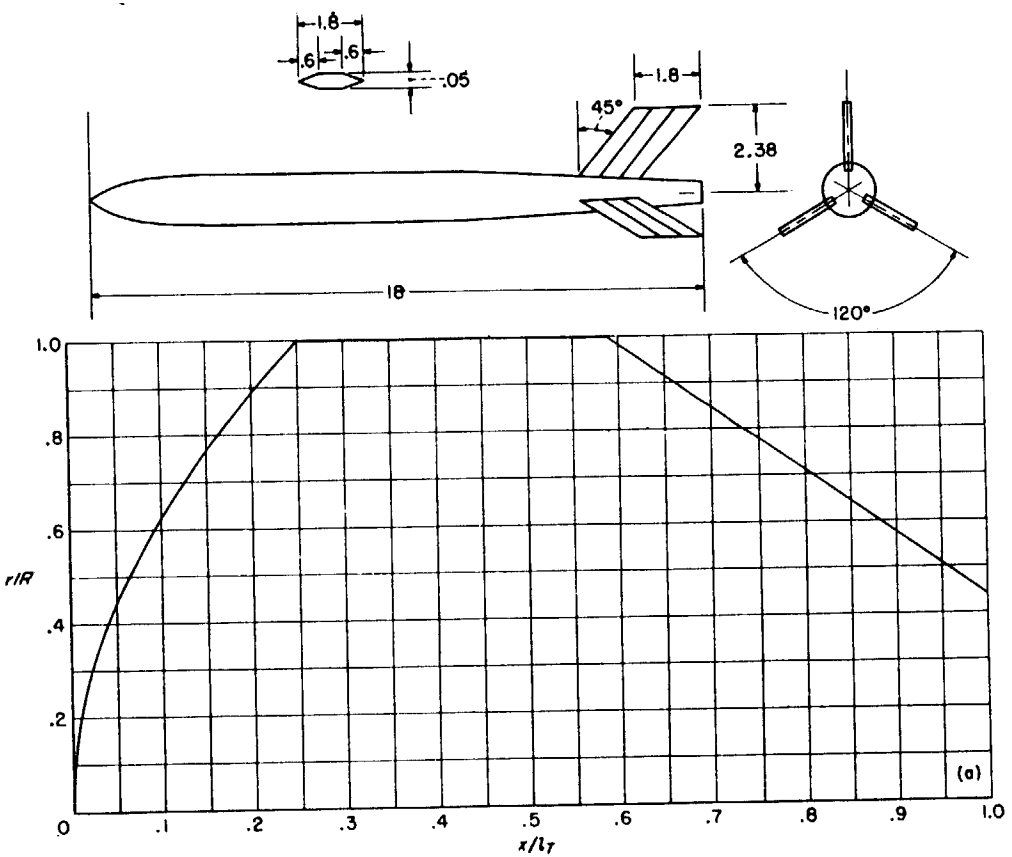

l_T/d	l_{N+A}/d	l_N/d	l_A/d	S_B/A_{max}	S_F/A_{max}	A_b/A_{max}	θ_b
12.00	8.00	3.00	5.00	38.40	11.0	.19	3.2°

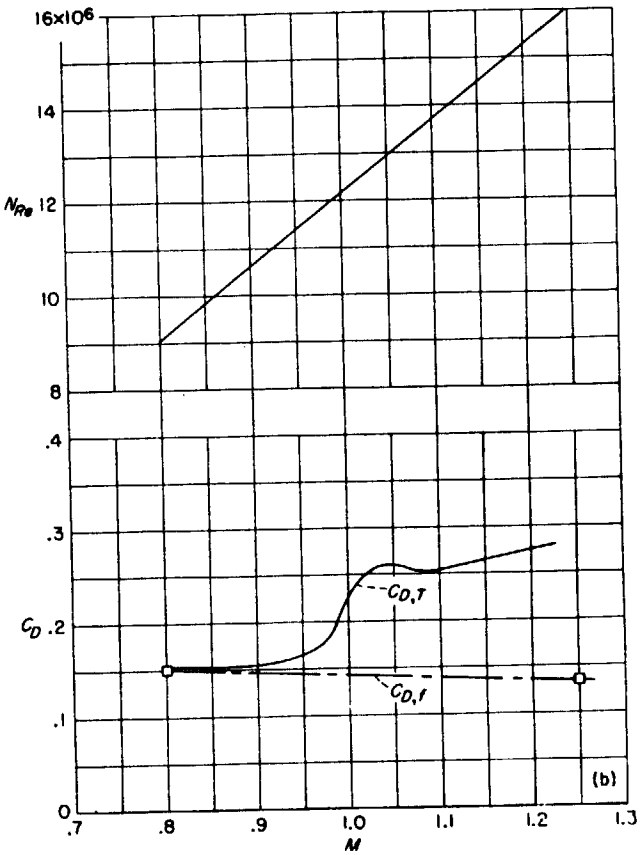

(a) Body shape. (Dimensions given are in inches.) (b) N_{R_θ} and C_D curves.

CONFIGURATION 63 $\left(\text{nose, } \frac{r}{R}=\frac{x}{l_N}\frac{1}{2}\text{; conical afterbody}\right)$; helium-gun test.

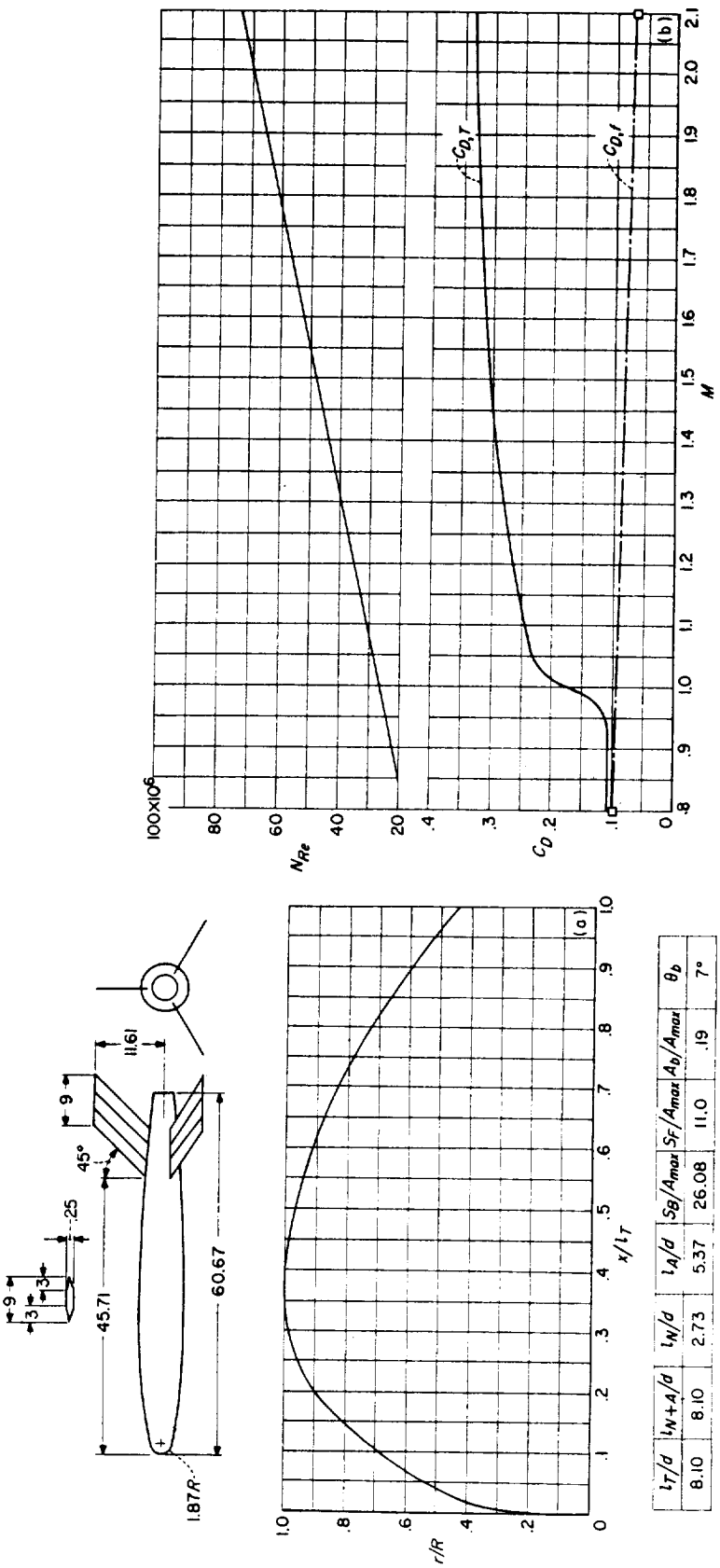

l_T/d	l_N+A/d	l_N/d	l_A/d	S_B/A_{max}	S_F/A_{max}	A_b/A_{max}	θ_b
8.10	8.10	2.73	5.37	26.08	11.0	.19	7°

(a) Body shape. (Dimensions given are in inches.) (b) N_{Re} and C_D curves.

CONFIGURATION 64 (nose consists of hemispherical and parabolic segments; parabolic afterbody); rocket test.

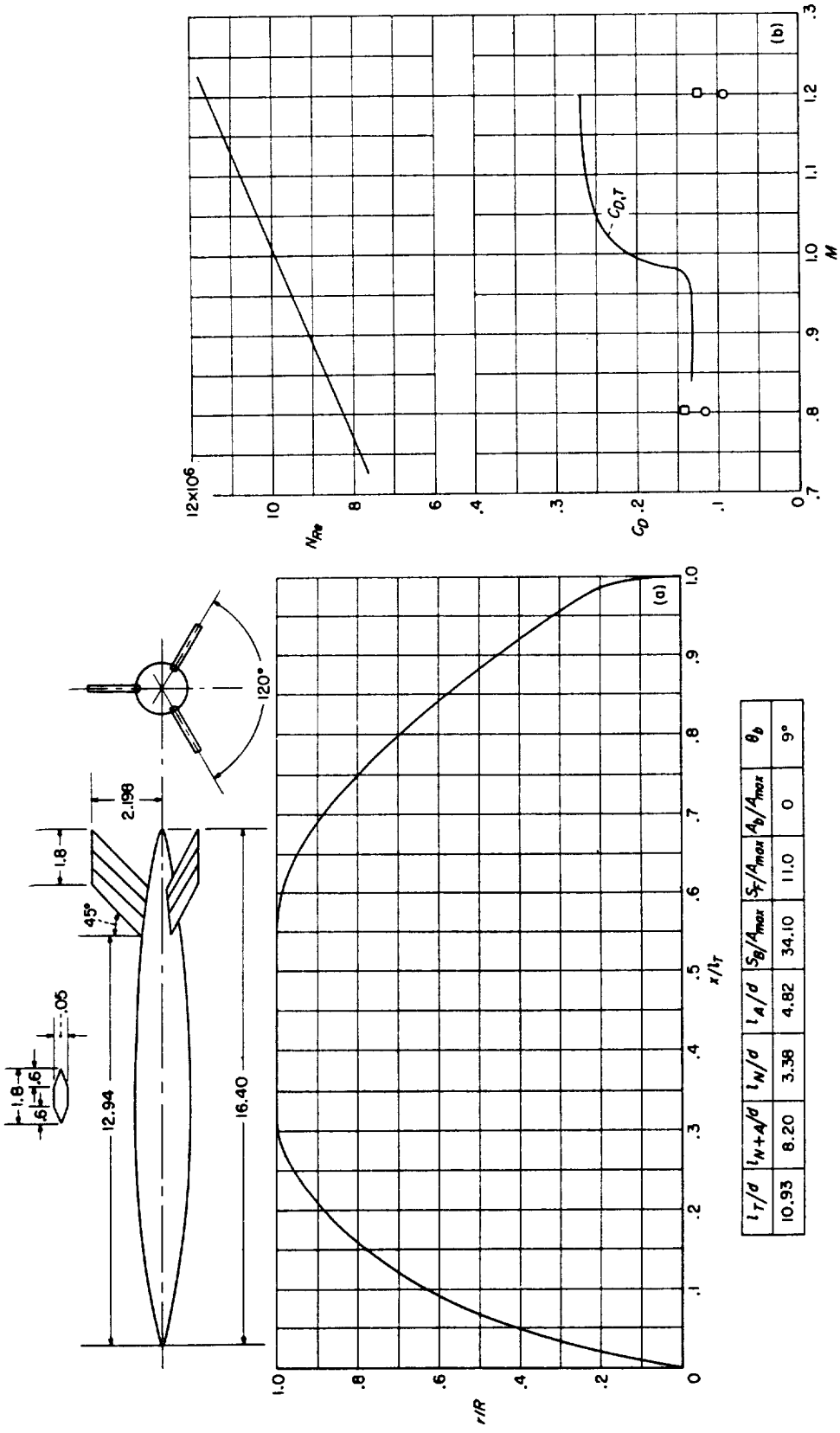

l_T/d	l_{N+A}/d	l_N/d	l_A/d	S_B/A_{max}	S_F/A_{max}	A_b/A_{max}	θ_b
10.93	8.20	3.38	4.82	34.10	11.0	0	9°

(a) Body shape. (Dimensions given are in inches.) (b) N_{Re} and C_D curves

CONFIGURATION 65; helium-gun test.

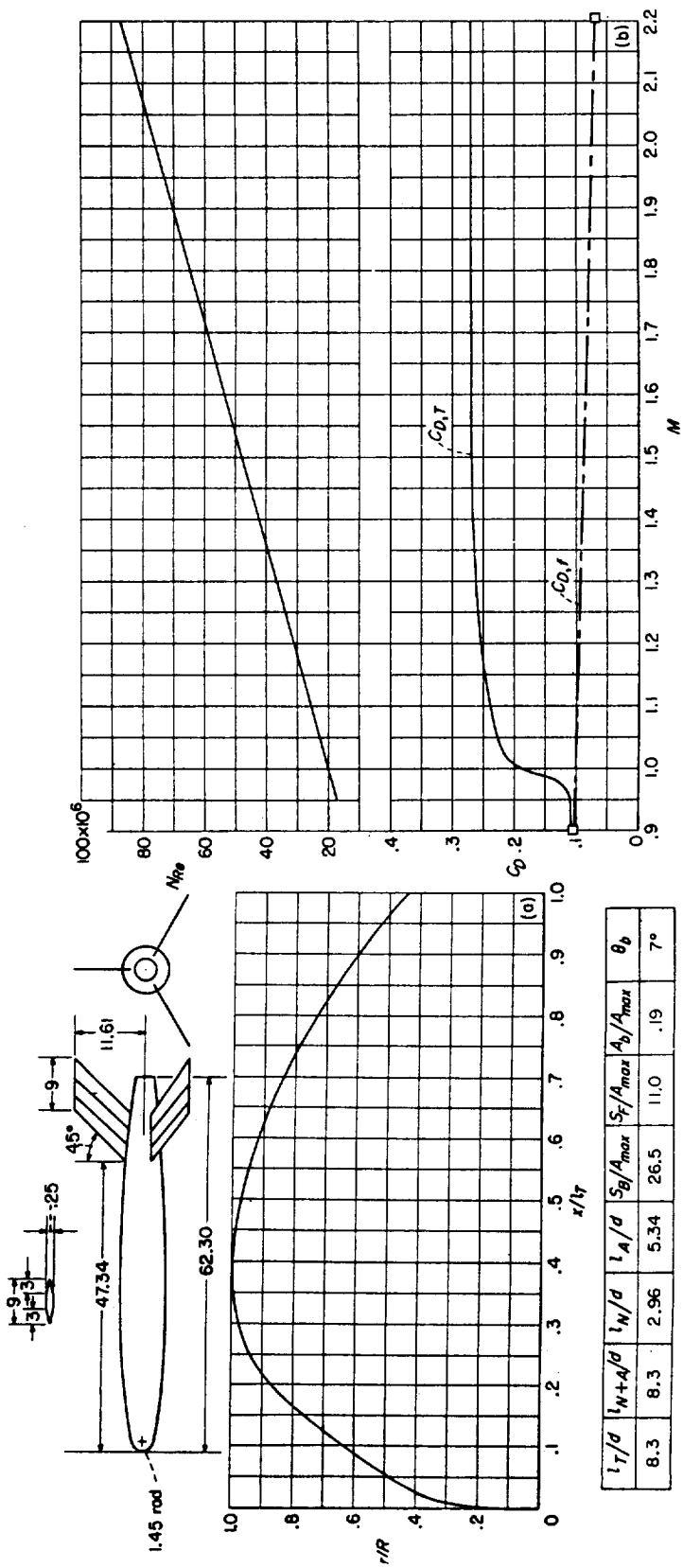

l_T/d	l_{N+A}/d	l_N/d	l_A/d	S_B/A_{max}	S_F/A_{max}	A_b/A_{max}	θ_b
8.3	8.3	2.96	5.34	26.5	11.0	.19	7°

(a) Body shape. (Dimensions given are in inches.) (b) N_{Re} and C_D curves.

CONFIGURATION 66 (nose consists of hemispherical and parabolic segments; parabolic afterbody); rocket test.

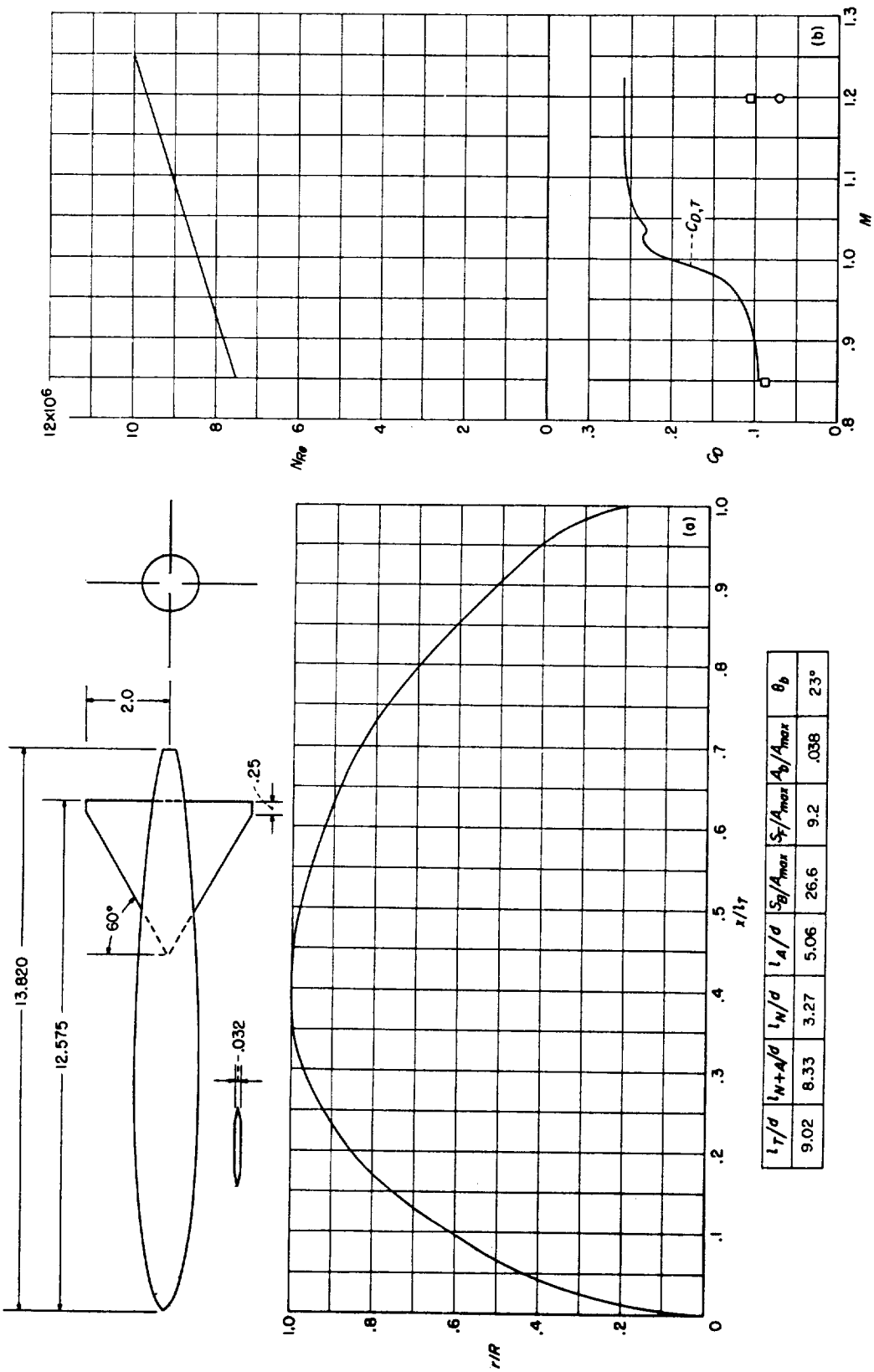

l_T/d	l_{N+A}/d	l_N/d	l_A/d	S_B/A_{max}	S_F/A_{max}	A_b/A_{max}	θ_b
9.02	8.33	3.27	5.06	26.6	9.2	.038	23°

(a) Body shape. (Dimensions given are in inches.) (b) N_{Re} and C_D curves.

CONFIGURATION 67; helium-gun test.

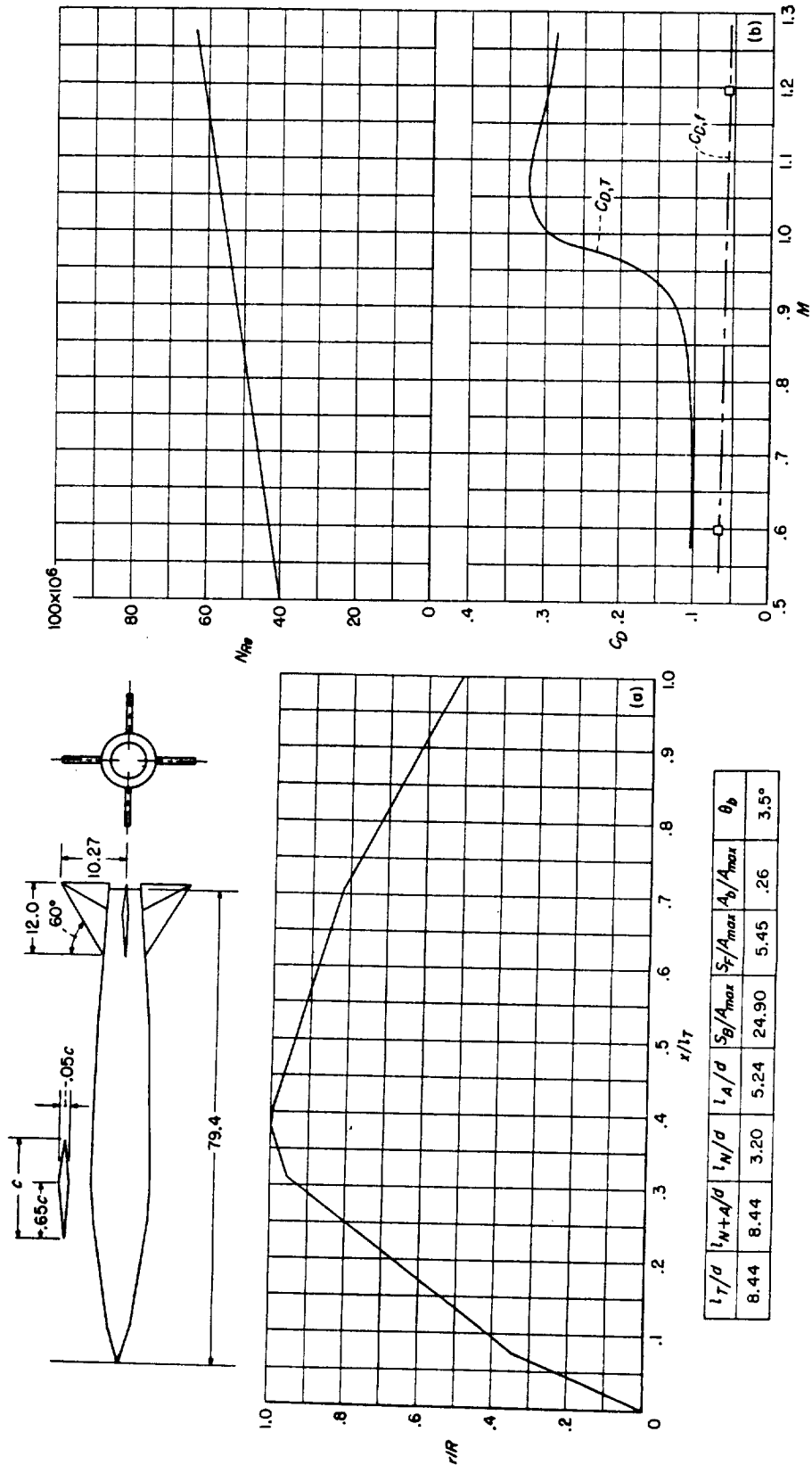

l_T/d	l_{N+A}/d	l_N/d	l_A/d	S_B/A_{max}	S_F/A_{max}	A_b/A_{max}	θ_b
8.44	8.44	3.20	5.24	24.90	5.45	.26	3.5°

(a) Body shape. (Dimensions given are in inches.) (b) N_{R_e} and C_D curves.

CONFIGURATION 68 (all conical sections); rocket test.

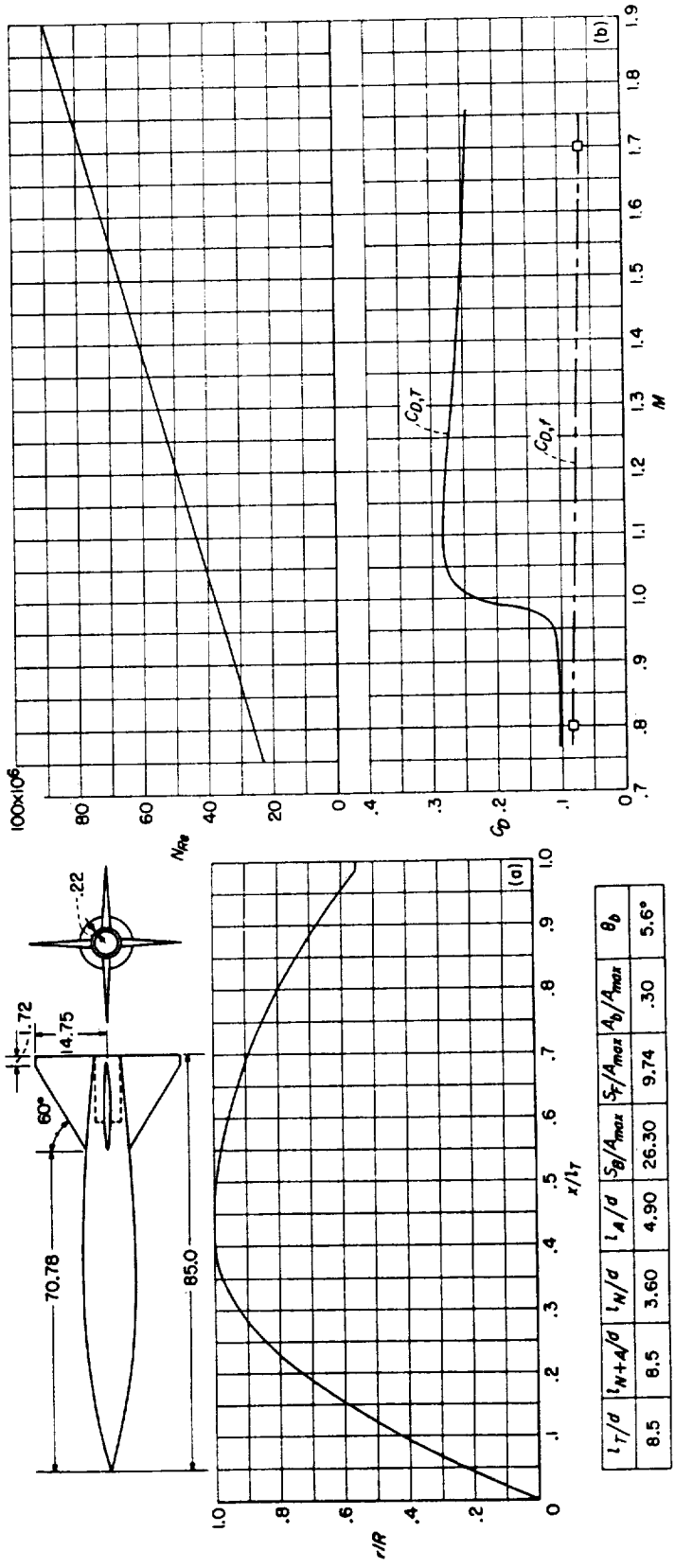

l_T/d	l_{N+A}/d	l_N/d	l_A/d	S_B/A_{max}	S_F/A_{max}	A_b/A_{max}	θ_b
8.5	8.5	3.60	4.90	26.30	9.74	.30	5.6°

(a) Body shape. (Dimensions given are in inches.) (b) N_{Re} and C_D curves.

CONFIGURATION 69; rocket test.

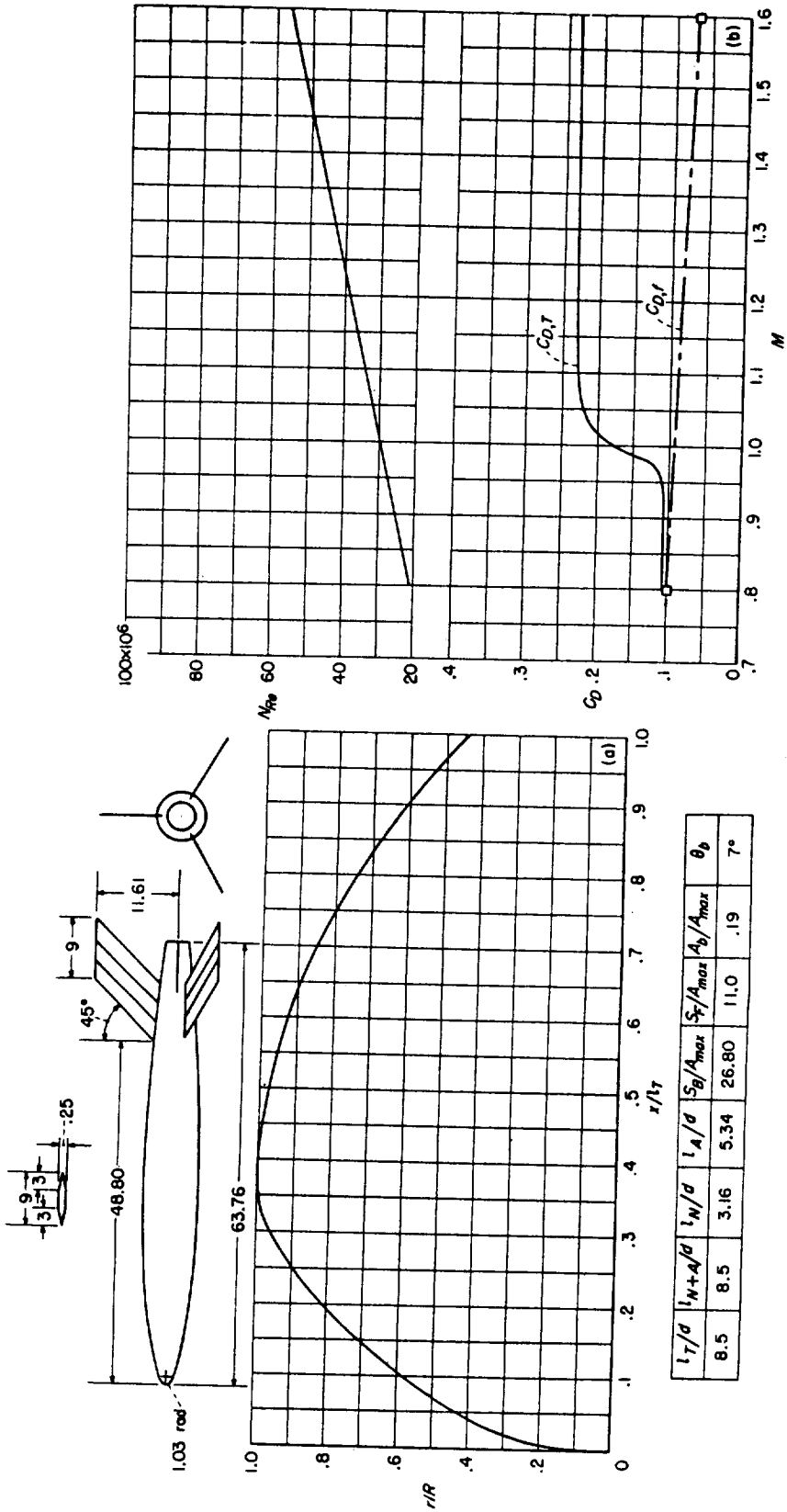

l_T/d	l_{N+A}/d	l_N/d	l_A/d	S_B/A_{max}	S_F/A_{max}	A_b/A_{max}	θ_b
8.5	8.5	3.16	5.34	26.80	11.0	.19	7°

(a) Body shape. (Dimensions given are in inches.) (b) N_{Re} and C_D curves.

CONFIGURATION 70 (nose consists of hemispherical and parabolic segments; parabolic afterbody); rocket test.

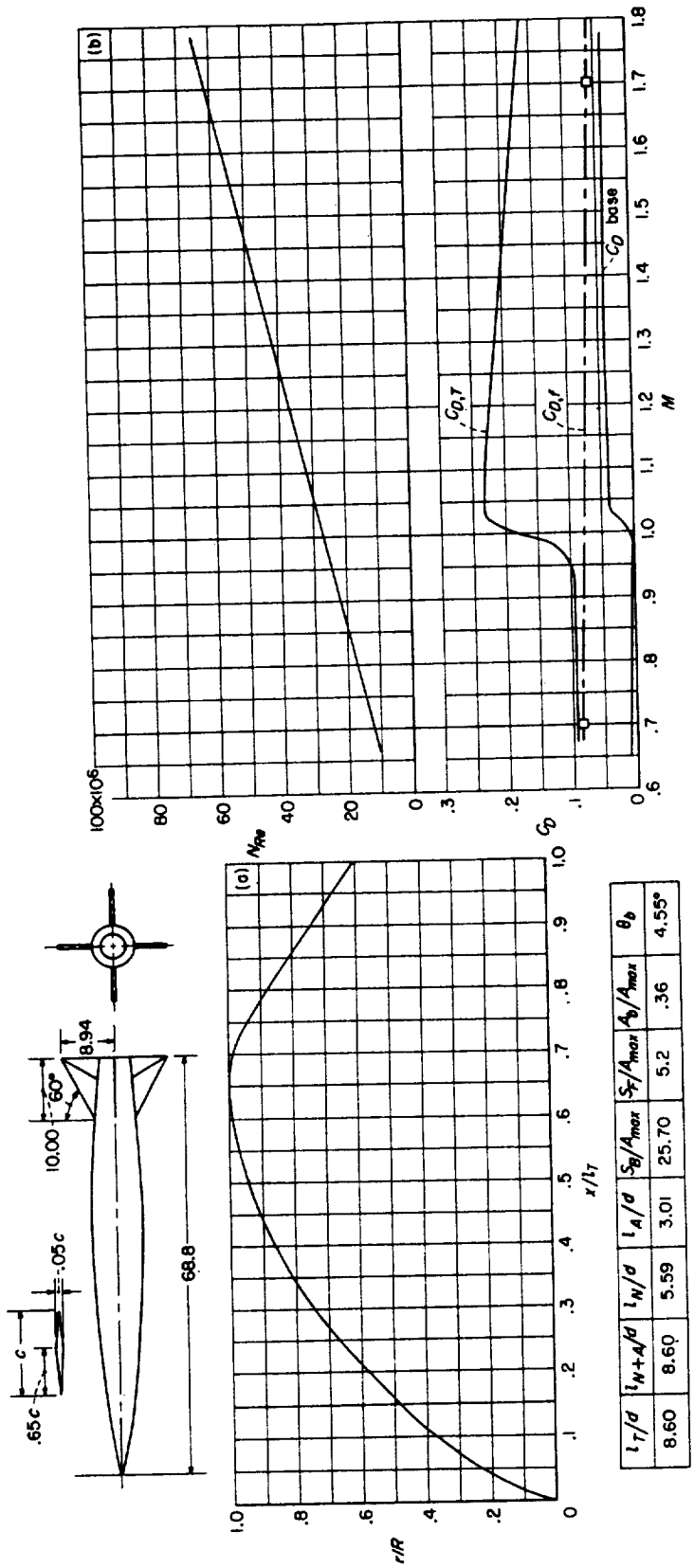

l_T/d	l_{N+A}/d	l_N/d	l_A/d	S_B/A_{max}	S_F/A_{max}	A_b/A_{max}	θ_b
8.60	8.60	5.59	3.01	25.70	5.2	.36	4.55°

(a) Body shape. (Dimensions given are in inches.) (b) N_{Re} and C_D curves.

CONFIGURATION 71; rocket test.

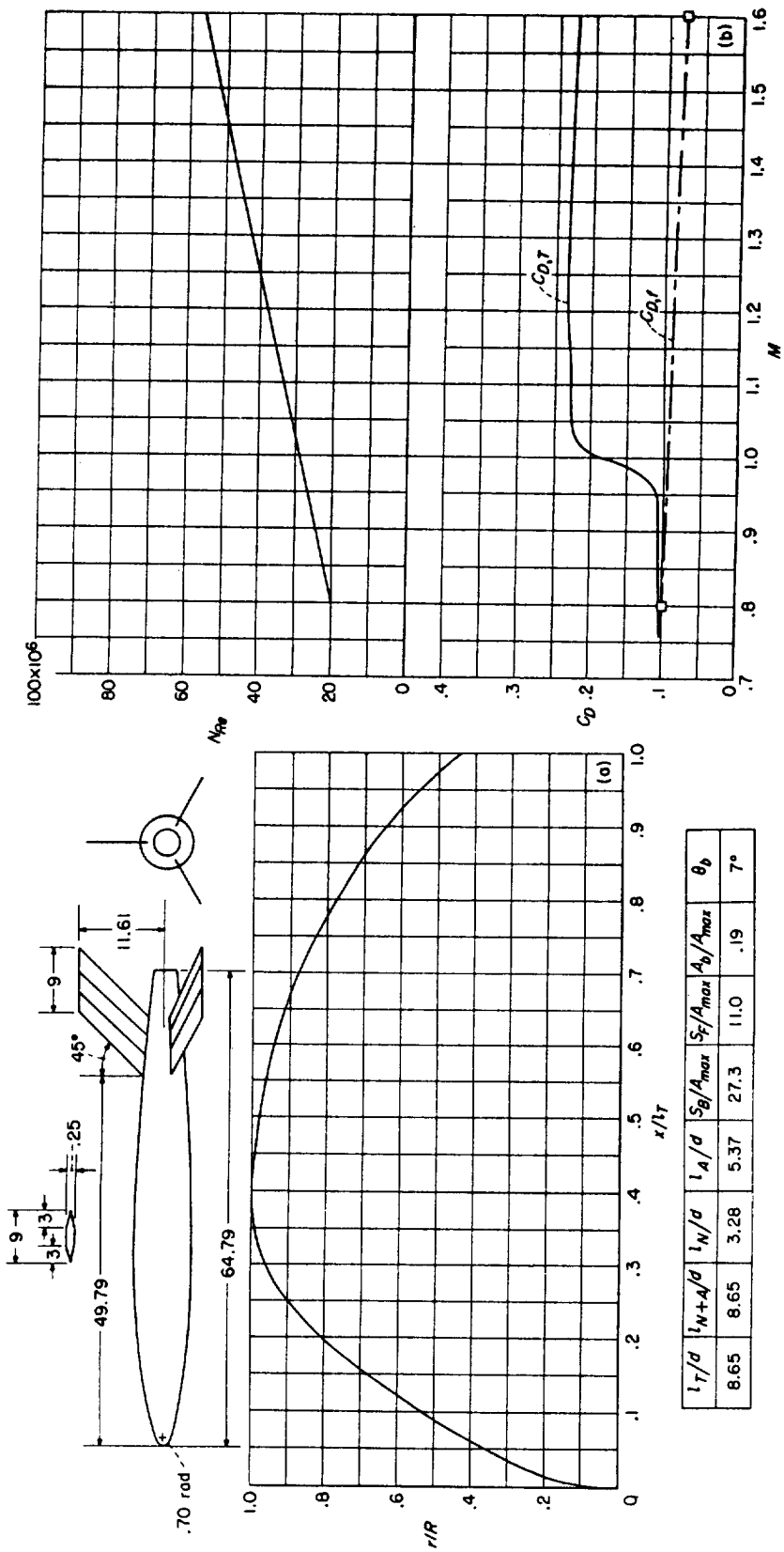

l_T/d	l_{N+A}/d	l_N/d	l_A/d	S_B/A_{max}	S_F/A_{max}	A_b/A_{max}	θ_b
8.65	8.65	3.28	5.37	27.3	11.0	.19	7°

(a) Body shape. (Dimensions given are in inches.) (b) N_{R_e} and C_D curves.

CONFIGURATION 72 (nose consists of hemispherical and parabolic segments; parabolic afterbody); rocket test.

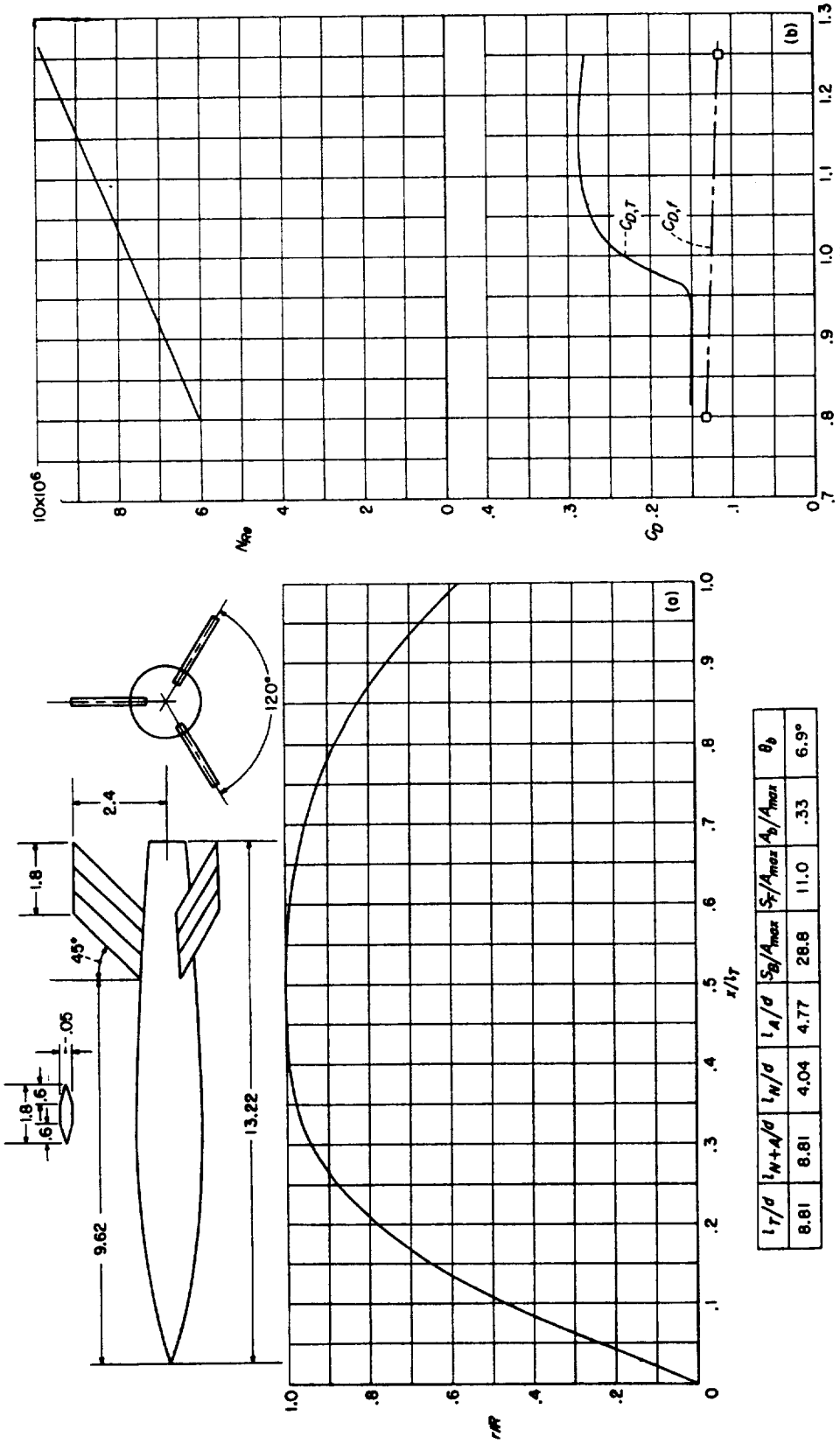

l_T/d	l_{N+A}/d	l_N/d	l_A/d	S_B/A_{max}	S_F/A_{max}	A_b/A_{max}	θ_b
8.81	8.81	4.04	4.77	28.8	11.0	.33	6.9°

(a) Body shape. (Dimensions given are in inches.) (b) N_{R_D} and C_D curves.

CONFIGURATION 73; helium-gun test.

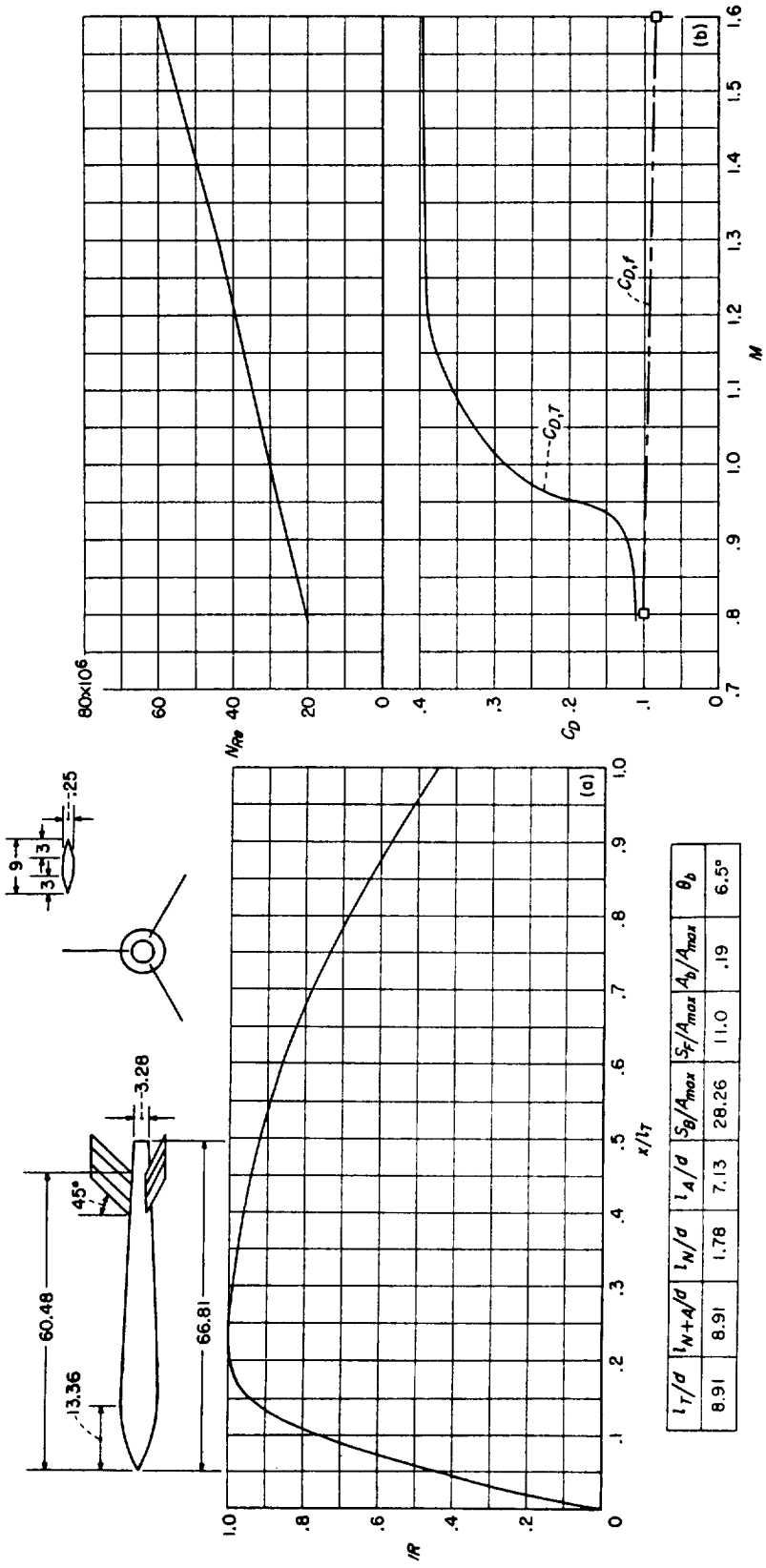

l_T/d	l_{N+A}/d	l_N/d	l_A/d	S_B/A_{max}	S_F/A_{max}	A_b/A_{max}	θ_b
8.91	8.91	1.78	7.13	28.26	11.0	.19	6.5°

(a) Body shape. (Dimensions given are in inches.) (b) N_{Re} and C_D curves.

CONFIGURATION 74 (parabolic nose and afterbody); rocket test.

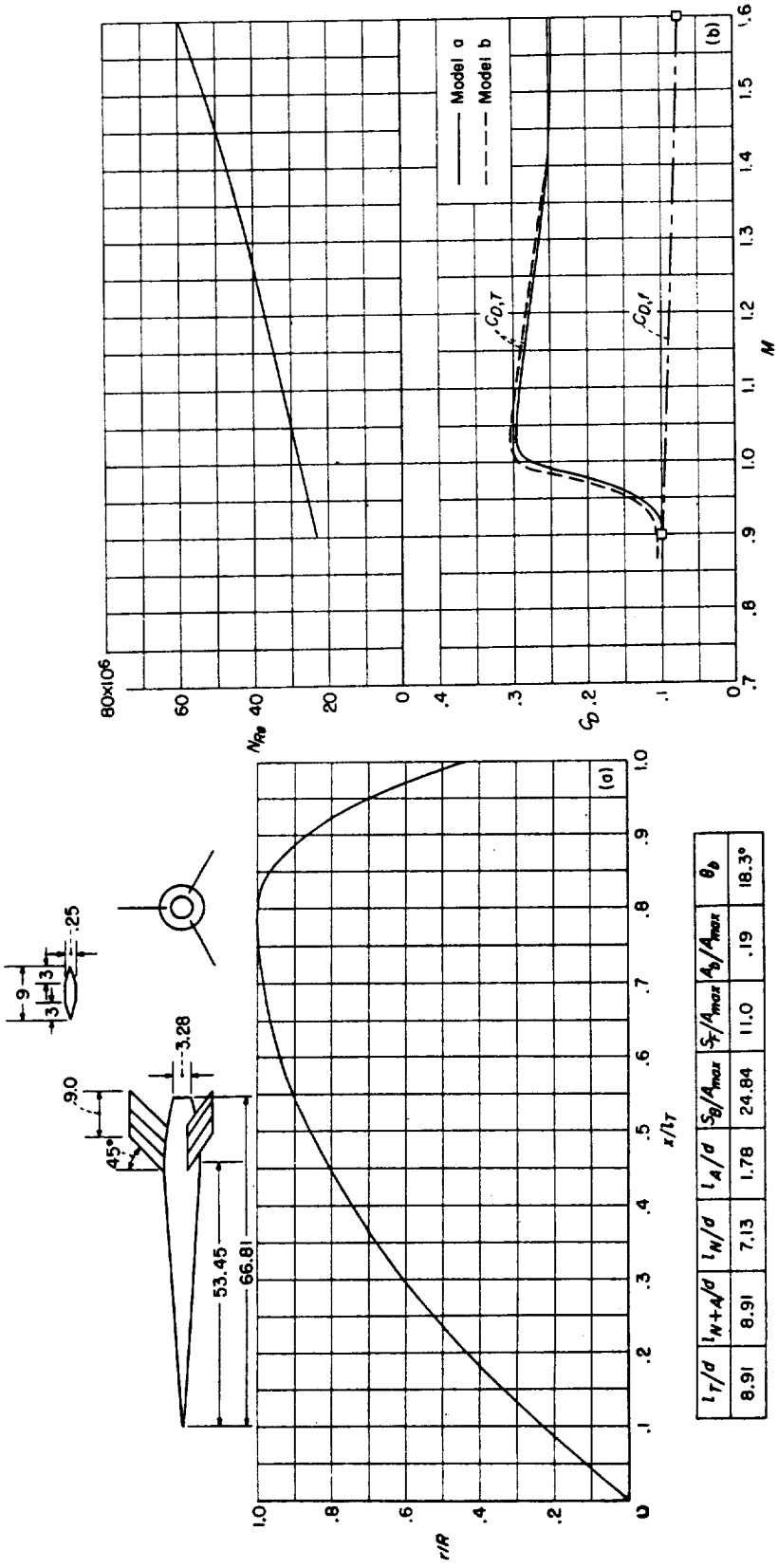

l_T/d	l_{N+A}/d	l_N/d	l_A/d	S_B/A_{max}	S_F/A_{max}	A_b/A_{max}	θ_b
8.91	8.91	7.13	1.78	24.84	11.0	.19	18.3°

(a) Body shape. (Dimensions given are in inches.) (b) N_{Re} and C_D curves.

CONFIGURATION 75 (parabolic nose and afterbody); rocket test.

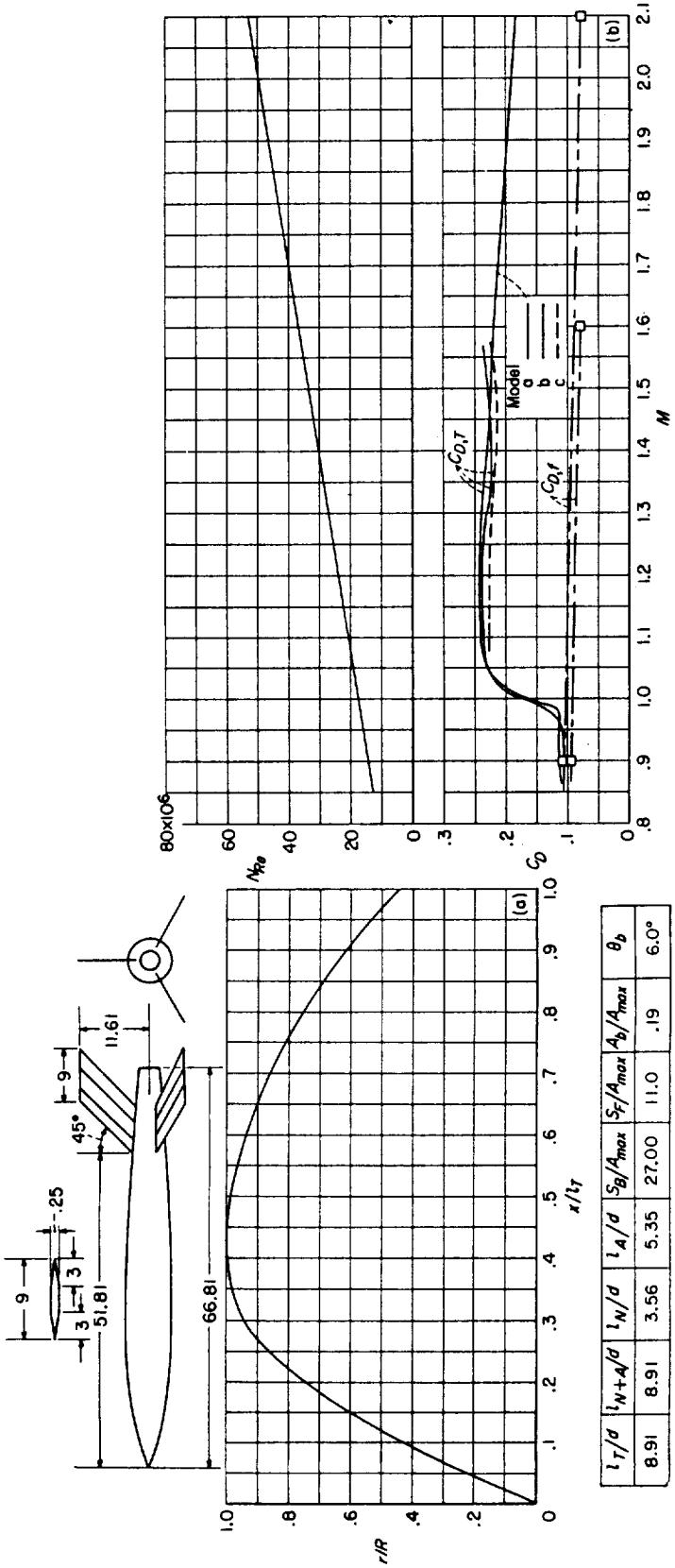

l_T/d	l_{N+A}/d	l_N/d	l_A/d	S_B/A_{max}	S_F/A_{max}	A_b/A_{max}	θ_b
8.91	8.91	3.56	5.35	27.00	11.0	.19	6.0°

(a) Body shape. (Dimensions given are in inches.) (b) N_{R_θ} and C_D curves.

CONFIGURATION 76 (parabolic nose and afterbody; waviness of coefficient of low Mach number models probably due to afterburning of their sustainer rockets); rocket test.

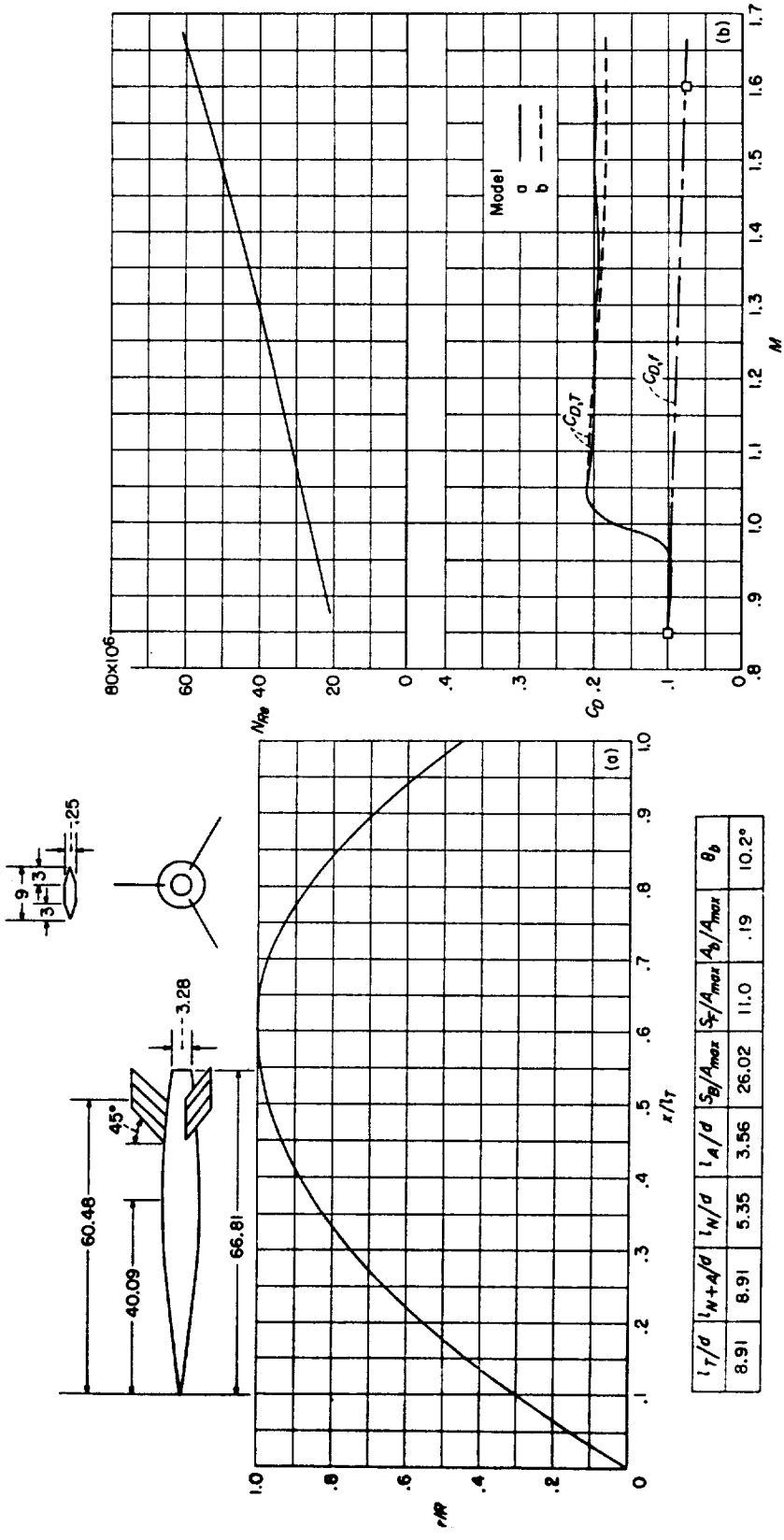

l_T/d	l_{N+A}/d	l_N/d	l_A/d	S_B/A_{max}	S_F/A_{max}	A_b/A_{max}	θ_b
8.91	8.91	5.35	3.56	26.02	11.0	.19	10.2°

(a) Body shape. (Dimensions given are in inches.) (b) N_{R_θ} and C_D curves.

CONFIGURATION 77 (parabolic nose and afterbody); rocket test.

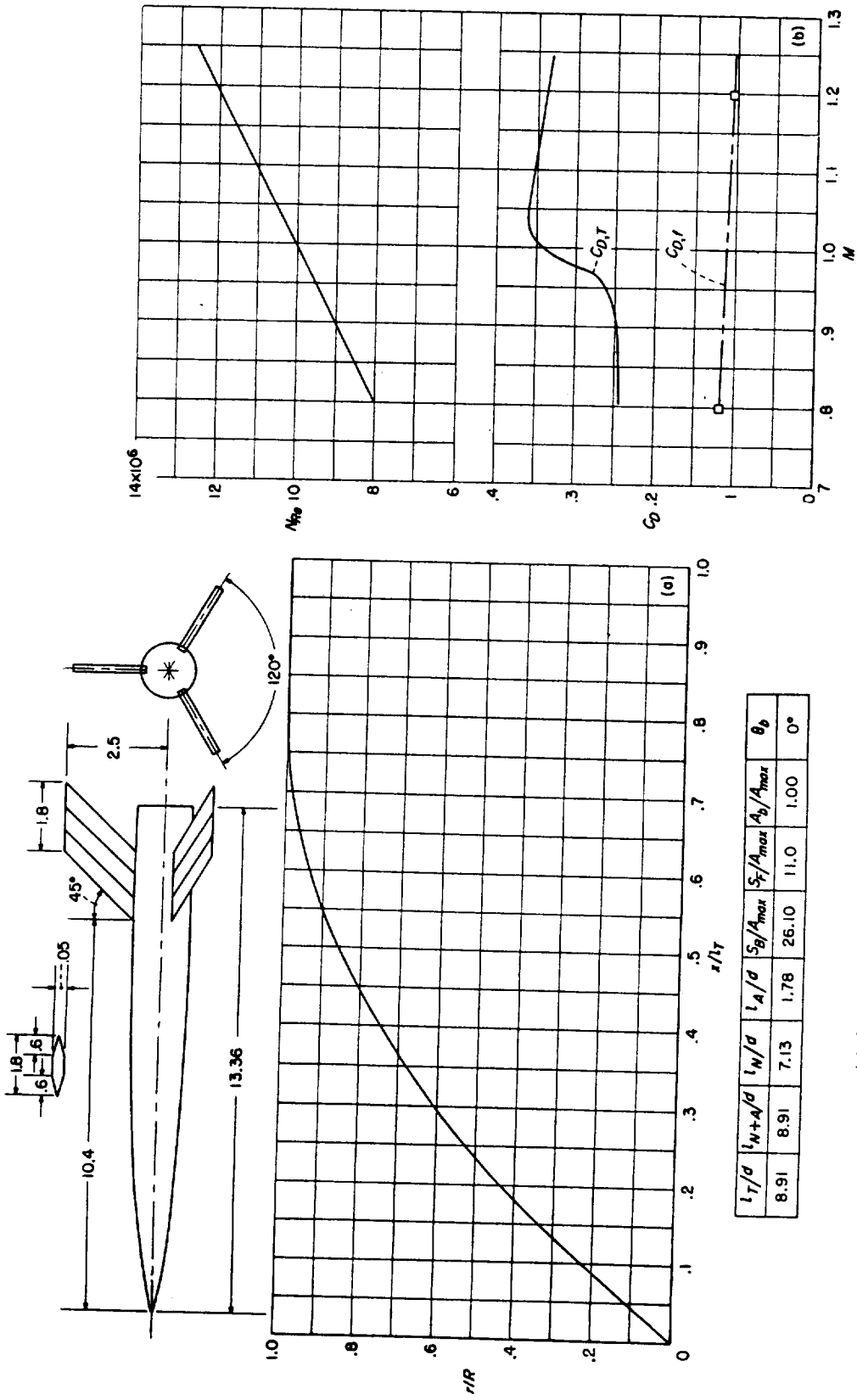

l_T/d	l_{N+A}/d	l_N/d	l_A/d	S_B/A_{max}	S_F/A_{max}	A_b/A_{max}	θ_b
8.91	8.91	7.13	1.78	26.10	11.0	1.00	0°

(a) Body shape. (Dimensions given are in inches.) (b) N_{Re} and C_D curves.

CONFIGURATION 78 (parabolic nose); helium-gun test.

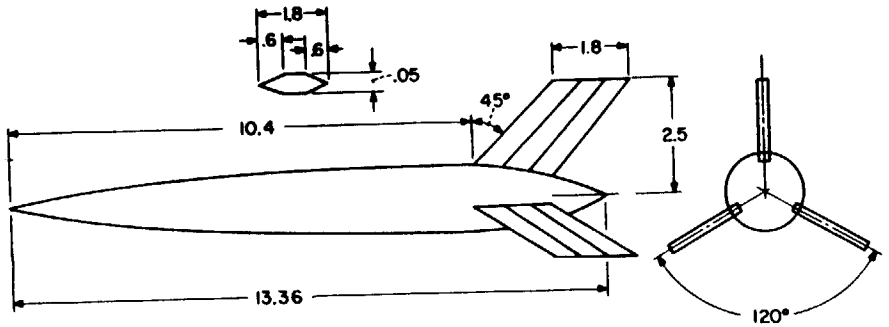

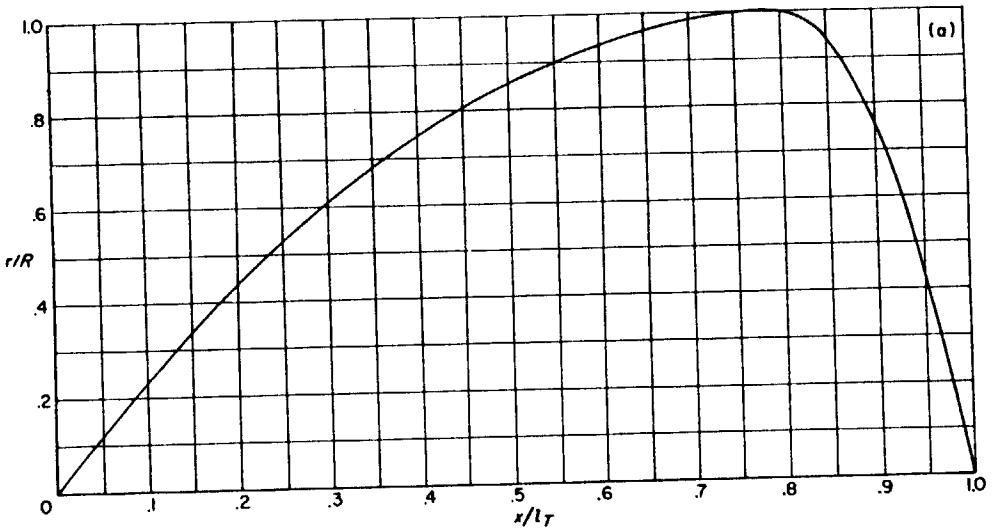

l_T/d	l_{N+A}/d	l_N/d	l_A/d	S_B/A_{max}	S_F/A_{max}	A_b/A_{max}	θ_b
8.91	8.91	7.13	1.78	23.70	11.0	0	29.3°

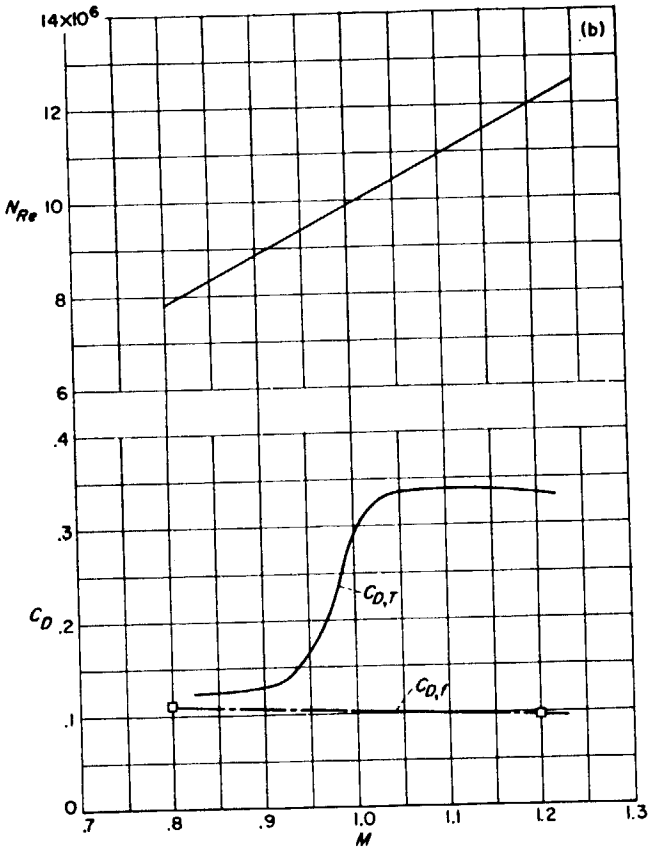

(a) Body shape. (Dimensions given are in inches.) (b) N_{Re} and C_D curves.

CONFIGURATION 79; helium-gun test.

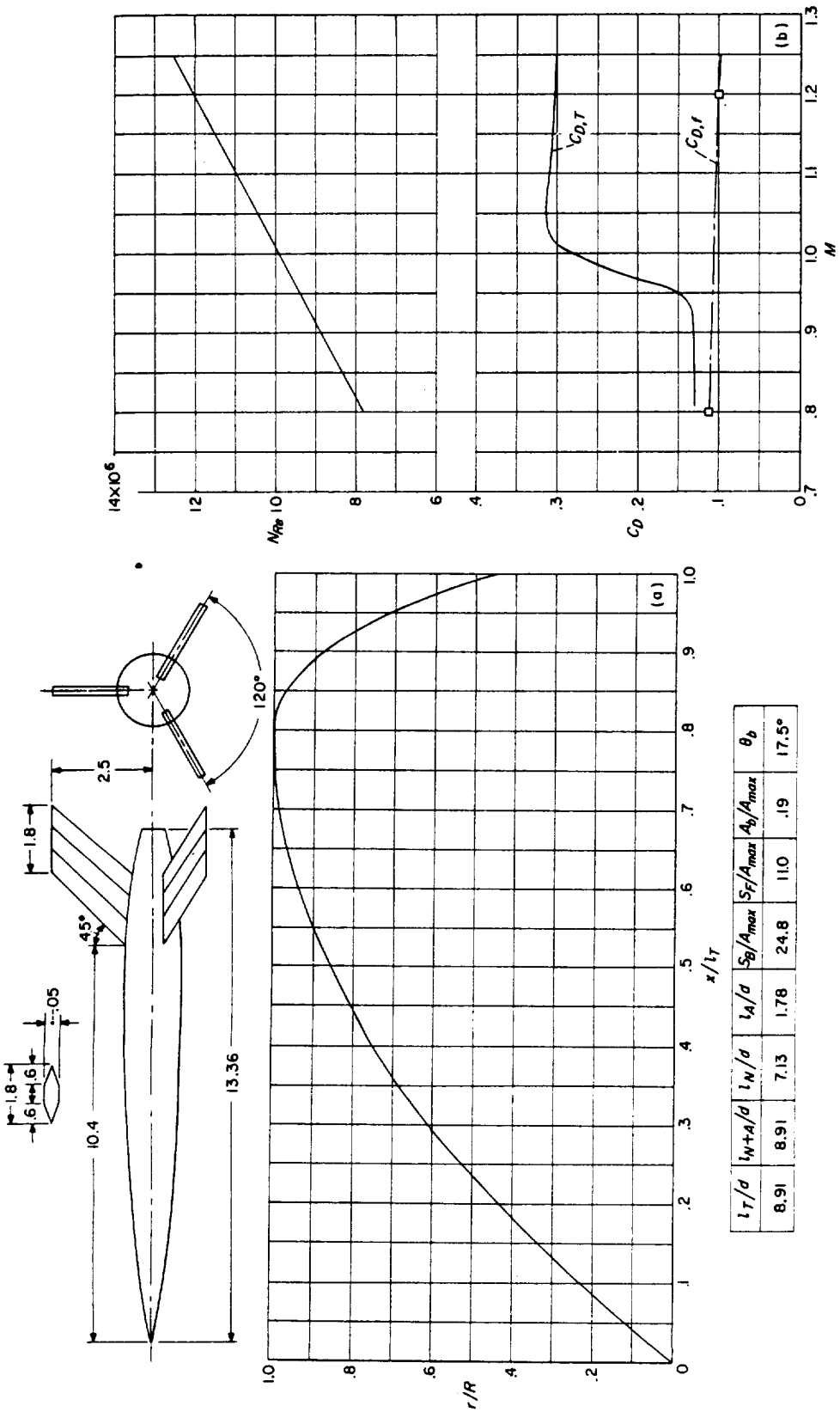

l_T/d	l_{N+A}/d	l_N/d	l_A/d	S_B/A_{max}	S_F/A_{max}	A_b/A_{max}	θ_b
8.91	8.91	7.13	1.78	24.8	11.0	.19	17.5°

(a) Body shape. (Dimensions given are in inches.) (b) N_{Re} and C_D curves.

CONFIGURATION 80 (parabolic nose and afterbody); helium-gun test.

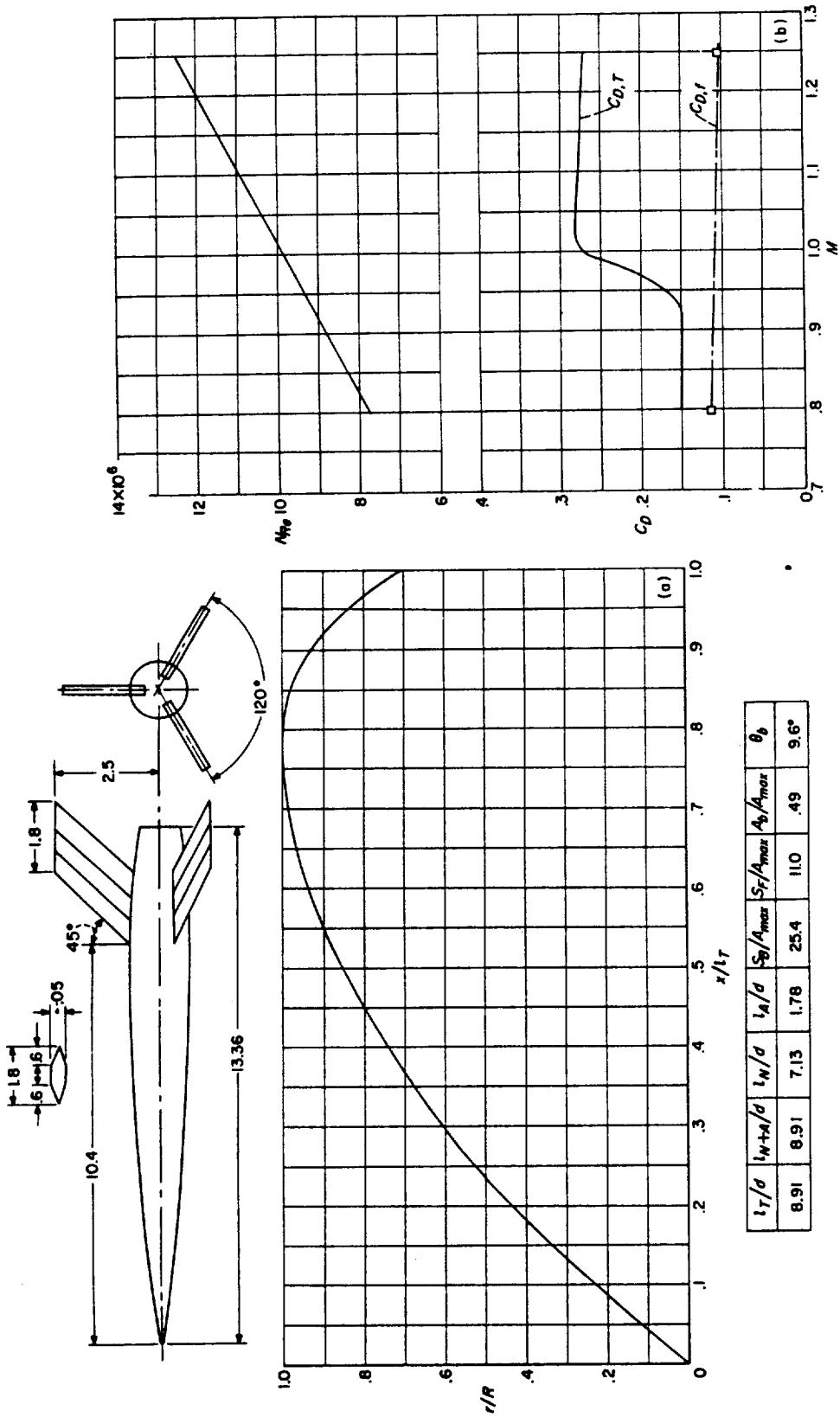

l_T/d	l_{W+A}/d	l_N/d	l_A/d	S_B/A_{max}	S_F/A_{max}	A_b/A_{max}	θ_b
8.91	8.91	7.13	1.78	25.4	11.0	.49	9.6°

(a) Body shape. (Dimensions given are in inches.) (b) N_{R_e} and C_D curves.

CONFIGURATION 81 (parabolic nose and afterbody); helium-gun test.

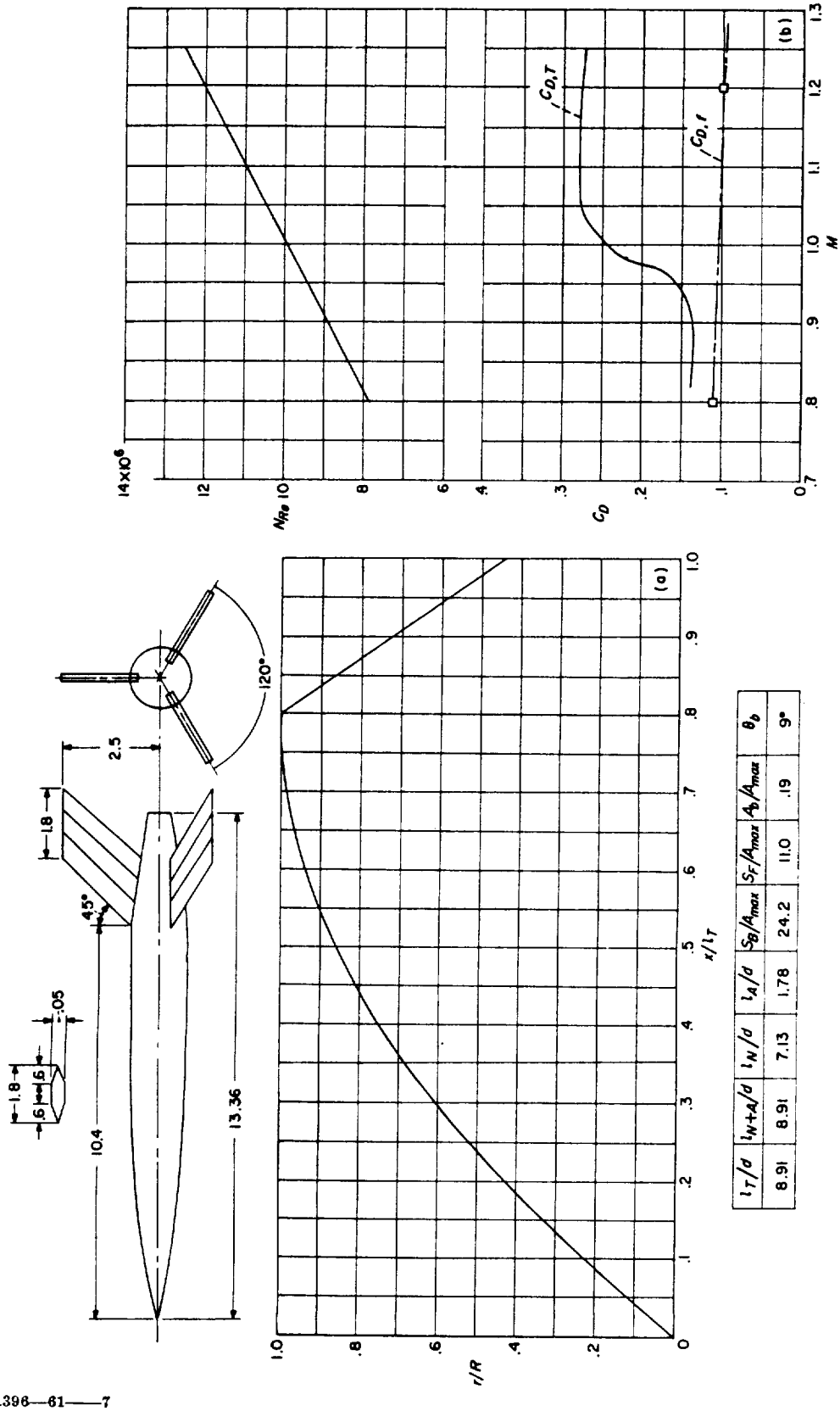

l_T/d	l_{N+A}/d	l_N/d	l_A/d	S_B/A_{max}	S_F/A_{max}	A_b/A_{max}	θ_b
8.91	8.91	7.13	1.78	24.2	11.0	.19	9°

(a) Body shape. (Dimensions given are in inches.) (b) N_{Re} and C_D curves.

CONFIGURATION 82 (parabolic nose; conical afterbody); helium-gun test.

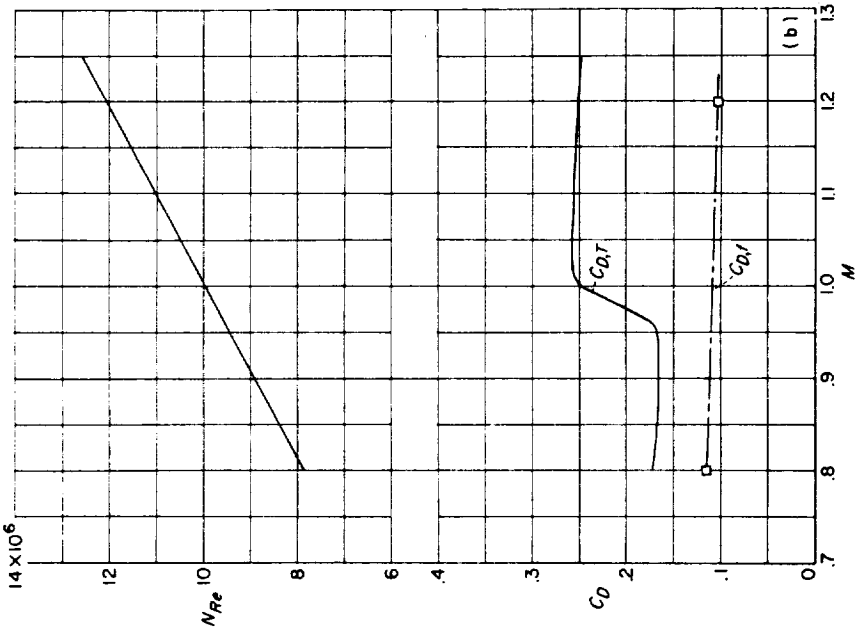

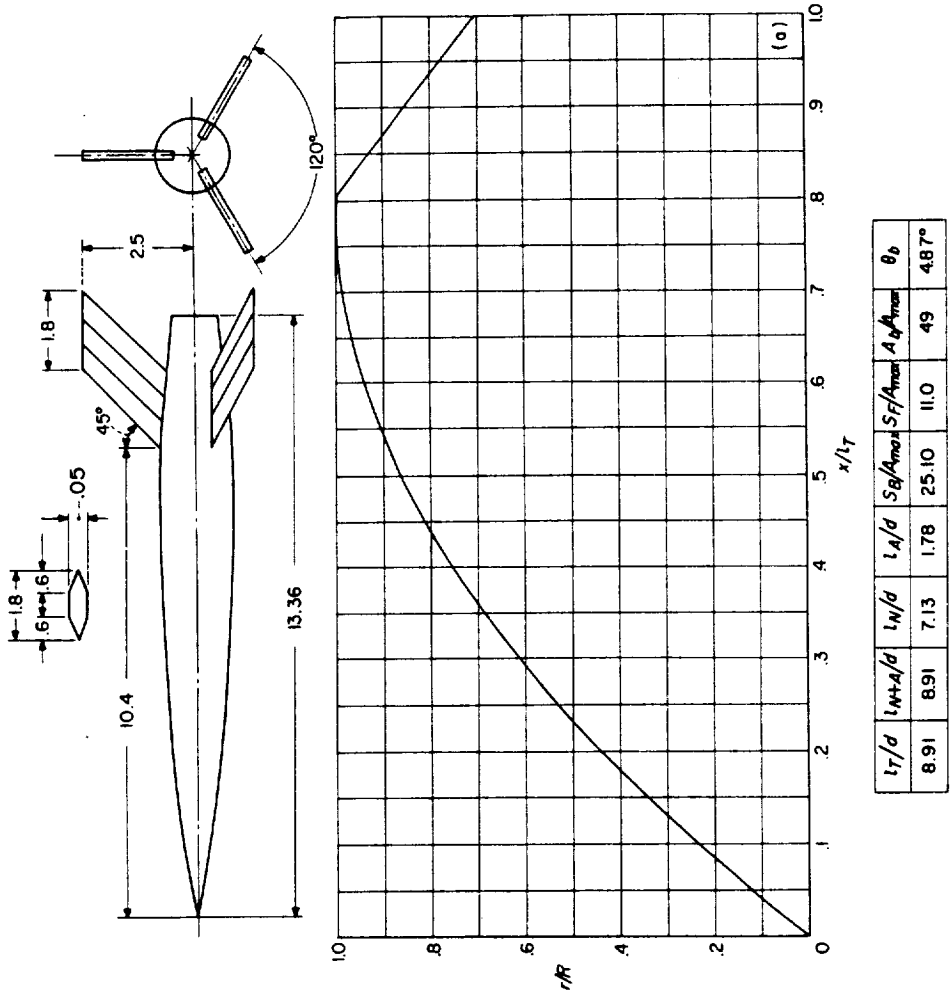

l_T/d	l_{N+A}/d	l_N/d	l_A/d	S_B/A_{max}	S_F/A_{max}	A_b/A_{max}	θ_b
8.91	8.91	7.13	1.78	25.10	11.0	49	48.7°

(a) Body shape. (Dimensions given are in inches.) (b) N_{Re} and C_D curves.

CONFIGURATION 83 (parabolic nose and afterbody); helium-gun test.

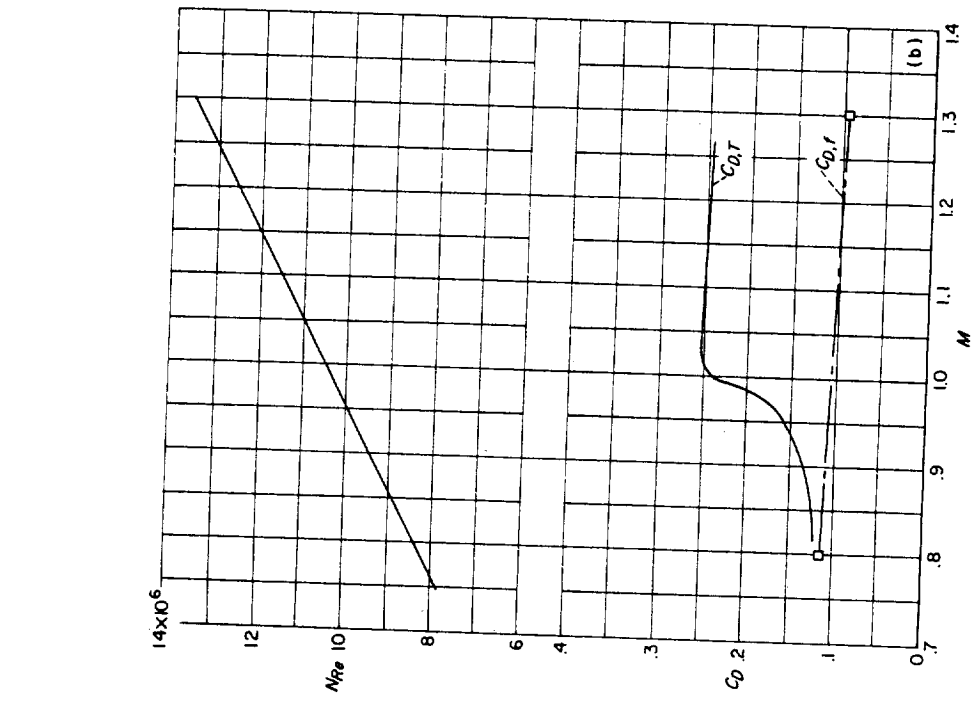

(b) N_{Re} and C_D curves.

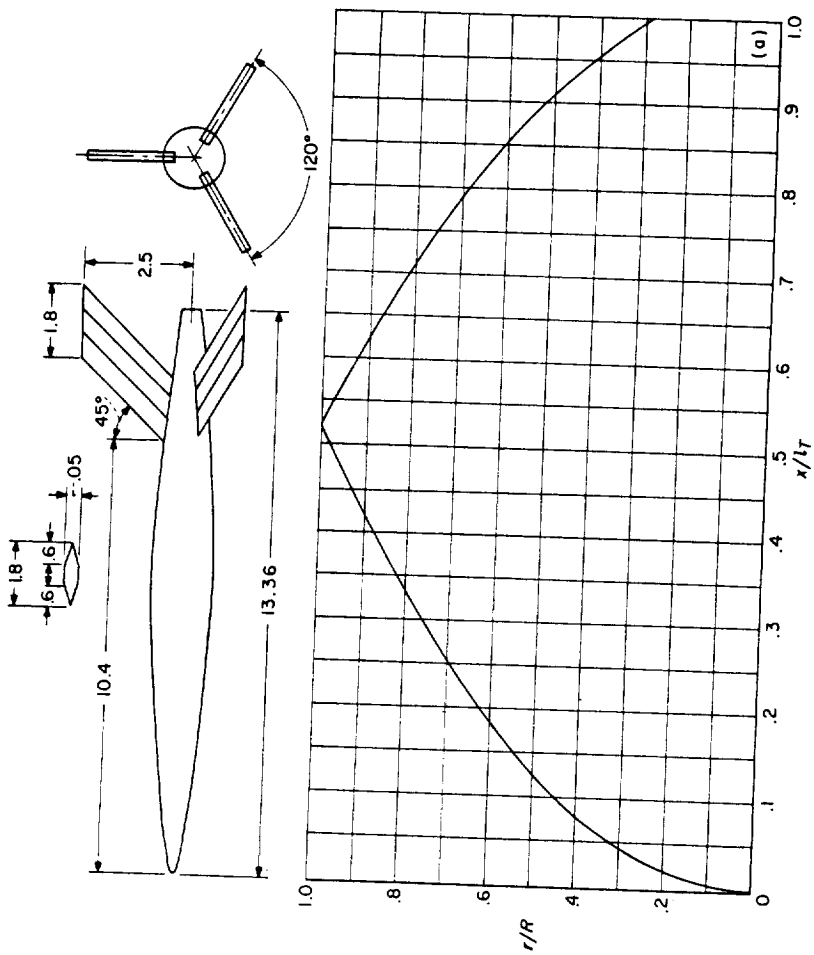

l_T/d	l_{W+A}/d	l_W/d	l_A/d	S_B/A_{max}	S_F/A_{max}	A_b/A_{max}	θ_b
8.91	8.91	4.66	4.25	24.5	110	.09	9.7°

(a) Body shape. (Dimensions given are in inches.)

CONFIGURATION 84 (contour of nose and afterbody exactly the same as those of configuration 85); helium-gun test.

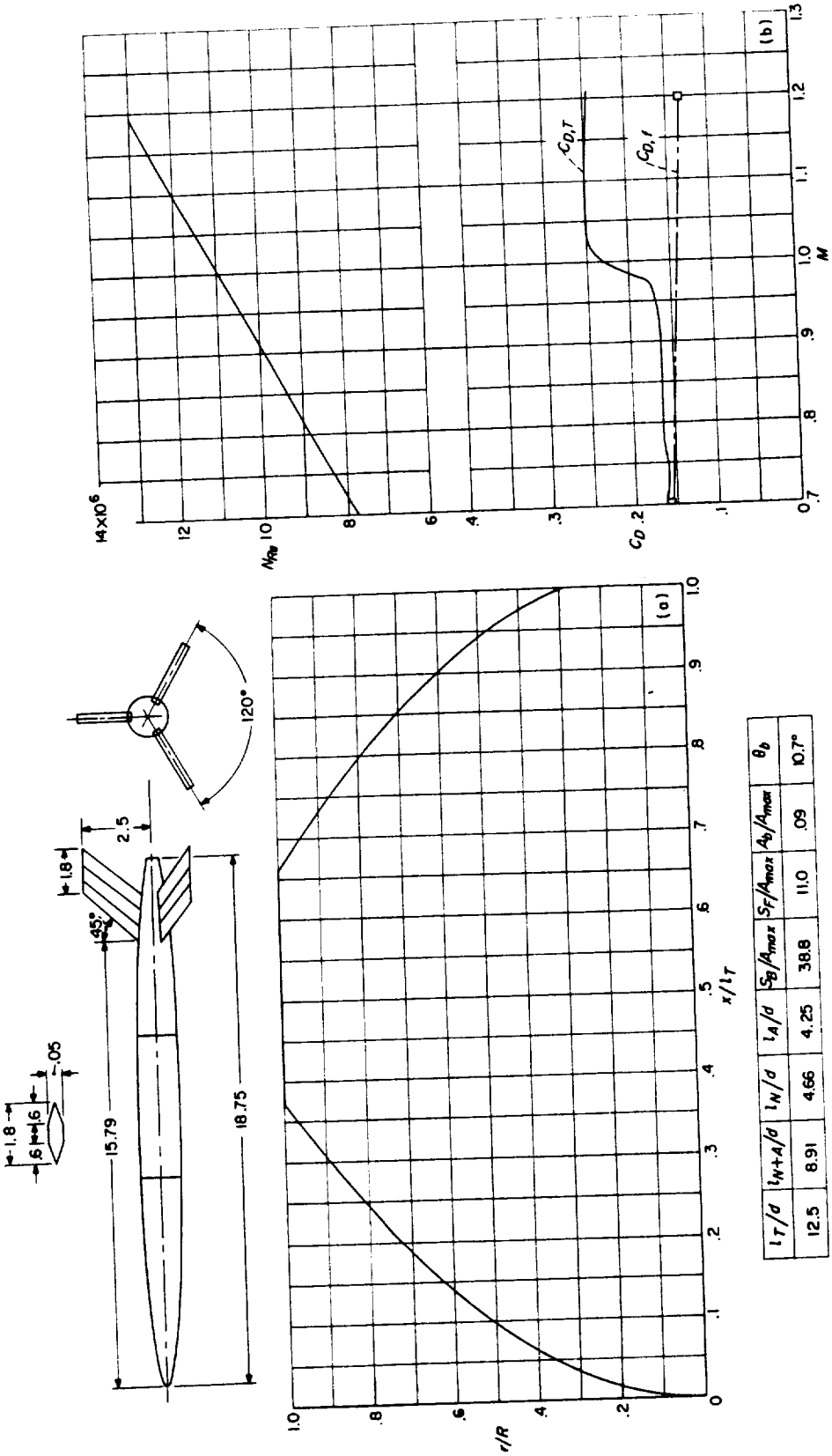

l_T/d	l_{N+A}/d	l_N/d	l_A/d	S_B/A_{max}	S_F/A_{max}	A_b/A_{max}	θ_b
12.5	8.91	4.66	4.25	38.8	11.0	.09	10.7°

(a) Body shape. (Dimensions given are in inches.) (b) N_{Re} and C_D curves.

CONFIGURATION 85 (contour of nose and afterbody exactly the same as those of configuration 84); helium-gun test.

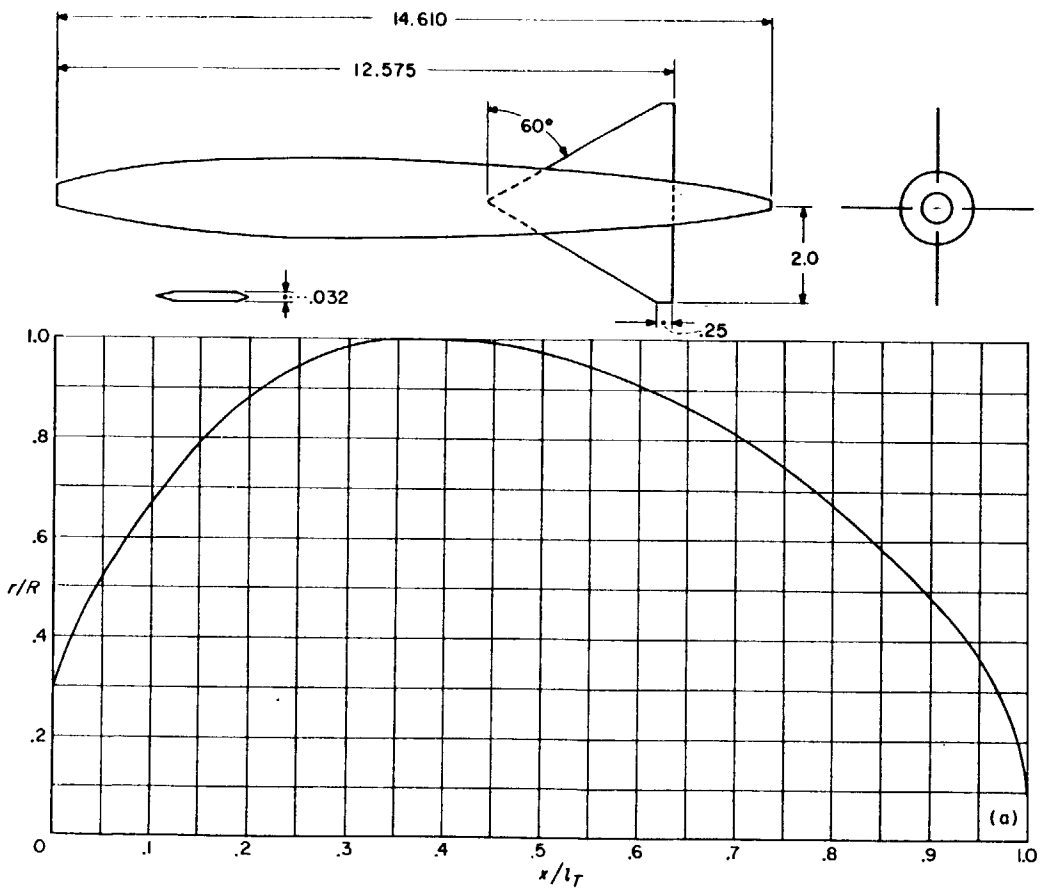

l_T/d	l_{N+A}/d	l_N/d	l_A/d	S_B/A_{max}	S_F/A_{max}	A_b/A_{max}	θ_b
9.13	9.13	3.28	5.85	28.0	8.30	.008	30°

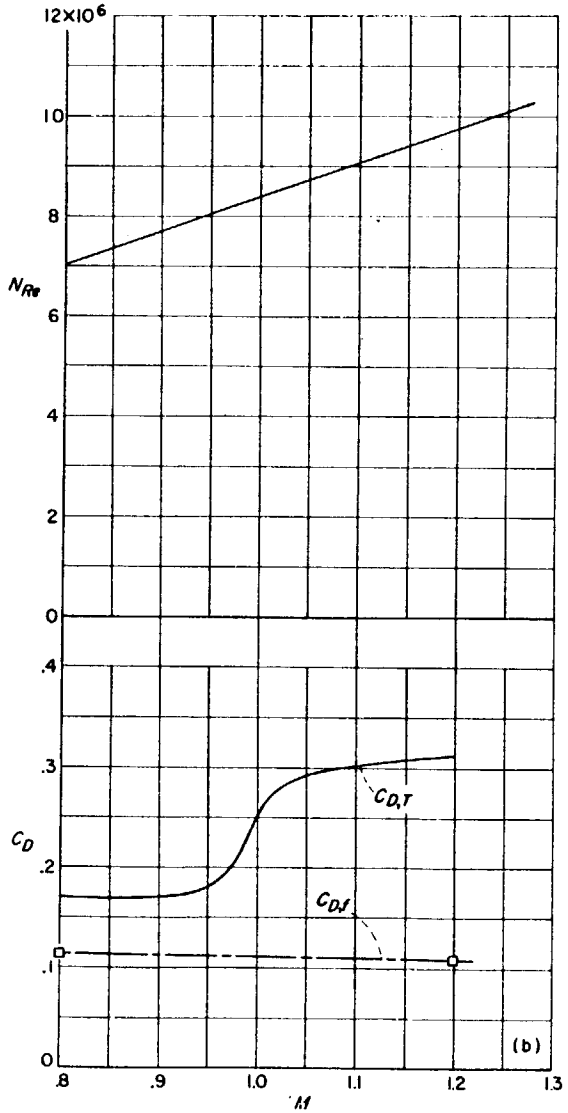

(a) Body shape. (Dimensions given are in inches.) (b) N_{Re} and C_D curves.

CONFIGURATION 86; helium-gun test. (Flat face of model caused high subsonic drag. See also configuration 47.)

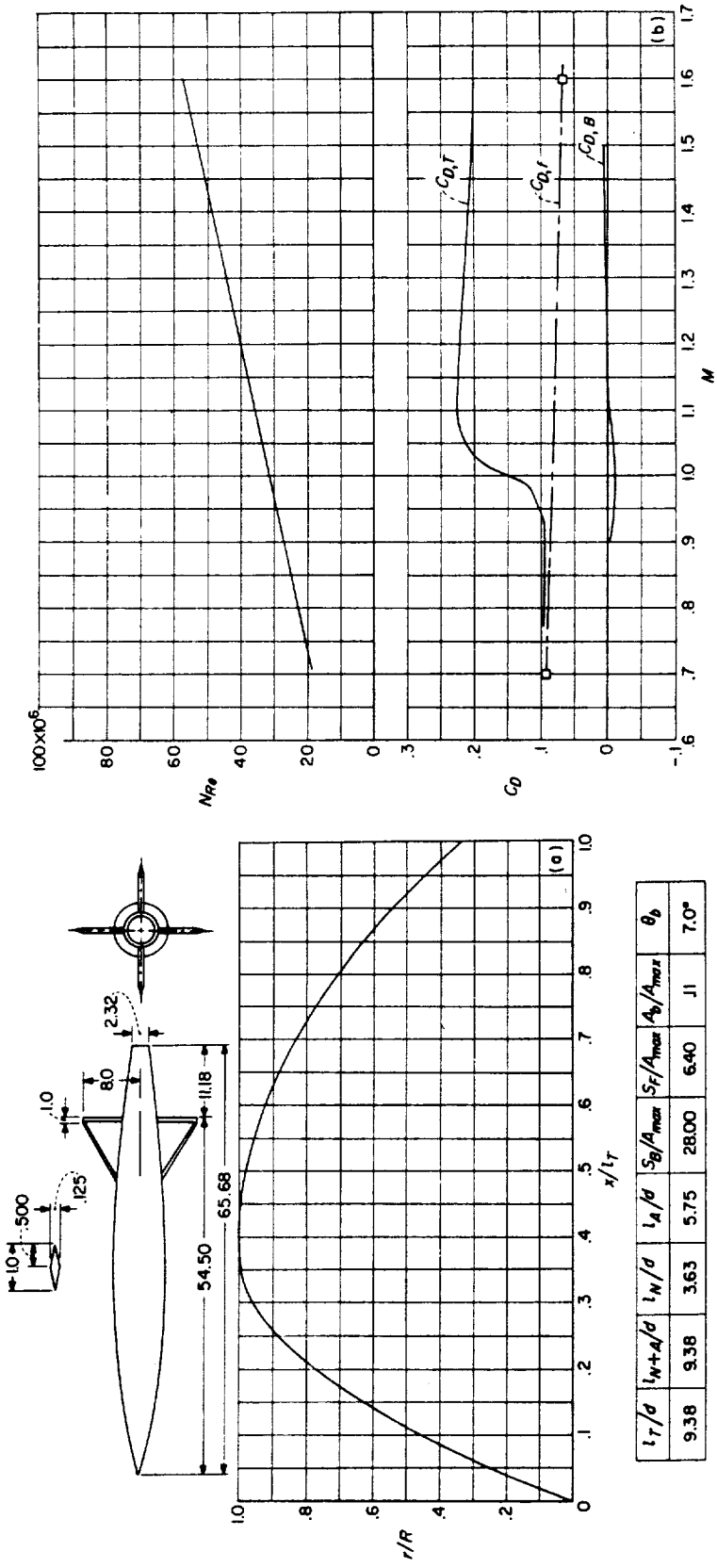

l_T/d	l_{N+A}/d	l_N/d	l_A/d	S_B/A_{max}	S_F/A_{max}	A_b/A_{max}	θ_b
9.38	9.38	3.63	5.75	28.00	6.40	.11	7.0°

(a) Body shape. (Dimensions given are in inches.) (b) N_{Re} and C_D curves.

CONFIGURATION 87 (parabolic nose and afterbody); rocket test.

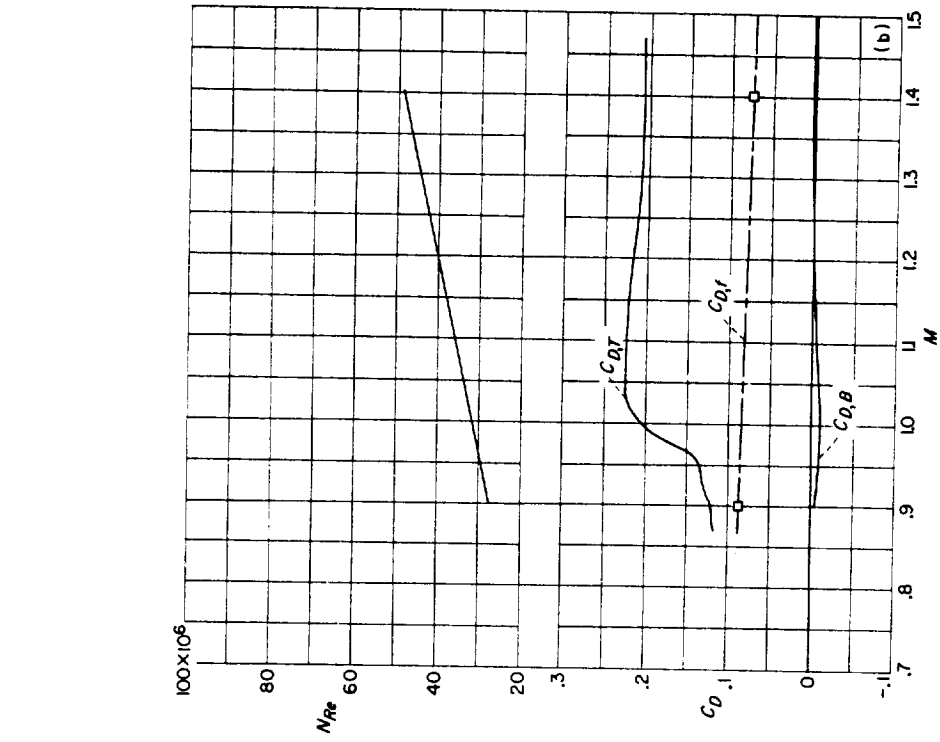

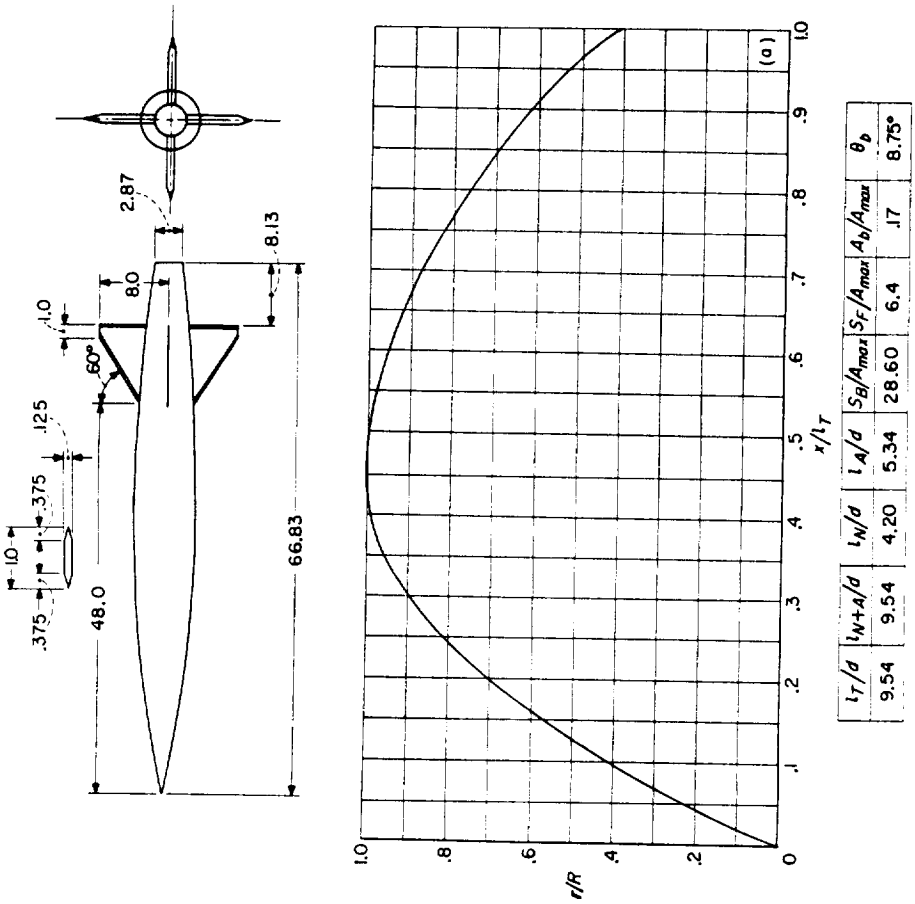

l_T/d	l_{N+A}/d	l_N/d	l_A/d	S_B/A_{max}	S_F/A_{max}	A_b/A_{max}	θ_b
9.54	9.54	4.20	5.34	28.60	6.4	.17	8.75°

(a) Body shape. (Dimensions given are in inches.) (b) N_{Re} and C_D curves.

CONFIGURATION 88 (parabolic nose and afterbody); rocket test.

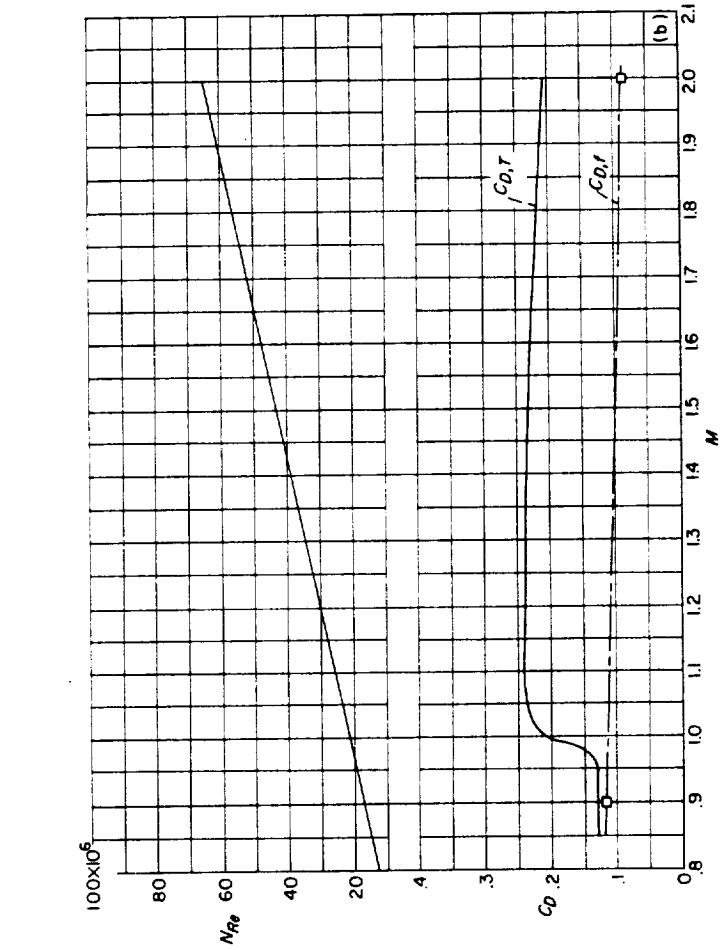

(b) N_{R_θ} and C_D curves.

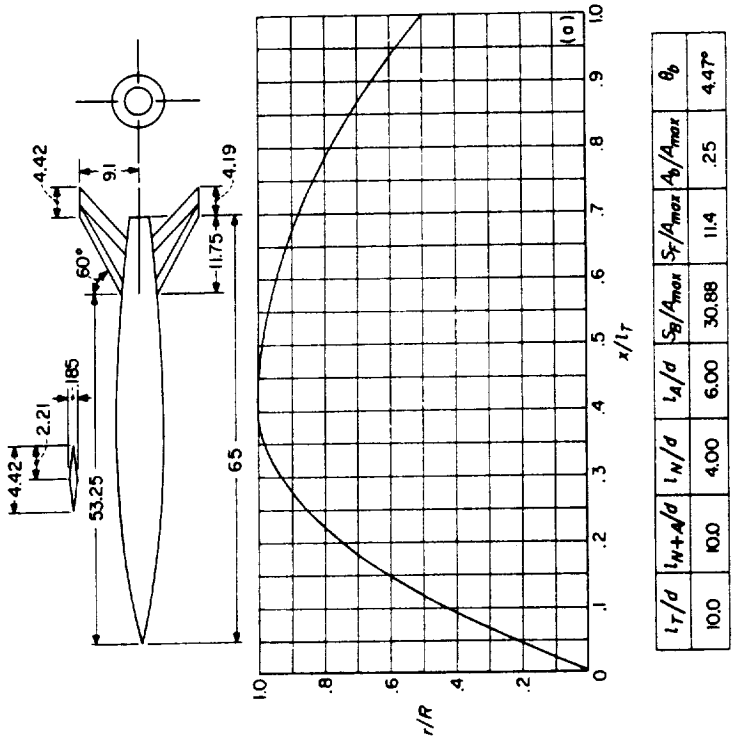

l_T/d	l_{N+A}/d	l_N/d	l_A/d	S_B/A_{max}	S_F/A_{max}	A_b/A_{max}	θ_b
10.0	10.0	4.00	6.00	30.88	11.4	.25	4.47°

(a) Body shape. (Dimensions given are in inches.)

CONFIGURATION 89 (parabolic nose and afterbody); rocket test.

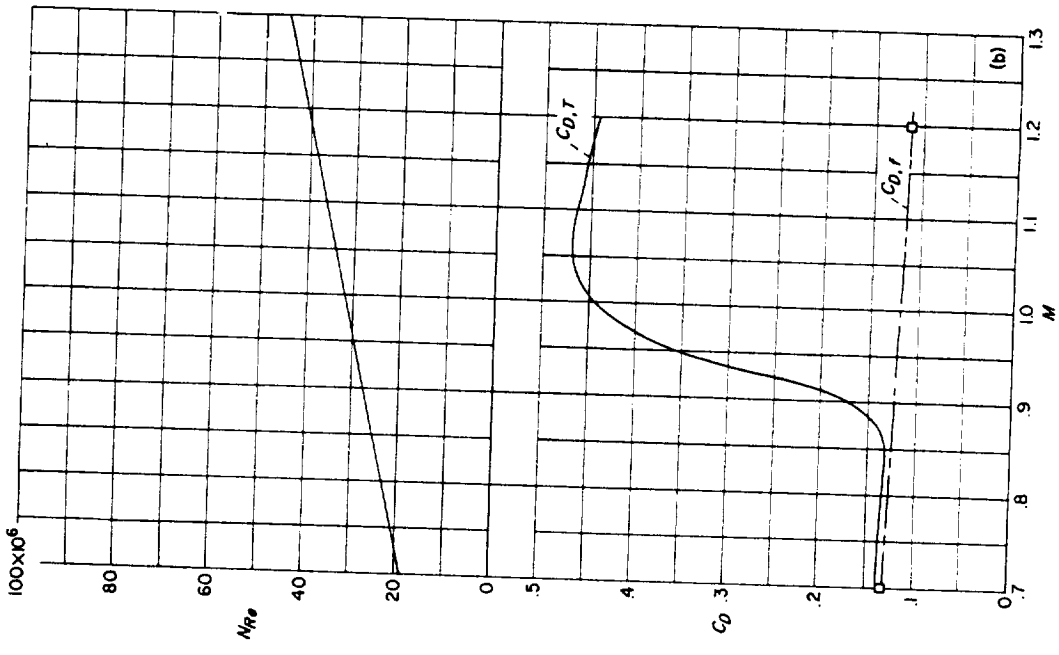

(b) N_R, and C_D curves.

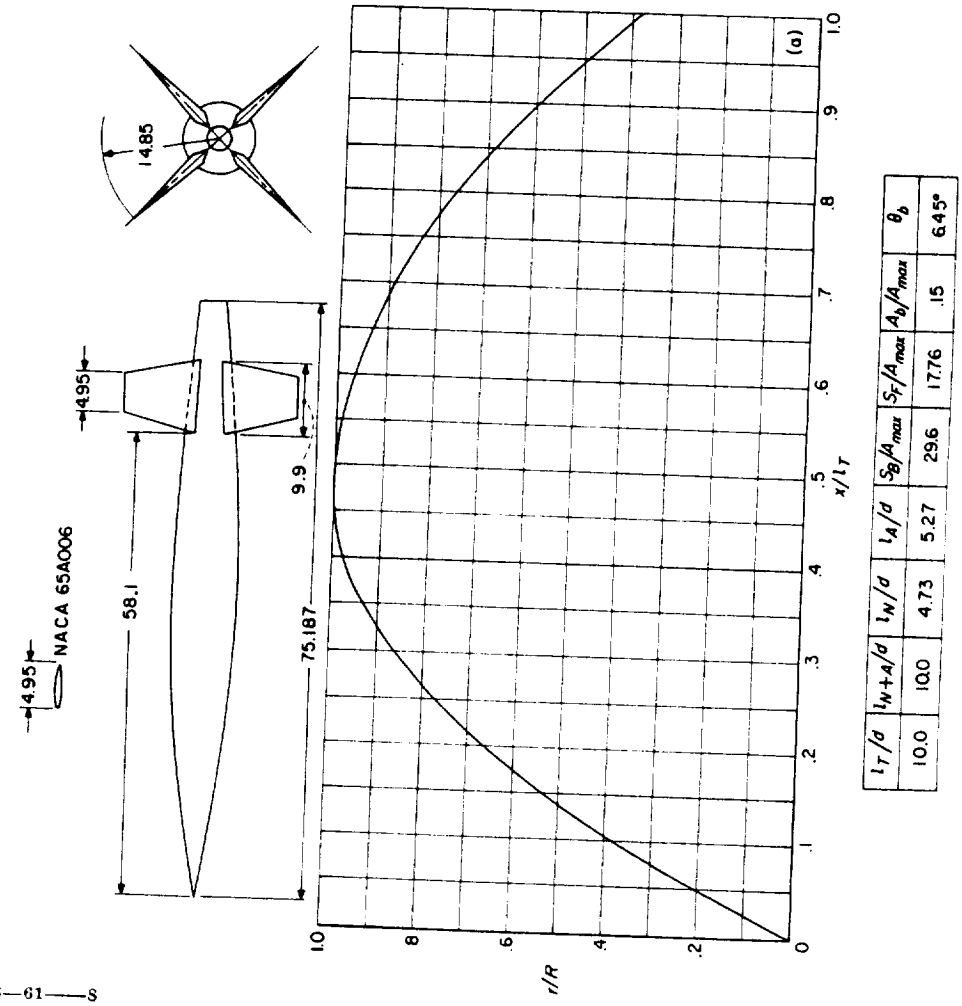

l_T/d	l_{N+A}/d	l_N/d	l_A/d	S_B/A_{max}	S_F/A_{max}	A_b/A_{max}	θ_b
10.0	10.0	4.73	5.27	29.6	17.76	.15	6.45°

(a) Body shape. (Dimensions given are in inches.)

CONFIGURATION 90; rocket test.

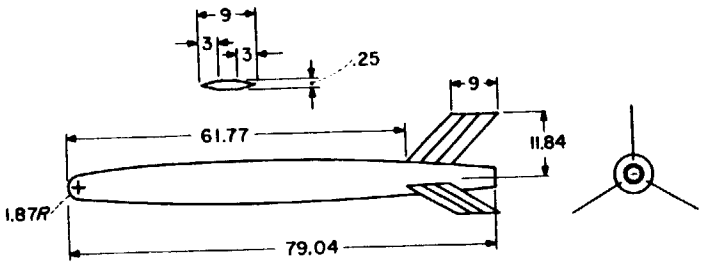

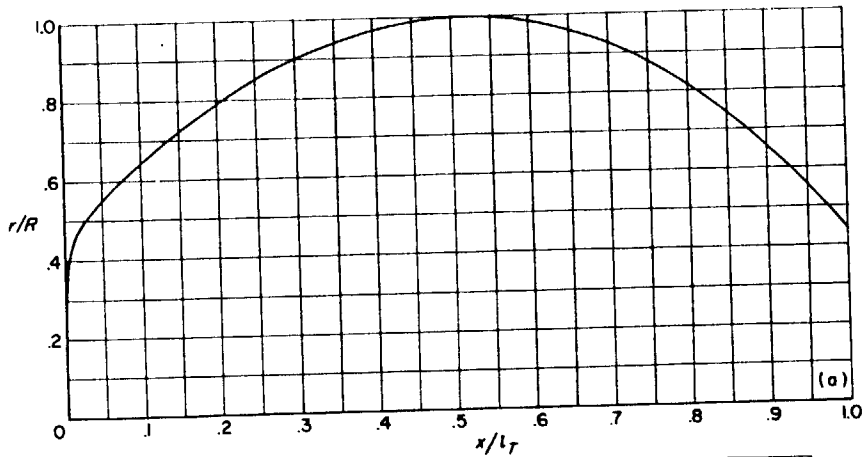

l_T/d	l_{N+A}/d	l_N/d	l_A/d	S_B/A_{max}	S_F/A_{max}	A_b/A_{max}	θ_b
10.54	10.54	5.38	5.16	34.40	11.0	.19	7.0°

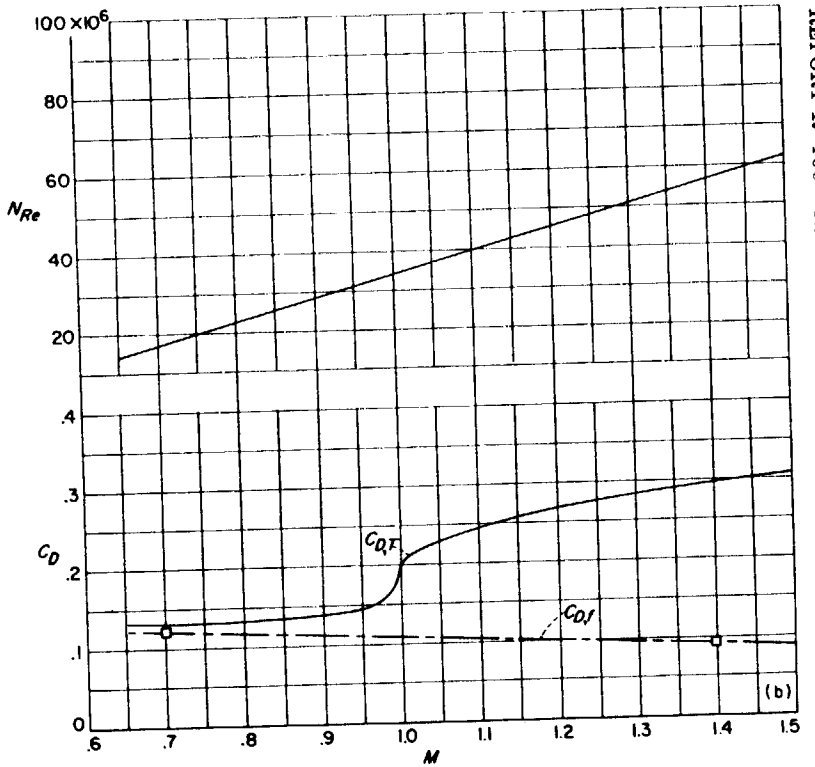

(a) Body shape. (Dimensions given are in inches.) (b) N_{R_e} and C_D curves.

CONFIGURATION 91 (nose consists of hemispherical and parabolic segments; parabolic afterbody); rocket test.

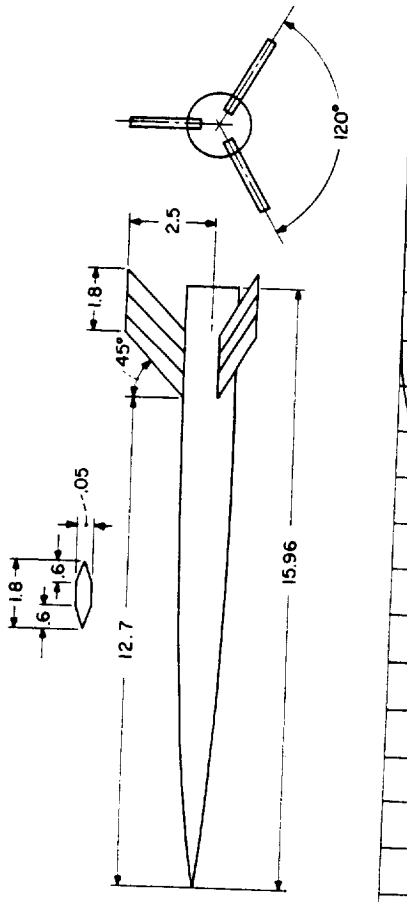

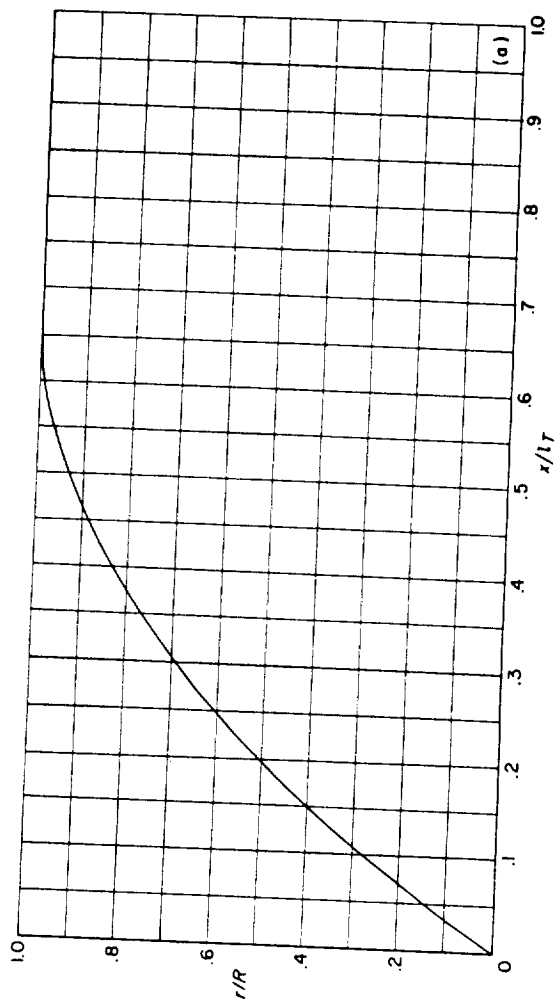

l_T/d	l_{N+A}/d	l_N/d	l_A/d	S_B/A_{max}	S_F/A_{max}	A_b/A_{max}	θ_b
10.63	10.63	7.13	3.50	33.0	11.0	1.0	0°

(a) Body shape. (Dimensions given are in inches.)

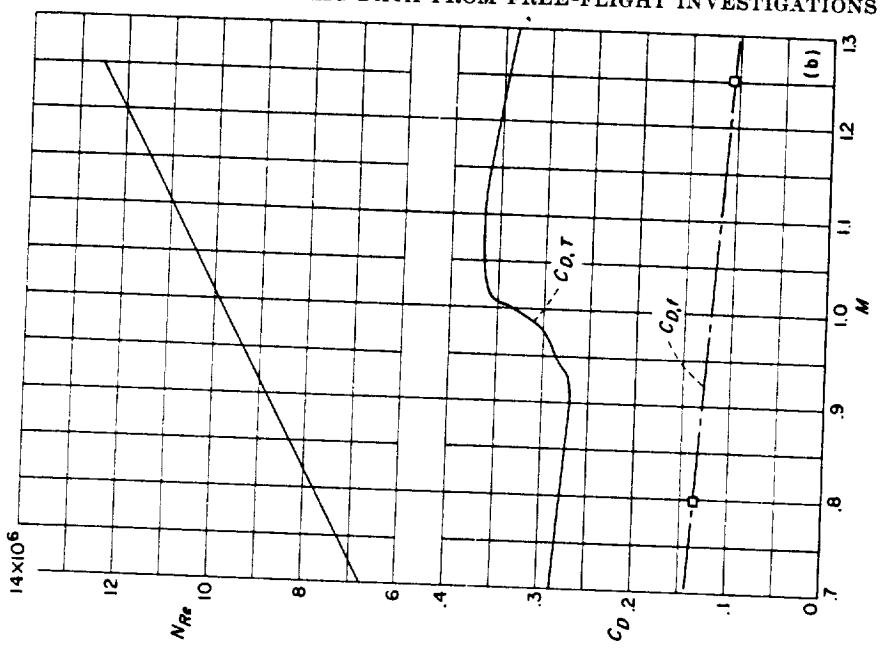

(b) N_{Re} and C_D curves.

CONFIGURATION 92 (parabolic nose; cylindrical afterbody); helium-gun test.

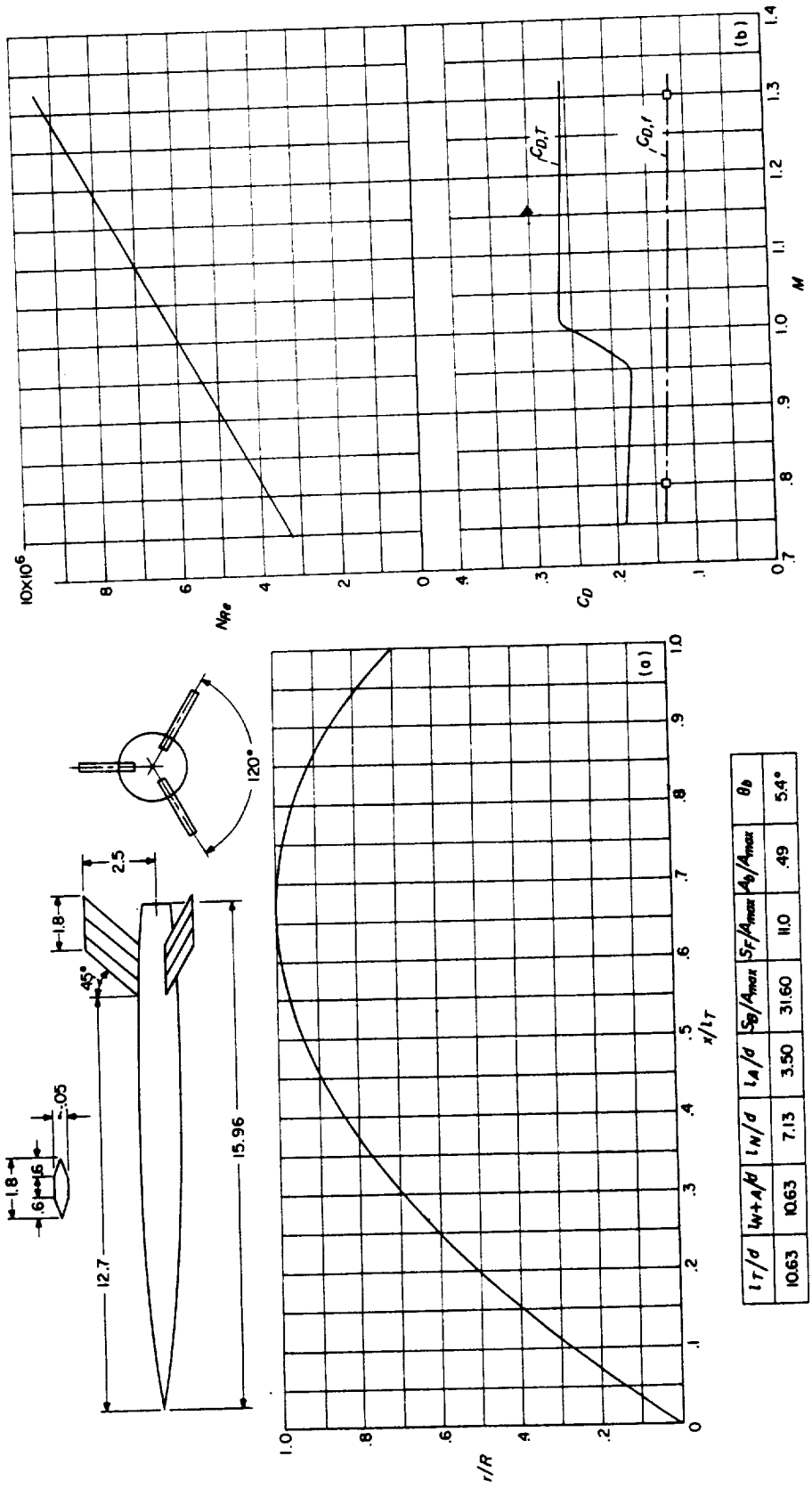

l_T/d	l_{N+A}/d	l_N/d	l_A/d	S_B/A_{max}	S_F/A_{max}	A_b/A_{max}	θ_b
10.63	10.63	7.13	3.50	31.60	11.0	.49	5.4°

(a) Body shape. (Dimensions given are in inches.) (b) N_{Re} and C_D curves.

CONFIGURATION 93 (parabolic nose and afterbody); helium-gun test.

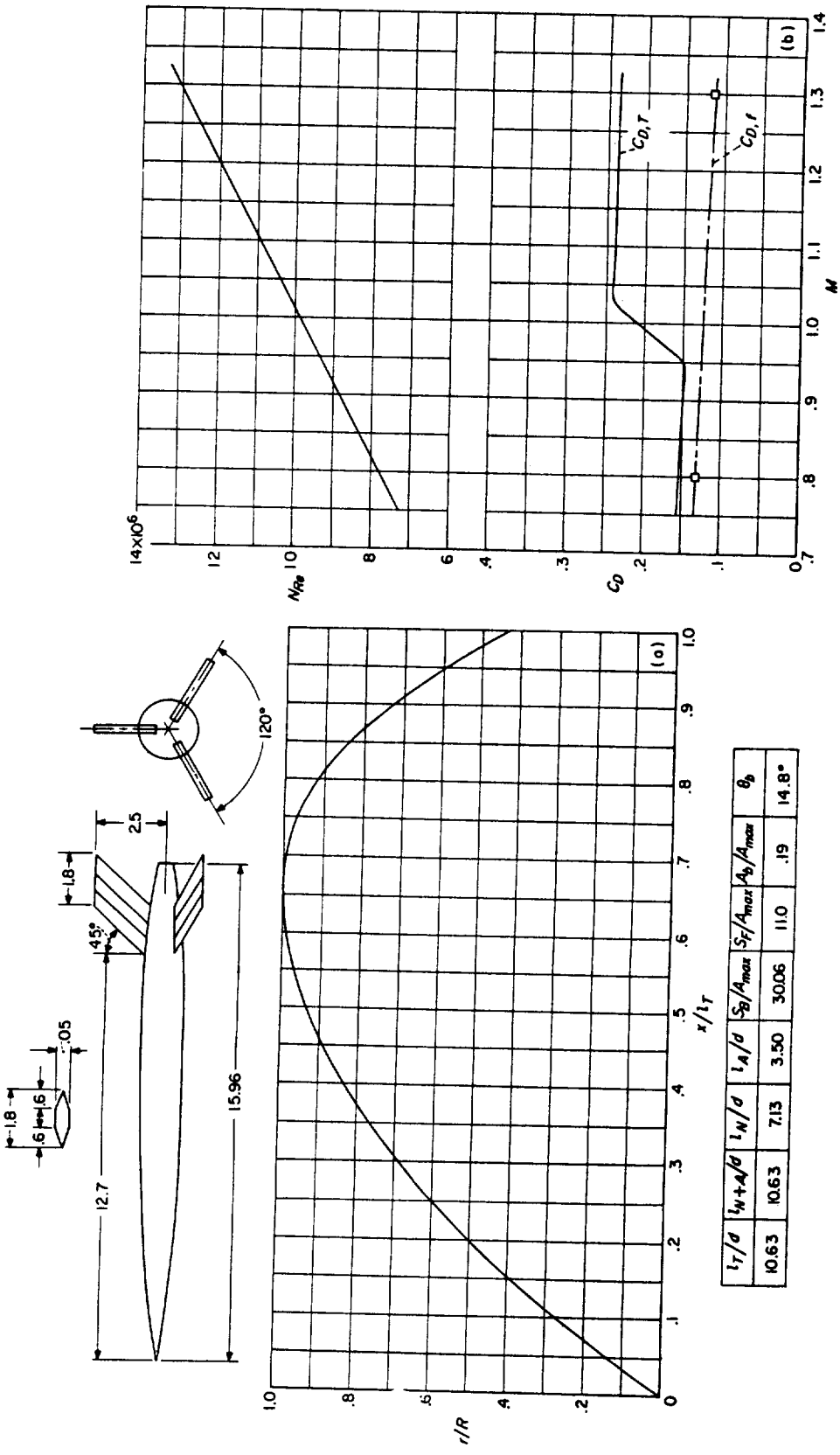

l_T/d	l_N+A/d	l_N/d	l_A/d	S_B/A_{max}	S_T/A_{max}	A_b/A_{max}	θ_b
10.63	10.63	7.13	3.50	30.06	11.0	.19	14.8°

(a) Body shape. (Dimensions given are in inches.) (b) N_{Re} and C_D curves.

CONFIGURATION 94 (parabolic nose and afterbody); helium-gun test.

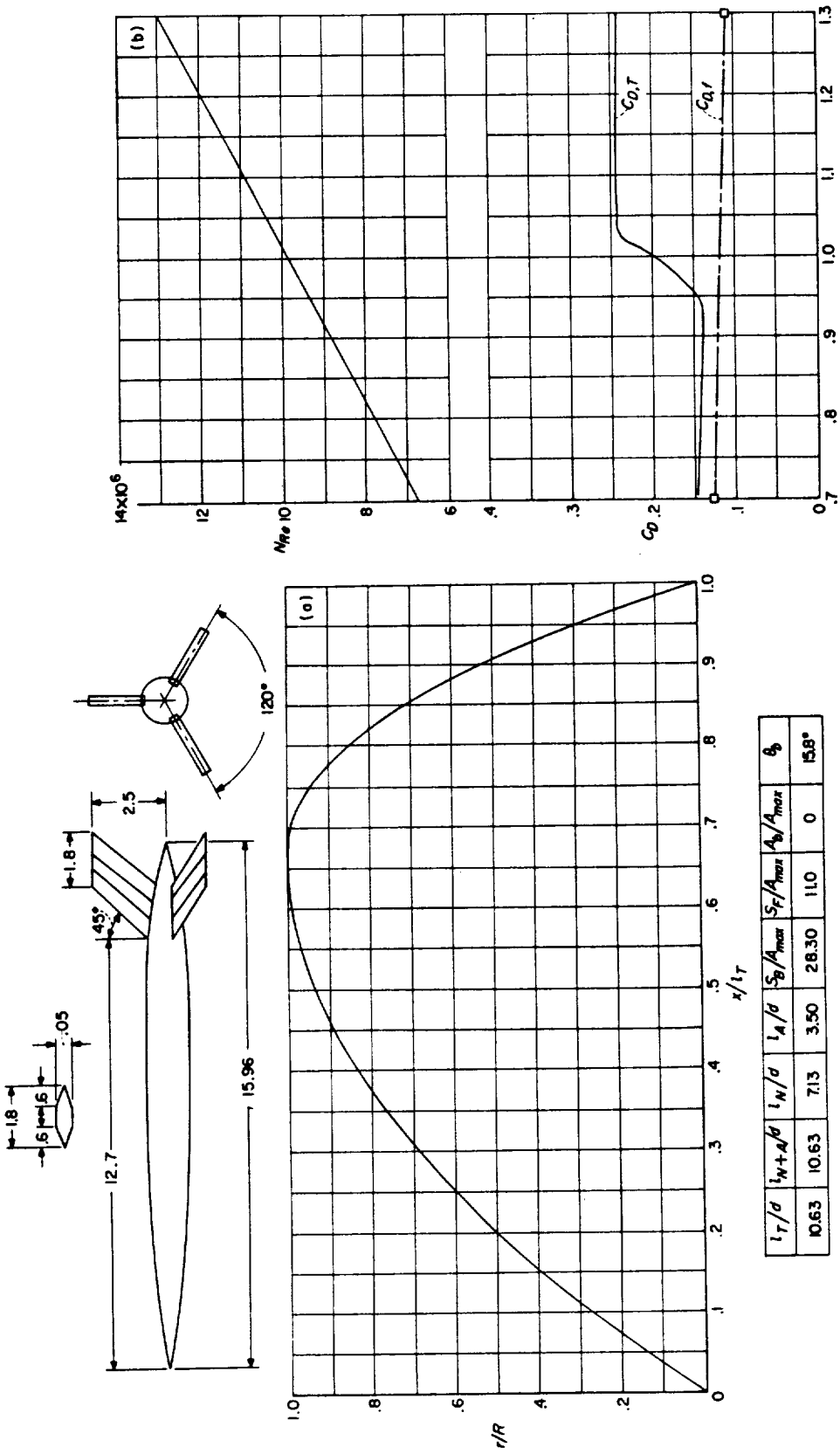

l_T/d	l_{N+A}/d	l_N/d	l_A/d	S_B/A_{max}	S_F/A_{max}	A_b/A_{max}	θ_b
10.63	10.63	7.13	3.50	28.30	11.0	0	15.8°

(a) Body shape. (Dimensions given are in inches.) (b) N_{Re} and C_D curves.

CONFIGURATION 95 (parabolic nose and afterbody); helium-gun test.

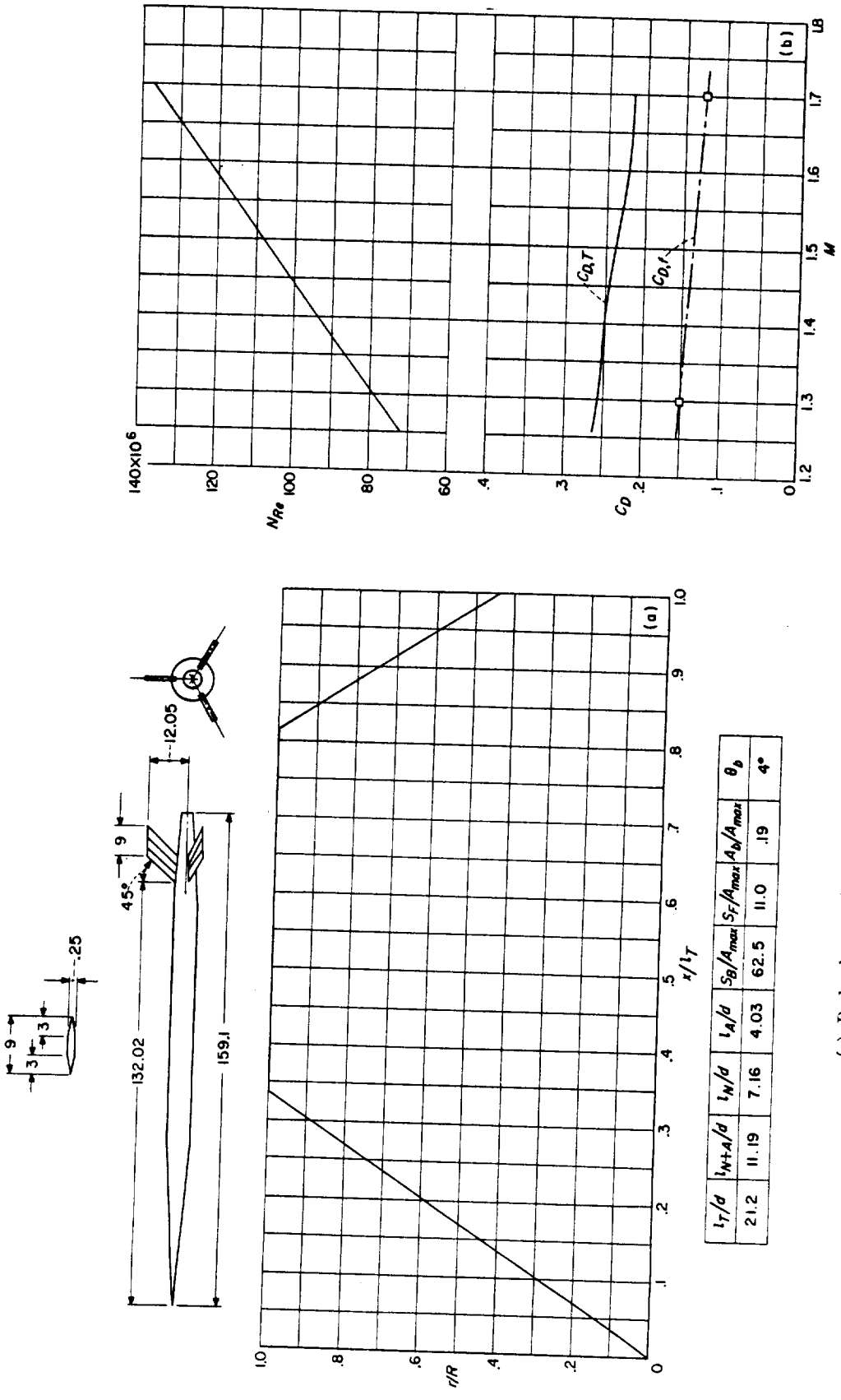

l_T/d	l_{N+A}/d	l_N/d	l_A/d	S_B/A_{max}	S_F/A_{max}	A_b/A_{max}	θ_b
21.2	11.19	7.16	4.03	62.5	11.0	.19	4°

(a) Body shape. (Dimensions given are in inches.) (b) N_{Re} and C_D curves.

CONFIGURATION 96 (conical nose and afterbody); rocket test.

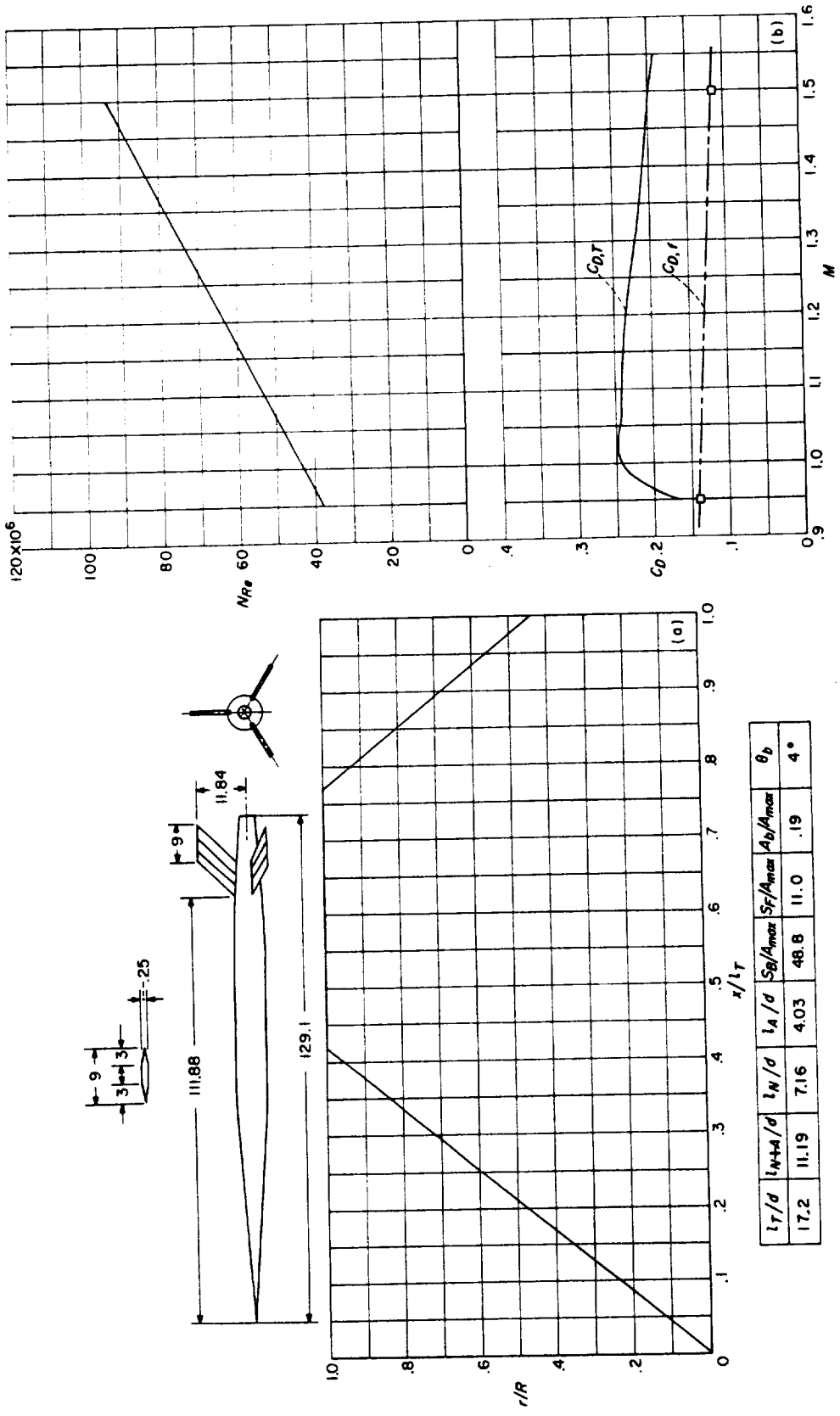

l_T/d	l_{N+A}/d	l_N/d	l_A/d	S_B/A_{max}	S_F/A_{max}	A_b/A_{max}	θ_b
17.2	11.19	7.16	4.03	48.8	11.0	.19	4°

(a) Body shape. (Dimensions given are in inches.) (b) N_{Re} and C_D curves.

CONFIGURATION 97 (conical nose and afterbody); rocket test.

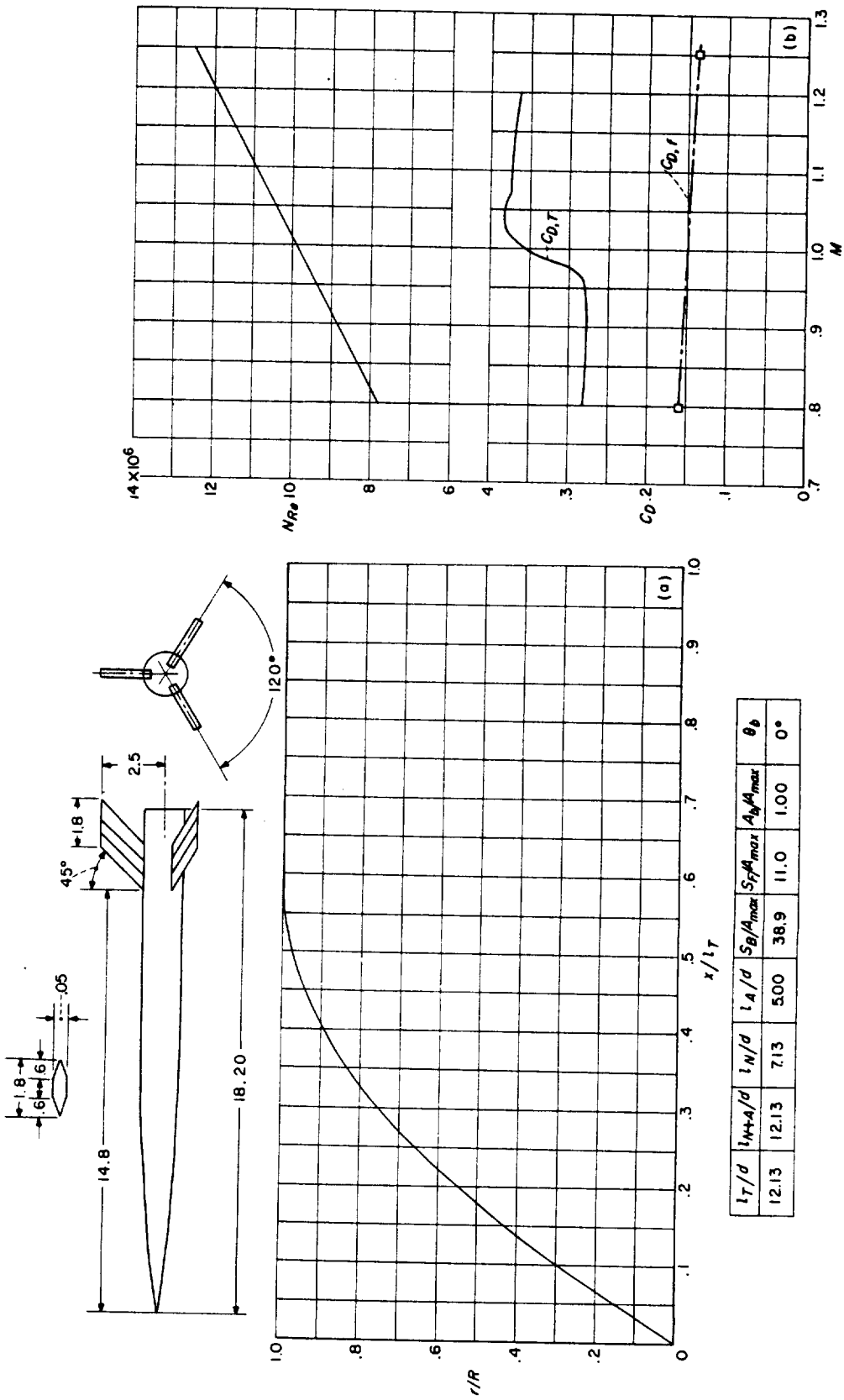

l_T/d	l_{N+A}/d	l_N/d	l_A/d	S_B/A_{max}	S_{fl}/A_{max}	A_b/A_{max}	θ_b
12.13	12.13	7.13	5.00	38.9	11.0	1.00	0°

(a) Body shape. (Dimensions given are in inches.) (b) N_{Re} and C_D curves.

CONFIGURATION 98 (parabolic nose; cylindrical afterbody); helium-gun test.

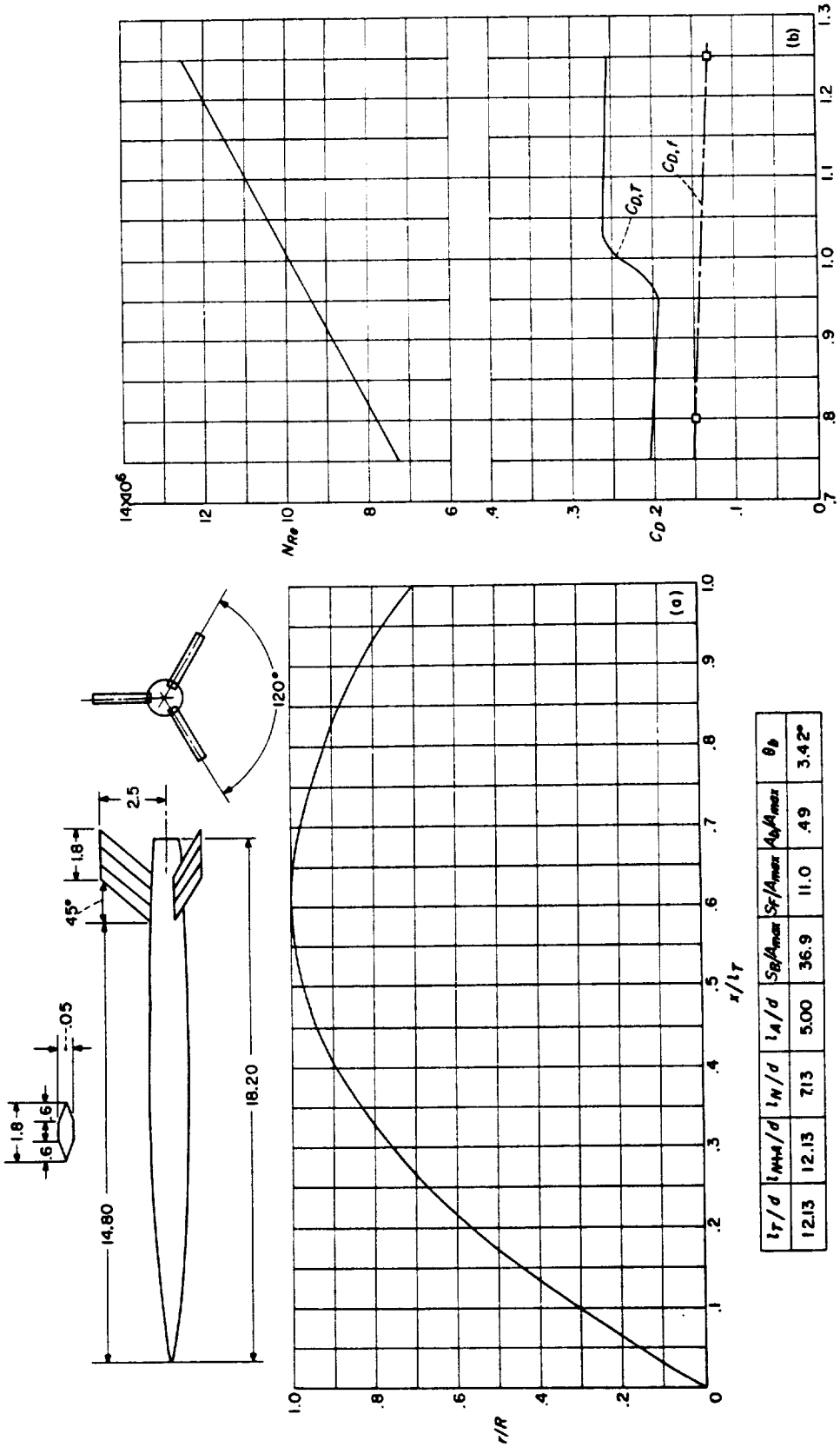

l_T/d	l_{NA}/d	l_N/d	l_A/d	S_B/A_{max}	S_F/A_{max}	A_b/A_{max}	θ_b
12.13	12.13	7.13	5.00	36.9	11.0	.49	3.42°

(a) Body shape. (Dimensions given are in inches.) (b) N_{Re} and C_D curves.

CONFIGURATION 99 (parabolic nose and afterbody); helium-gun test.

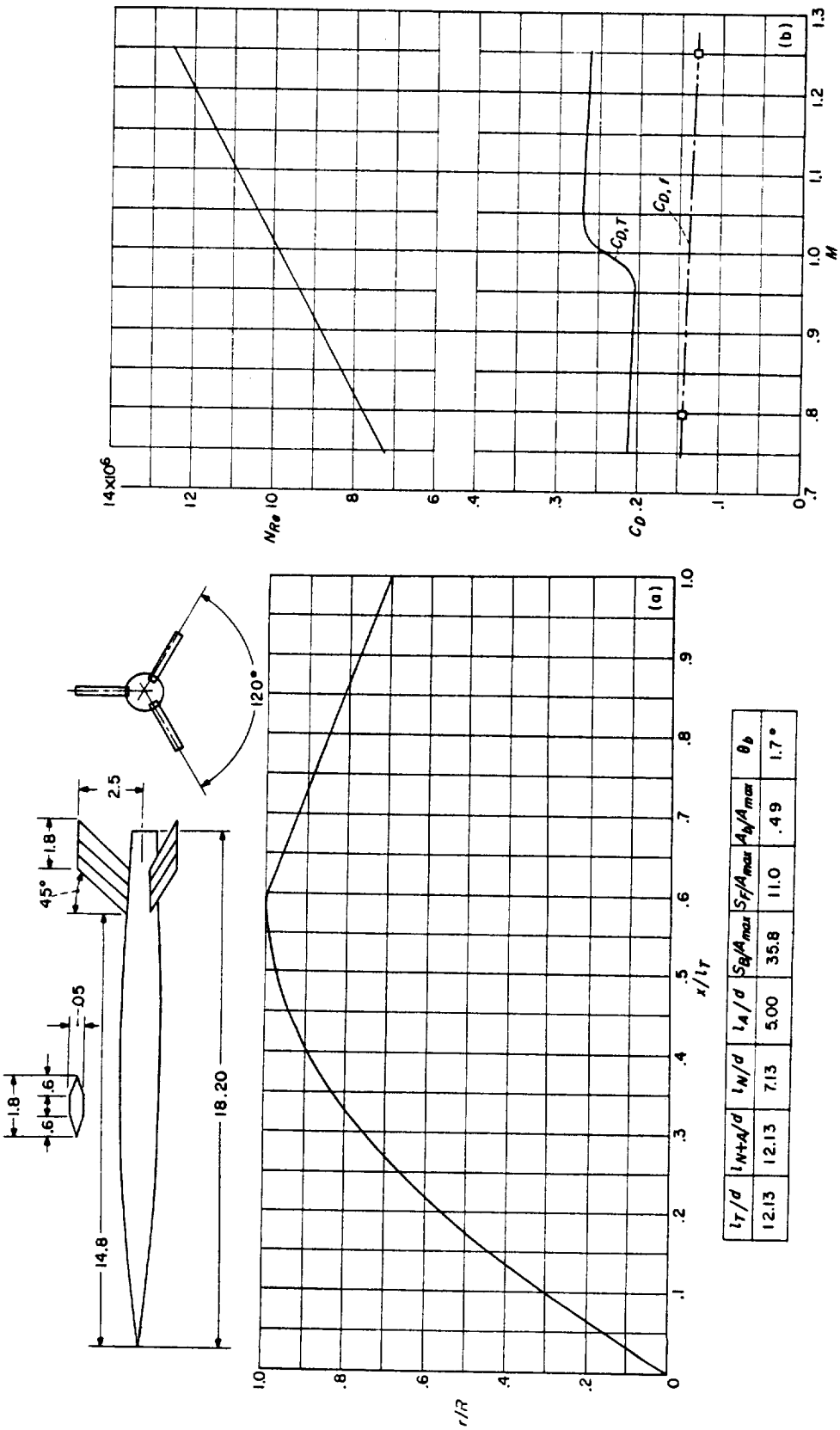

l_T/d	l_{N+A}/d	l_N/d	l_A/d	S_B/A_{max}	S_F/A_{max}	A_b/A_{max}	θ_b
12.13	12.13	7.13	5.00	35.8	11.0	.49	1.7°

(a) Body shape. (Dimensions given are in inches.) (b) N_{Re} and C_D curves.

CONFIGURATION 100 (parabolic nose; conical afterbody); helium-gun test.

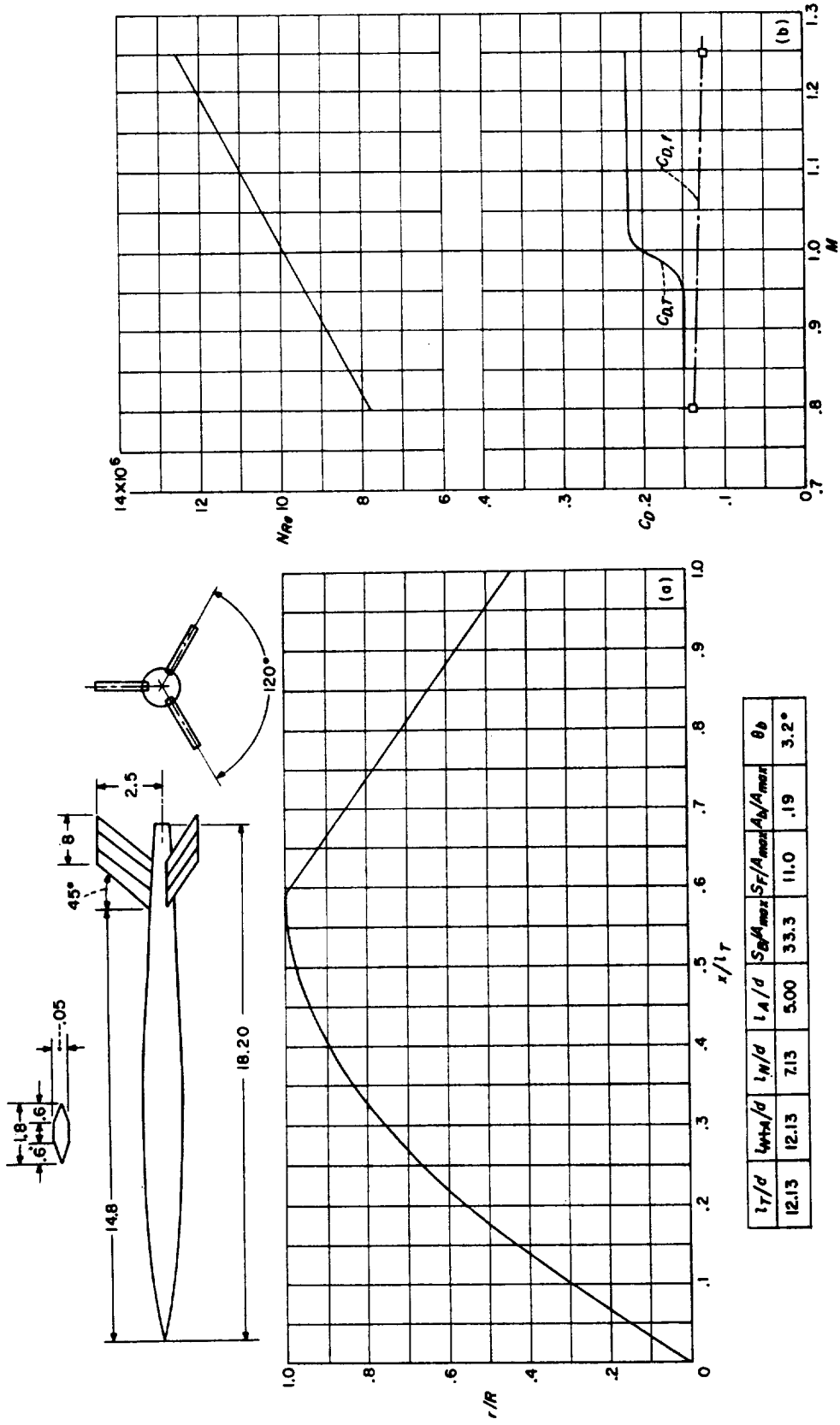

l_T/d	l_{W+A}/d	l_N/d	l_A/d	S_B/A_{max}	S_F/A_{max}	A_b/A_{max}	θ_b
12.13	12.13	7.13	5.00	33.3	11.0	.19	3.2°

(a) Body shape. (Dimensions given are in inches.) (b) N_{Re} and C_D curves.

CONFIGURATION 101 (parabolic nose; conical afterbody); helium-gun test.

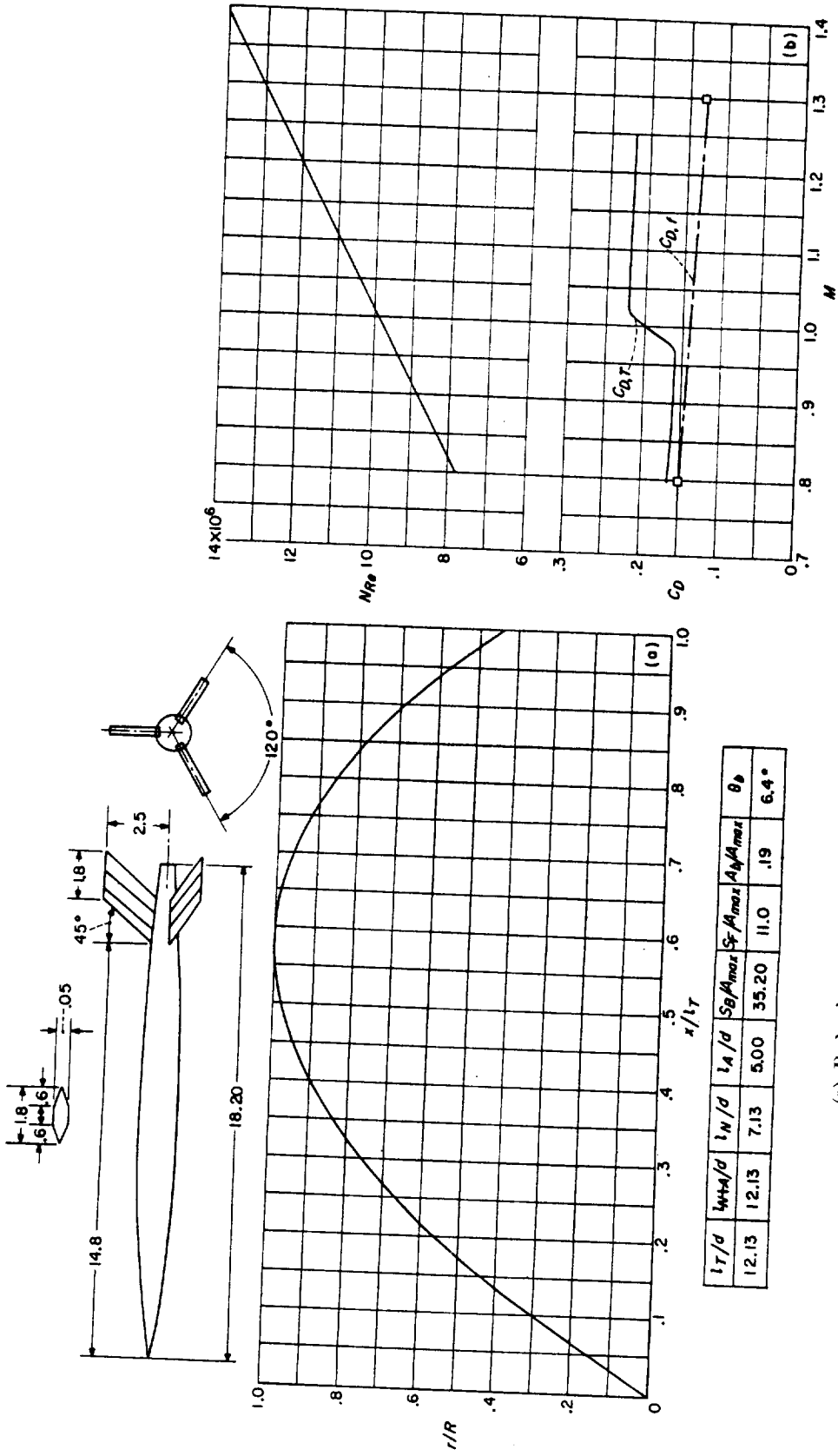

l_T/d	l_{N+A}/d	l_N/d	l_A/d	S_B/A_{max}	S_F/A_{max}	A_b/A_{max}	θ_b
12.13	12.13	7.13	5.00	35.20	11.0	.19	6.4°

(a) Body shape. (Dimensions given are in inches.) (b) N_{Re} and C_D curves.

CONFIGURATION 102 (parabolic nose and afterbody); helium-gun test.

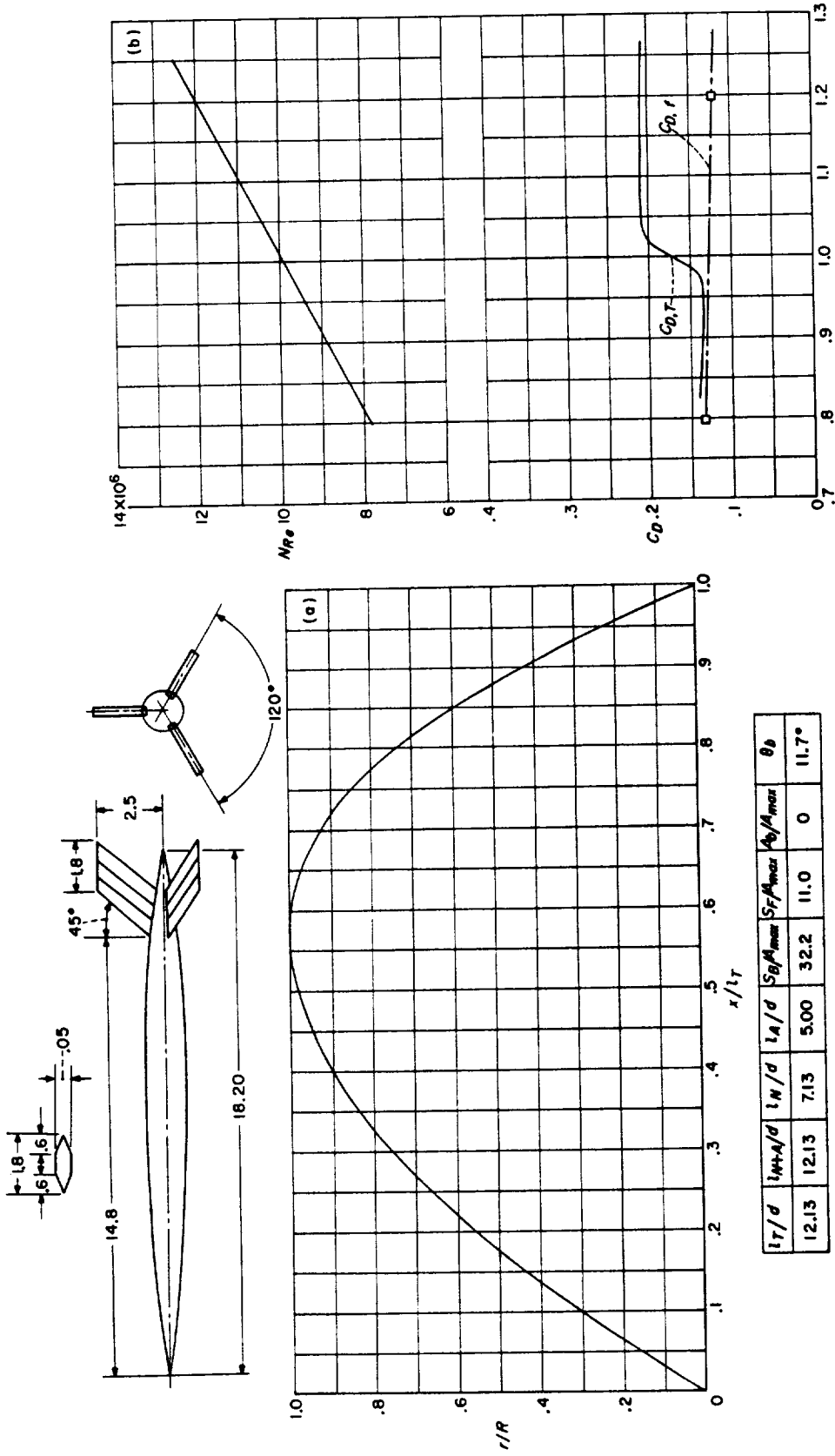

l_T/d	l_{M+A}/d	l_N/d	l_A/d	S_B/A_{max}	S_F/A_{max}	A_b/A_{max}	θ_b
12.13	12.13	7.13	5.00	32.2	11.0	0	11.7°

(a) Body shape. (Dimensions given are in inches.) (b) N_{Re} and C_D curves.

CONFIGURATION 103 (parabolic nose and afterbody); helium-gun test.

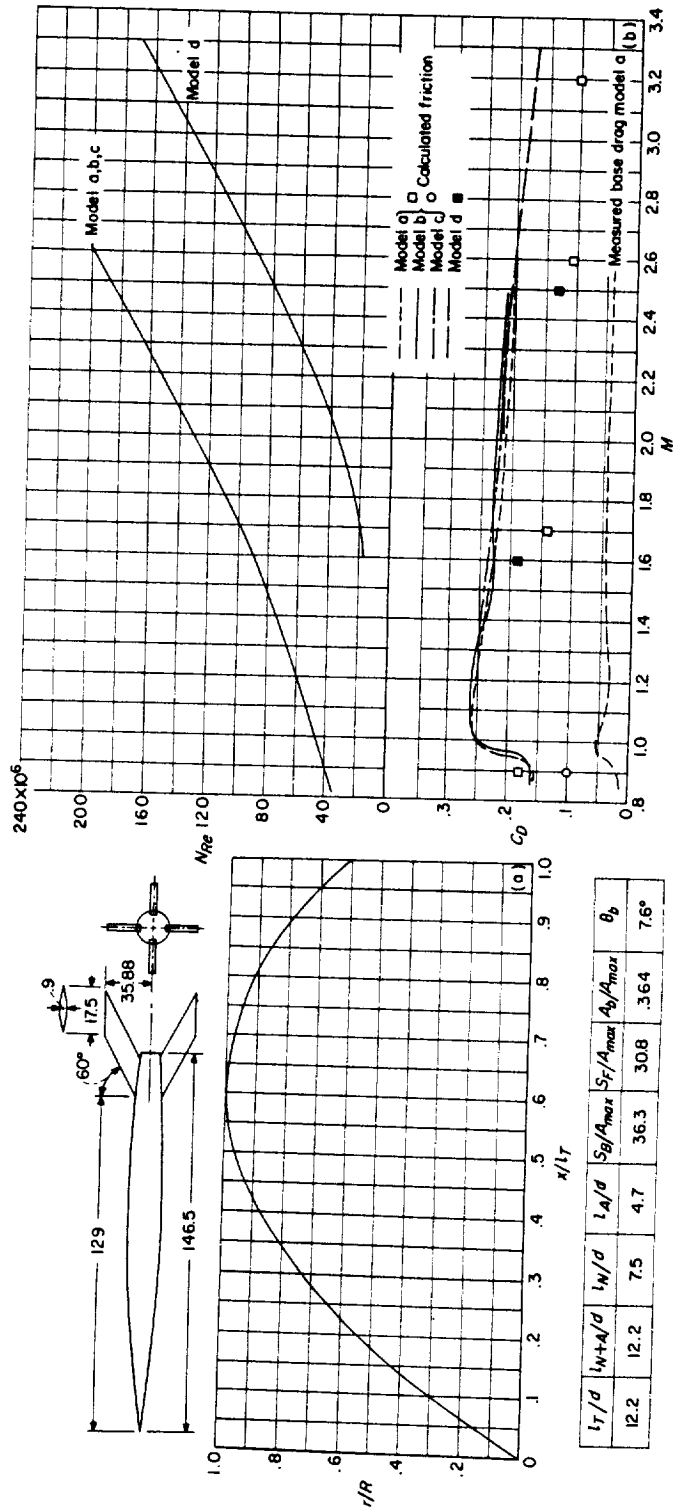

l_T/d	l_{N+A}/d	l_N/d	l_A/d	S_B/A_{max}	S_F/A_{max}	A_b/A_{max}	θ_b
12.2	12.2	7.5	4.7	36.3	30.8	.364	7.6°

(a) Body shape. (Dimensions given are in inches.) (b) N_{Re} and C_D curves.

CONFIGURATION 104 (parabolic nose and afterbody twice scale of configuration 105. Calculated friction drag coefficients are obviously too high. See note for configuration 105 about oscillations in drag curves); rocket test.

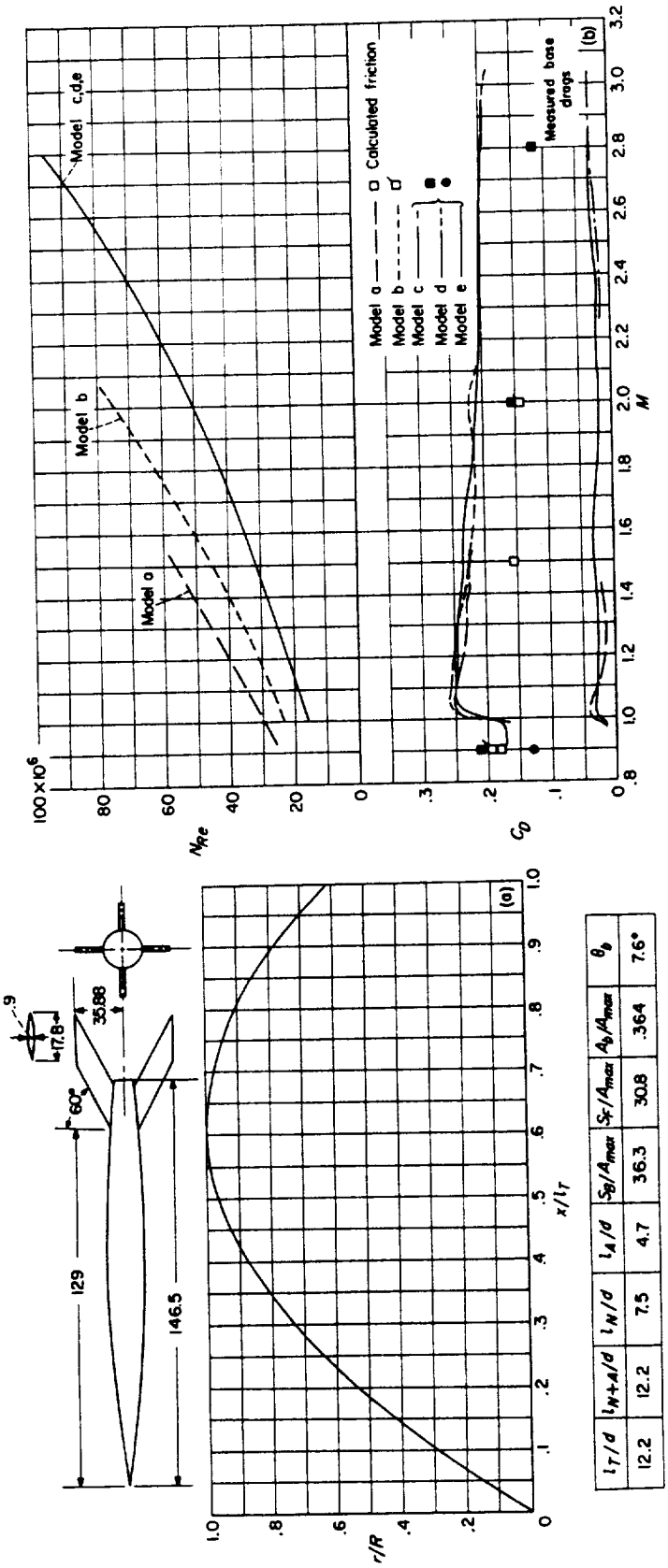

l_T/d	l_{W+A}/d	l_W/d	l_A/d	S_B/A_{max}	S_F/A_{max}	A_b/A_{max}	θ_b
12.2	12.2	7.5	4.7	36.3	30.8	.364	7.6°

(a) Body shape. (Dimensions given are in inches.) (b) N_{Re} and C_D curves.

CONFIGURATION 105; rocket test.

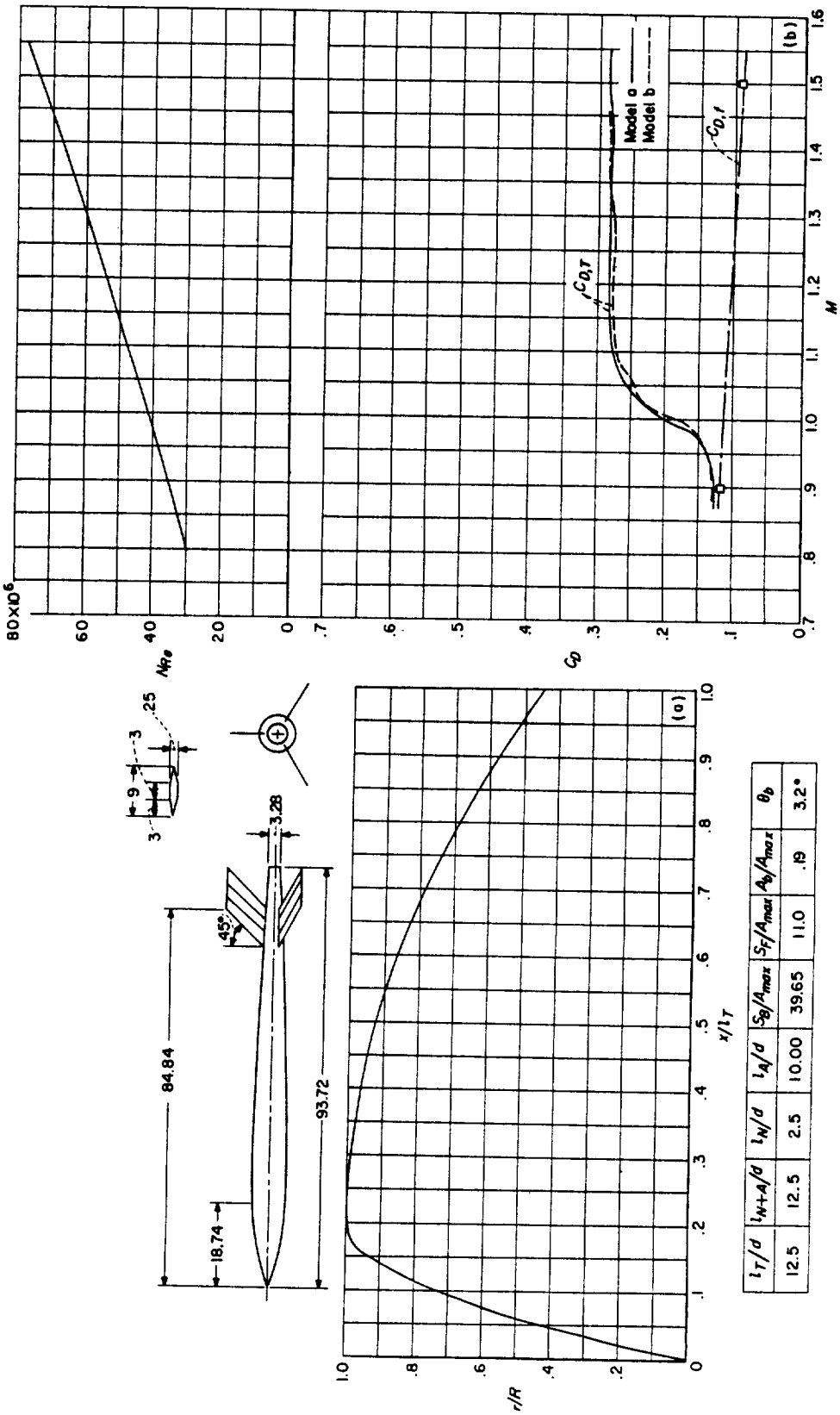

l_T/d	l_{N+A}/d	l_N/d	l_A/d	S_B/A_{max}	S_F/A_{max}	A_b/A_{max}	θ_b
12.5	12.5	2.5	10.00	39.65	11.0	.19	3.2°

(a) Body shape. (Dimensions given are in inches.) (b) N_{Re} and C_D curves.

CONFIGURATION 106 (parabolic nose and afterbody); rocket test.

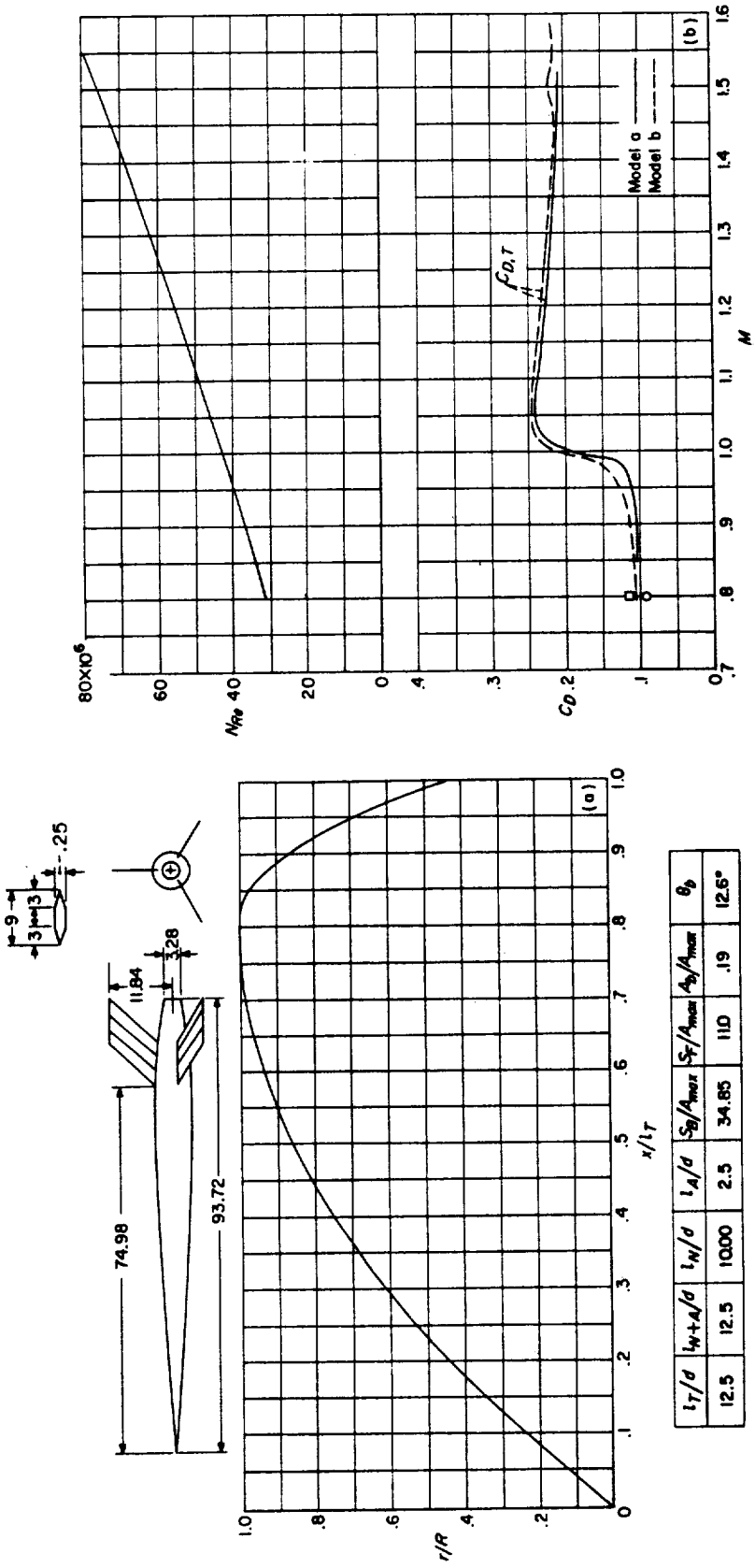

l_T/d	l_{W+A}/d	l_W/d	l_A/d	S_B/A_{MAX}	S_F/A_{MAX}	A_b/A_{MAX}	θ_b
12.5	12.5	10.00	2.5	34.85	110	.19	12.6°

(a) Body shape. (Dimensions given are in inches.) (b) N_{R_θ} and C_D curves.

CONFIGURATION 107 (parabolic nose and afterbody); rocket test.

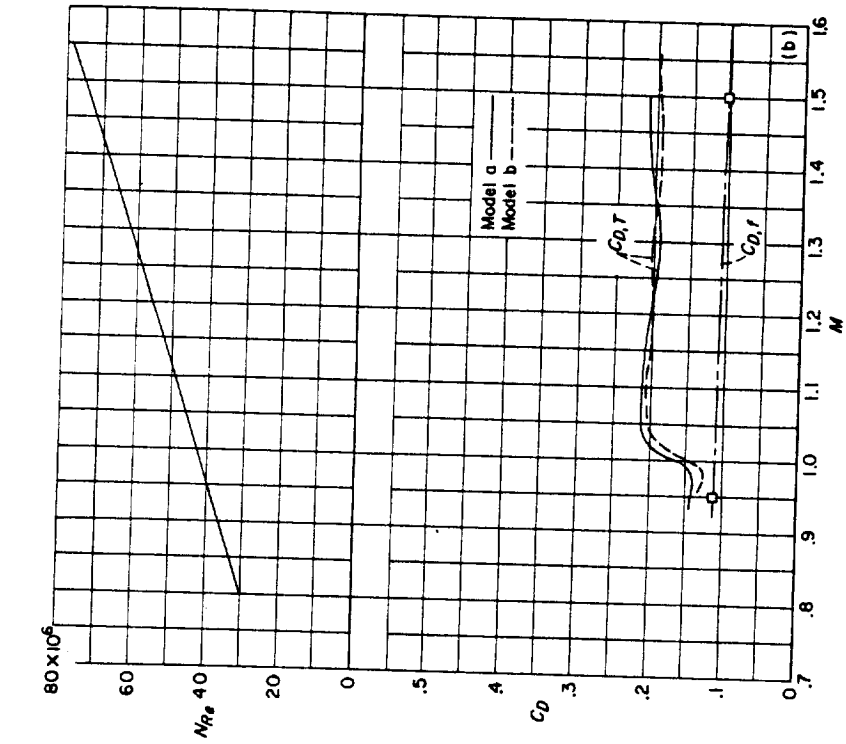

(b) N_{Re} and C_D curves.

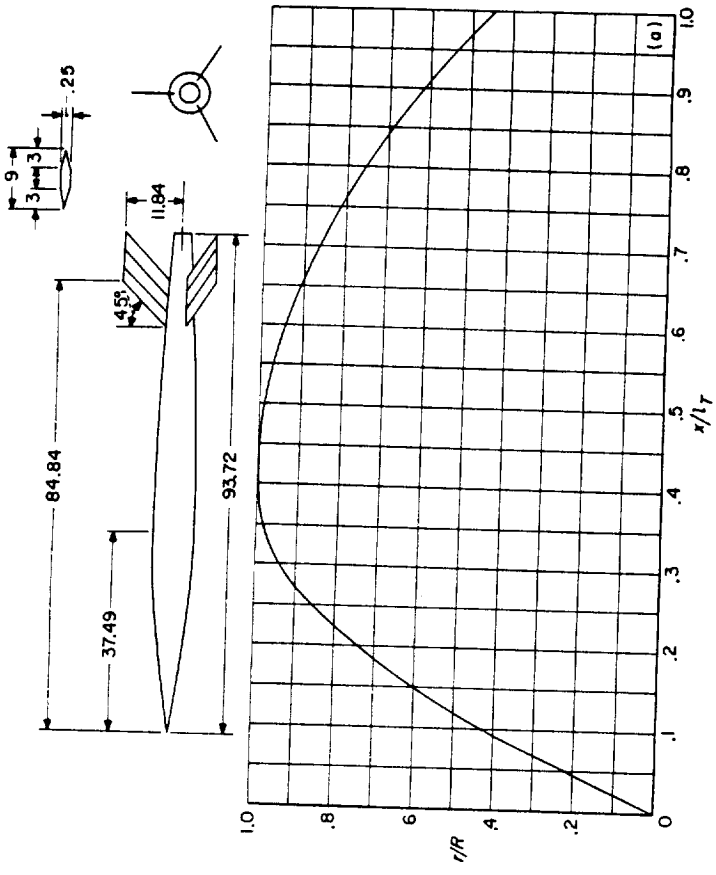

l_T/d	l_{N+A}/d	l_N/d	l_A/d	S_B/A_{max}	S_F/A_{max}	A_b/A_{max}	θ_b
12.5	12.5	5.00	7.50	38.10	11.0	.19	4.3°

(a) Body shape. (Dimensions given are in inches.)

CONFIGURATION 108 (parabolic nose and afterbody; both models appear to have been affected by rocket afterburning, which caused the wavy curve of C_D at supersonic Mach numbers); rocket test.

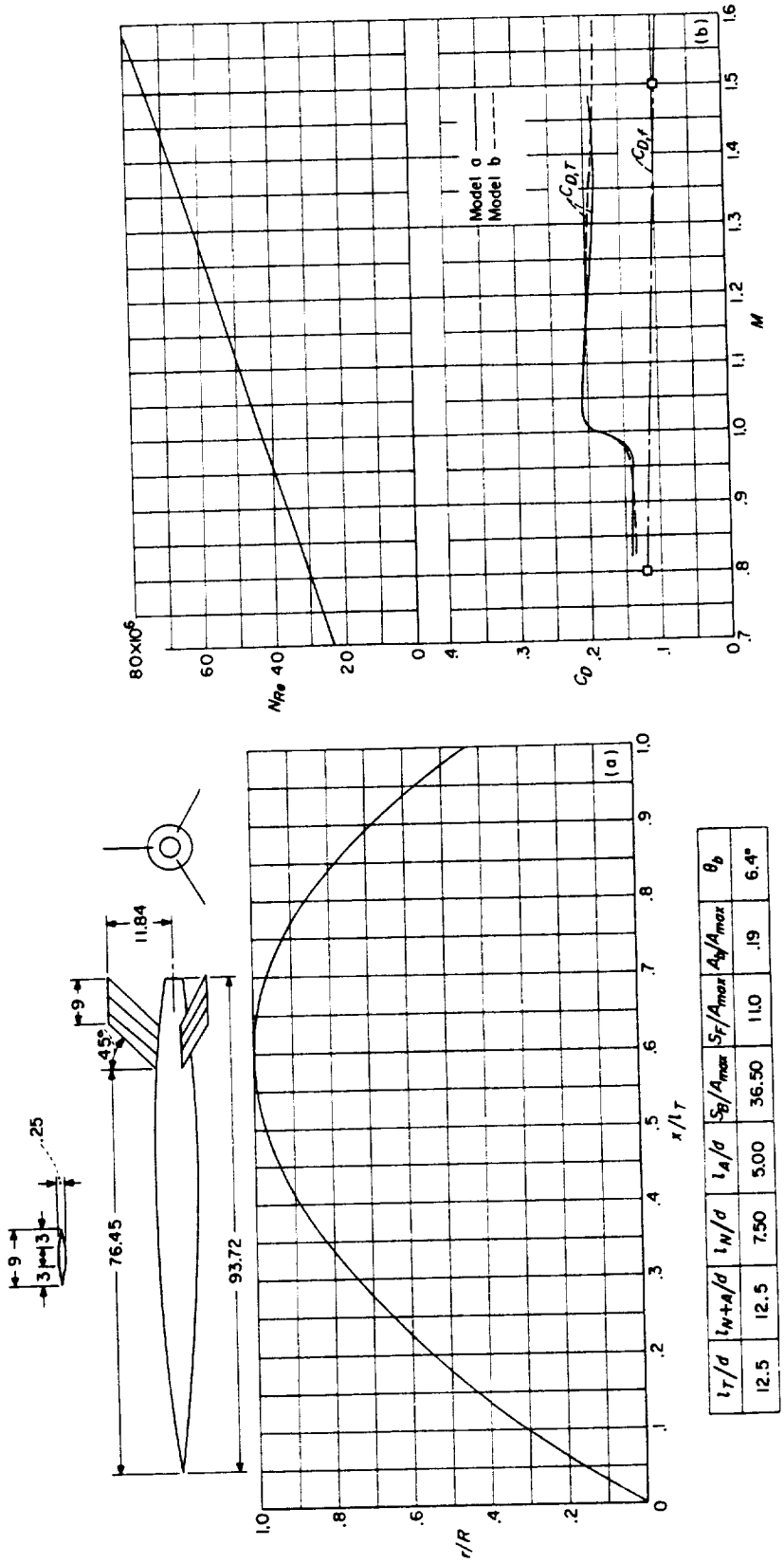

l_T/d	l_{N+A}/d	l_N/d	l_A/d	S_B/A_{max}	S_F/A_{max}	A_B/A_{max}	θ_b
12.5	12.5	7.50	5.00	36.50	11.0	.19	6.4°

(a) Body shape. (Dimensions given are in inches.) (b) N_{Re} and C_D curves.

CONFIGURATION 109 (parabolic nose and afterbody); rocket test.

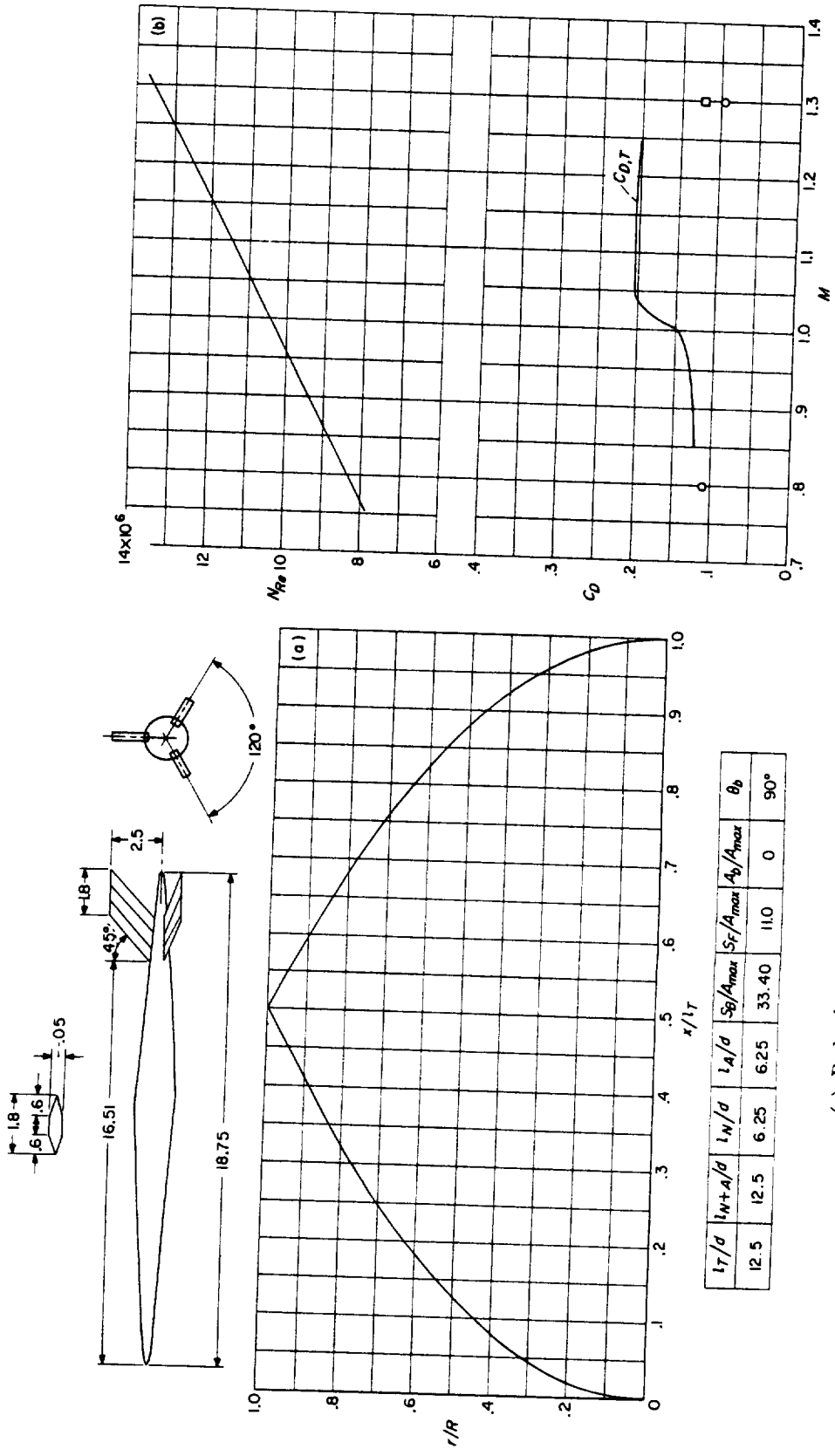

l_T/d	l_{N+A}/d	l_N/d	l_A/d	S_B/A_{max}	S_T/A_{max}	A_b/A_{max}	θ_b
12.5	12.5	6.25	6.25	33.40	11.0	0	90°

(a) Body shape. (Dimensions given are in inches.) (b) N_{Re} and C_D curves.

CONFIGURATION 110 (nose and afterbody, $\frac{r}{R}=\frac{x^{3/4}}{l^{3/4}}$); helium-gun test.

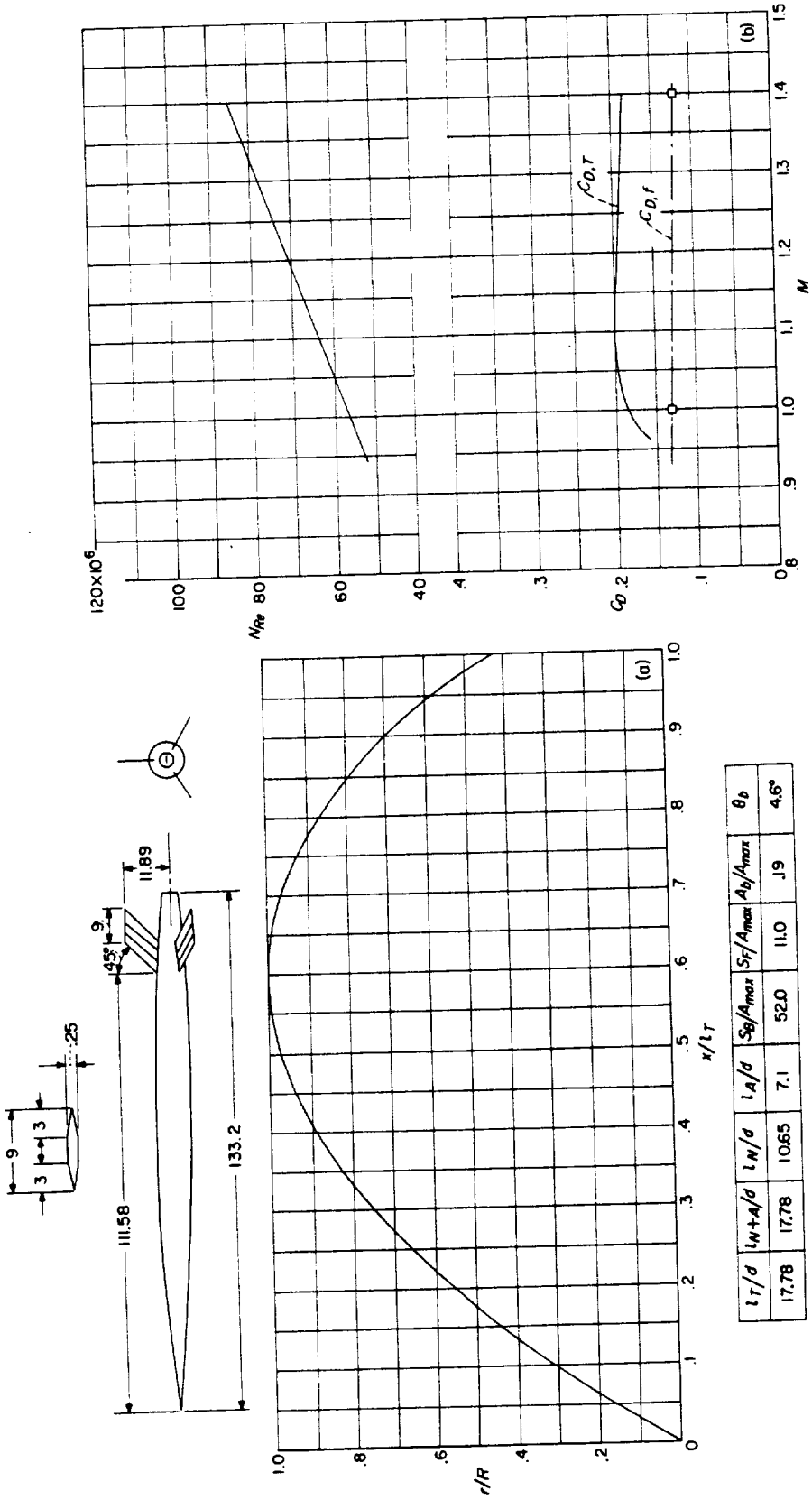

l_T/d	l_{N+A}/d	l_N/d	l_A/d	S_B/A_{max}	S_F/A_{max}	A_b/A_{max}	θ_b
17.78	17.78	10.65	7.1	52.0	11.0	.19	4.6°

(a) Body shape. (Dimensions given are in inches.) (b) N_{Re} and C_D curves.

CONFIGURATION 111 (parabolic nose and afterbody); rocket test.

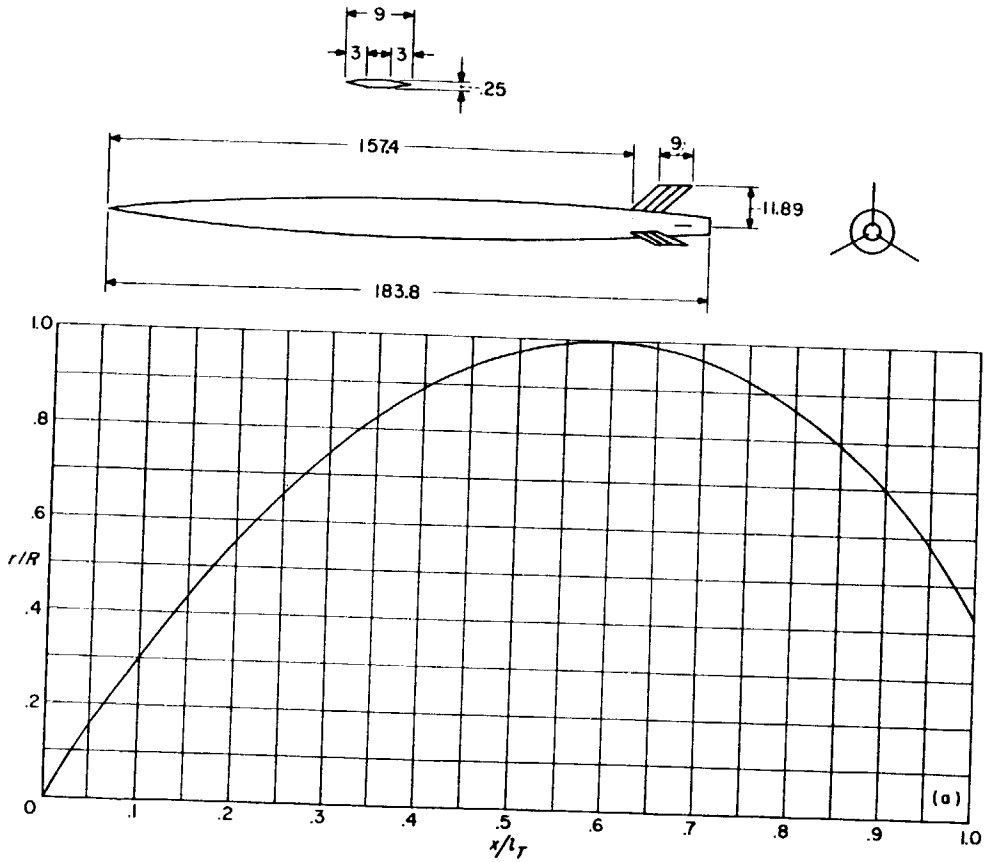

l_T/d	l_{N+A}/d	l_N/d	l_A/d	S_B/A_{max}	S_F/A_{max}	A_b/A_{max}	θ_b
24.5	24.5	14.7	9.8	71.6	11.0	.19	3.3°

(a) Body shape. (Dimensions given are in inches.)

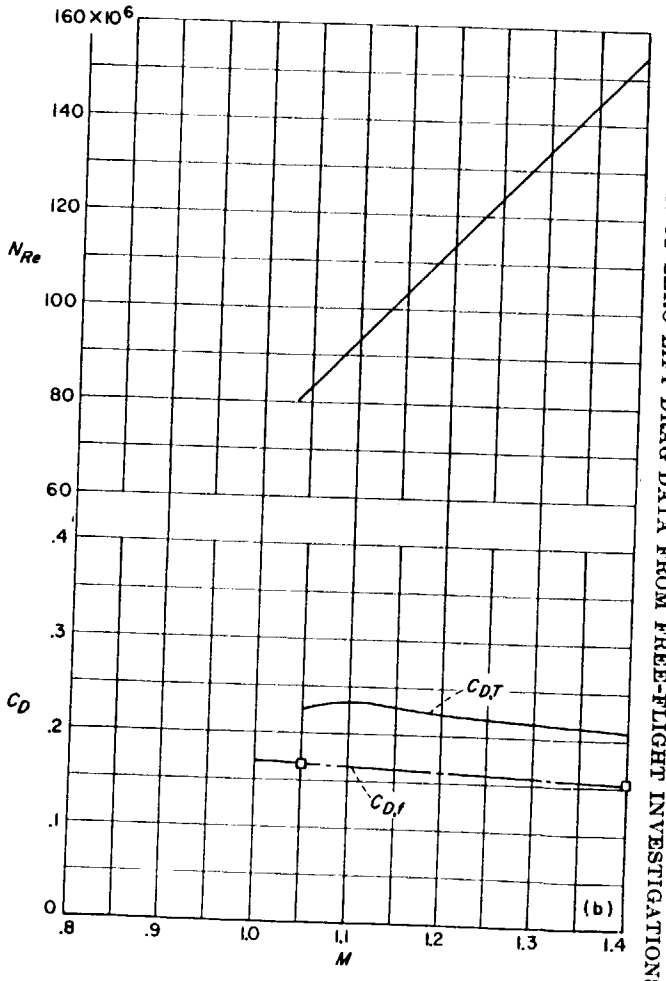

(b) N_{Re} and C_D curves.

CONFIGURATION 112; rocket test.

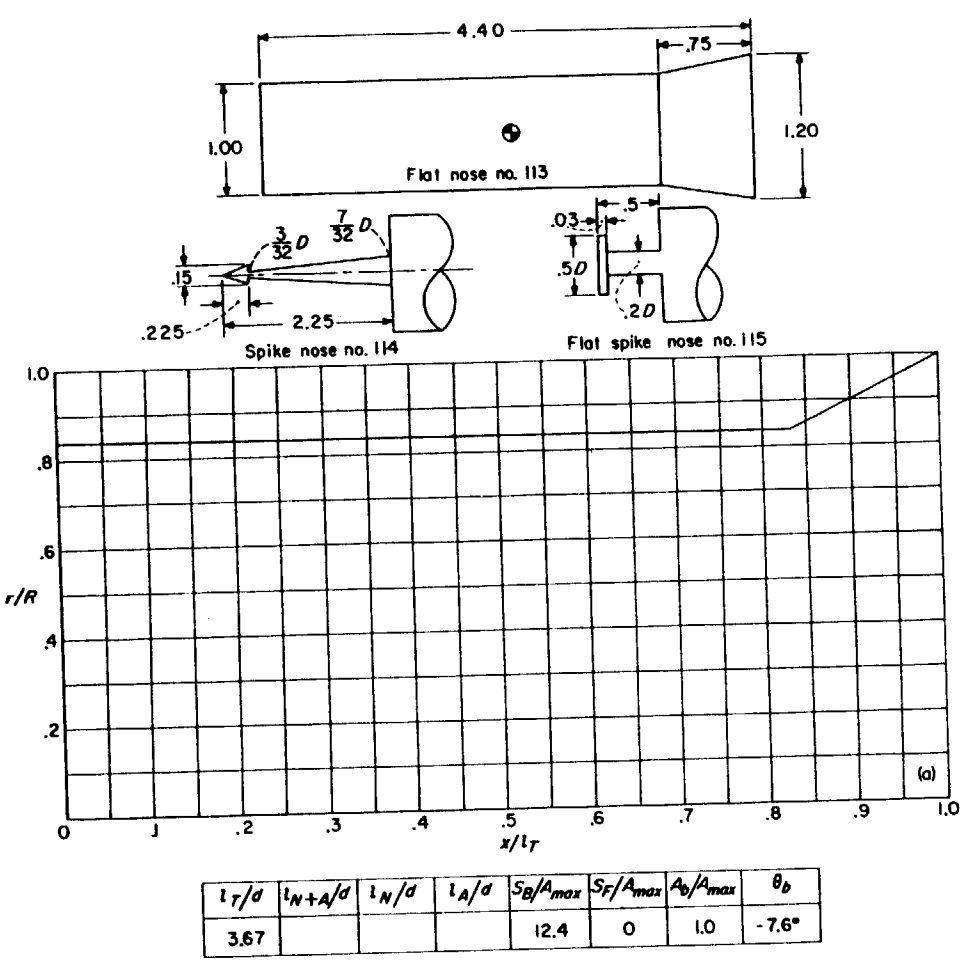

l_T/d	l_{N+A}/d	l_N/d	l_A/d	S_B/A_{max}	S_F/A_{max}	A_b/A_{max}	θ_b
3.67				12.4	0	1.0	-7.6°

(a) Body shape. (Dimensions given are in inches.)

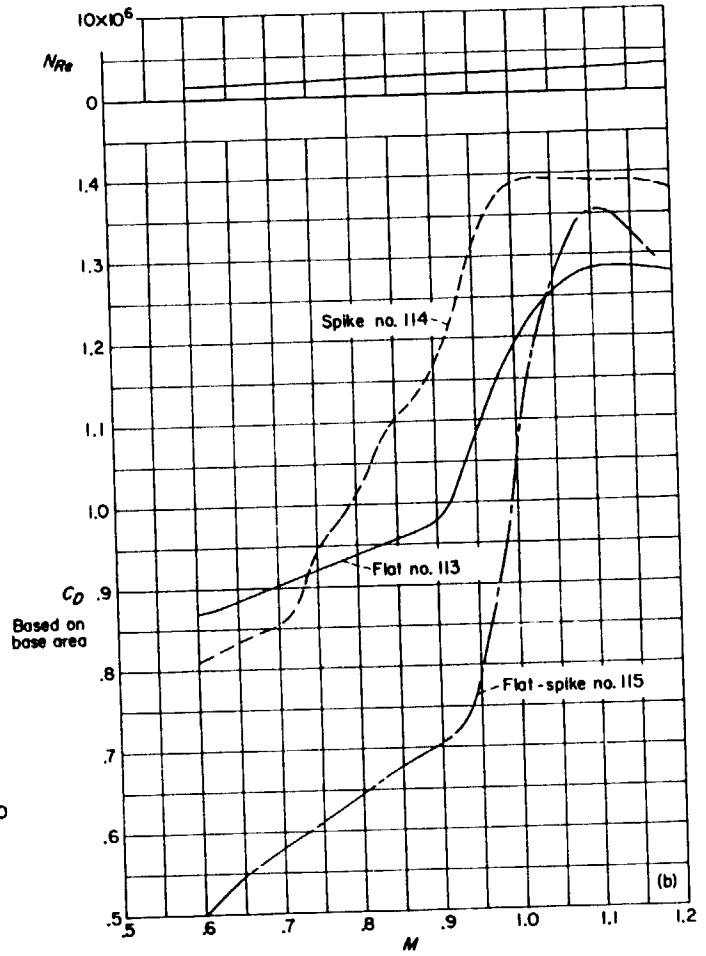

(b) N_{Re} and C_D curves.

CONFIGURATIONS 113, 114, 115; helium-gun test. (Curves presented are faired values obtained from the drag of two models for each of the configurations. In each case the drags of the identical models were quite close, indicating that the models were at essentially 0° angle of attack since it does not appear reasonable that the drag due to oscillations would be a repeatable phenomena.)

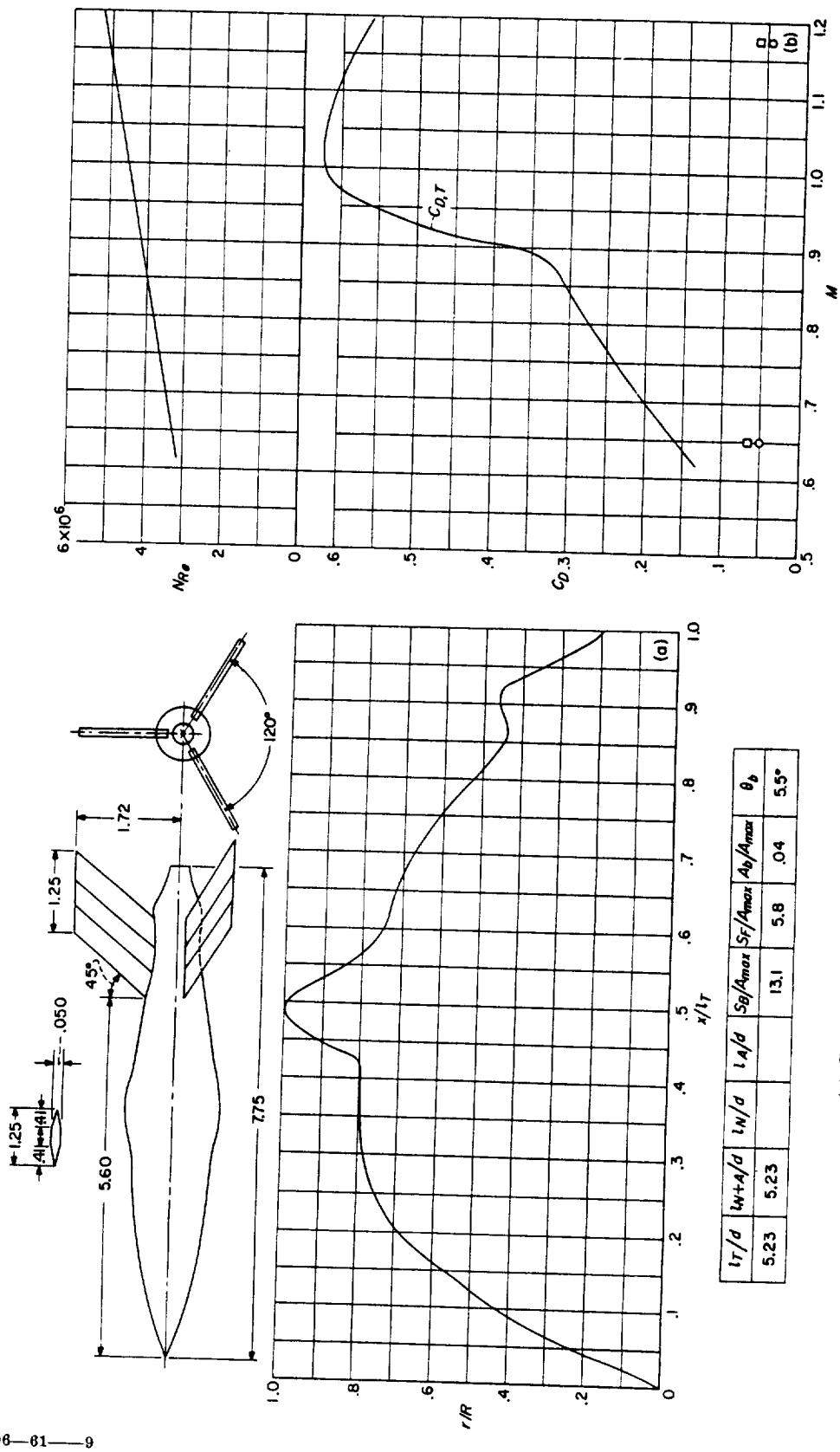

l_T/d	l_{N+A}/d	l_N/d	l_A/d	S_B/A_{max}	S_F/A_{max}	A_b/A_{max}	θ_b
5.23	5.23			13.1	5.8	.04	5.5°

(a) Body shape. (Dimensions given are in inches.) (b) N_{Re} and C_D curves.

CONFIGURATION 116; helium-gun test.

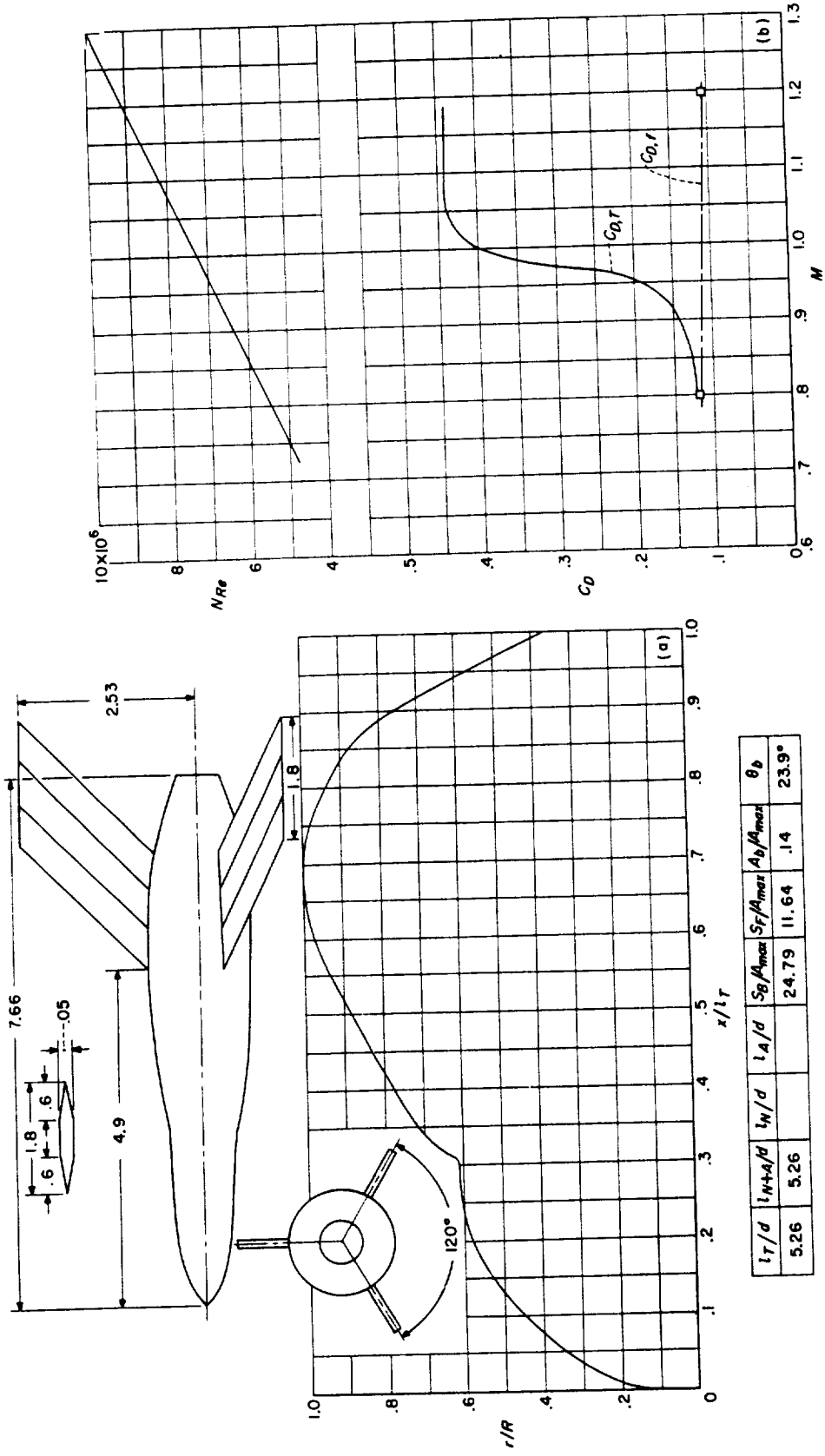

l_T/d	l_{N+A}/d	l_N/d	l_A/d	S_B/A_{max}	S_F/A_{max}	A_b/A_{max}	θ_b
5.26	5.26			24.79	11.64	.14	23.9°

(a) Body shape. (Dimensions given are in inches.) (b) N_{Re} and C_D curves.

CONFIGURATION 117; helium-gun test.

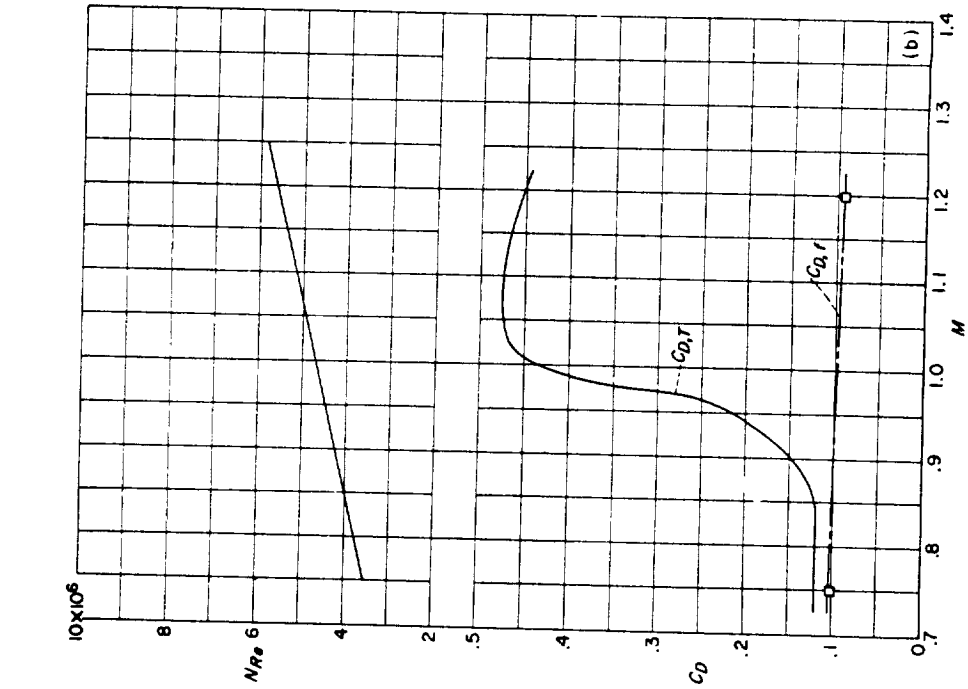

(b) N_{Re} and C_D curves.

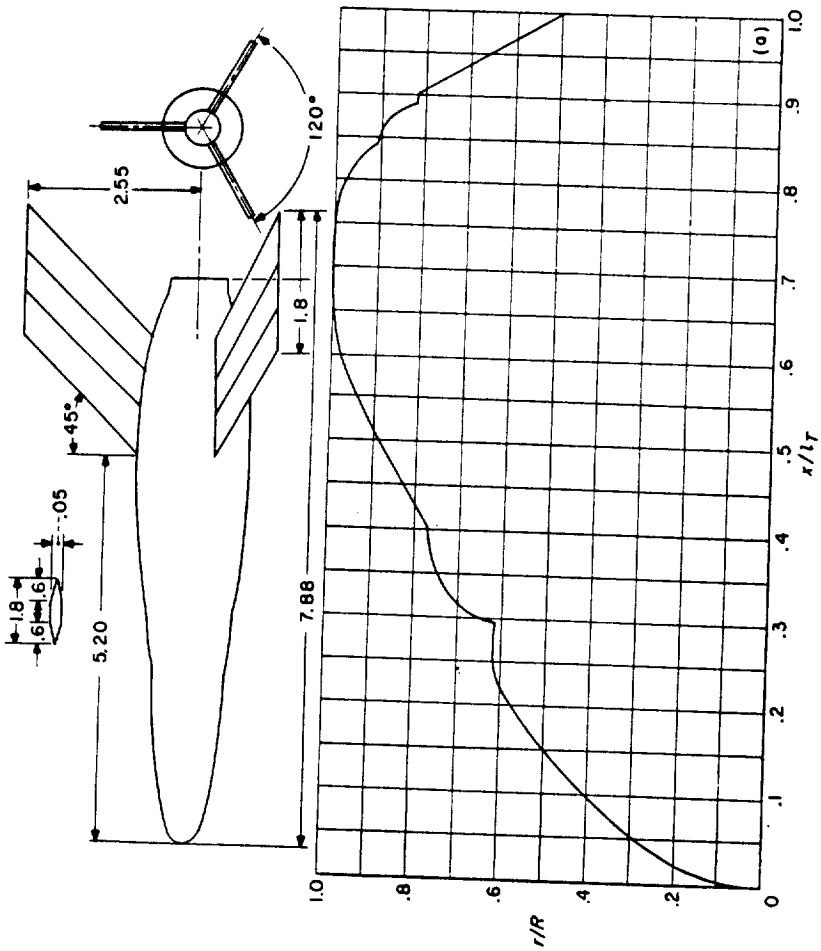

l_T/d	l_{M+A}/d	l_W/d	l_A/d	S_B/A_{max}	S_F/A_{max}	A_b/A_{max}	θ_b
5.29	5.29			16.0	11.64	.23	17.3°

(a) Body shape. (Dimensions given are in inches.)

CONFIGURATION 118; helium-gun test.

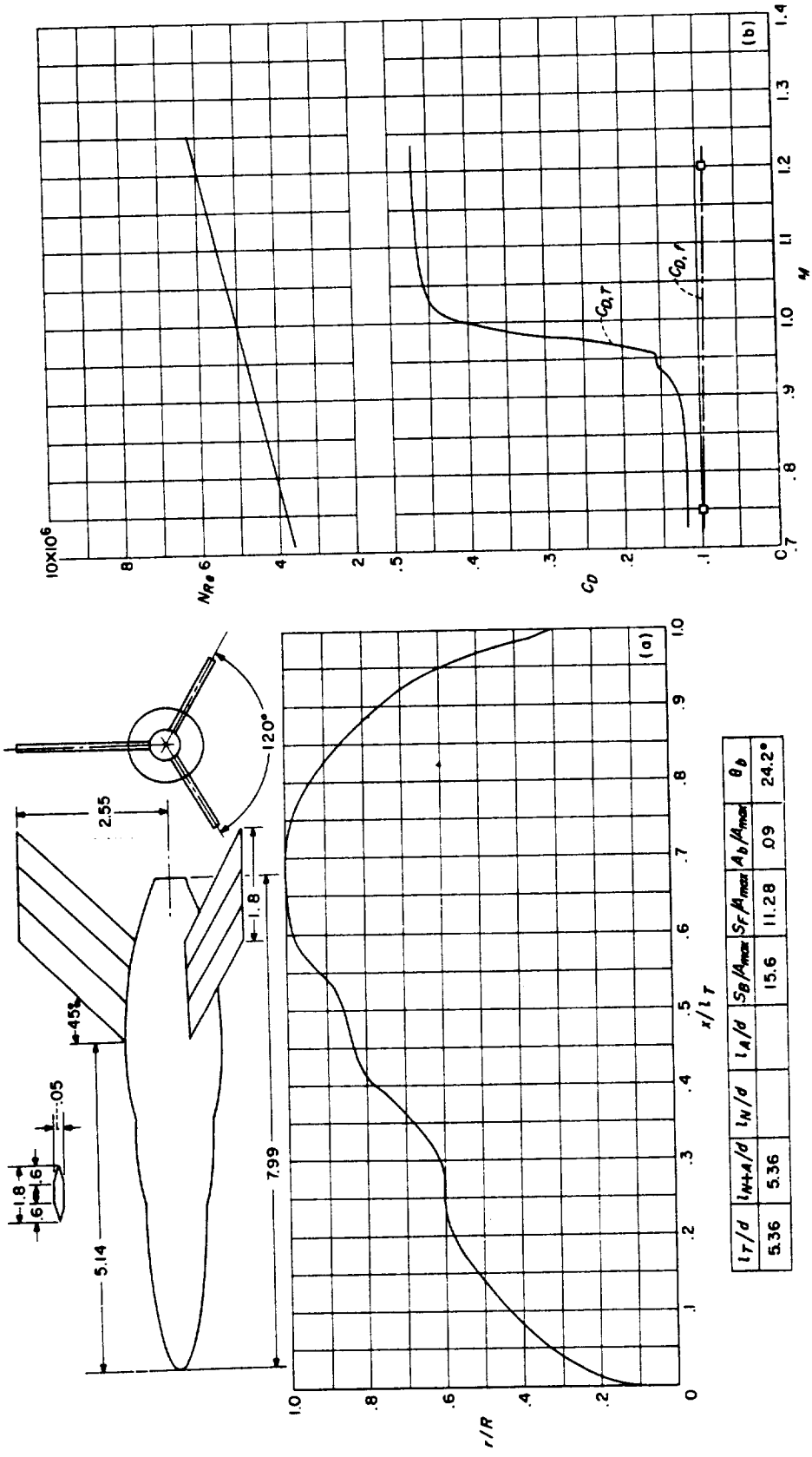

l_T/d	l_{N+A}/d	l_N/d	l_A/d	S_B/A_{max}	S_F/A_{max}	A_b/A_{max}	θ_b
5.36	5.36			15.6	11.28	.09	24.2°

(a) Body shape. (Dimensions given are in inches.) (b) N_{Re} and C_D curves.

CONFIGURATION 119; helium-gun test.

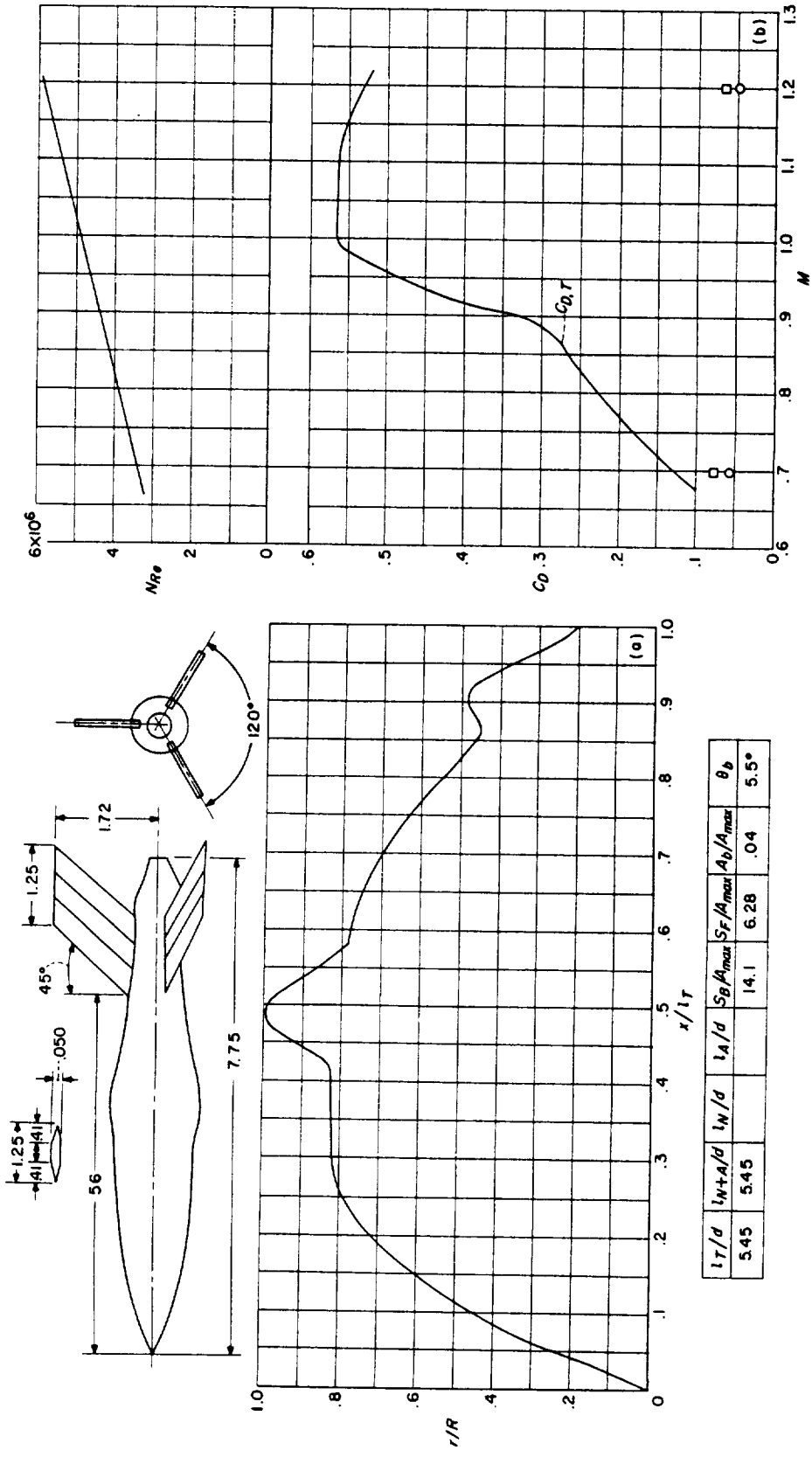

l_T/d	l_{N+A}/d	l_N/d	l_A/d	S_B/A_{max}	S_F/A_{max}	A_b/A_{max}	θ_b
5.45	5.45			14.1	6.28	.04	5.5°

(a) Body shape. (Dimensions given are in inches.) (b) N_{Re} and C_D curves.

CONFIGURATION 120; helium-gun test.

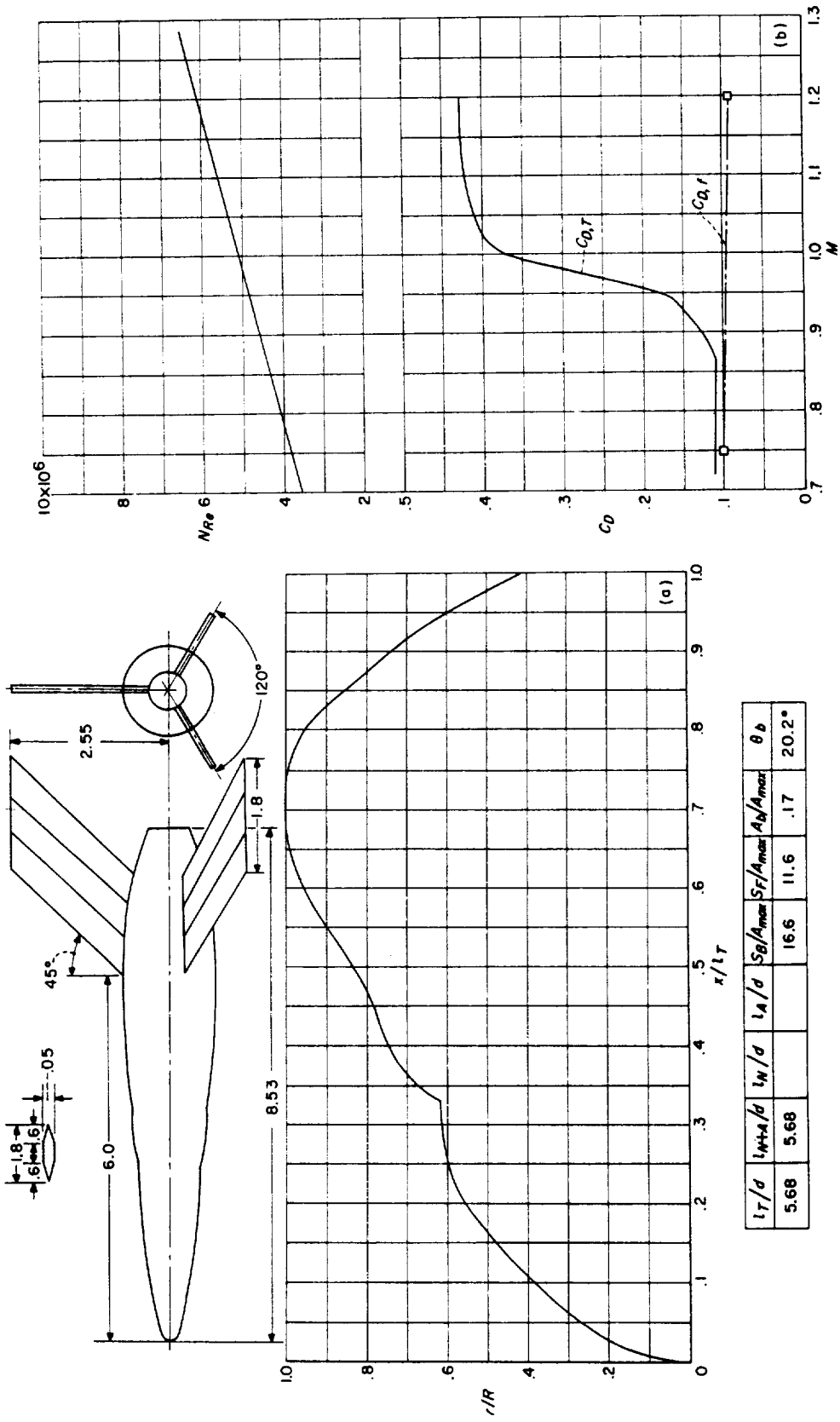

l_T/d	l_{N+A}/d	l_N/d	l_A/d	S_B/A_{max}	S_F/A_{max}	A_b/A_{max}	θ_b
5.68	5.68			16.6	11.6	.17	20.2°

(a) Body shape. (Dimensions given are in inches.) (b) N_{Re} and C_D curves.

CONFIGURATION 121; helium-gun test.

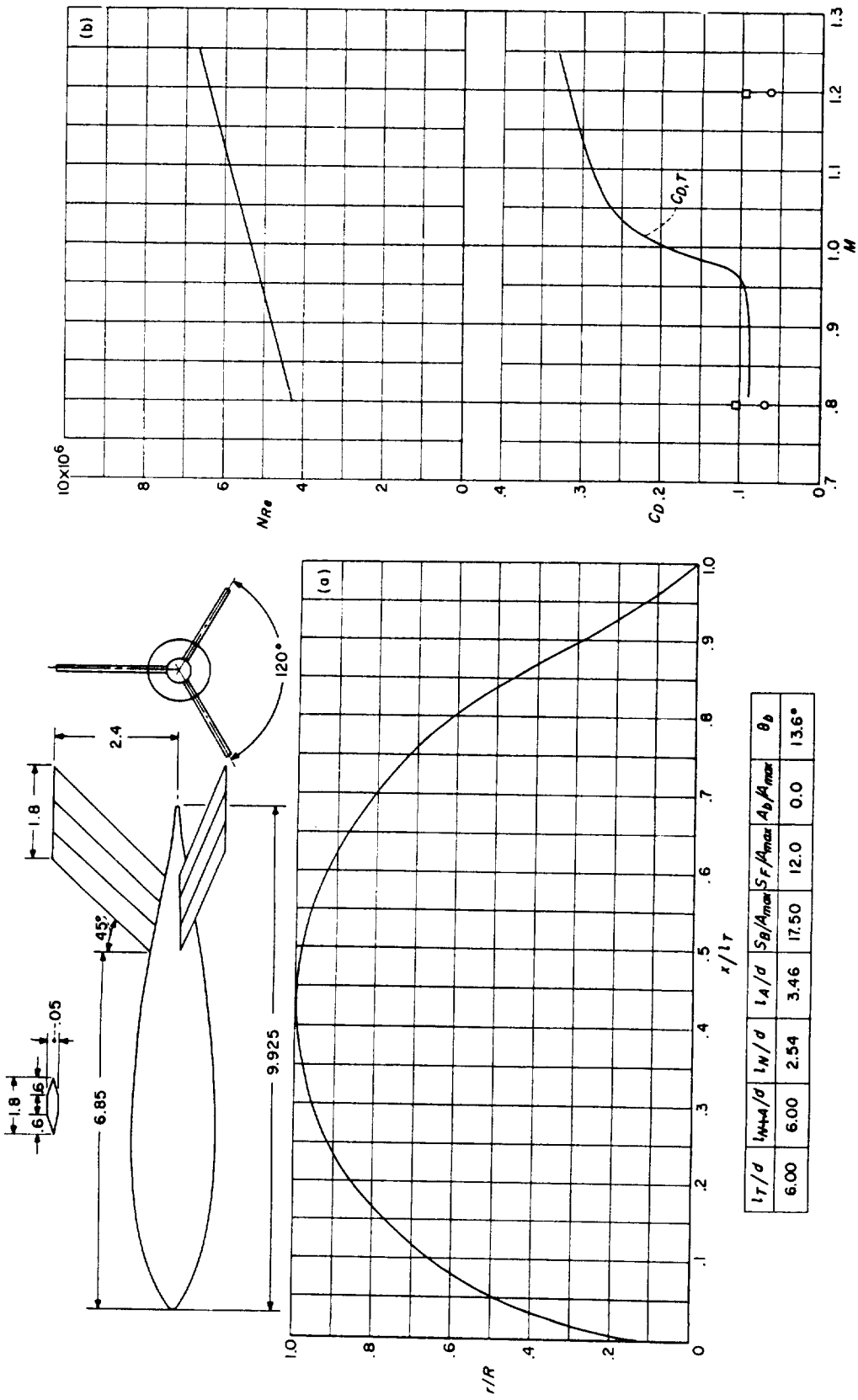

l_T/d	l_{N+A}/d	l_N/d	l_A/d	S_B/A_{max}	S_F/A_{max}	A_b/A_{max}	θ_b
6.00	6.00	2.54	3.46	17.50	12.0	0.0	13.6°

(a) Body shape (Dimensions given are in inches.) (b) N_{Re} and C_D curves.

CONFIGURATION 122; helium-gun test.

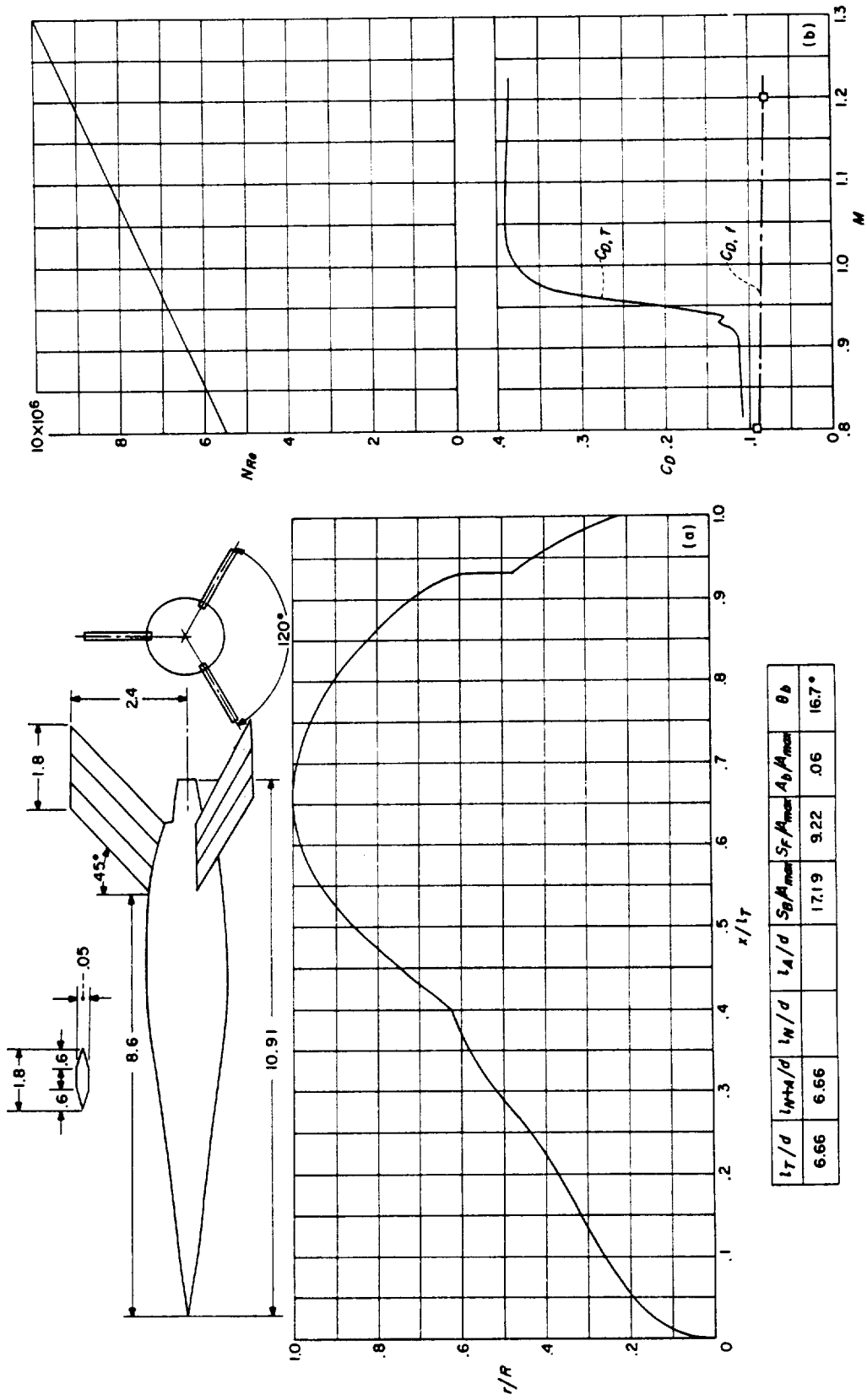

l_T/d	l_{N+A}/d	l_N/d	l_A/d	S_B/A_{max}	S_F/A_{max}	A_b/A_{max}	θ_b
6.66	6.66			17.19	9.22	.06	16.7°

(a) Body shape. (Dimensions given are in inches.) (b) N_R, and C_D curves.

CONFIGURATION 123; helium-gun test. (Subsonic flow probably separated at rear step.)

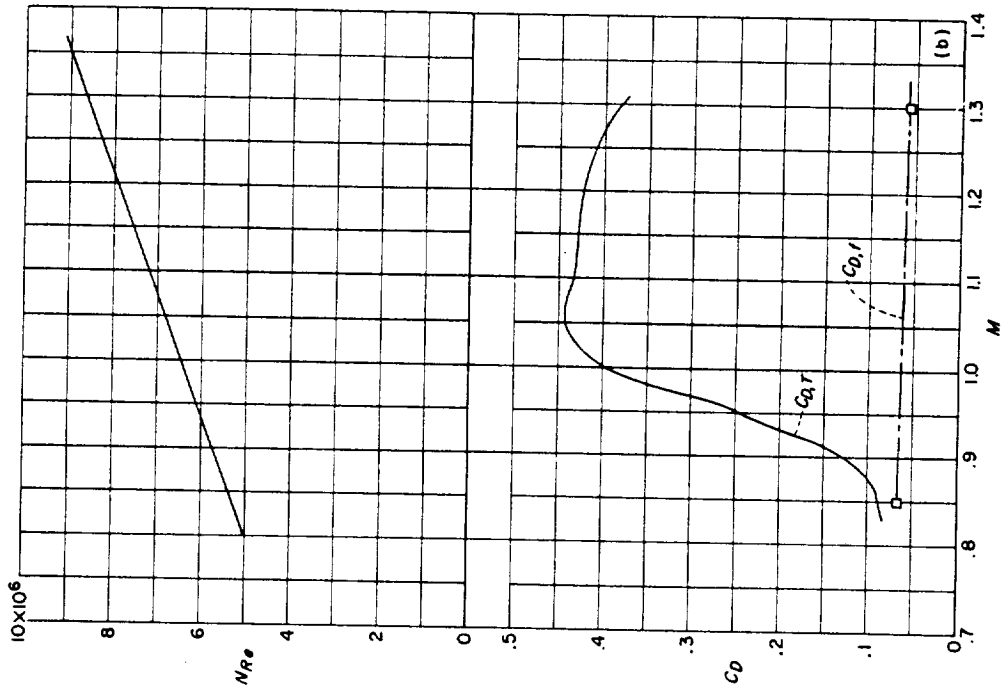

(b) N_{Re} and C_D curves.

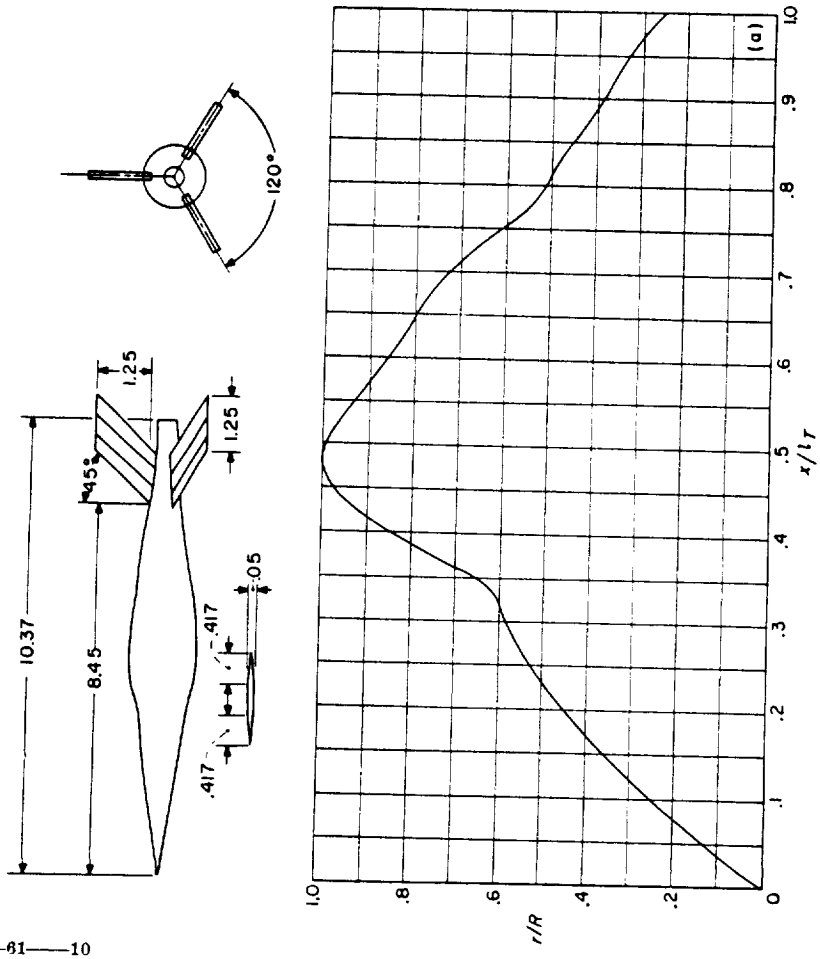

l_T/d	l_{N+A}/d	l_N/d	l_A/d	S_B/A_{max}	S_F/A_{max}	A_b/A_{max}	θ_b
6.82	6.82			15.7	5.43	.065	5.0°

(a) Body shape. (Dimensions given are in inches.)

CONFIGURATION 124; helium-gun test.

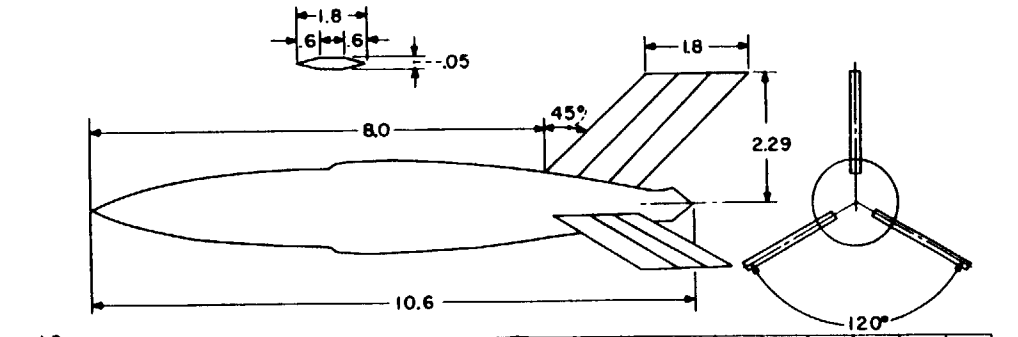

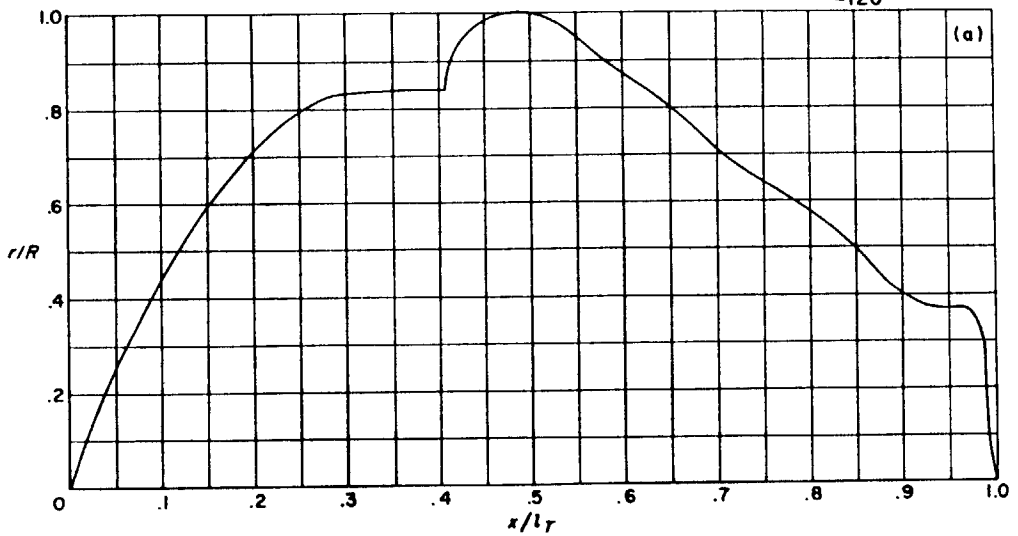

l_T/d	l_{N+A}/d	l_N/d	l_A/d	S_B/A_{max}	S_F/A_{max}	A_b/A_{max}	θ_b
6.84	6.84			18.2	10.76	0	90°

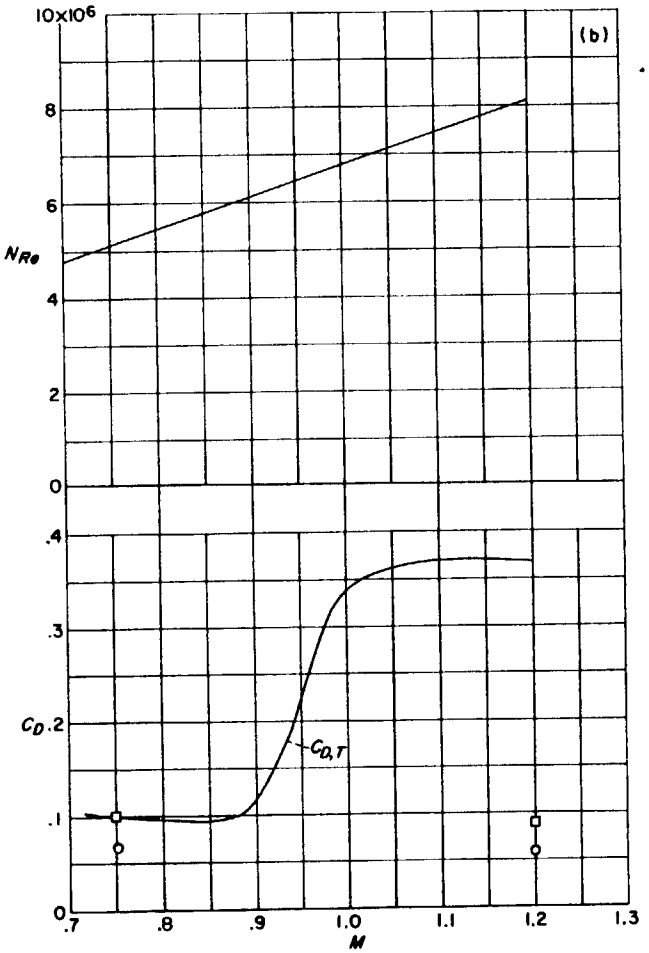

(a) Body shape. (Dimensions given are in inches.) (b) N_{Re} and C_D curves.

CONFIGURATION 125; helium-gun test. (Although the calculated friction drag indicates that the fins may be in turbulent flow at subsonic values of M, it is possible that they may be in laminar as their low Reynolds number would predict. The drag difference between the laminar friction calculations and the experimental subsonic values may be due to separation over the base $\left(\frac{x}{l_T} \approx 0.970\right)$ and over the forward step at $\frac{x}{l_T} = 0.4$.)

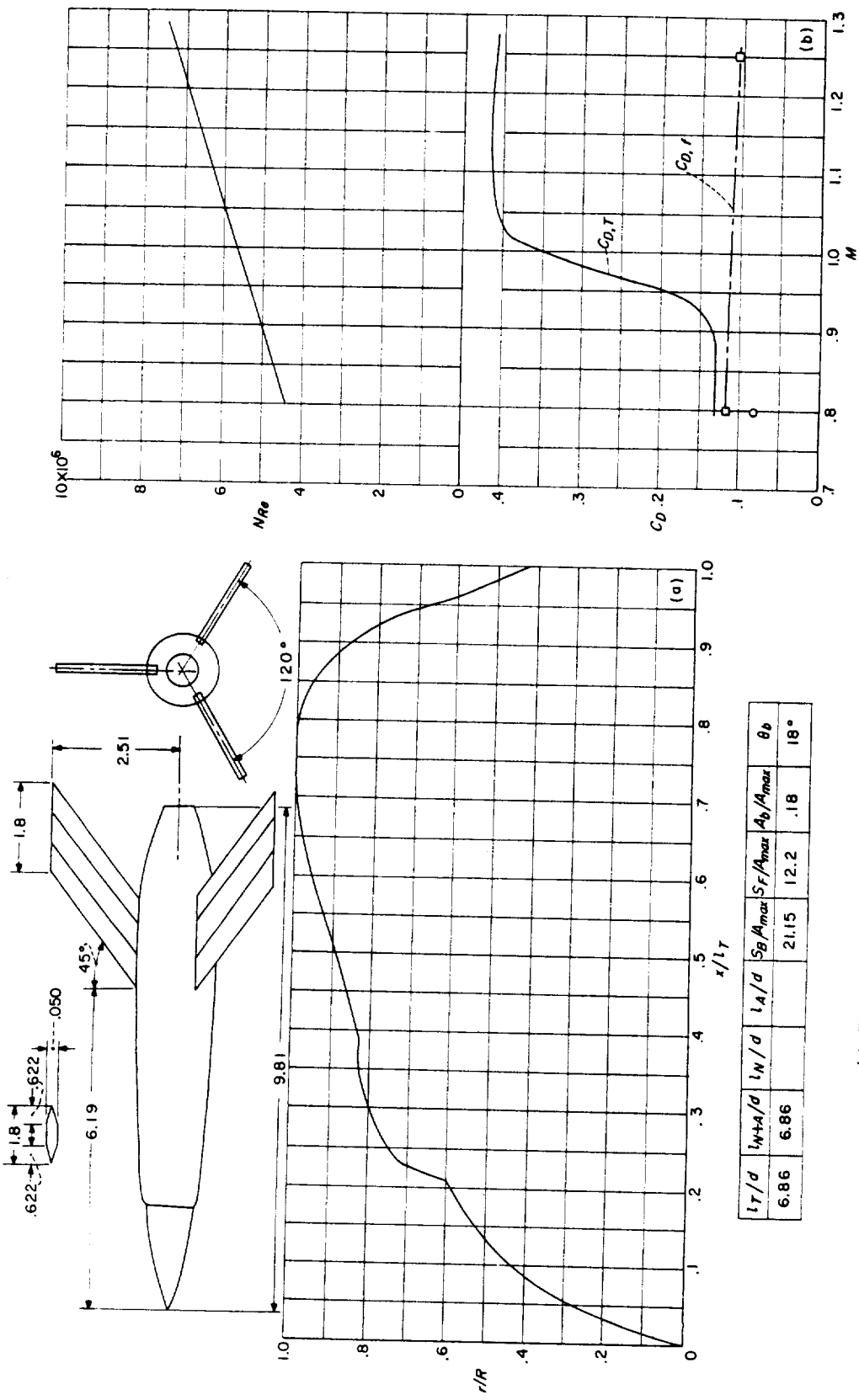

l_T/d	l_{N+A}/d	l_N/d	l_A/d	S_B/A_{max}	S_F/A_{max}	A_b/A_{max}	θ_b
6.86	6.86			21.15	12.2	.18	18°

(a) Body shape. (Dimensions given are in inches.) (b) N_{Re} and C_D curves.

CONFIGURATION 126; helium-gun test.

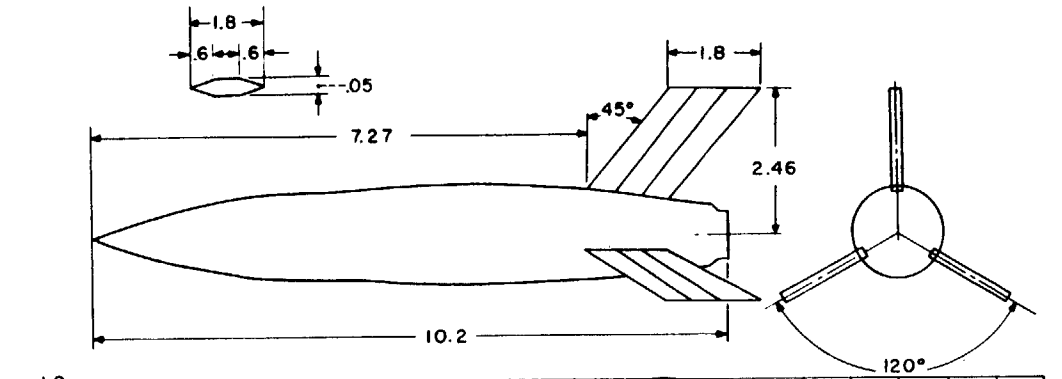

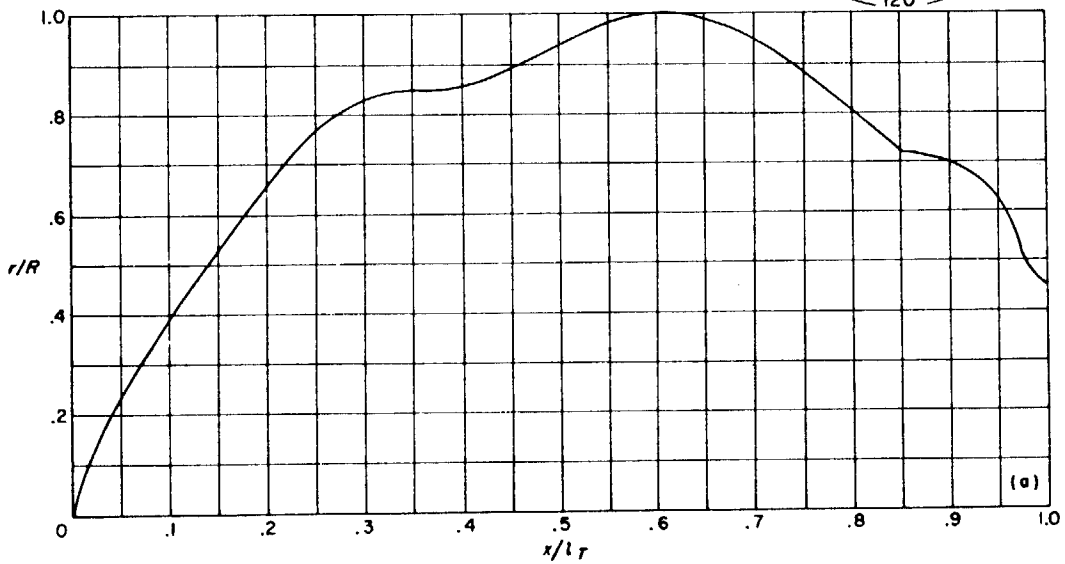

l_T/d	l_{N+A}/d	l_N/d	l_A/d	S_B/A_{max}	S_F/A_{max}	A_b/A_{max}	θ_b
6.95	6.95			19.90	11.64	.20	8.8°

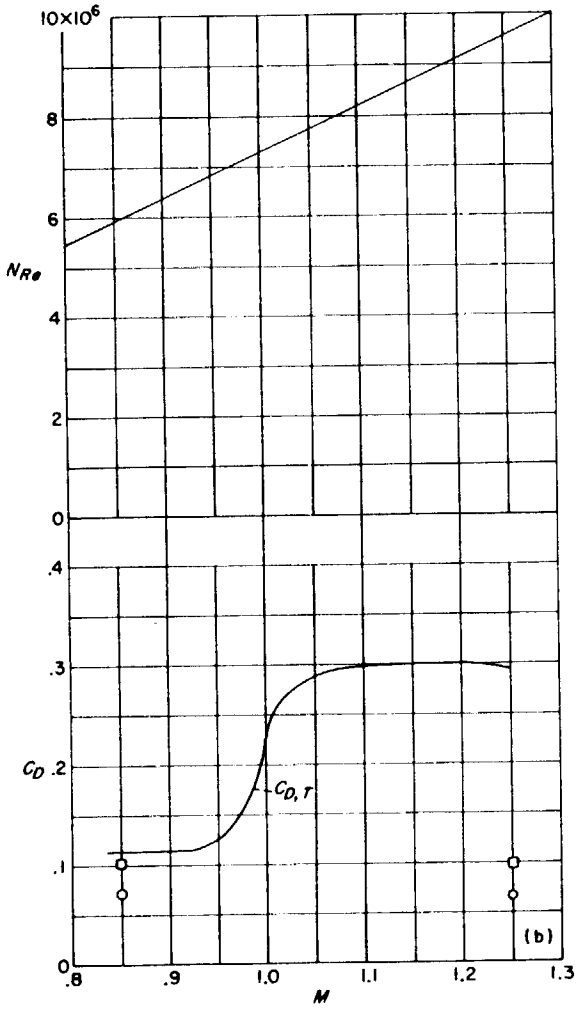

(a) Body shape. (Dimensions given are in inches.) (b) N_{R_θ} and C_D curves.

CONFIGURATION 127; helium-gun test. (Assuming separation at step $\left(\frac{x}{l_T} \approx 0.9\right)$ and subsonic $C_p = -0.1$, the subsonic base drag would be $C_{D,B} = 0.1 \times 0.5 = 0.05$. This would indicate that subsonic fin flow was laminar.)

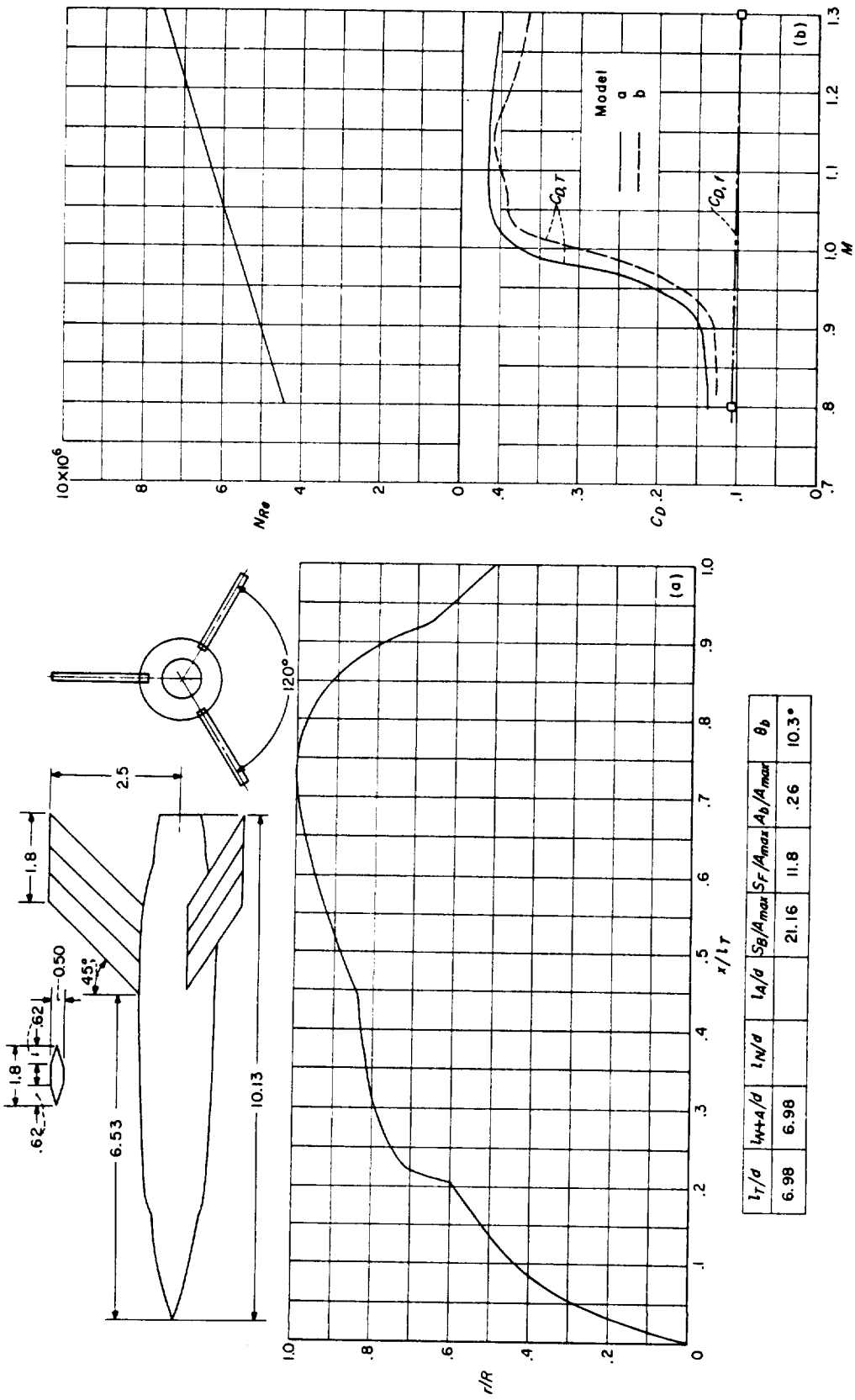

l_T/d	l_{N+A}/d	l_N/d	l_A/d	S_B/A_{max}	S_F/A_{max}	A_b/A_{max}	θ_b
6.98	6.98			21.16	11.8	.26	10.3°

(a) Body shape. (Dimensions given are in inches.) (b) N_{Re} and C_D curves.

CONFIGURATION 128; helium-gun test.

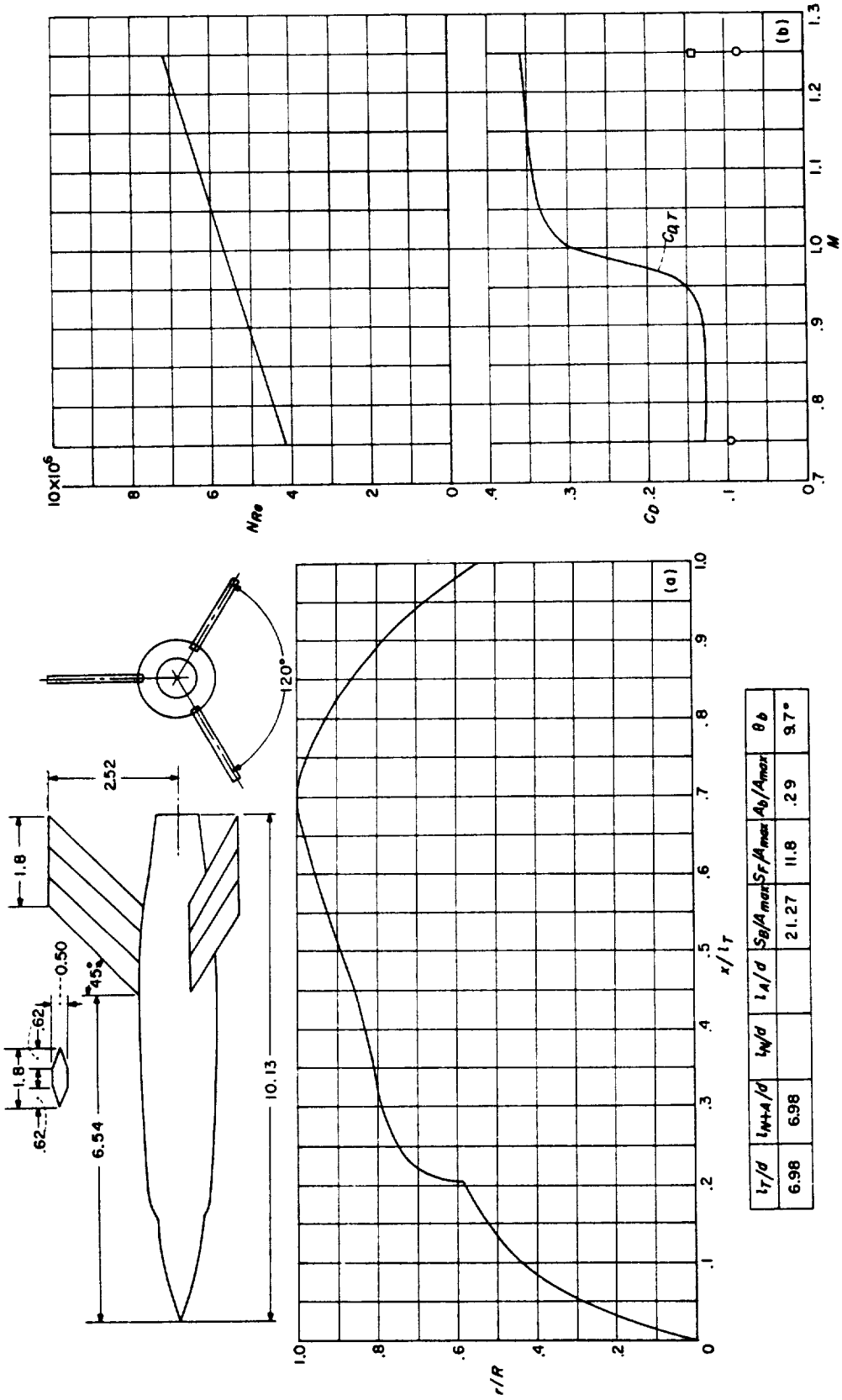

l_T/d	l_{N+A}/d	l_W/d	l_A/d	S_B/A_{max}	S_F/A_{max}	A_b/A_{max}	θ_b
6.98	6.98			21.27	11.8	.29	9.7°

(a) Body shape. (Dimensions given are in inches.) (b) N_{Re} and C_D curves

CONFIGURATION 129; helium-gun test.

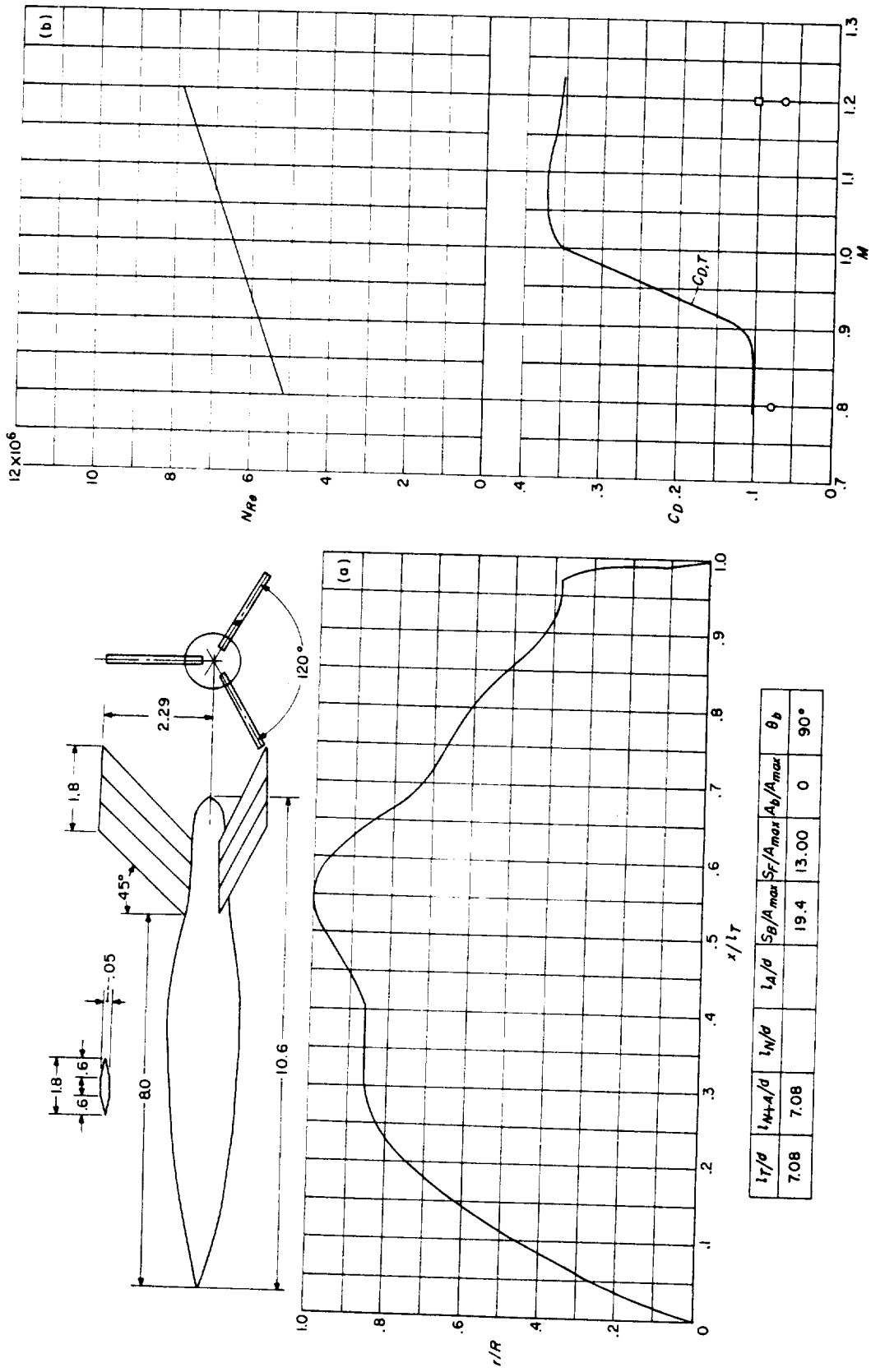

l_T/d	l_{N+A}/d	l_N/d	l_A/d	S_B/A_{max}	S_F/A_{max}	A_b/A_{max}	θ_b
7.08	7.08			19.4	13.00	0	90°

(a) Body shape. (Dimensions given are in inches.) (b) N_{R_e} and C_D curves.

CONFIGURATION 130; helium-gun test. $\left(\text{Subsonic flow probably separated about } \frac{x}{l_T}=0.97.\right)$

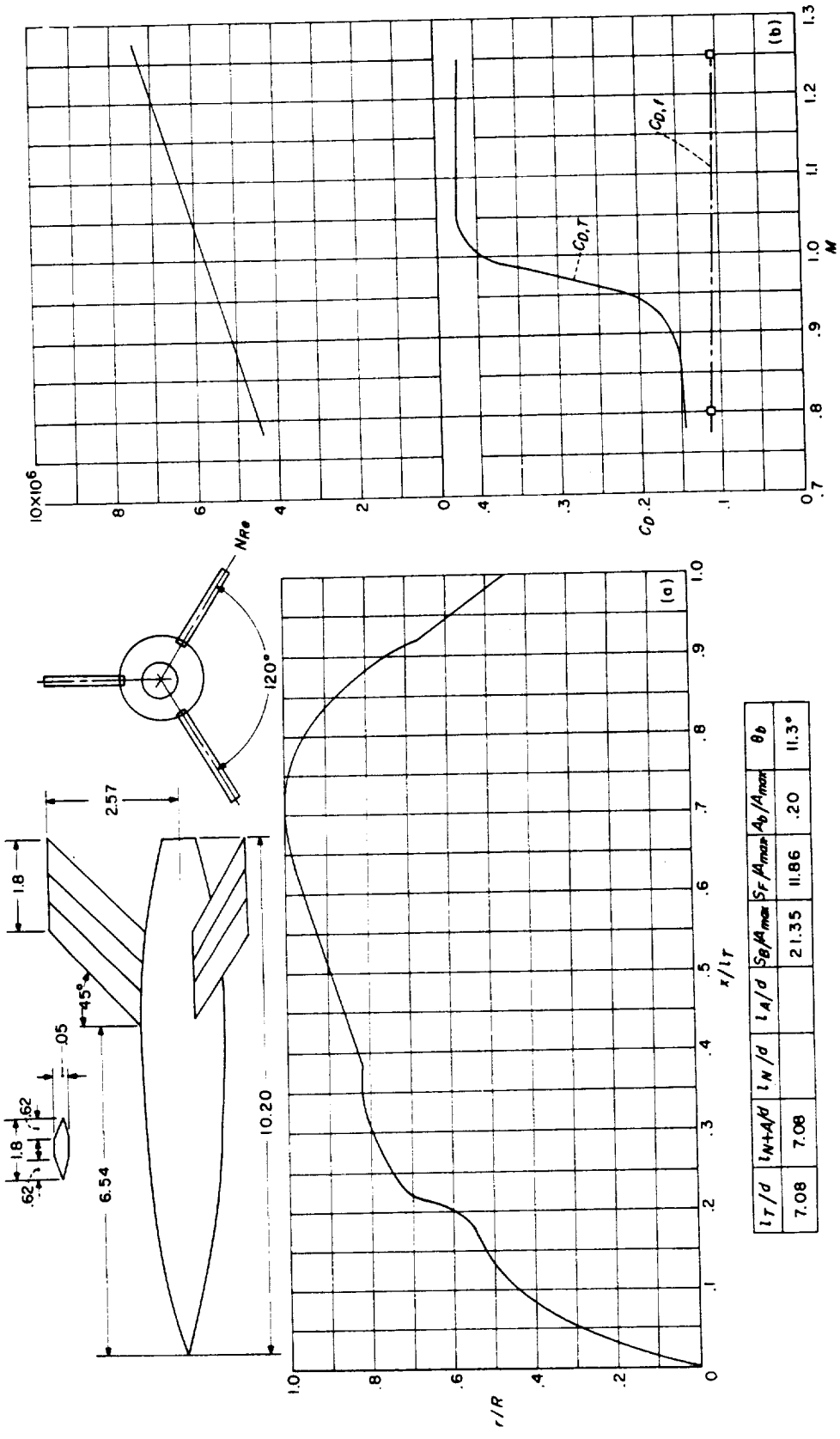

l_T/d	l_{N+A}/d	l_N/d	l_A/d	S_B/A_{max}	S_F/A_{max}	A_b/A_{max}	θ_b
7.08	7.08			21.35	11.86	.20	11.3°

(a) Body shape. (Dimensions given are in inches.) (b) N_{Re} and C_D curves.

CONFIGURATION 131; helium-gun test.

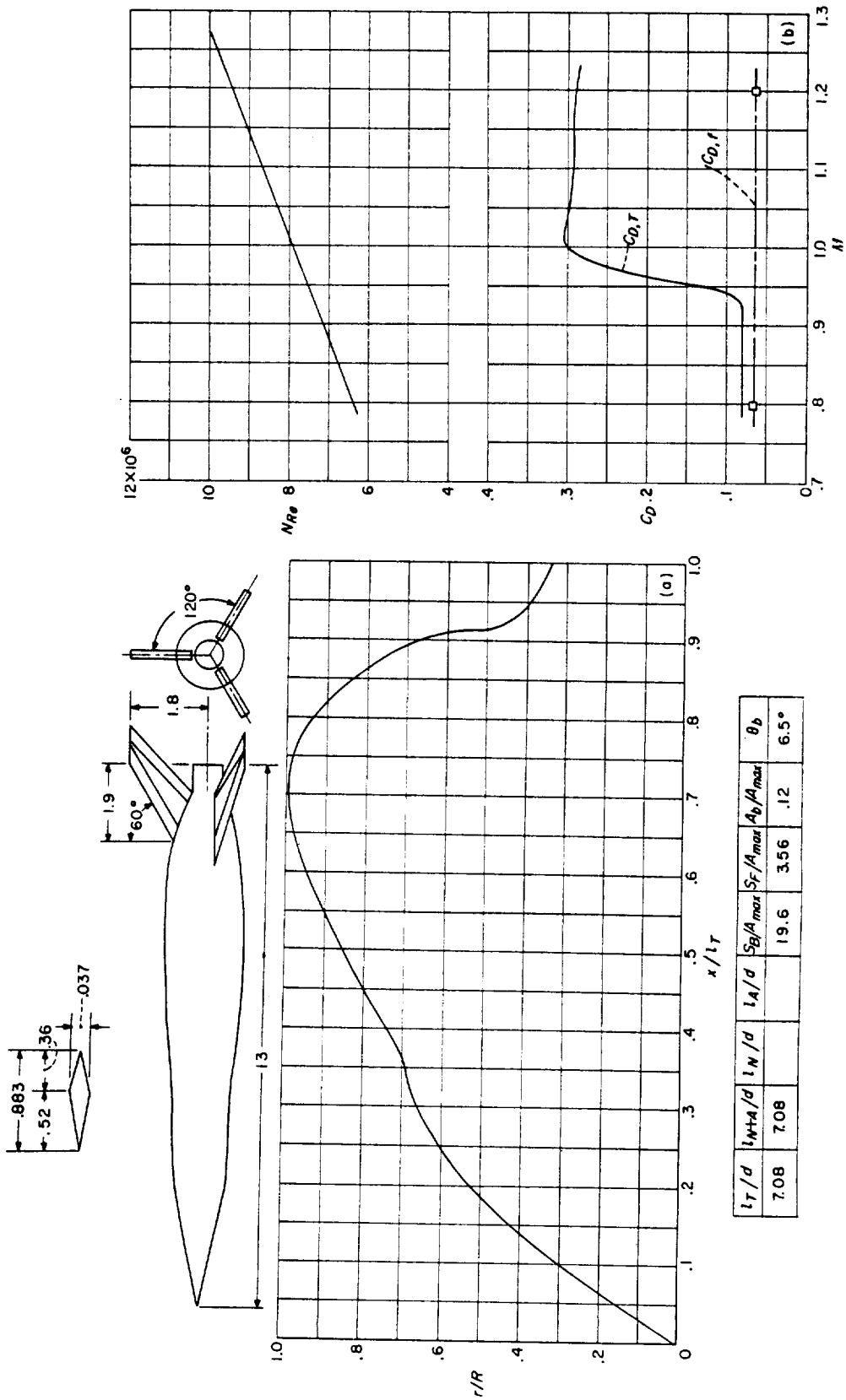

l_T/d	l_{N+A}/d	l_N/d	l_A/d	S_B/A_{max}	S_F/A_{max}	A_b/A_{max}	θ_b
7.08	7.08			19.6	3.56	.12	6.5°

(a) Body shape. (Dimensions given are in inches.) (b) N_{Re} and C_D curves.

Configuration 132; helium-gun test.

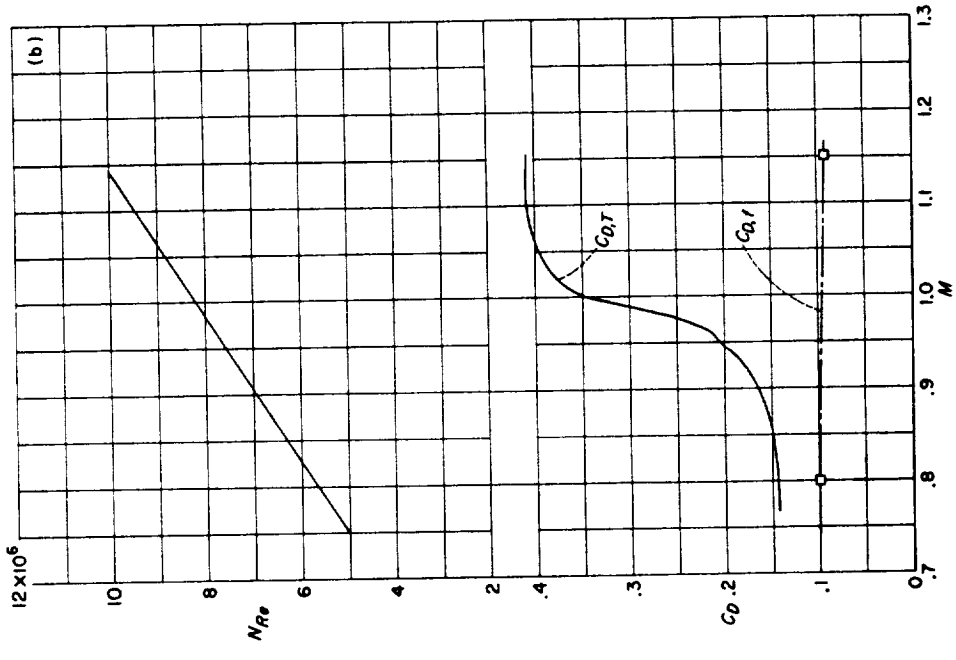

(b) N_{Re} and C_D curves.

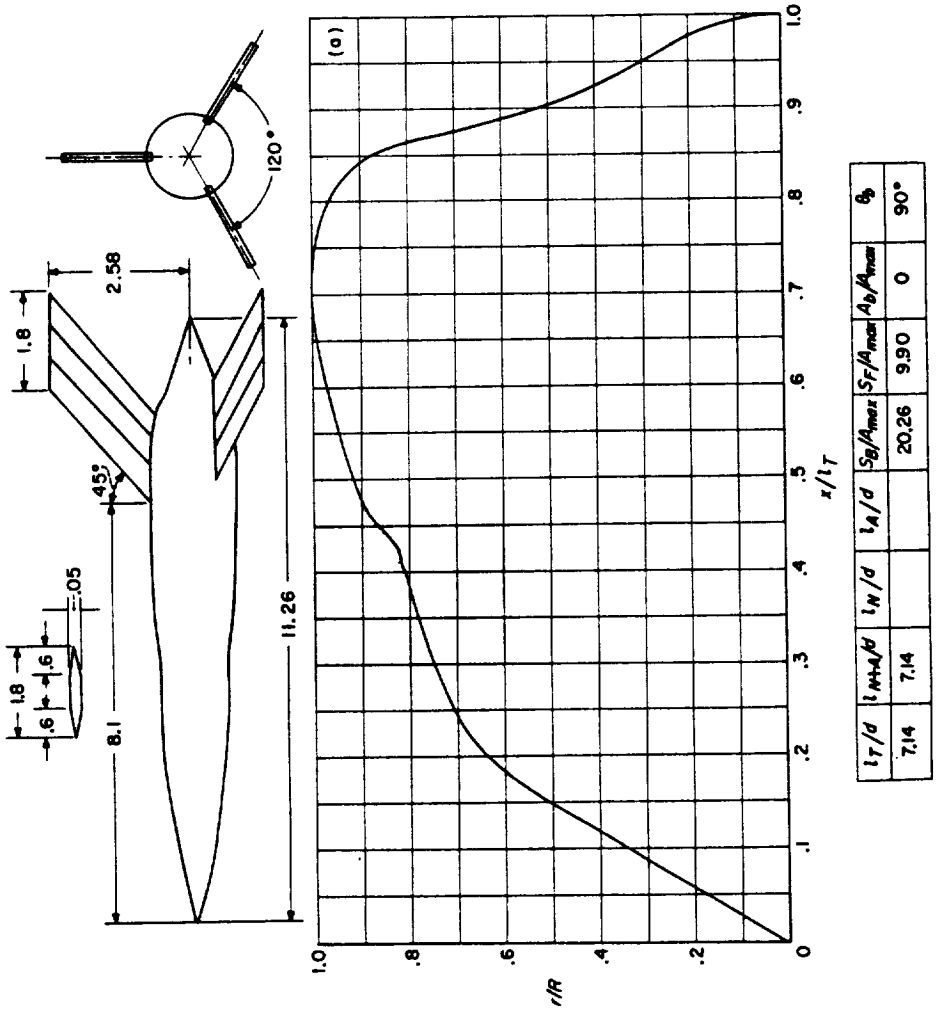

l_T/d	l_{NH+A}/d	l_W/d	l_A/d	S_B/A_{max}	S_F/A_{max}	A_b/A_{max}	θ_b
7.14	7.14			20.26	9.90	0	90°

(a) Body shape. (Dimensions given are in inches.)

CONFIGURATION 133; helium-gun test. (Flow is probably separated at subsonic speeds.)

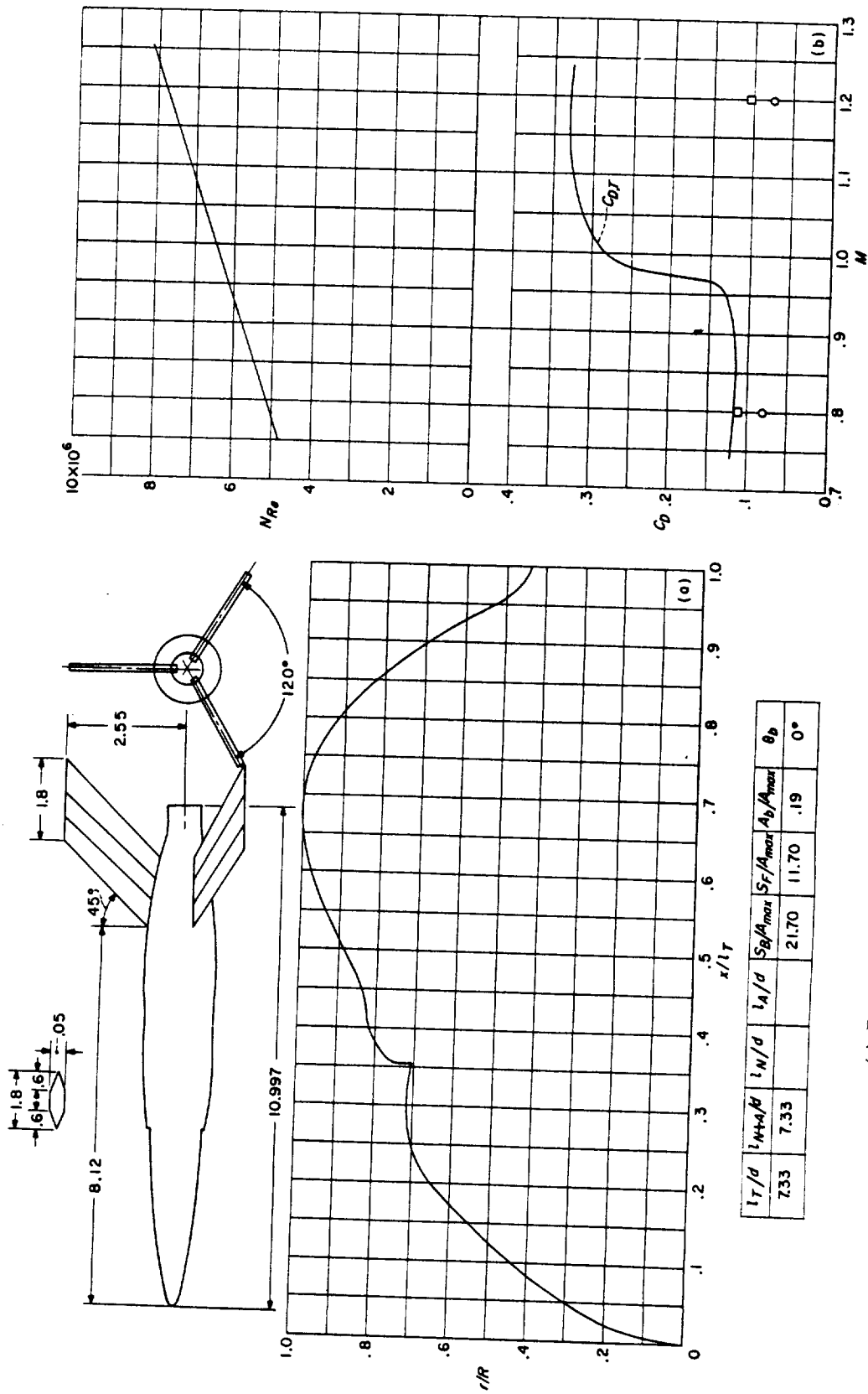

l_T/d	l_{N+A}/d	l_N/d	l_A/d	S_B/A_{max}	S_F/A_{max}	A_b/A_{max}	θ_b
7.33	7.33			21.70	11.70	.19	0°

(a) Body shape. (Dimensions given are in inches.) (b) N_{Re} and C_D curves.

CONFIGURATION 134; helium-gun test. (Subsonic flow was probably laminar. See note for configuration 125.)

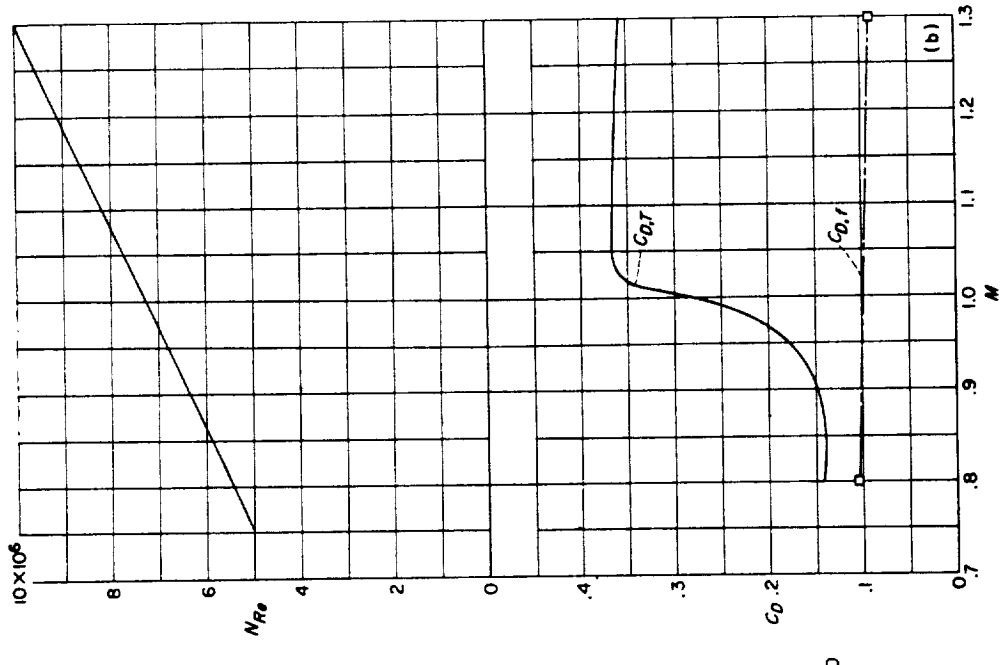

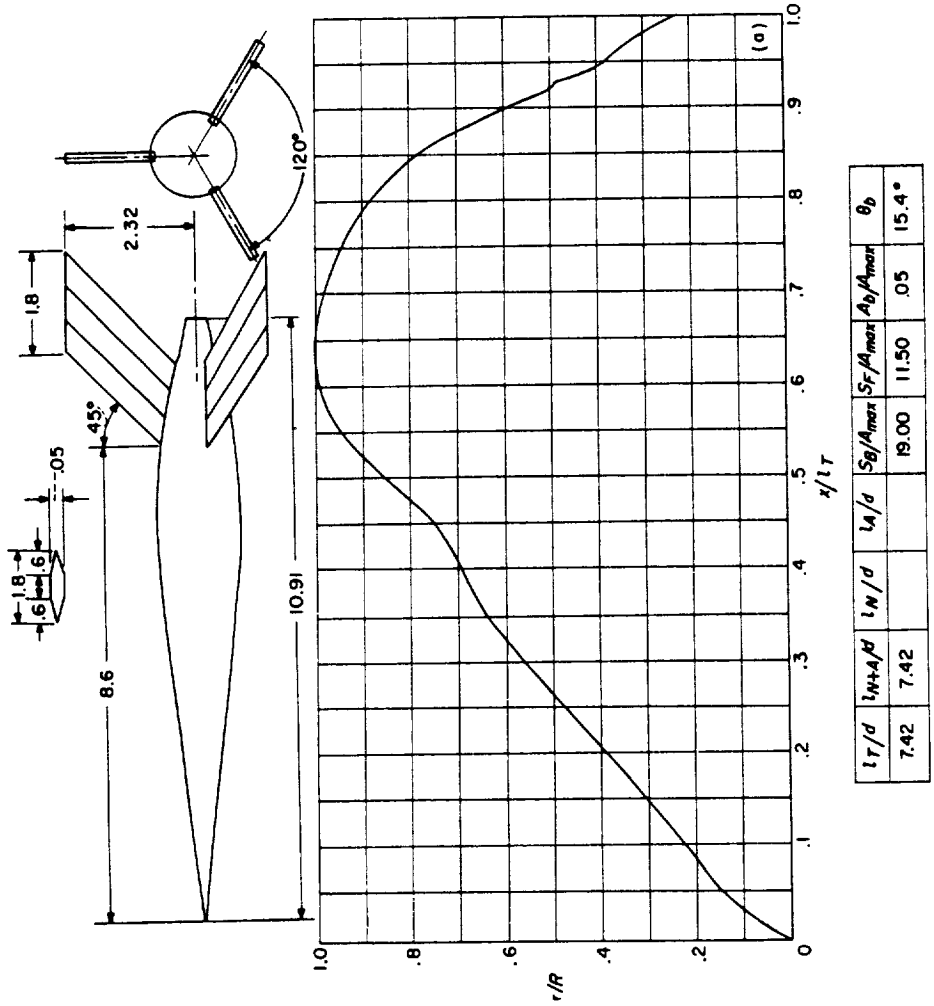

l_T/d	l_{N+A}/d	l_N/d	l_A/d	S_B/A_{max}	S_F/A_{max}	A_b/A_{max}	θ_b
7.42	7.42			19.00	11.50	.05	15.4°

(a) Body shape. (Dimensions given are in inches.) (b) N_{Re} and C_D curves.

CONFIGURATION 135; helium-gun test. (Subsonic drag looks too high.)

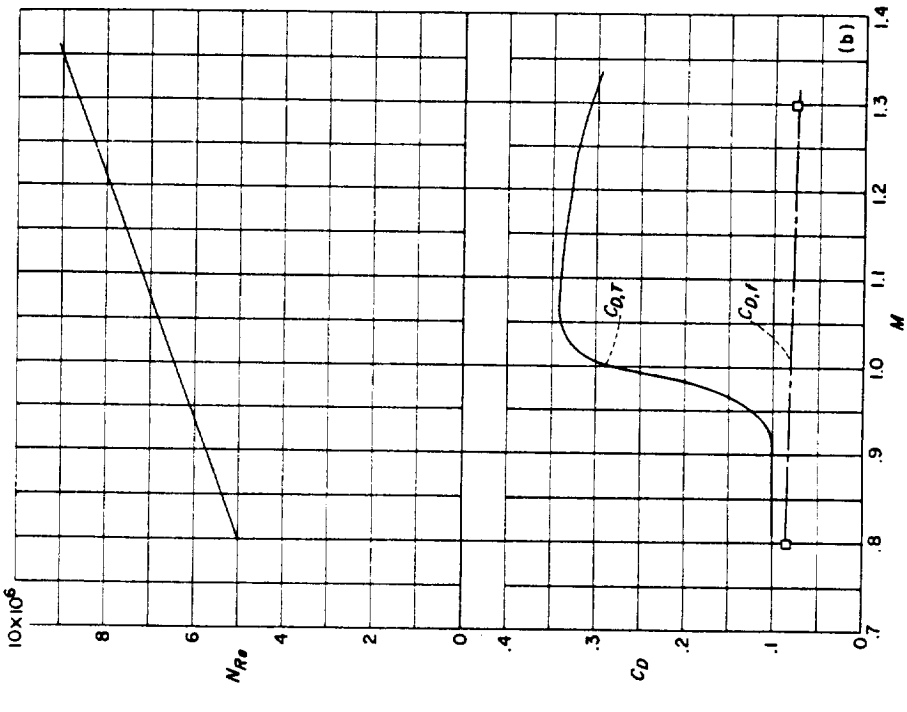

(b) N_{Re} and C_D curves.

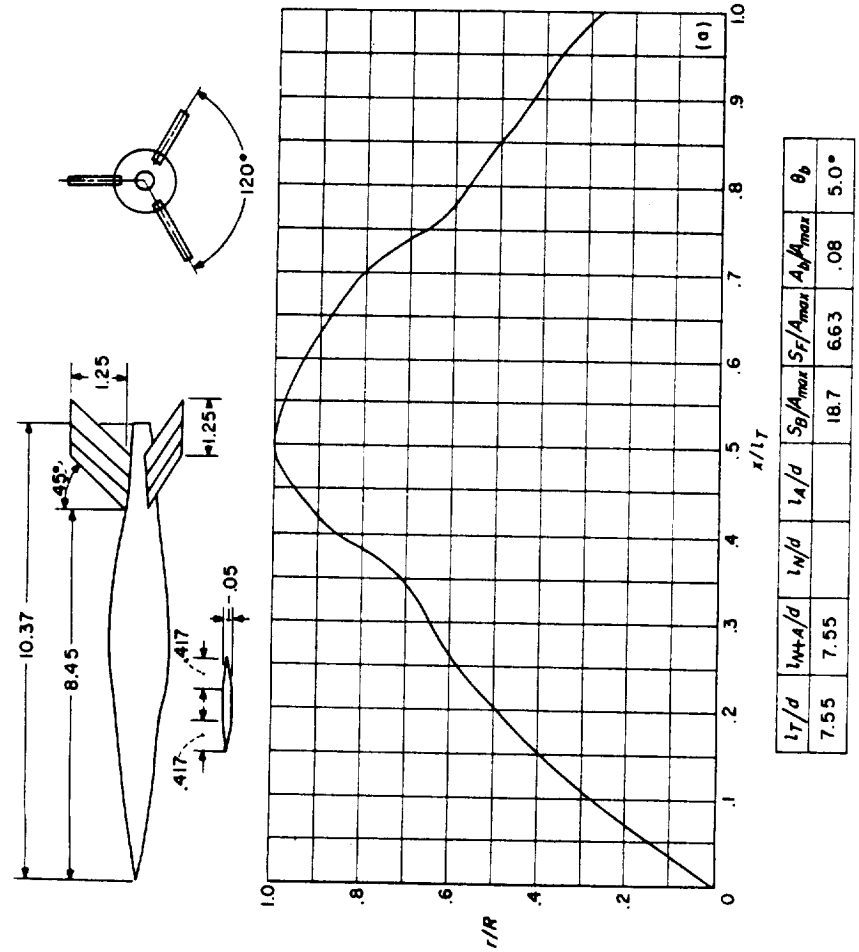

l_T/d	l_{N+A}/d	l_N/d	l_A/d	S_B/A_{max}	S_F/A_{max}	A_b/A_{max}	θ_b
7.55	7.55			18.7	6.63	.08	5.0°

(a) Body shape. (Dimensions given are in inches.)

Configuration 136; helium-gun test.

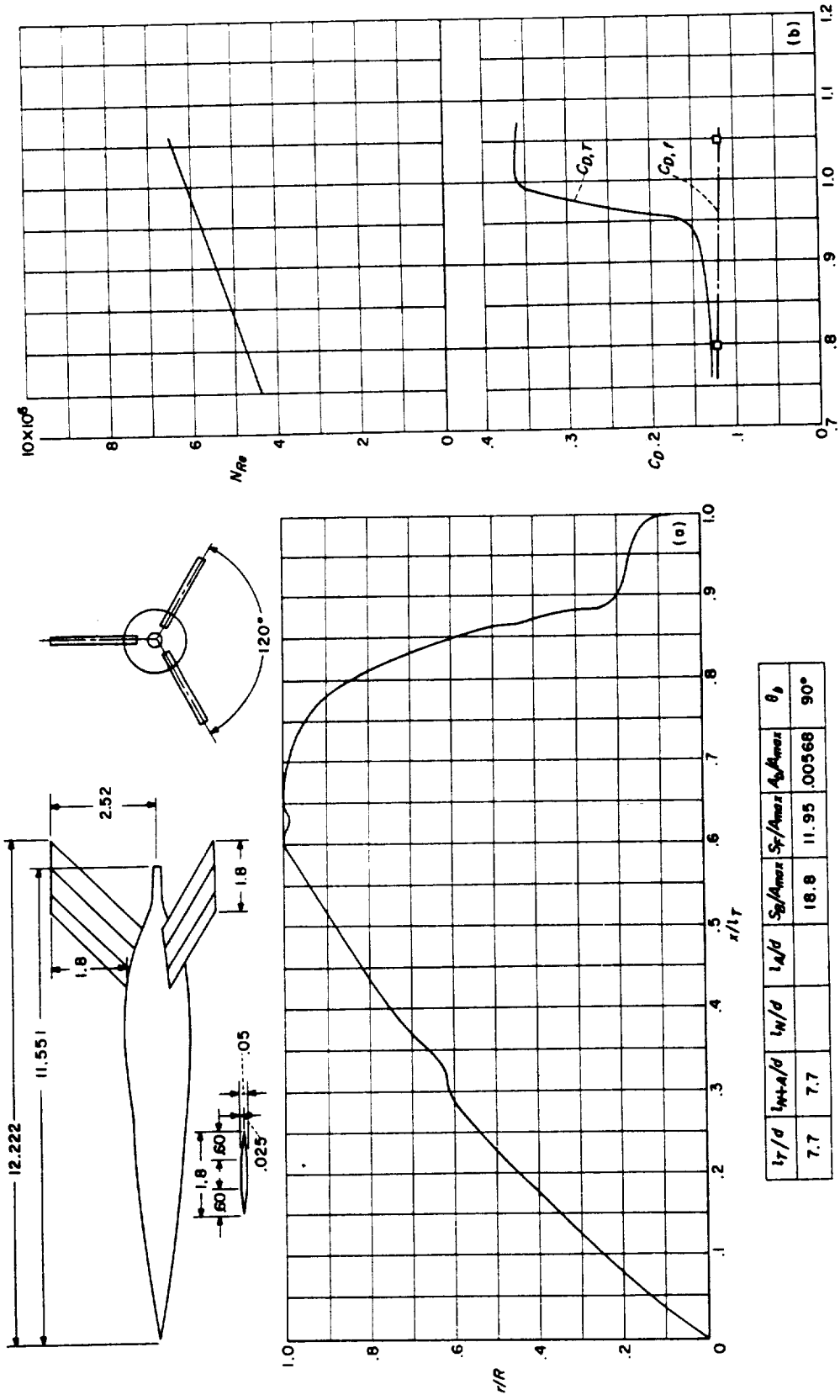

l_T/d	l_{N+A}/d	l_N/d	l_A/d	S_B/A_{max}	S_F/A_{max}	A_b/A_{max}	θ_b
7.7	7.7			18.8	11.95	.00568	90°

(a) Body shape. (Dimensions given are in inches.) (b) N_{Re} and C_D curves.

Configuration 137; helium-gun test.

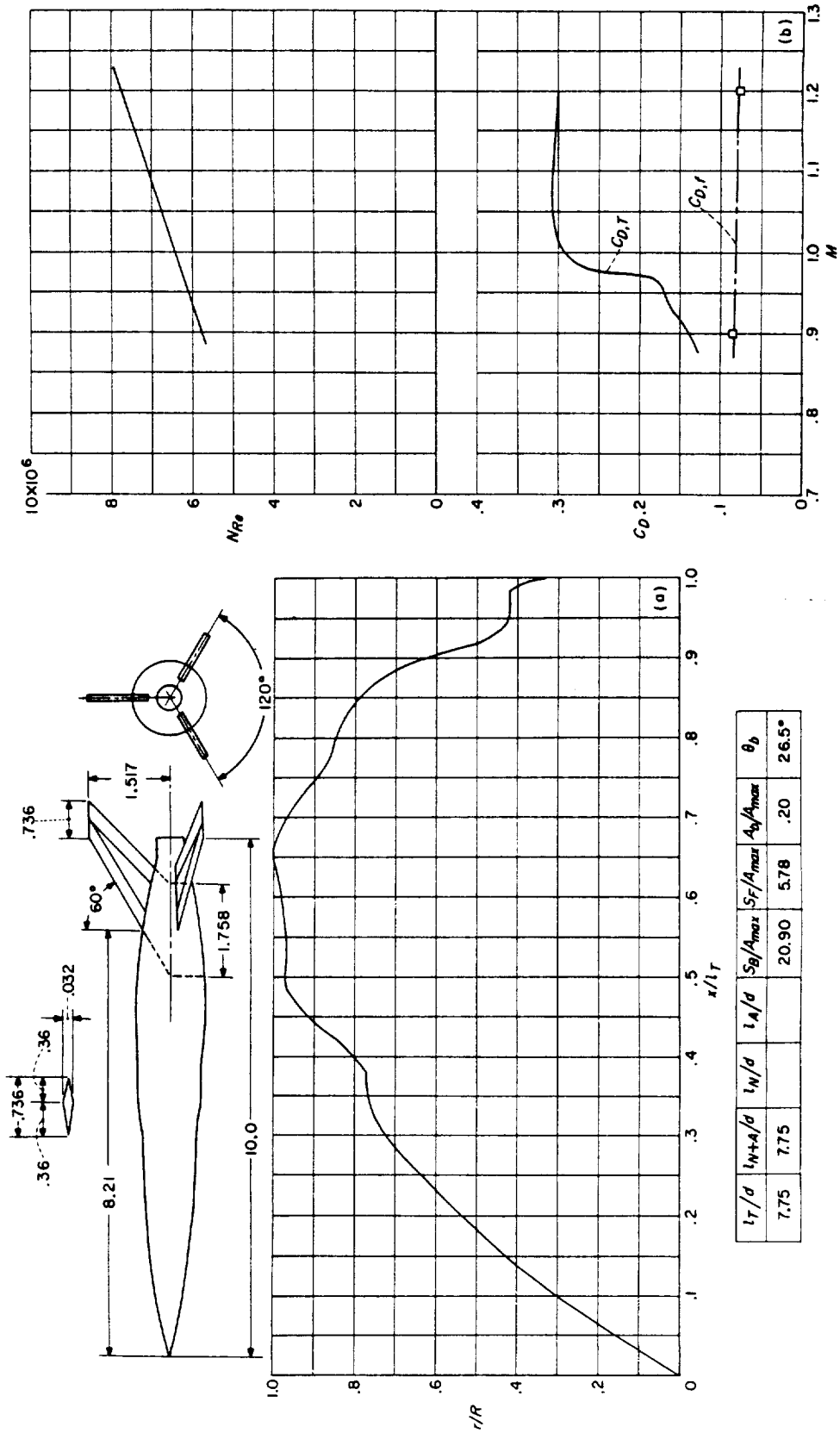

l_T/d	l_{N+A}/d	l_N/d	l_A/d	S_B/A_{max}	S_F/A_{max}	A_b/A_{max}	θ_b
7.75	7.75			20.90	5.78	.20	26.5°

(a) Body shape. (Dimensions given are in inches.) (b) N_{Re} and C_D curves.

CONFIGURATION 138; helium-gun test. (Remarks for configuration 125 may apply to these models also.)

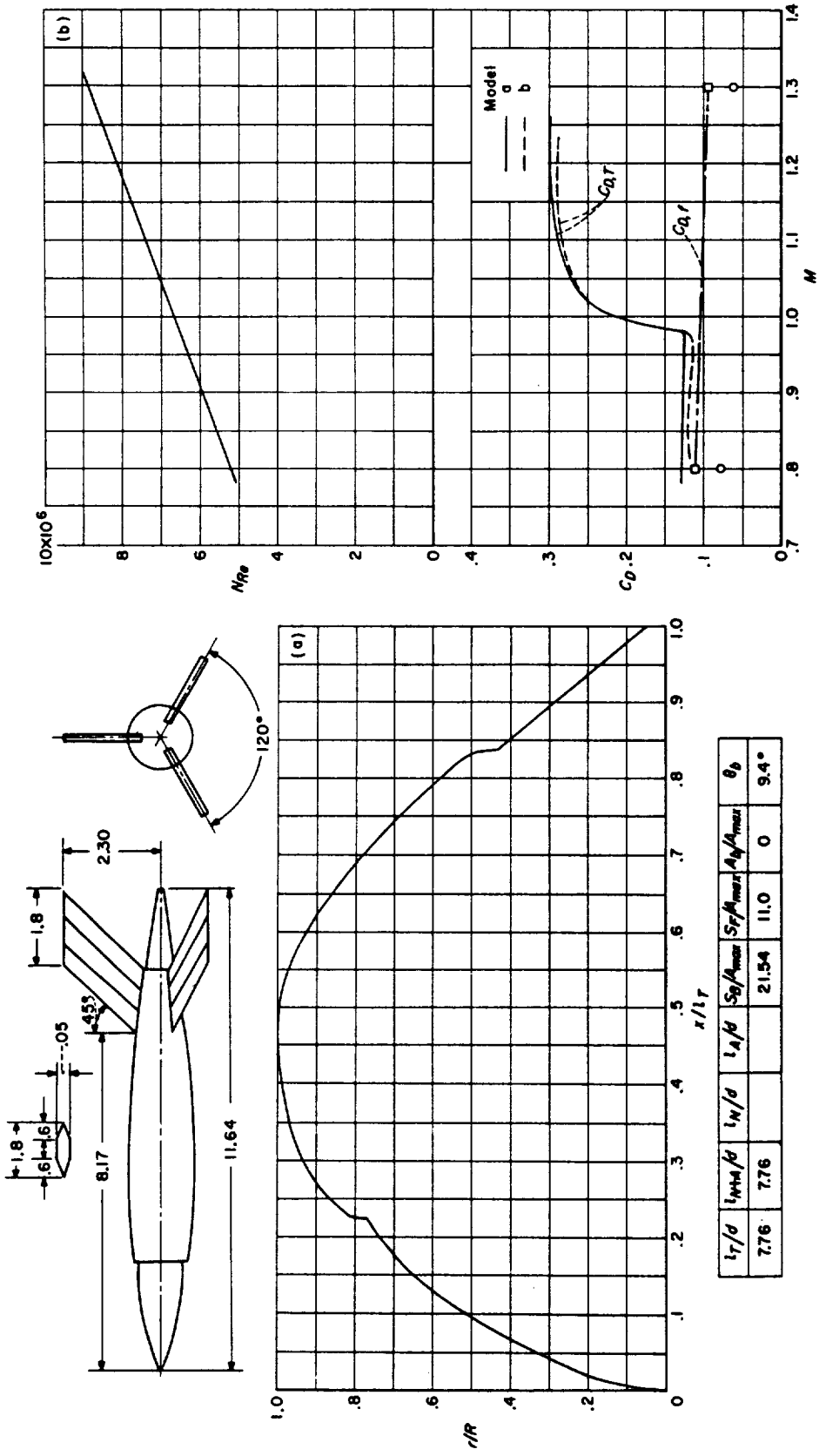

l_T/d	l_{NH}/d	l_N/d	l_A/d	S_0/A_{max}	S_T/A_{max}	A_b/A_{max}	θ_b
7.76	7.76			21.54	11.0	0	9.4°

(a) Body shape. (Dimensions given are in inches.) (b) N_{Re} and C_D curves.

CONFIGURATION 139; helium-gun test. (Remarks for configuration 125 may apply to these models also.)

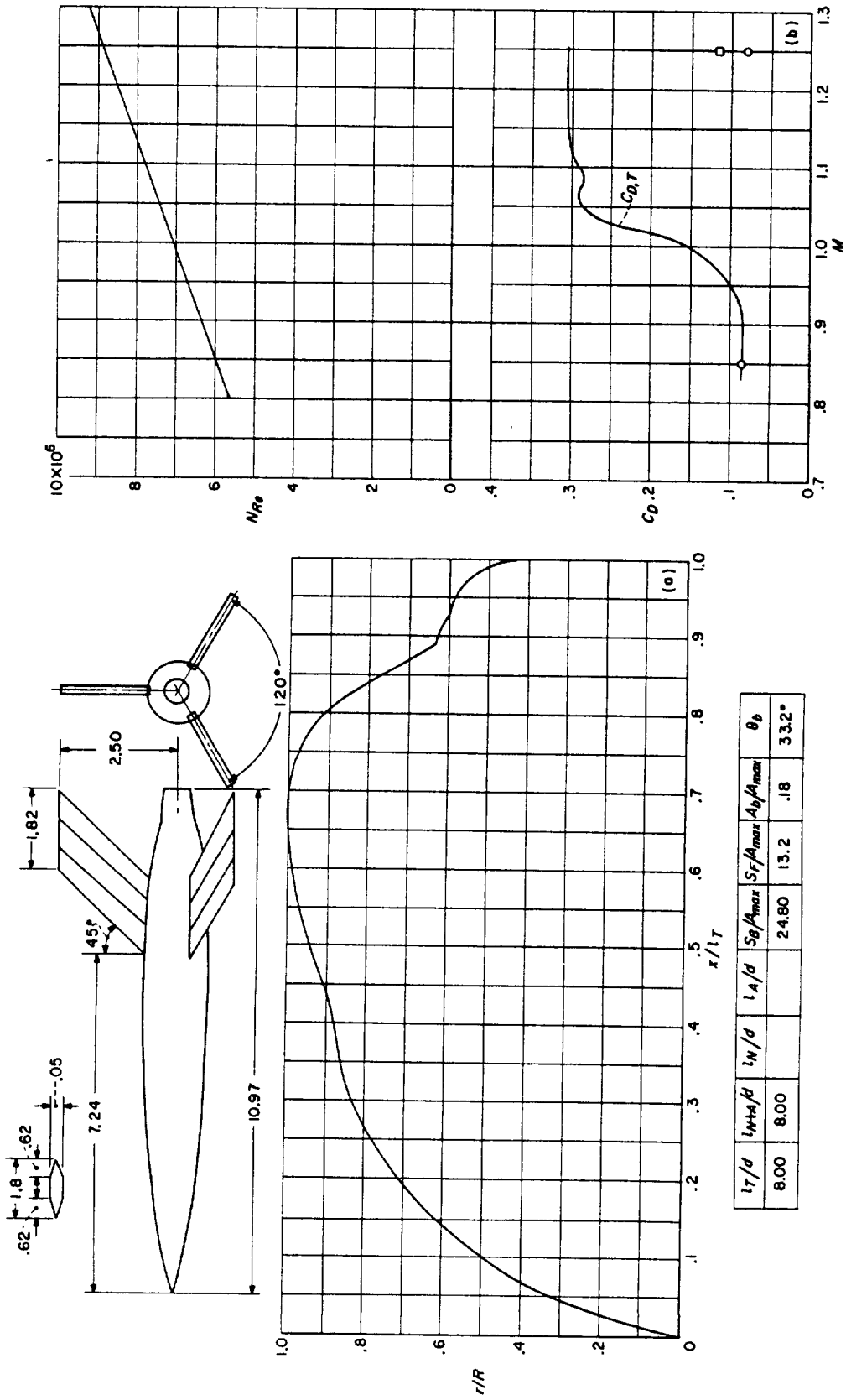

l_T/d	l_{NT+A}/d	l_W/d	l_A/d	S_B/A_{max}	S_F/A_{max}	A_b/A_{max}	θ_b
8.00	8.00			24.80	13.2	.18	33.2°

(a) Body shape. (Dimensions given are in inches.) (b) N_{Re} and C_D curves.

CONFIGURATION 140; helium-gun test.

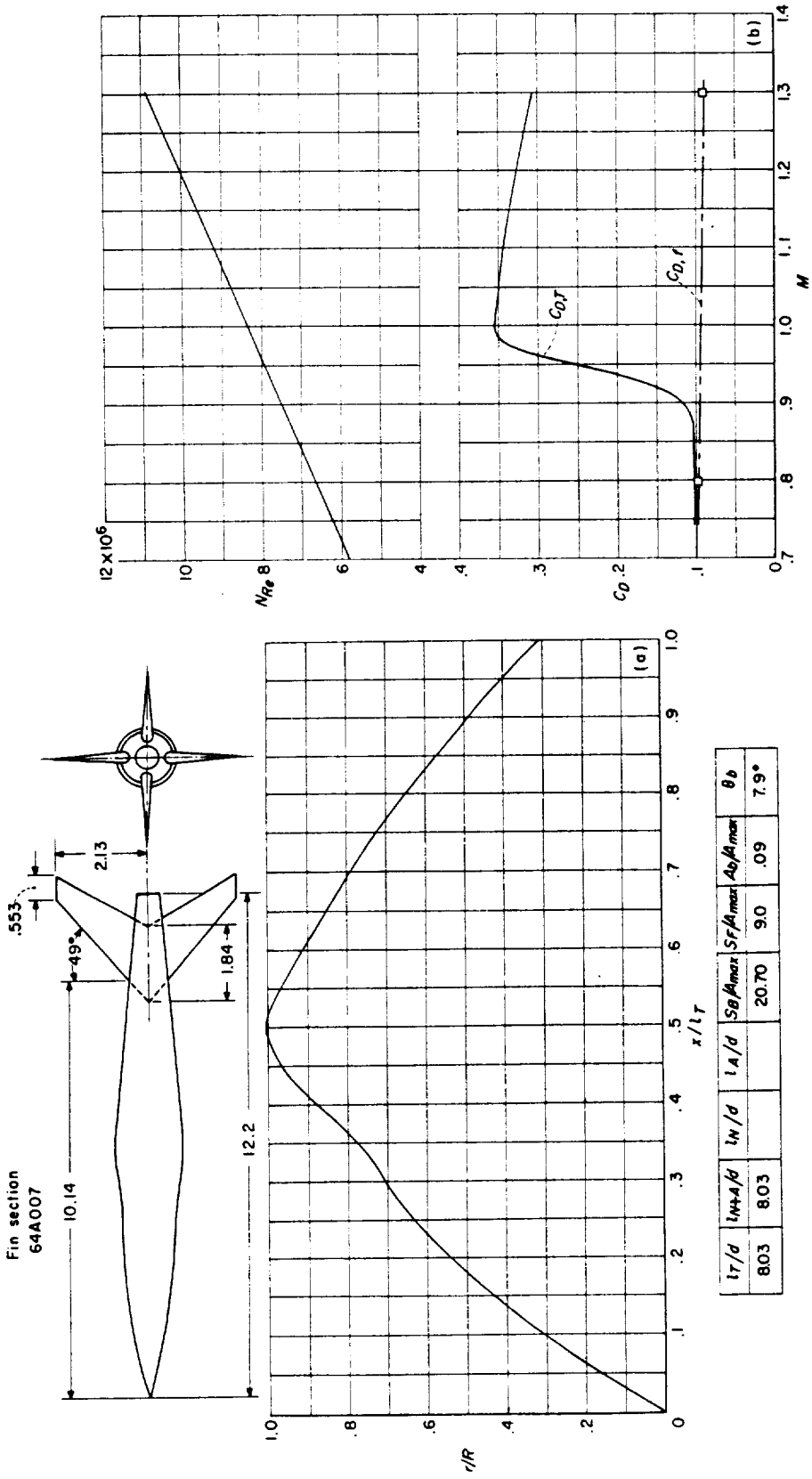

l_T/d	l_{W+A}/d	l_N/d	l_A/d	S_B/A_{max}	S_F/A_{max}	A_b/A_{max}	θ_b
8.03	8.03			20.70	9.0	.09	7.9°

(a) Body shape. (Dimensions given are in inches.) (b) N_{Re} and C_D curves.

CONFIGURATION 141; helium-gun test.

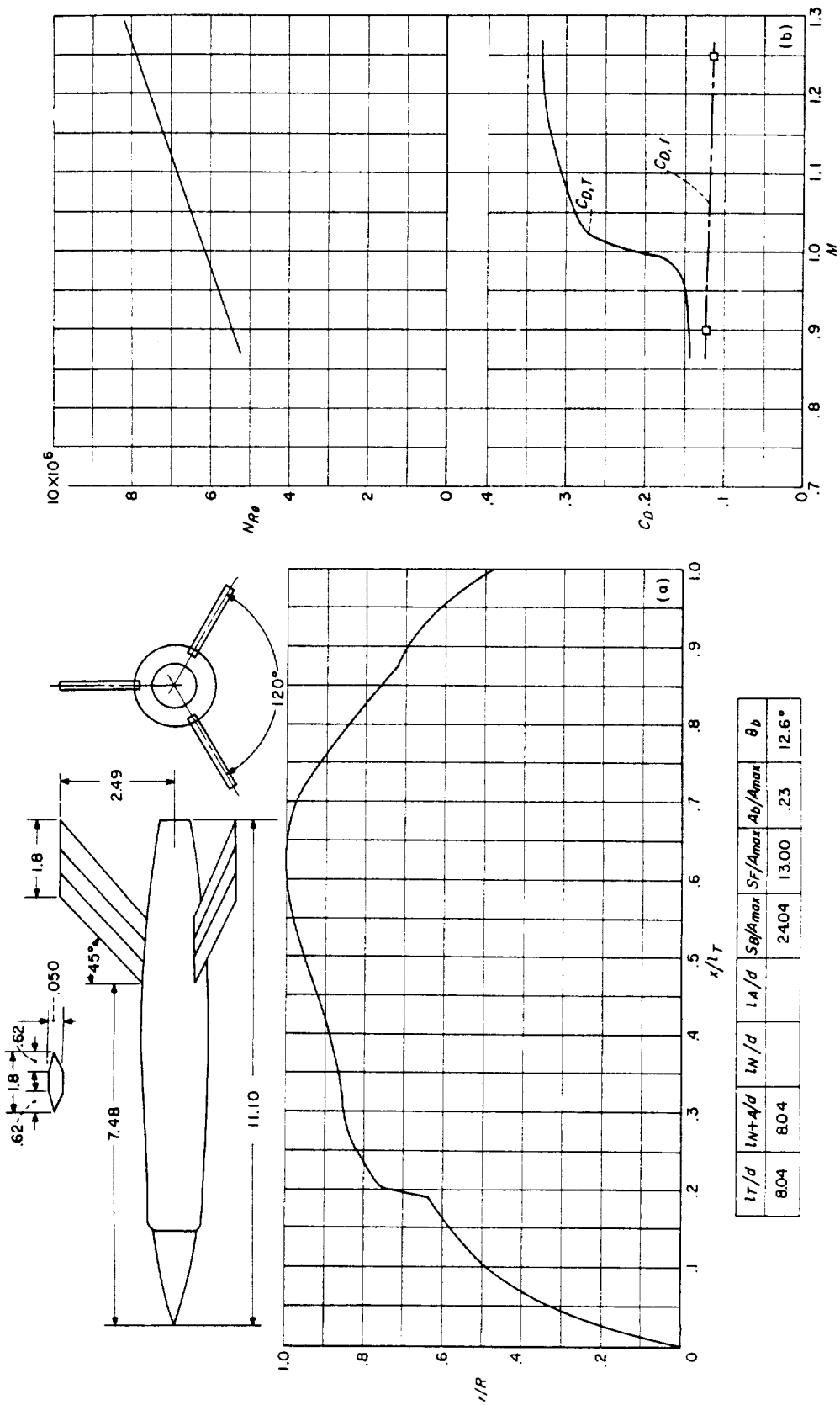

l_T/d	l_{N+4}/d	l_N/d	l_A/d	S_B/A_{max}	S_F/A_{max}	A_b/A_{max}	θ_b
8.04	8.04			24.04	13.00	.23	12.6°

(a) Body shape. (Dimensions given are in inches.) (b) N_{Re} and C_D curves.

CONFIGURATION 142; helium-gun test.

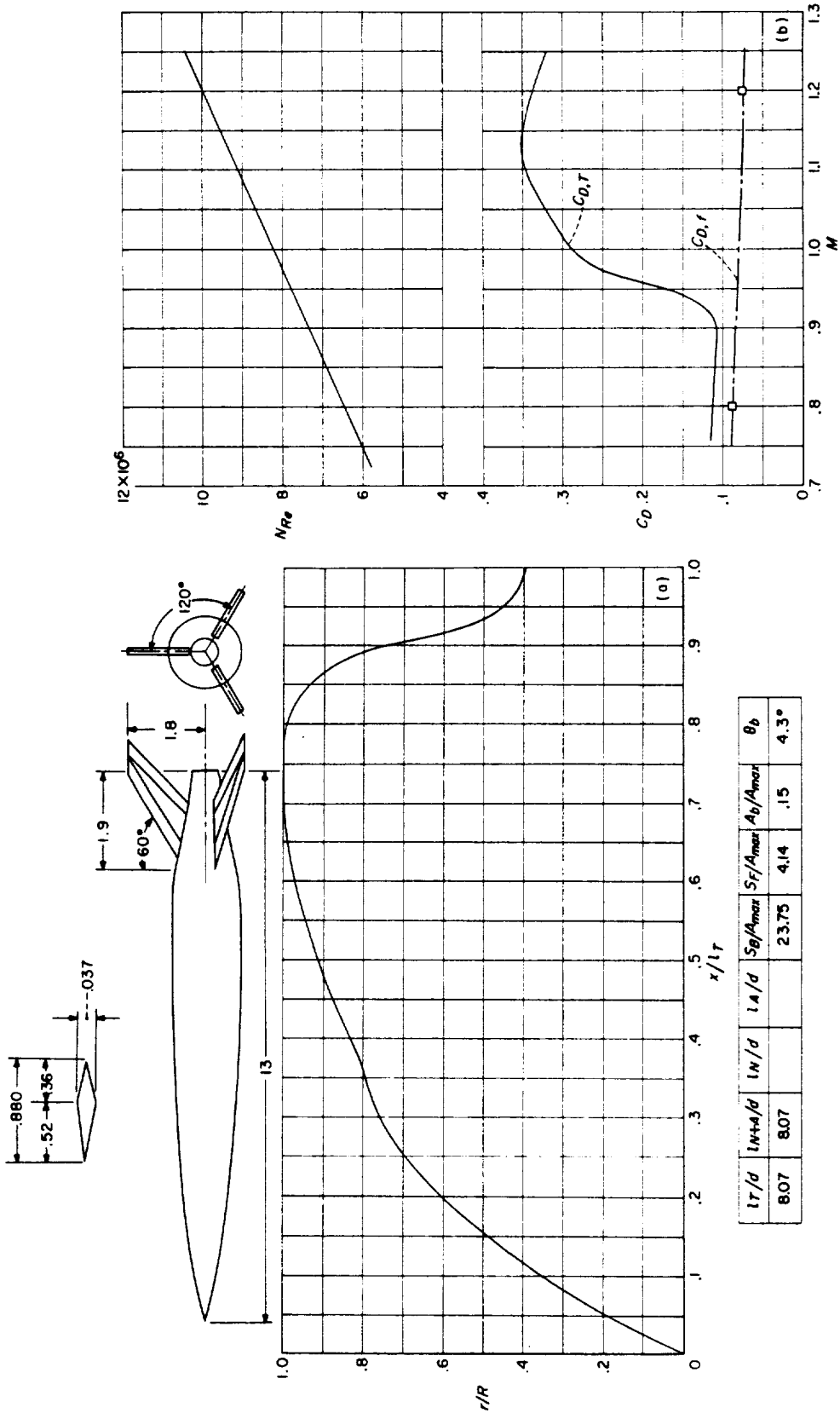

l_T/d	l_{N+A}/d	l_N/d	l_A/d	S_B/A_{max}	S_F/A_{max}	A_b/A_{max}	θ_b
8.07	8.07			23.75	4.14	.15	4.3°

(a) Body shape. (Dimensions given are in inches.) (b) N_{Re} and C_D curves.

CONFIGURATION 143; helium-gun test.

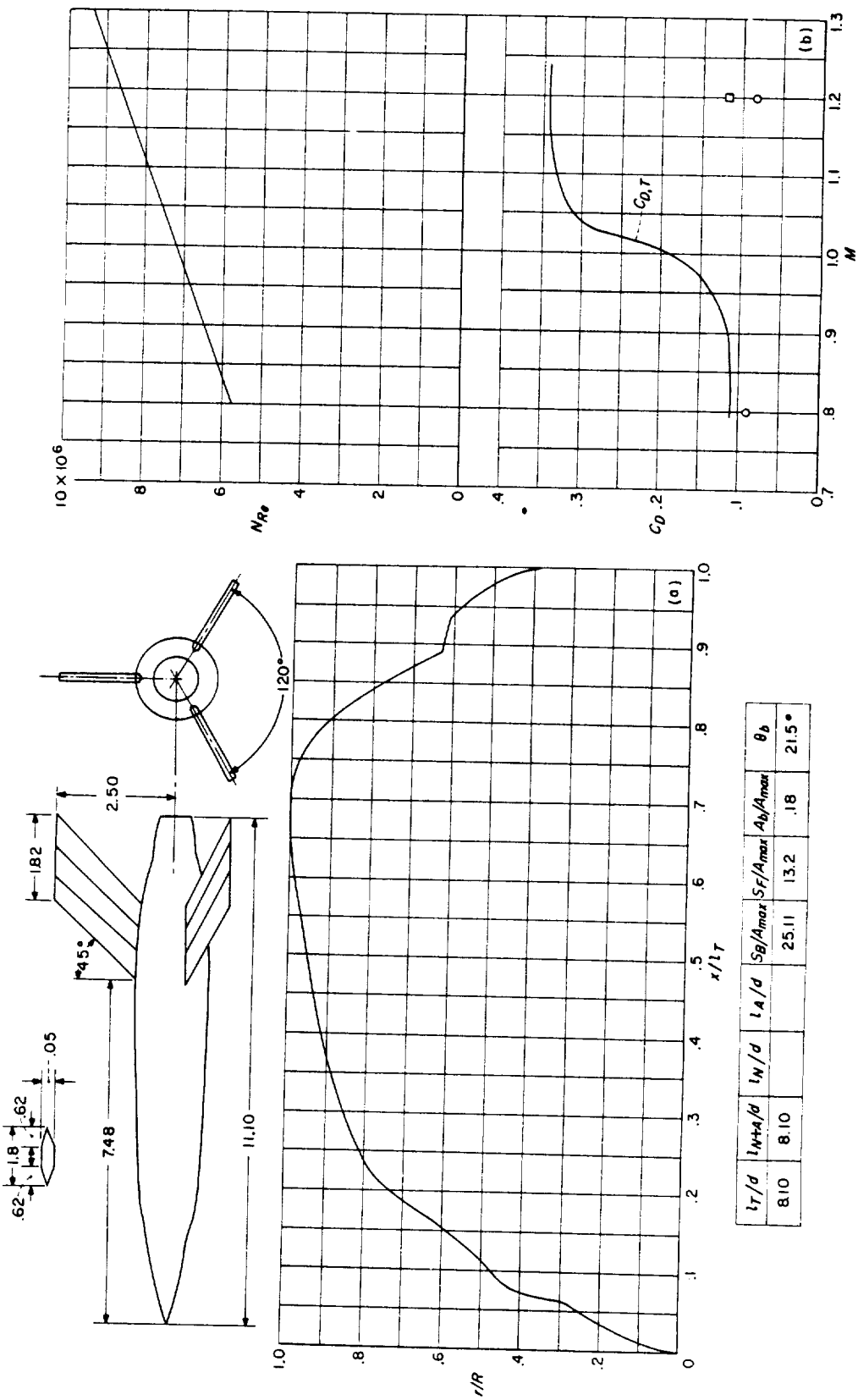

l_T/d	l_{N+A}/d	l_N/d	l_A/d	S_B/A_{max}	S_F/A_{max}	A_b/A_{max}	θ_b
8.10	8.10			25.11	13.2	.18	21.5°

(a) Body shape. (Dimensions given are in inches.) (b) N_{Re} and C_D curves.

CONFIGURATION 144; helium-gun test.

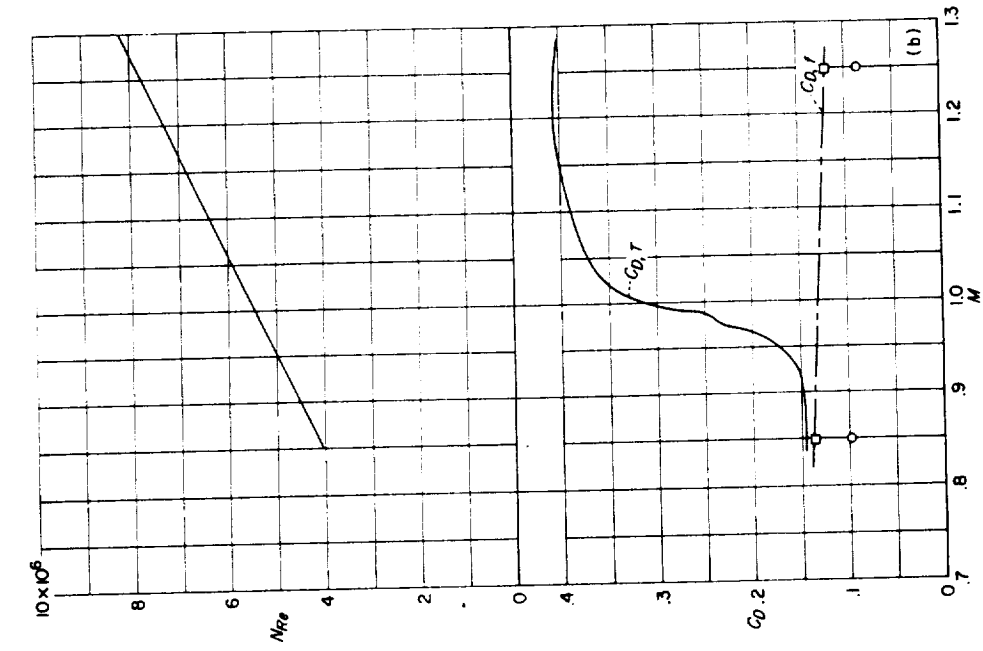

(b) N_{Re} and C_D curves.

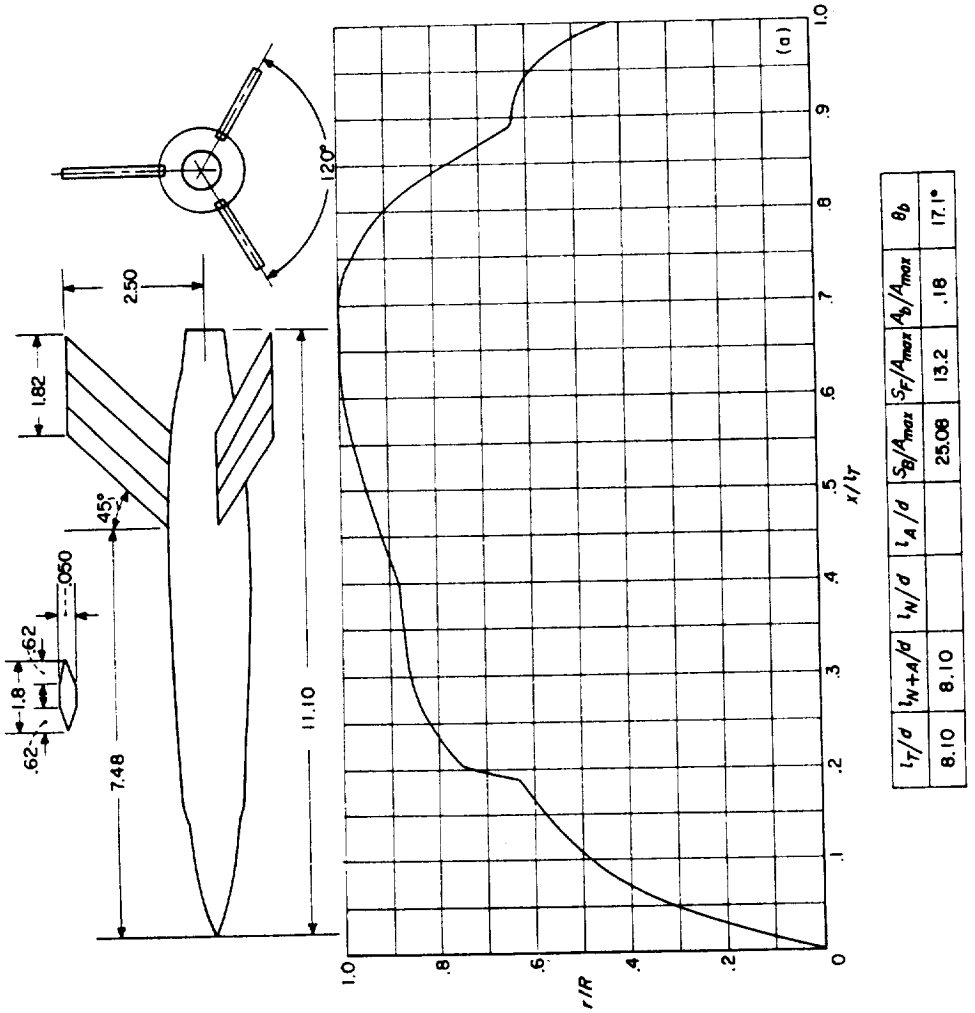

l_T/d	l_{N+A}/d	l_N/d	l_A/d	S_B/A_{max}	S_F/A_{max}	A_b/A_{max}	θ_b
8.10	8.10			25.08	13.2	.18	17.1°

(a) Body shape. (Dimensions given are in inches.)

CONFIGURATION 145; helium-gun test.

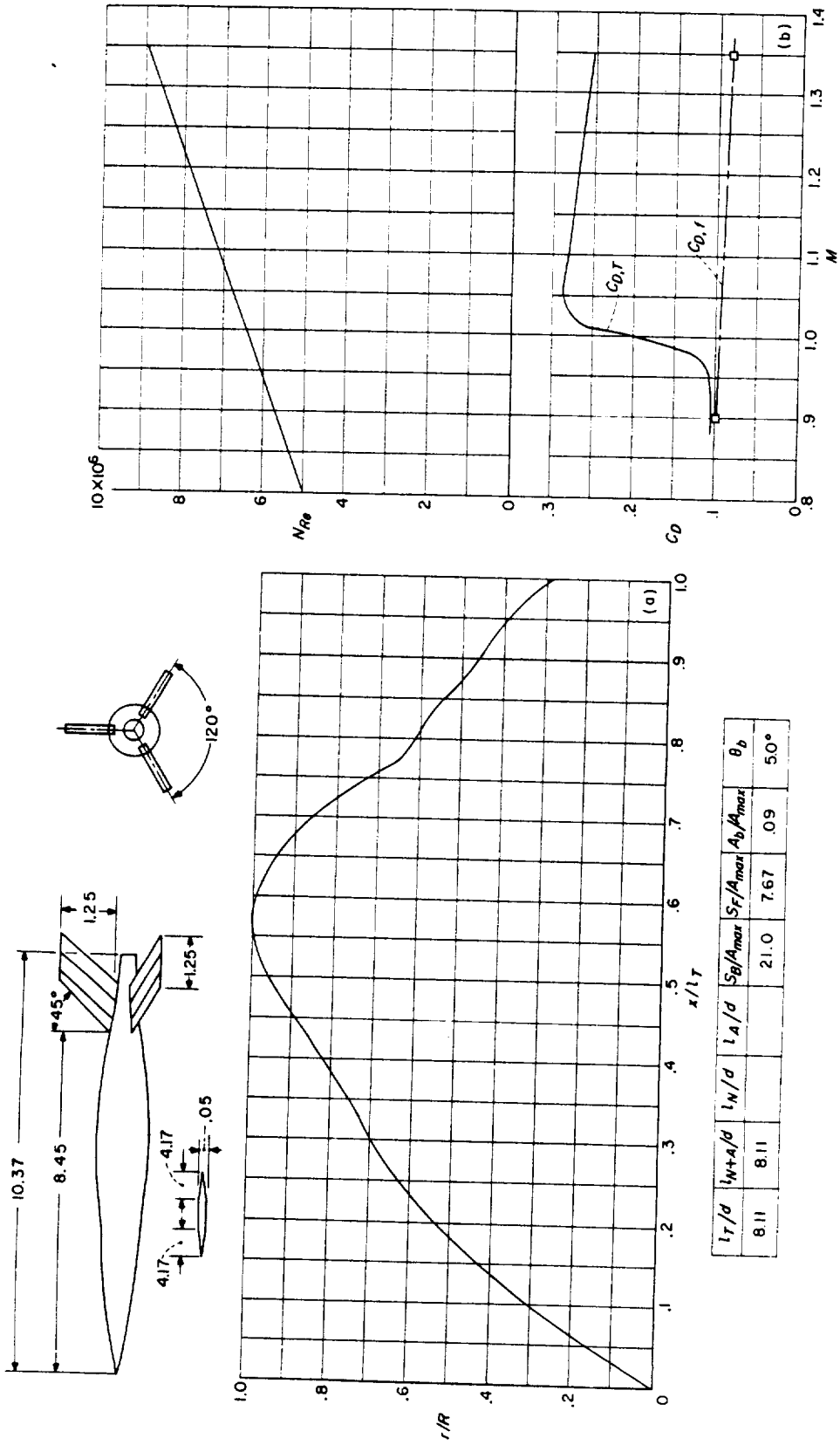

l_T/d	l_{N+A}/d	l_N/d	l_A/d	S_B/A_{max}	S_F/A_{max}	A_b/A_{max}	θ_b
8.11	8.11			21.0	7.67	.09	50°

(a) Body shape. (Dimensions given are in inches.) (b) N_{Re} and C_D curves.

CONFIGURATION 146; helium-gun test.

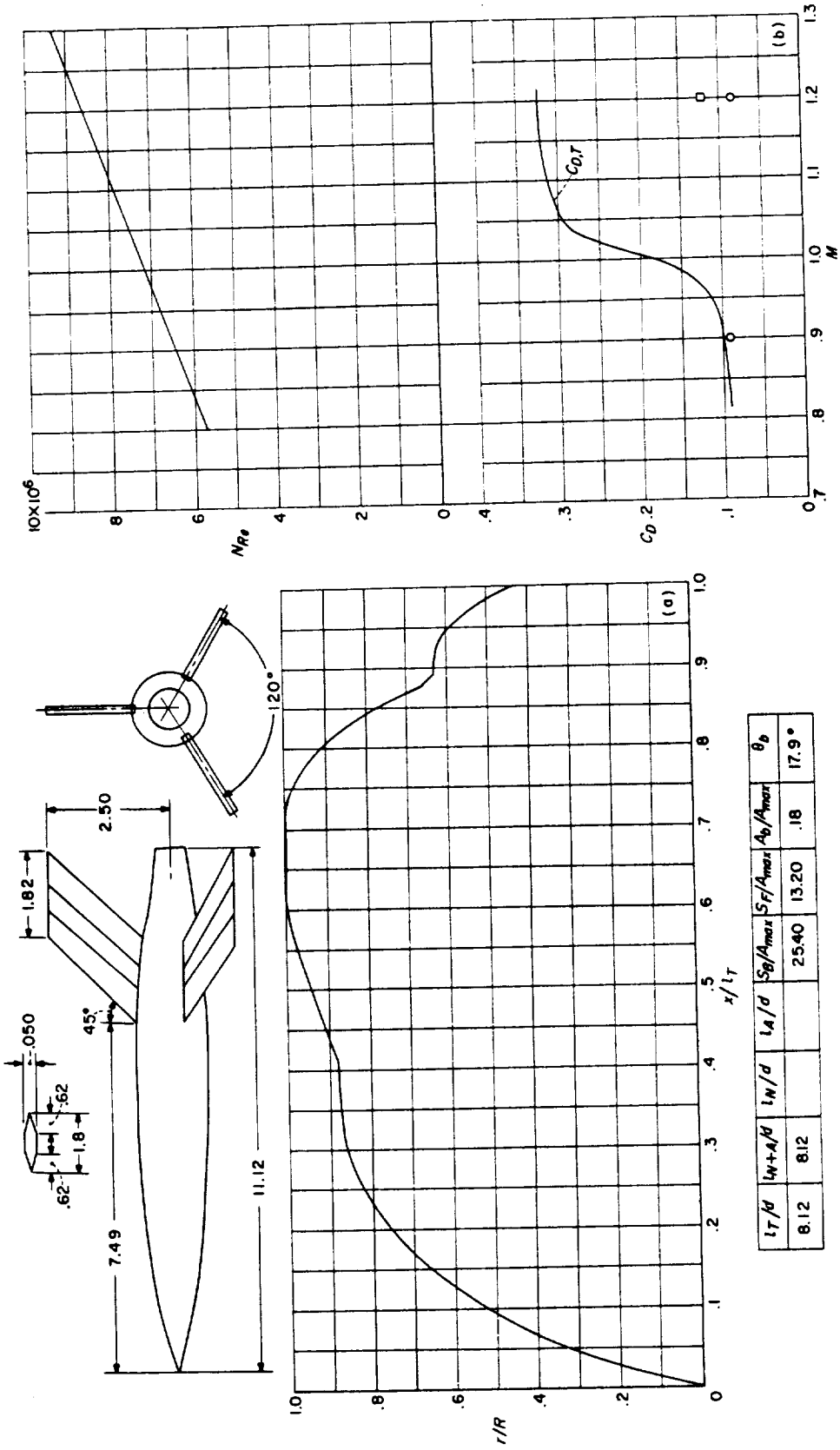

l_T/d	l_{N+A}/d	l_N/d	l_A/d	S_B/A_{max}	S_F/A_{max}	A_b/A_{max}	θ_b
8.12	8.12			25.40	13.20	.18	17.9°

(a) Body shape. (Dimensions given are in inches.) (b) N_{Re} and C_D curves.

Configuration 147; helium-gun test.

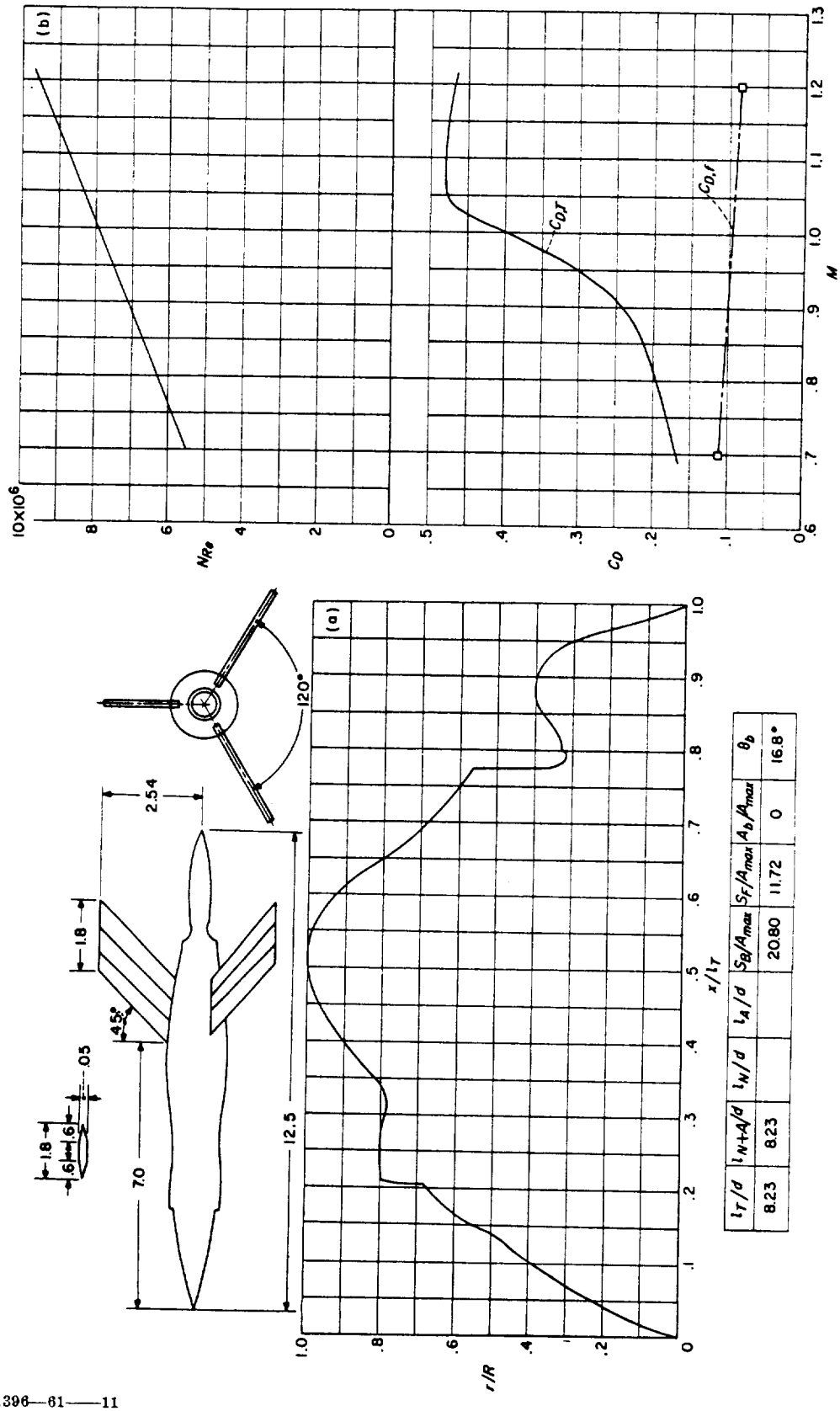

l_T/d	l_{N+A}/d	l_N/d	l_A/d	S_B/A_{max}	S_F/A_{max}	A_b/A_{max}	θ_b
8.23	8.23			20.80	11.72	0	16.8°

(a) Body shape. (Dimensions given are in inches.) (b) N_{Re} and C_D curves.

CONFIGURATION 148; helium-gun test.

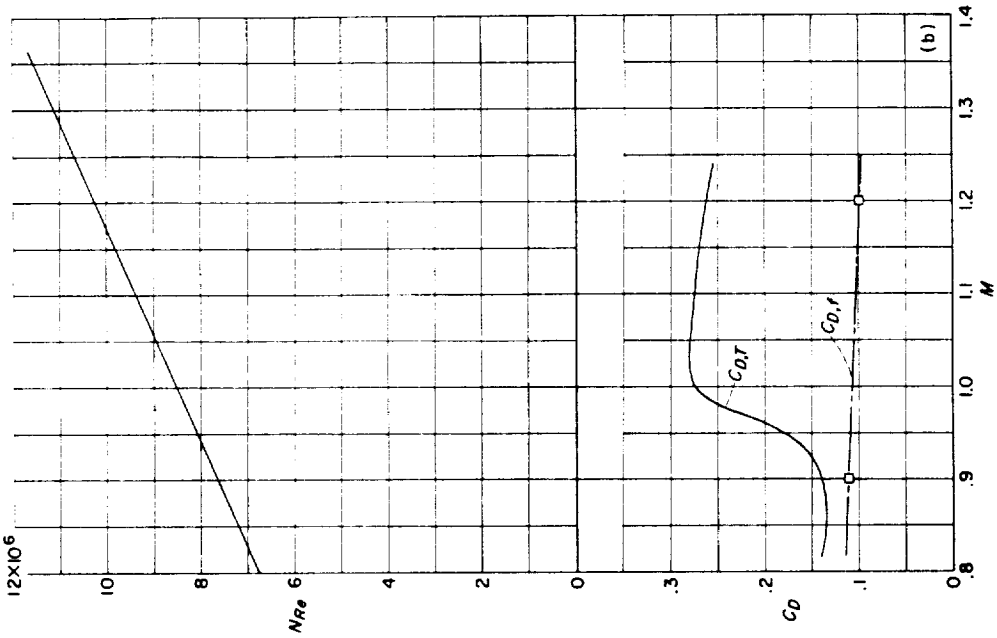

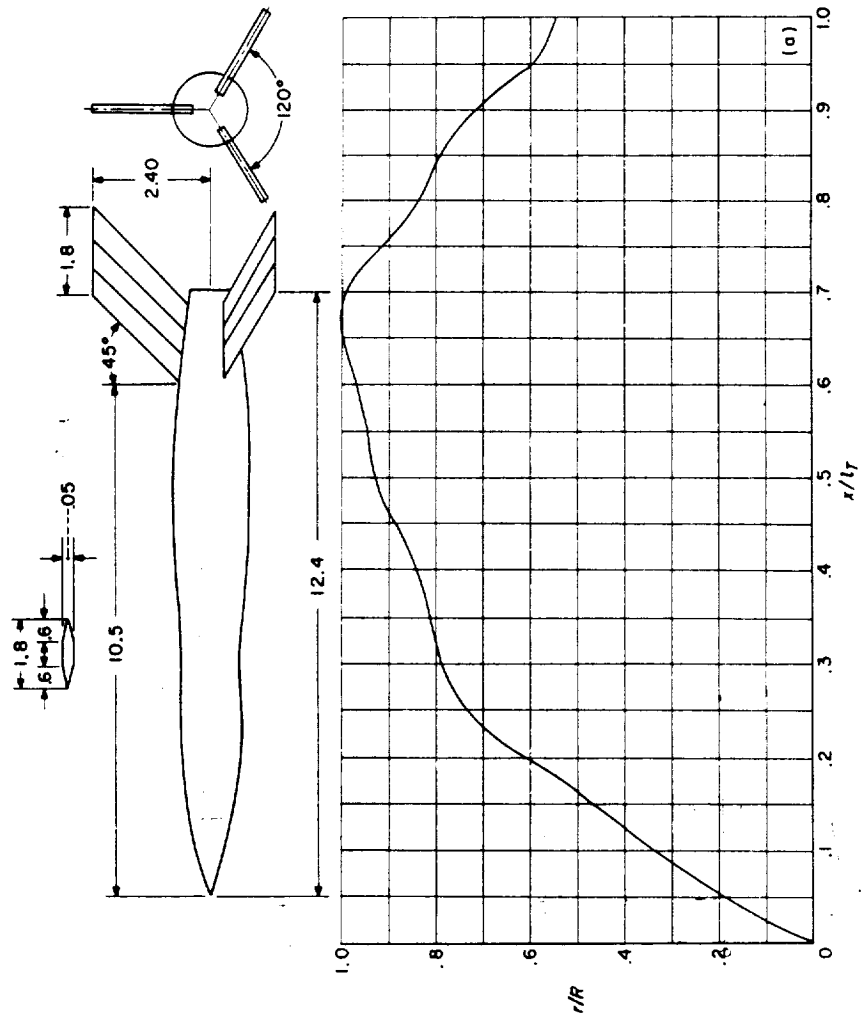

l_T/d	l_{N+A}/d	l_N/d	l_A/d	S_B/A_{max}	S_F/A_{max}	A_b/A_{max}	θ_b
8.27	8.27			24.0	10.9	.29	2.8°

(a) Body shape. (Dimensions given are in inches.) (b) N_{Re} and C_D curves.

CONFIGURATION 149; helium-gun test.

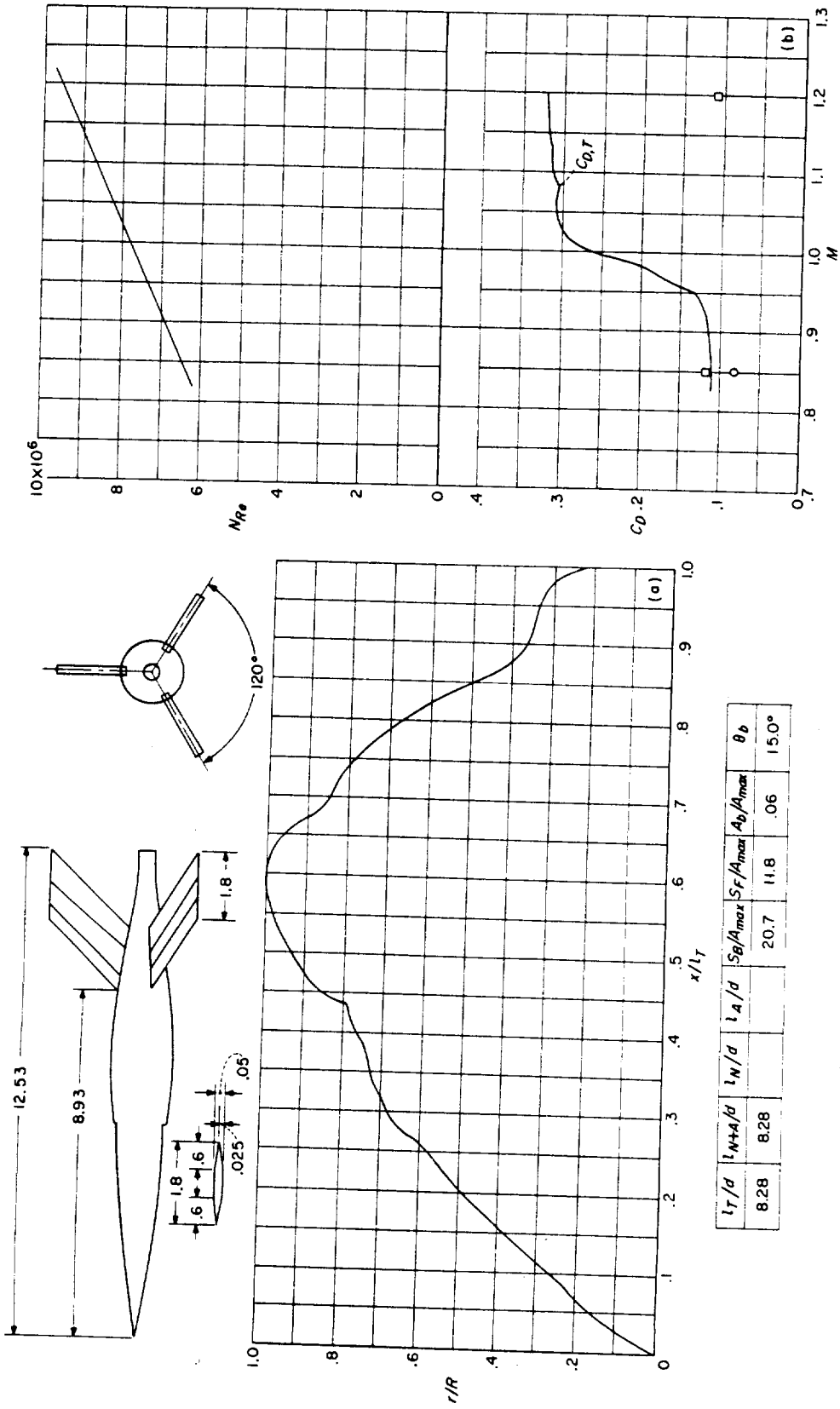

l_T/d	l_{N+A}/d	l_N/d	l_A/d	S_B/A_{max}	S_F/A_{max}	A_b/A_{max}	θ_b
8.28	8.28			20.7	11.8	.06	15.0°

(a) Body shape. (Dimensions given are in inches.) (b) N_{R_e} and C_D curves.

CONFIGURATION 150; helium-gun test.

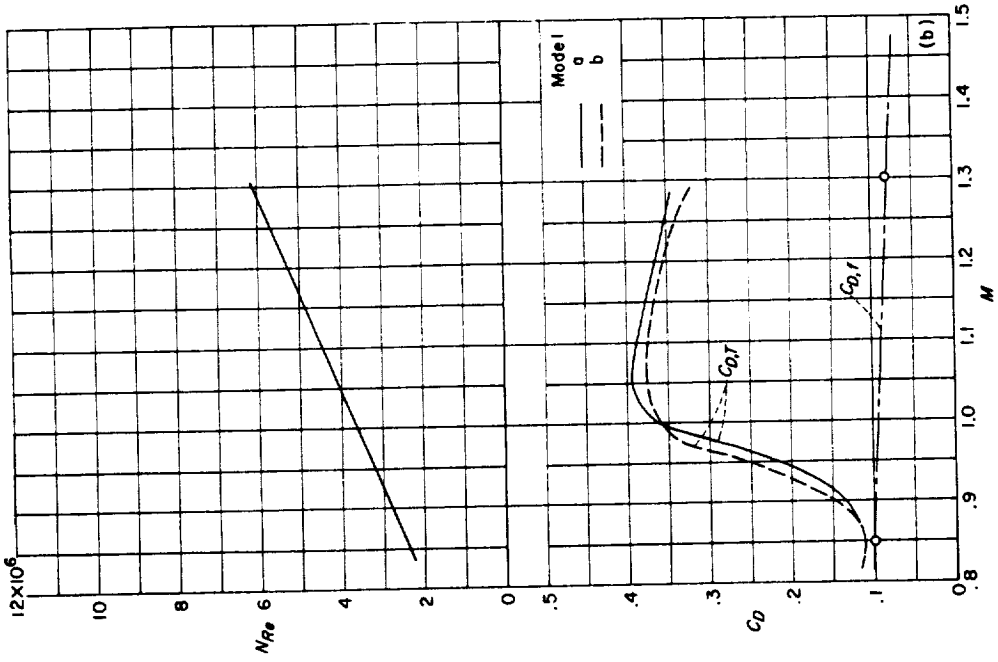

(b) N_{Re} and C_D curves.

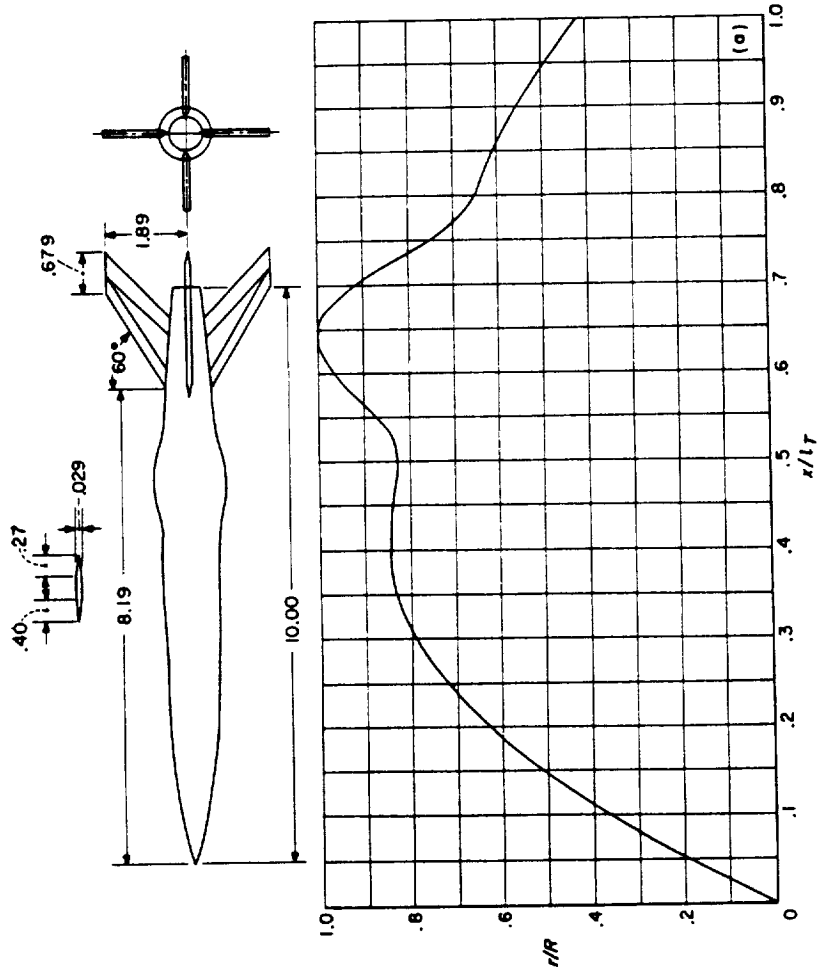

l_T/d	l_{N+A}/d	l_N/d	l_A/d	S_B/A_{max}	S_F/A_{max}	A_b/A_{max}	θ_b
8.40	8.40			23.00	7.88	.17	6.1°

(a) Body shape. (Dimensions given are in inches.)

CONFIGURATION 151; helium-gun test.

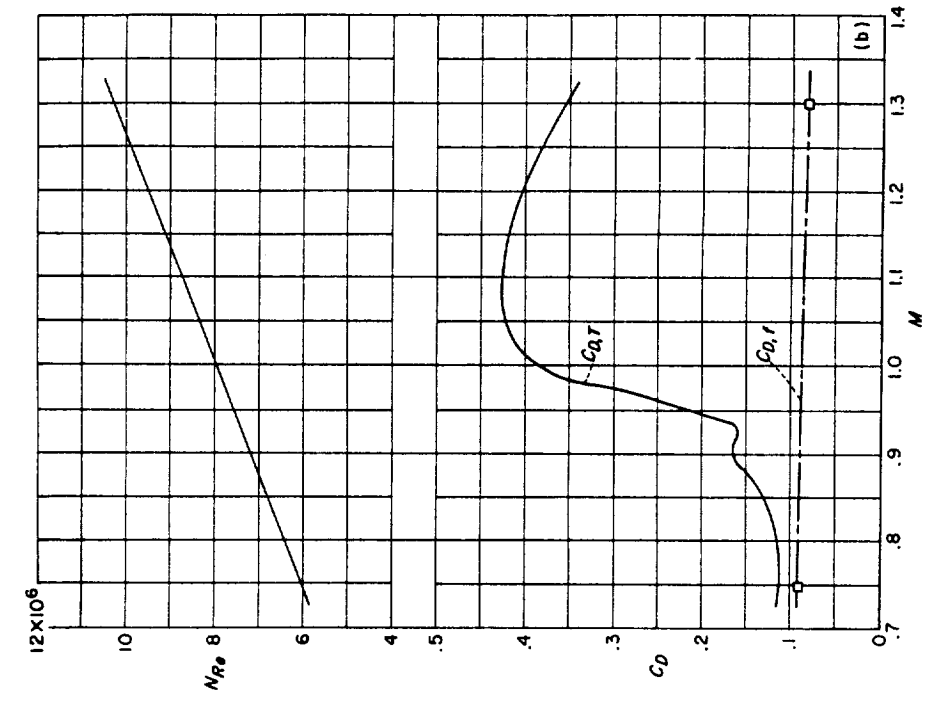

(b) N_{Re} and C_D curves.

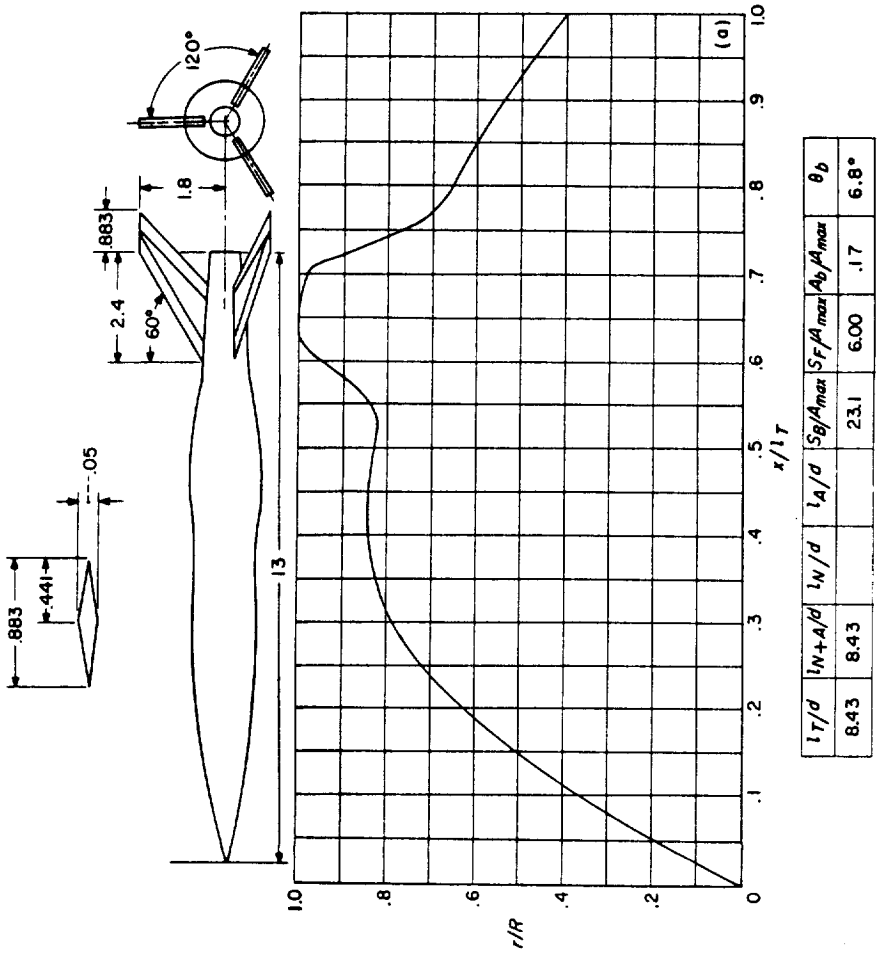

l_T/d	l_{N+A}/d	l_N/d	l_A/d	S_B/A_{max}	S_F/A_{max}	A_b/A_{max}	θ_b
8.43	8.43			23.1	6.00	.17	6.8°

(a) Body shape. (Dimensions given are in inches.)

CONFIGURATION 152; helium-gun test.

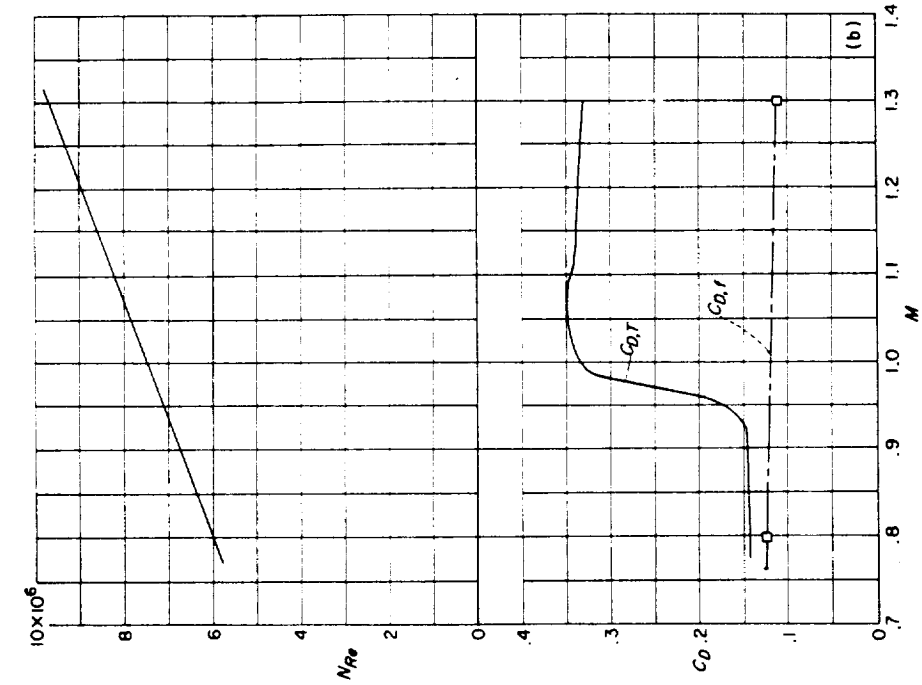

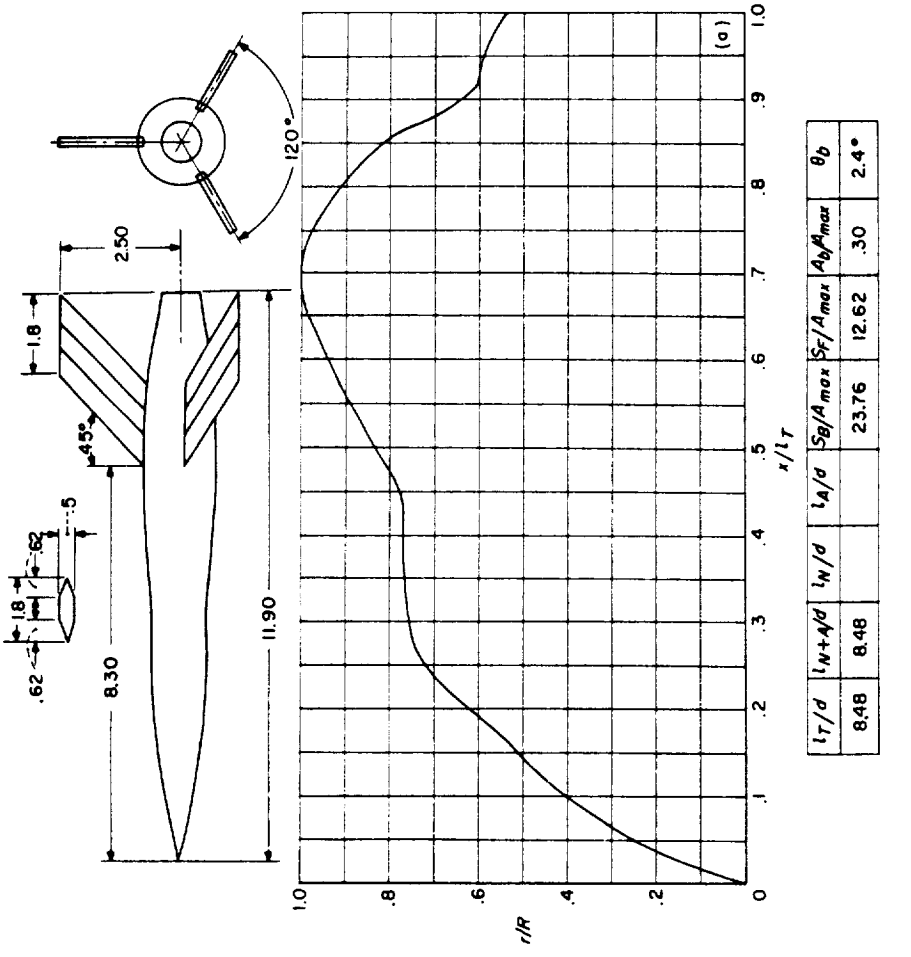

l_T/d	l_{N+A}/d	l_N/d	l_A/d	S_B/A_{max}	S_F/A_{max}	A_b/A_{max}	θ_b
8.48	8.48			23.76	12.62	.30	2.4°

(a) Body shape. (Dimensions given are in inches.) (b) N_{Re} and C_D curves.

CONFIGURATION 153; helium-gun test.

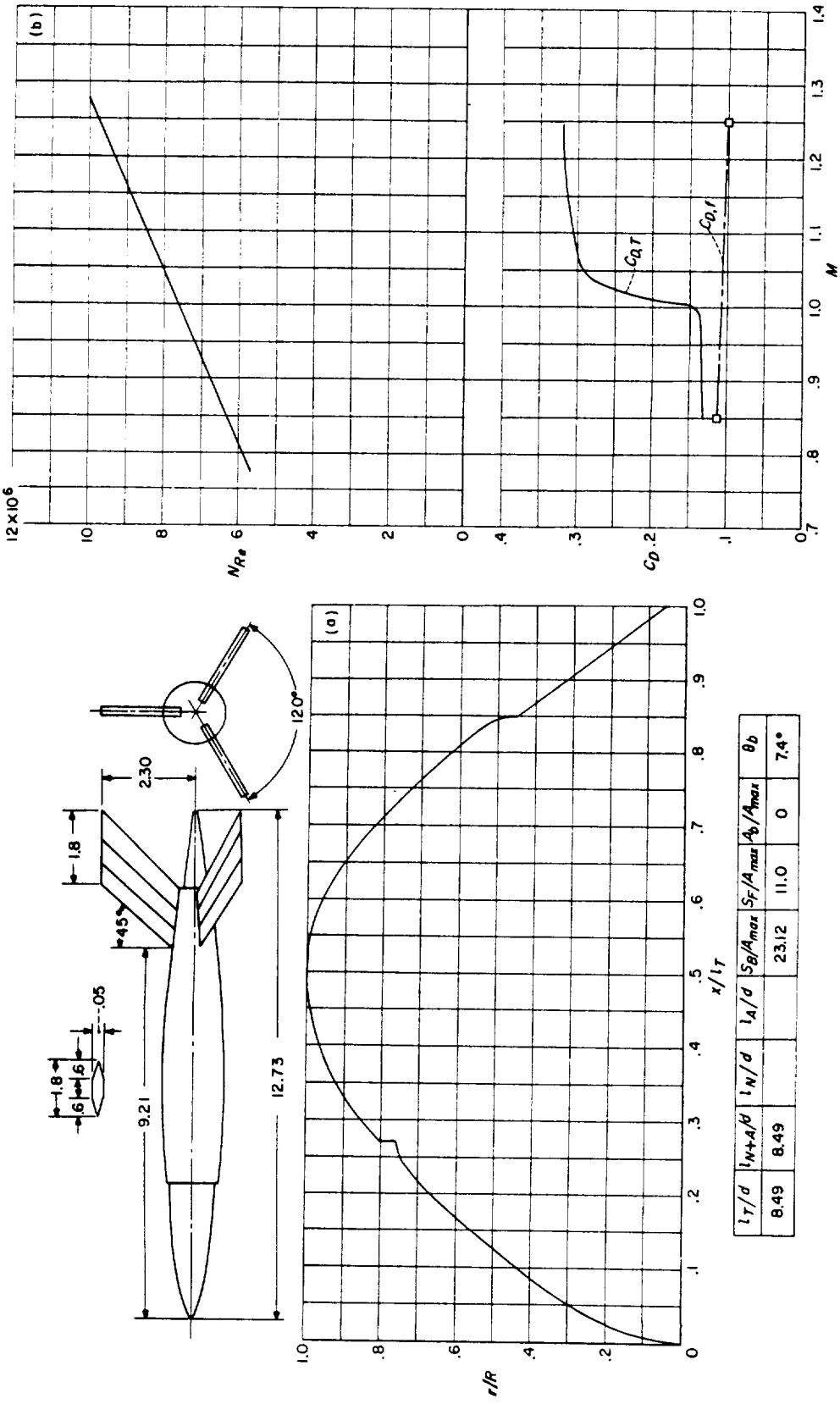

l_T/d	l_{N+A}/d	l_N/d	l_A/d	S_B/A_{max}	S_F/A_{max}	A_b/A_{max}	θ_b
8.49	8.49			23.12	11.0	0	7.4°

(a) Body shape. (Dimensions given are in inches.) (b) N_{Re} and C_D curves.

CONFIGURATION 154; helium-gun test.

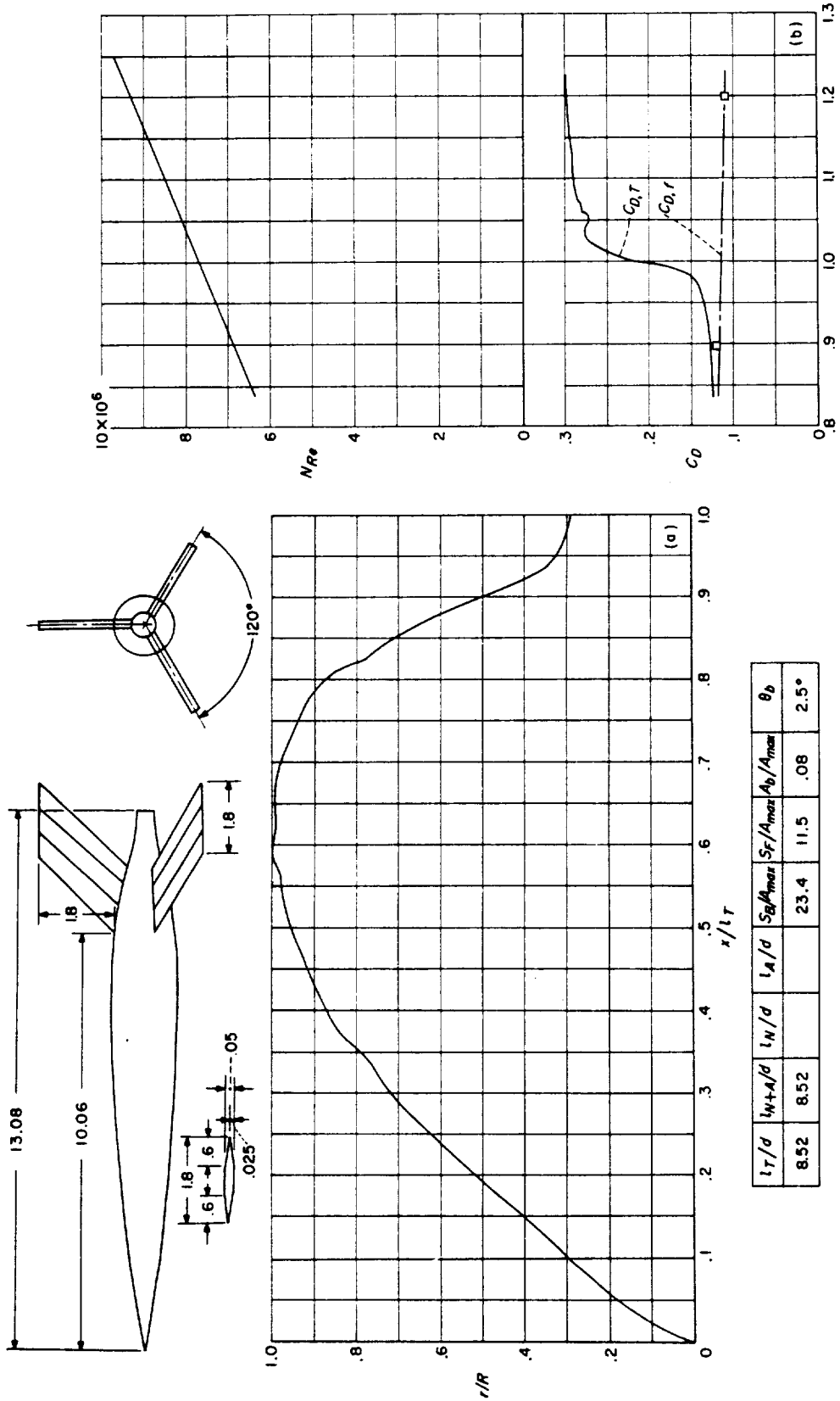

l_T/d	l_{N+A}/d	l_N/d	l_A/d	S_B/A_{max}	S_F/A_{max}	A_b/A_{max}	θ_b
8.52	8.52			23.4	11.5	.08	2.5°

(a) Body shape. (Dimensions given are in inches.) (b) N_{Re} and C_D curves.

CONFIGURATION 155; helium-gun test.

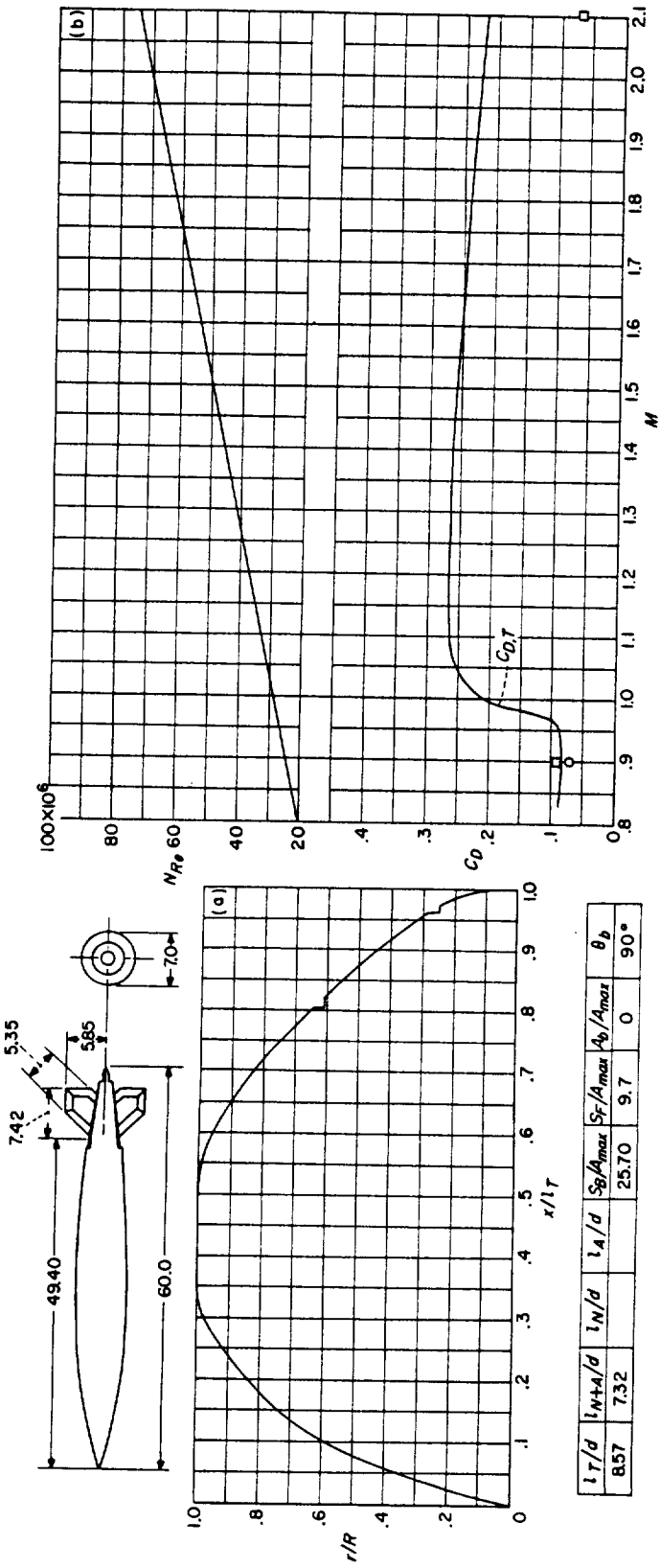

l_T/d	l_{N+A}/d	l_N/d	l_A/d	S_B/A_{max}	S_F/A_{max}	A_b/A_{max}	θ_b
8.57	7.32			25.70	9.7	0	90°

(a) Body shape. (Dimensions given are in inches.) (b) N_{Re} and C_D curves.

CONFIGURATION 156; rocket test.

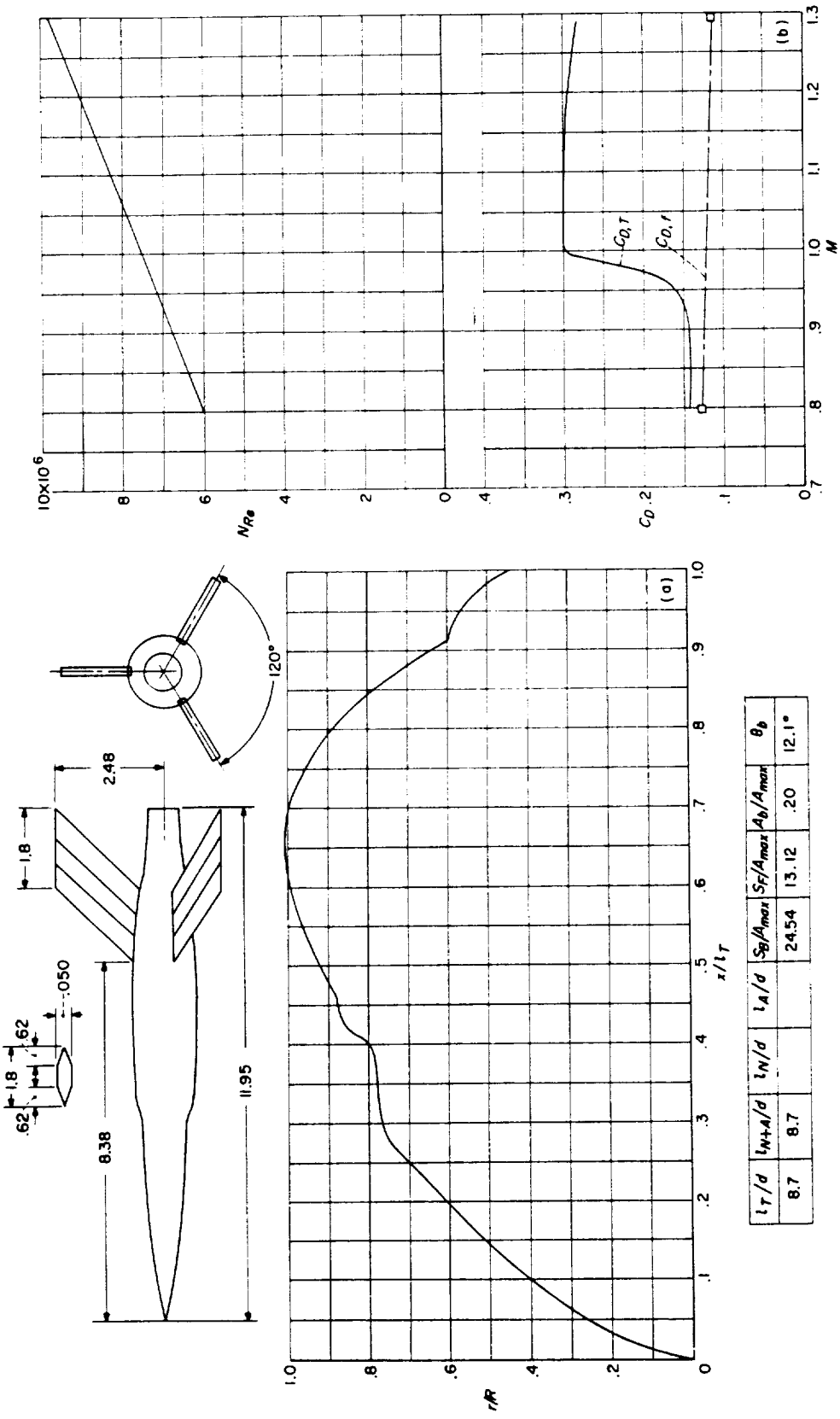

l_T/d	l_{N+A}/d	l_N/d	l_A/d	S_B/A_{max}	S_F/A_{max}	A_b/A_{max}	θ_b
8.7	8.7			24.54	13.12	.20	12.1°

(a) Body shape. (Dimensions given are in inches.) (b) N_{Re} and C_D curves.

CONFIGURATION 157; helium-gun test.

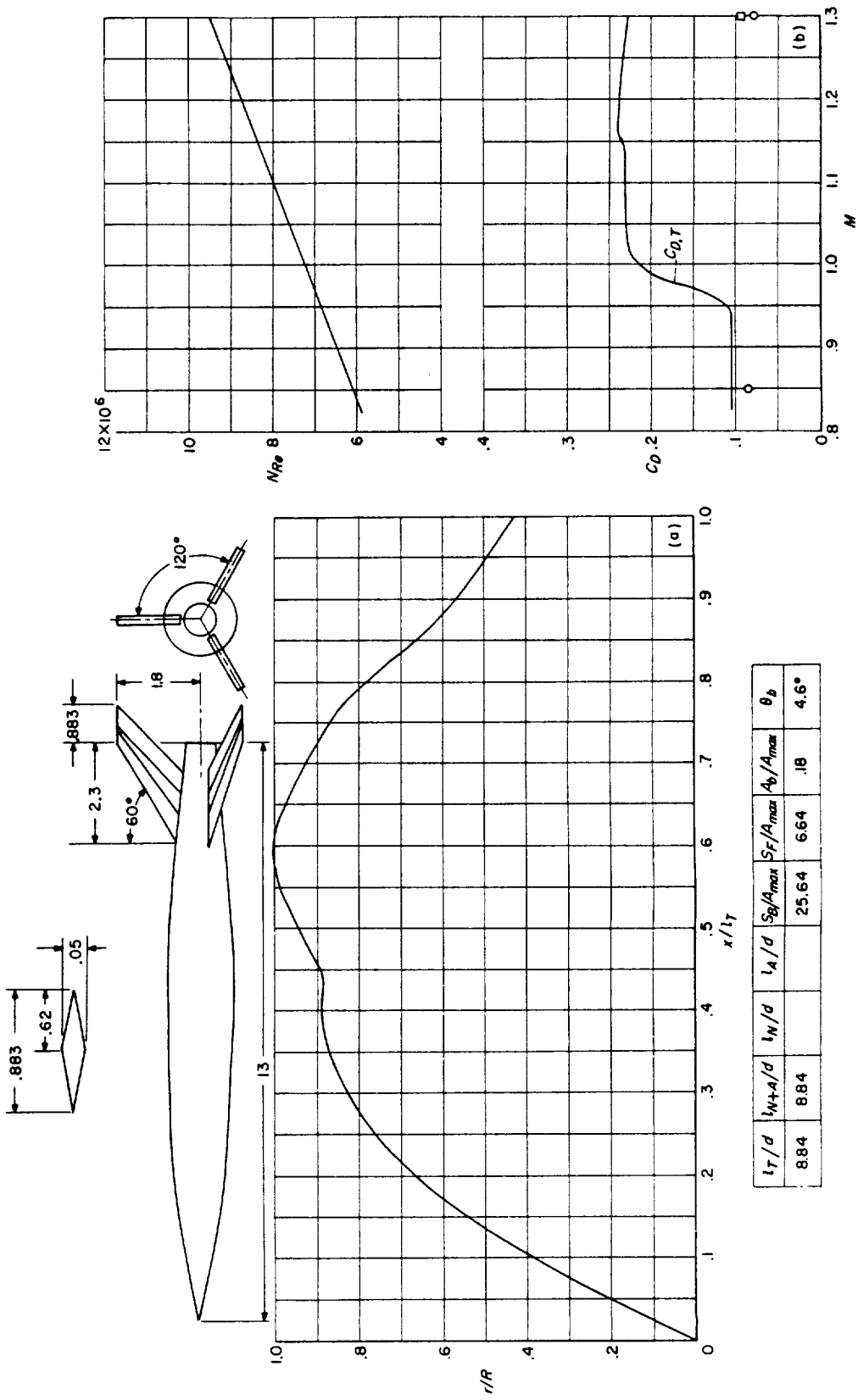

l_T/d	l_{N+A}/d	l_N/d	l_A/d	S_B/A_{max}	S_F/A_{max}	A_b/A_{max}	θ_b
8.84	8.84			25.64	6.64	.18	4.6°

(a) Body shape. (Dimensions given are in inches.) (b) N_{Re} and C_D curves.

CONFIGURATION 158; helium-gun test.

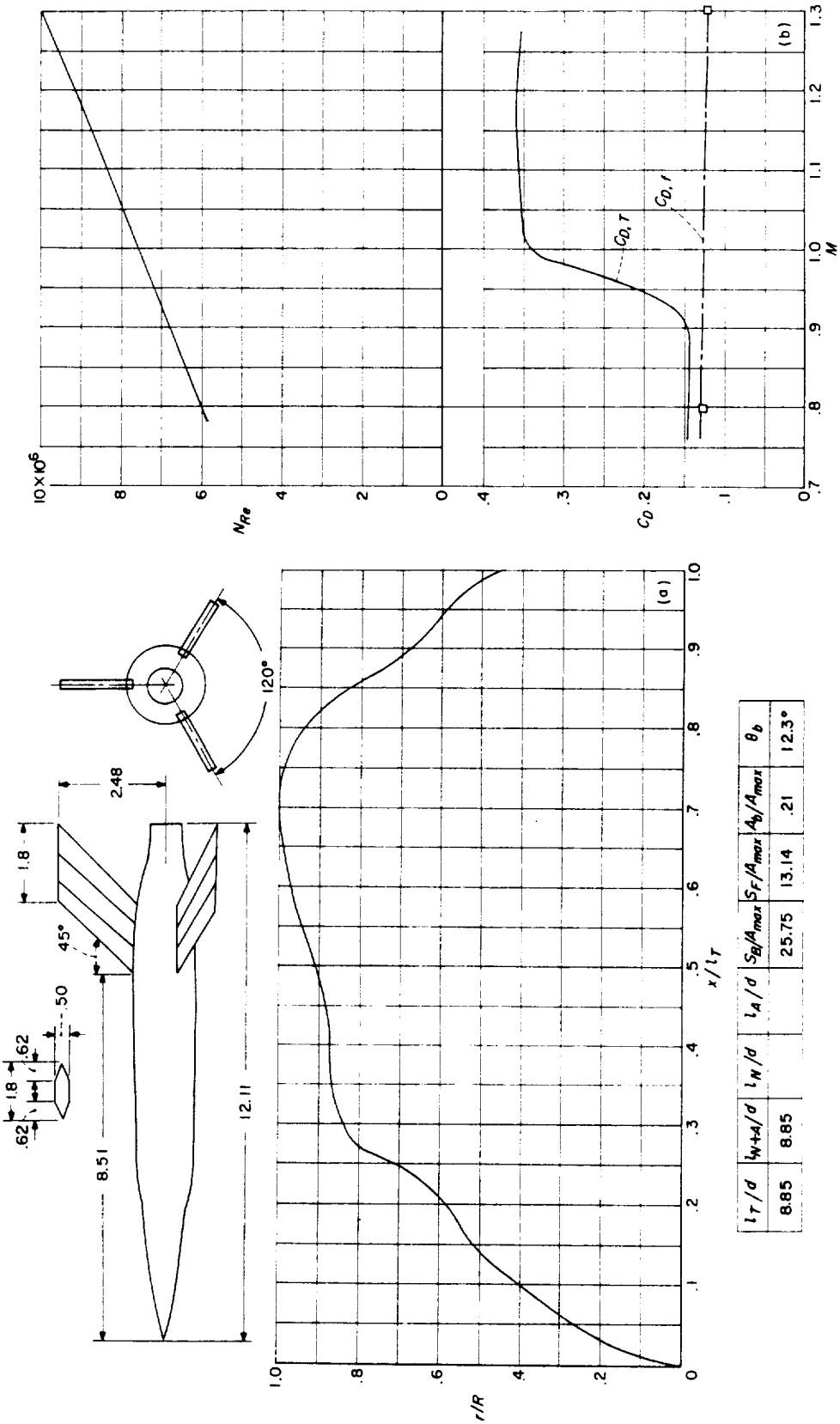

l_T/d	l_{W+A}/d	l_N/d	l_A/d	S_B/A_{max}	S_F/A_{max}	A_b/A_{max}	θ_b
8.85	8.85			25.75	13.14	.21	12.3°

(a) Body shape. (Dimensions given are in inches.) (b) N_{Re} and C_D curves.

CONFIGURATION 159; helium-gun test.

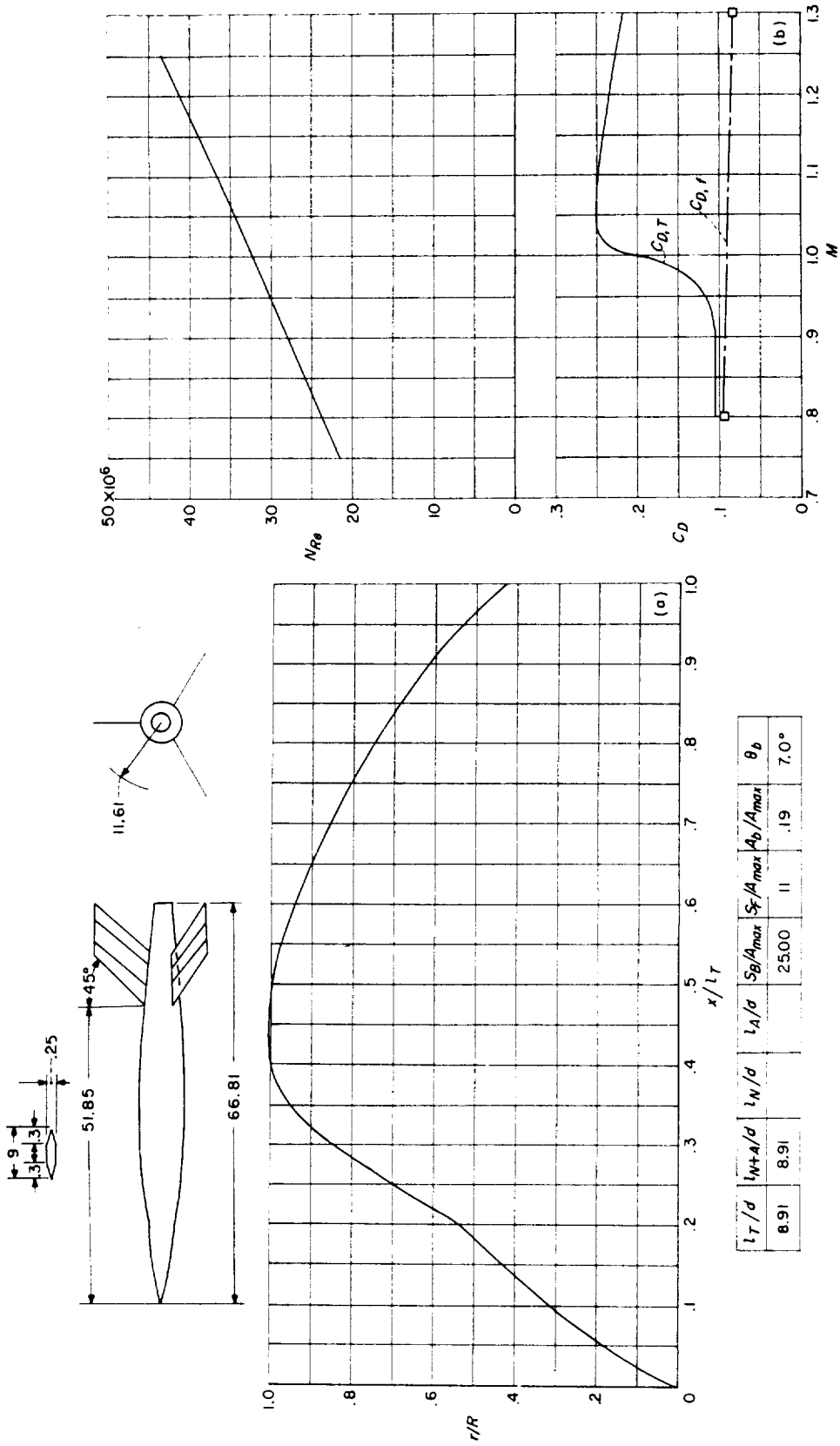

l_T/d	l_{N+A}/d	l_N/d	l_A/d	S_B/A_{max}	S_F/A_{max}	A_b/A_{max}	θ_b
8.91	8.91			25.00	11	.19	7.0°

(a) Body shape. (Dimensions given are in inches.) (b) N_{Re} and C_D curves.

CONFIGURATION 160 (parabolic afterbody); rocket test.

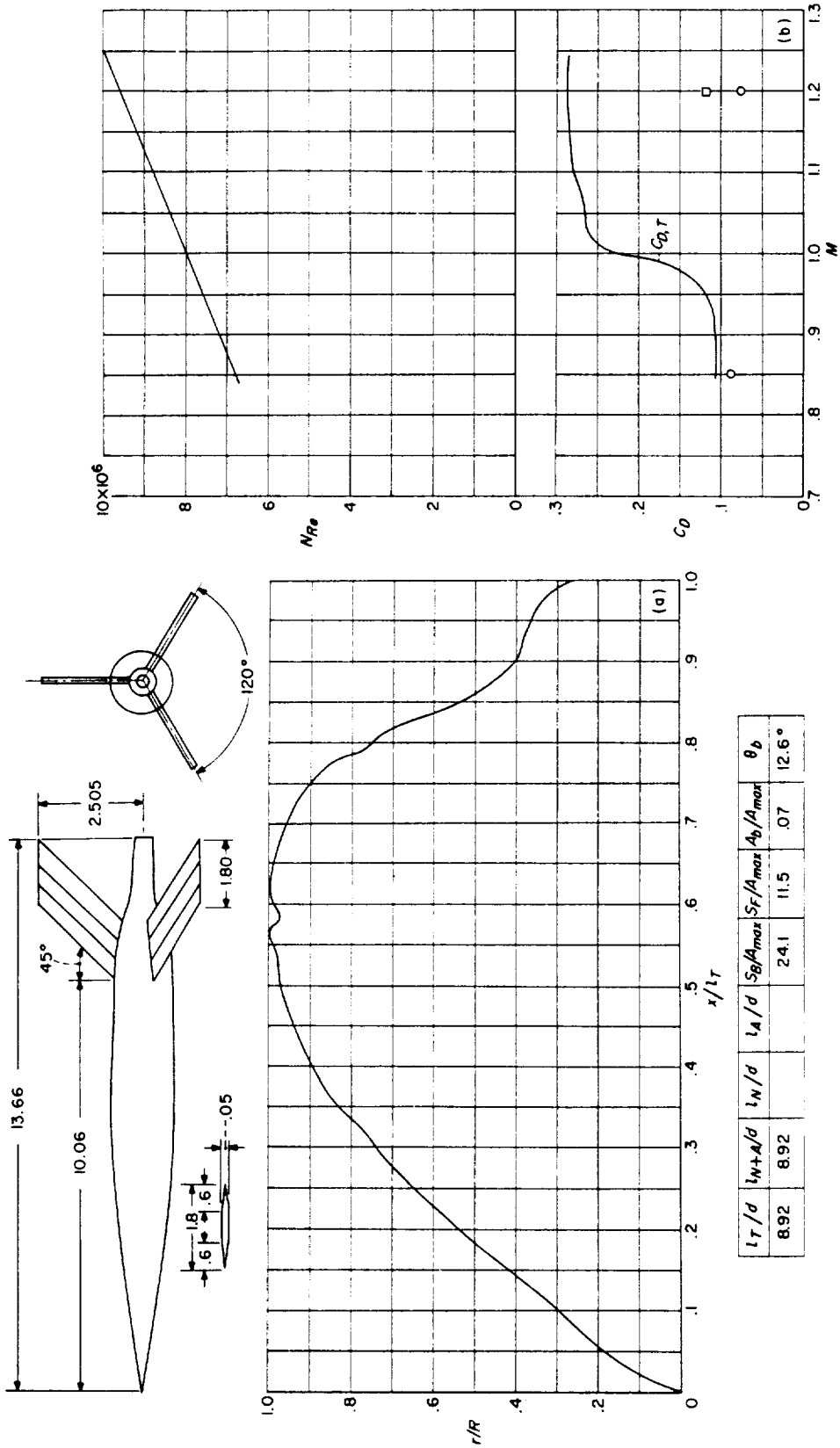

l_T/d	l_{N+A}/d	l_N/d	l_A/d	S_B/A_{max}	S_F/A_{max}	A_b/A_{max}	θ_b
8.92	8.92			24.1	11.5	.07	12.6°

(a) Body shape. (Dimensions given are in inches.) (b) N_{Re} and C_D curves.

CONFIGURATION 161; helium-gun test.

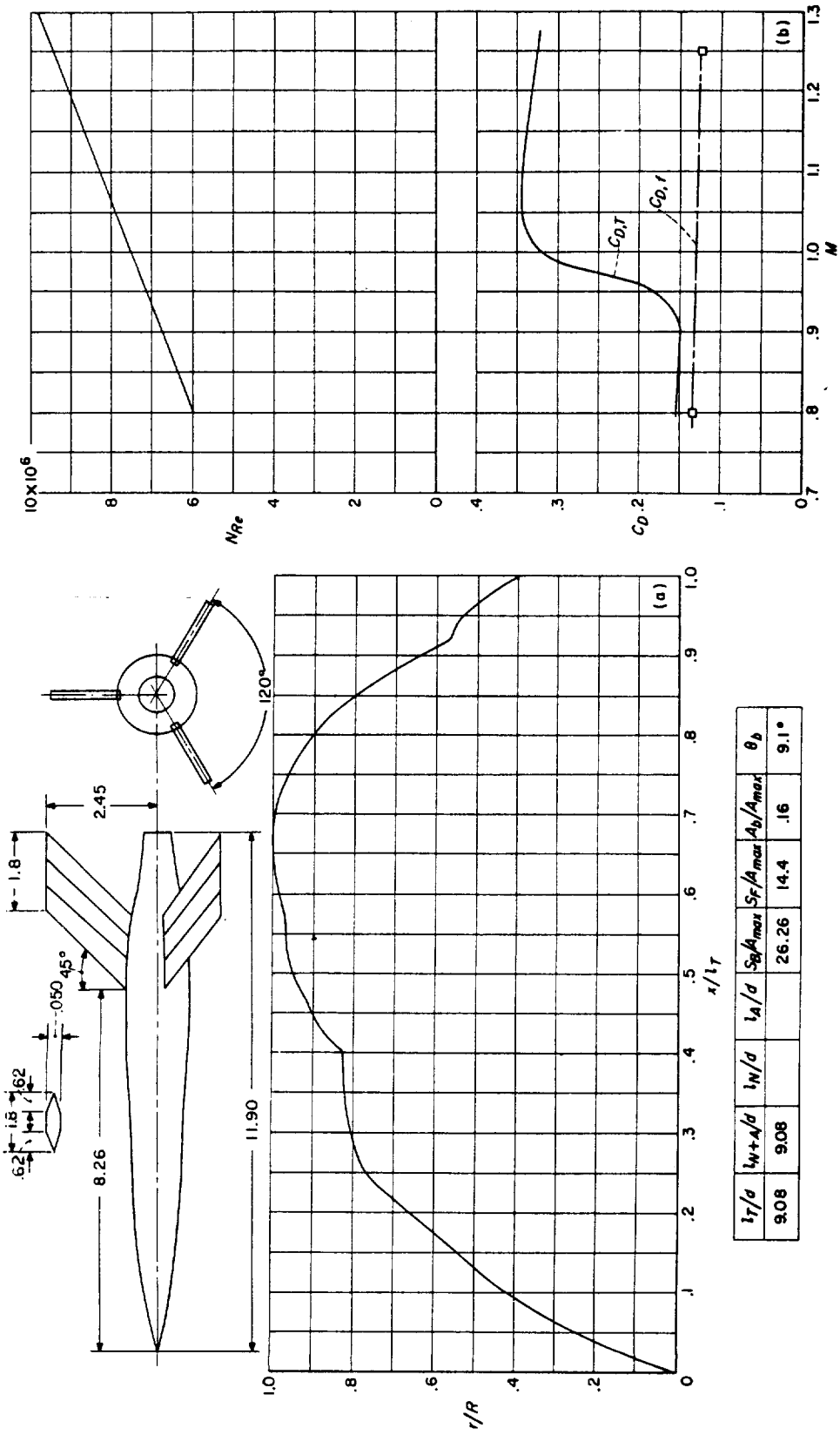

l_T/d	l_{N+A}/d	l_N/d	l_A/d	S_B/A_{max}	S_F/A_{max}	A_b/A_{max}	θ_b
9.08	9.08			26.26	14.4	.16	9.1°

(a) Body shape. (Dimensions given are in inches.) (b) N_{Re} and C_D curves.

CONFIGURATION 162; helium-gun test.

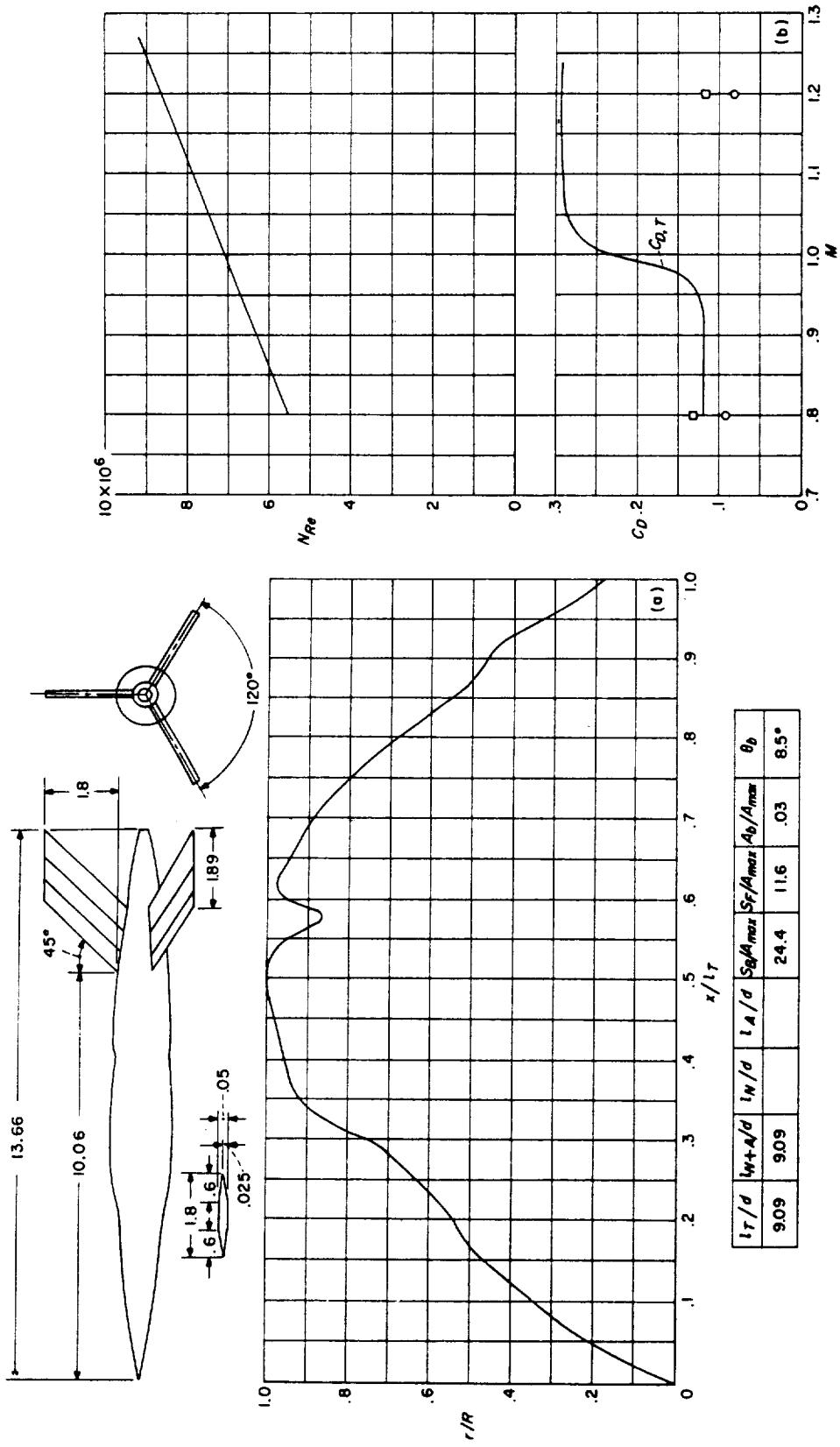

l_T/d	l_{N+A}/d	l_N/d	l_A/d	S_B/A_{max}	S_F/A_{max}	A_b/A_{max}	θ_b
9.09	9.09			24.4	11.6	.03	8.5°

(a) Body shape. (Dimensions given are in inches.) (b) N_{Re} and C_D curves.

CONFIGURATION 163; helium-gun test.

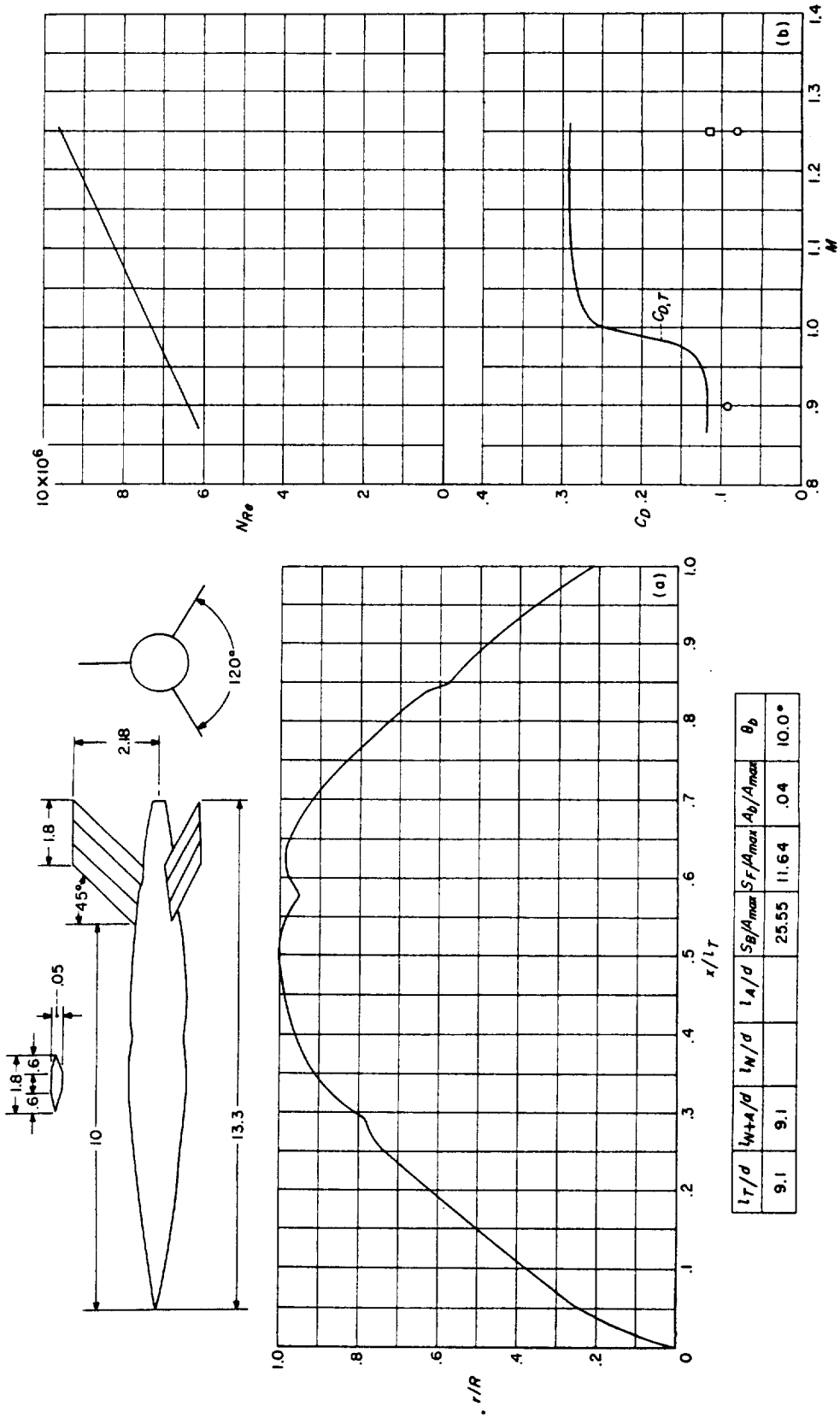

l_T/d	l_{W+A}/d	l_W/d	l_A/d	S_B/A_{max}	S_F/A_{max}	A_b/A_{max}	θ_b
9.1	9.1			25.55	11.64	.04	10.0°

(a) Body shape. (Dimensions given are in inches.) (b) N_{Re} and C_D curves.

CONFIGURATION 164; helium-gun test.

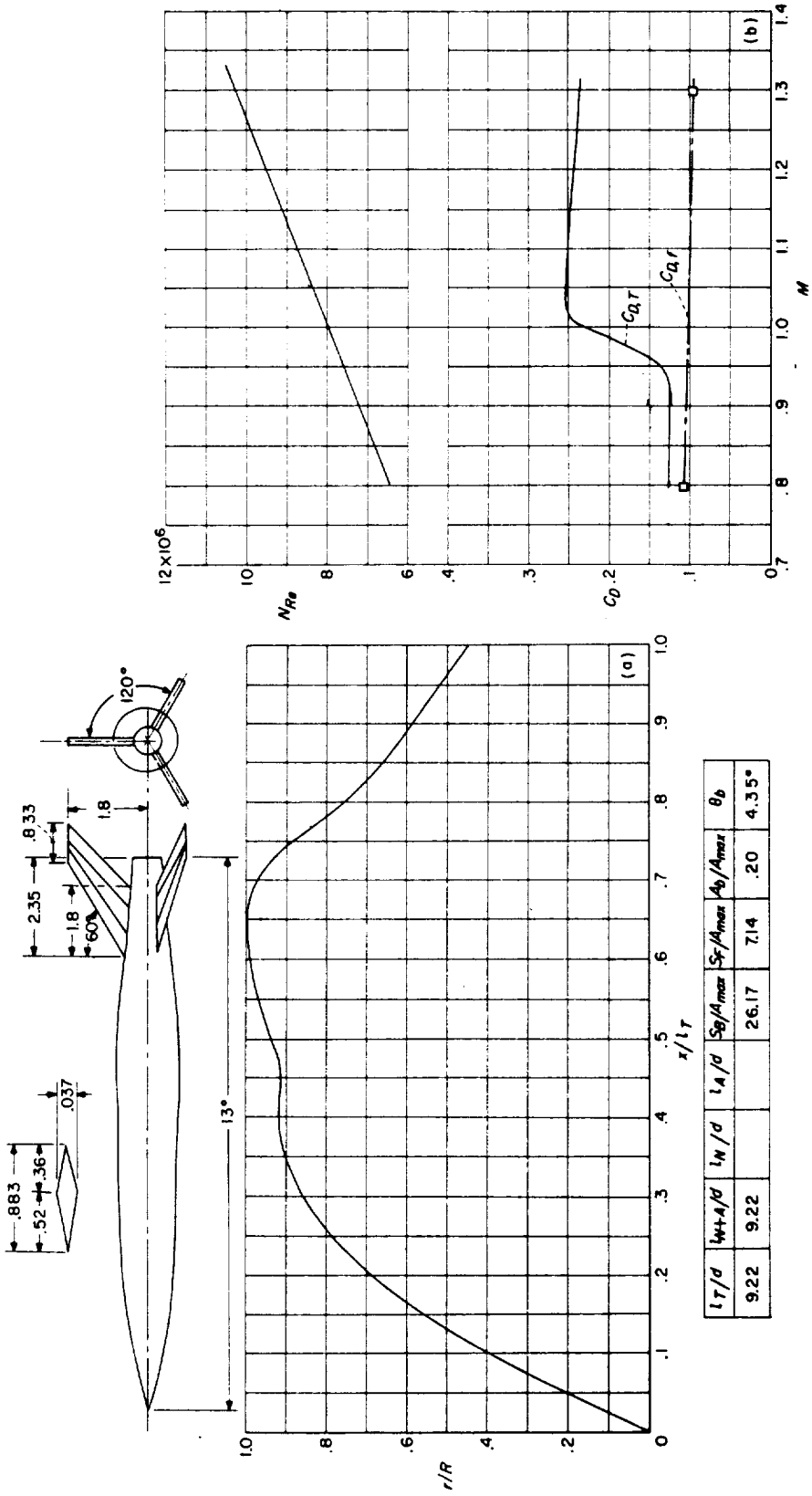

l_T/d	l_{N+A}/d	l_N/d	l_A/d	S_B/A_{max}	S_F/A_{max}	A_b/A_{max}	θ_b
9.22	9.22			26.17	7.14	.20	4.35°

(a) Body shape. (Dimensions given are in inches.) (b) N_{Re} and C_D curves

CONFIGURATION 165; helium-gun test.

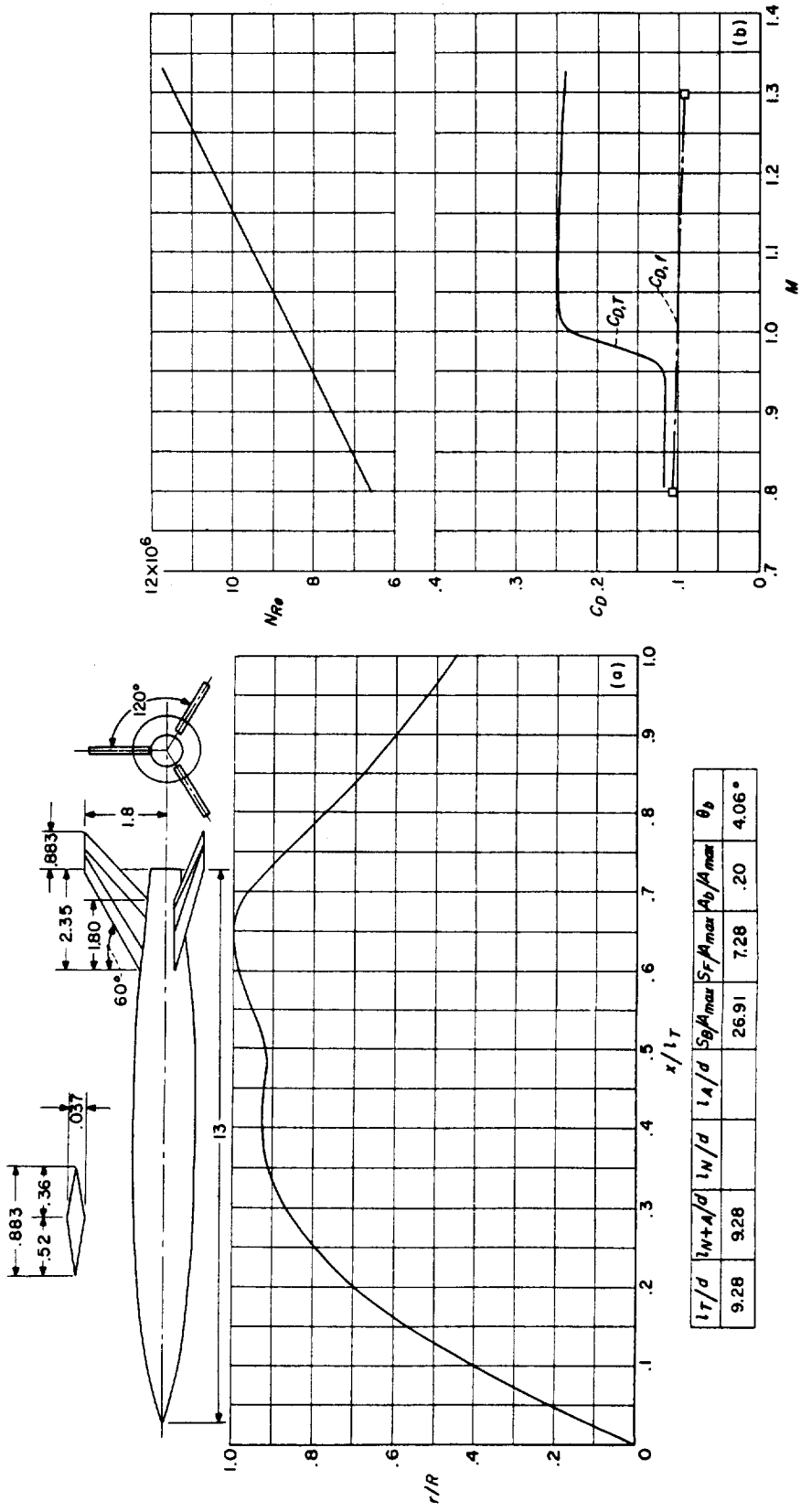

l_T/d	l_{N+A}/d	l_N/d	l_A/d	S_B/A_{max}	S_F/A_{max}	A_b/A_{max}	θ_b
9.28	9.28			26.91	7.28	.20	4.06°

(a) Body shape. (Dimensions given are in inches.) (b) N_{Re} and C_D curves.

Configuration 166; helium-gun test.

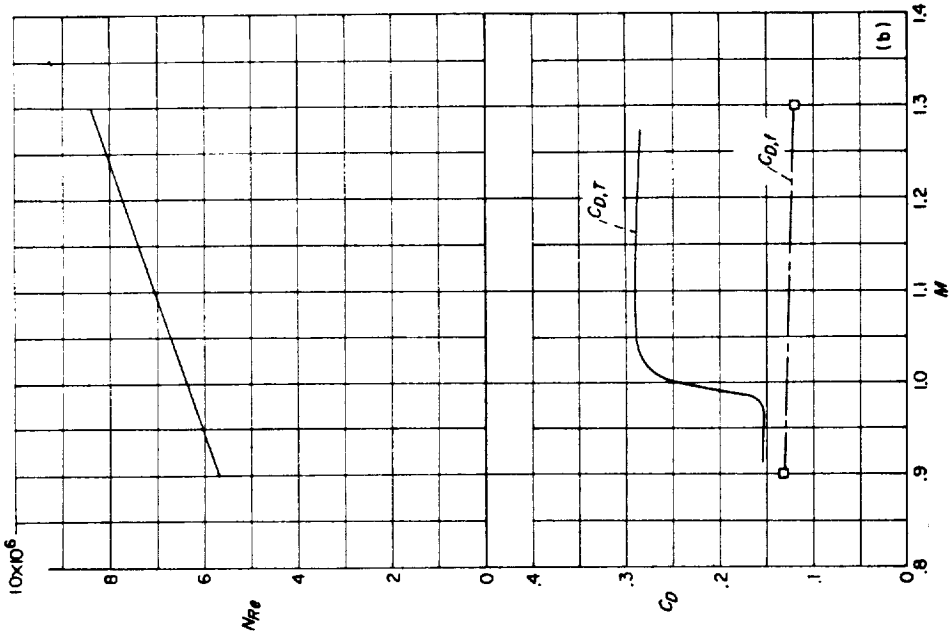

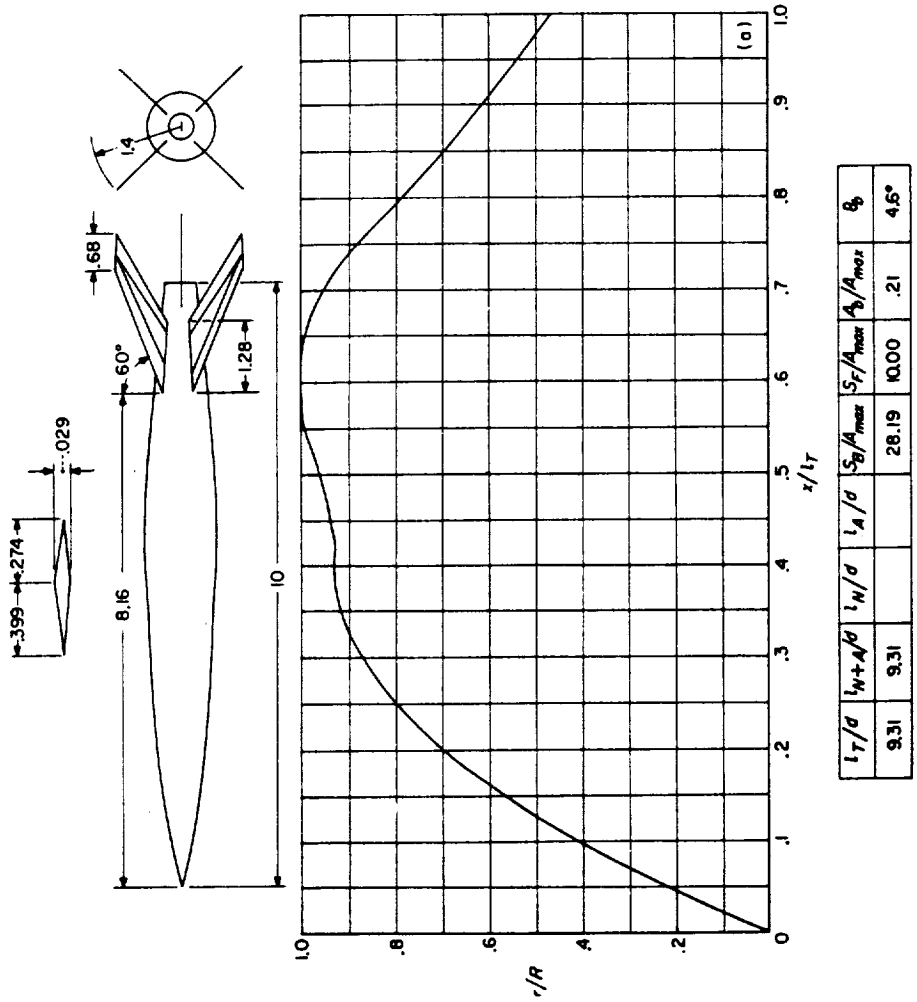

l_T/d	l_{N+A}/d	l_N/d	l_A/d	S_B/A_{max}	S_T/A_{max}	A_b/A_{max}	θ_b
9.31	9.31			28.19	10.00	.21	4.6°

(a) Body shape. (Dimensions given are in inches.) (b) N_{Re} and C_D curves.

CONFIGURATION 167; helium-gun test.

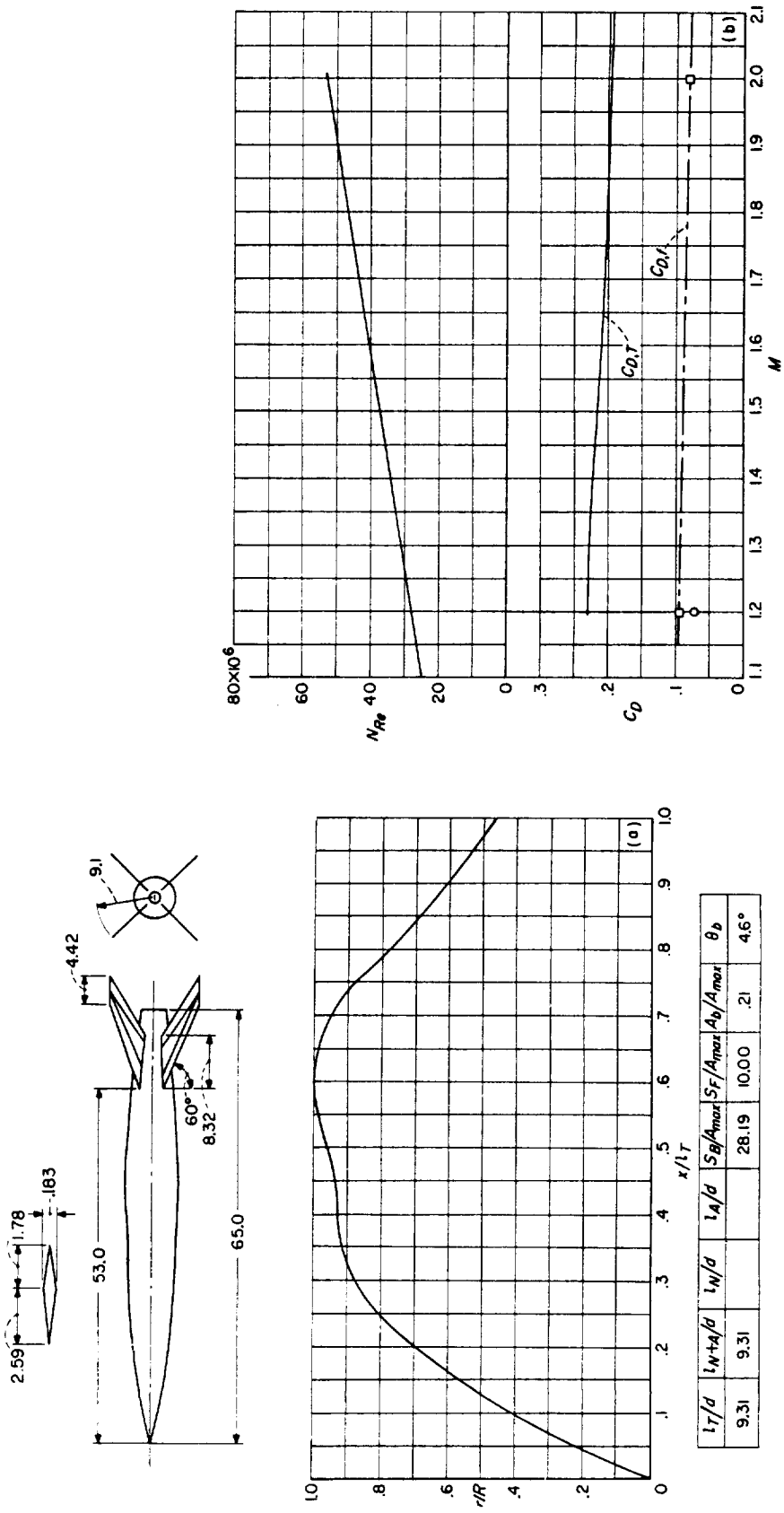

l_T/d	l_{N+A}/d	l_N/d	l_A/d	S_B/A_{max}	S_F/A_{max}	A_b/A_{max}	θ_b
9.31	9.31			28.19	10.00	.21	4.6°

(a) Body shape. (Dimensions given are in inches.) (b) N_{Re} and C_D curves.

CONFIGURATION 168; rocket test.

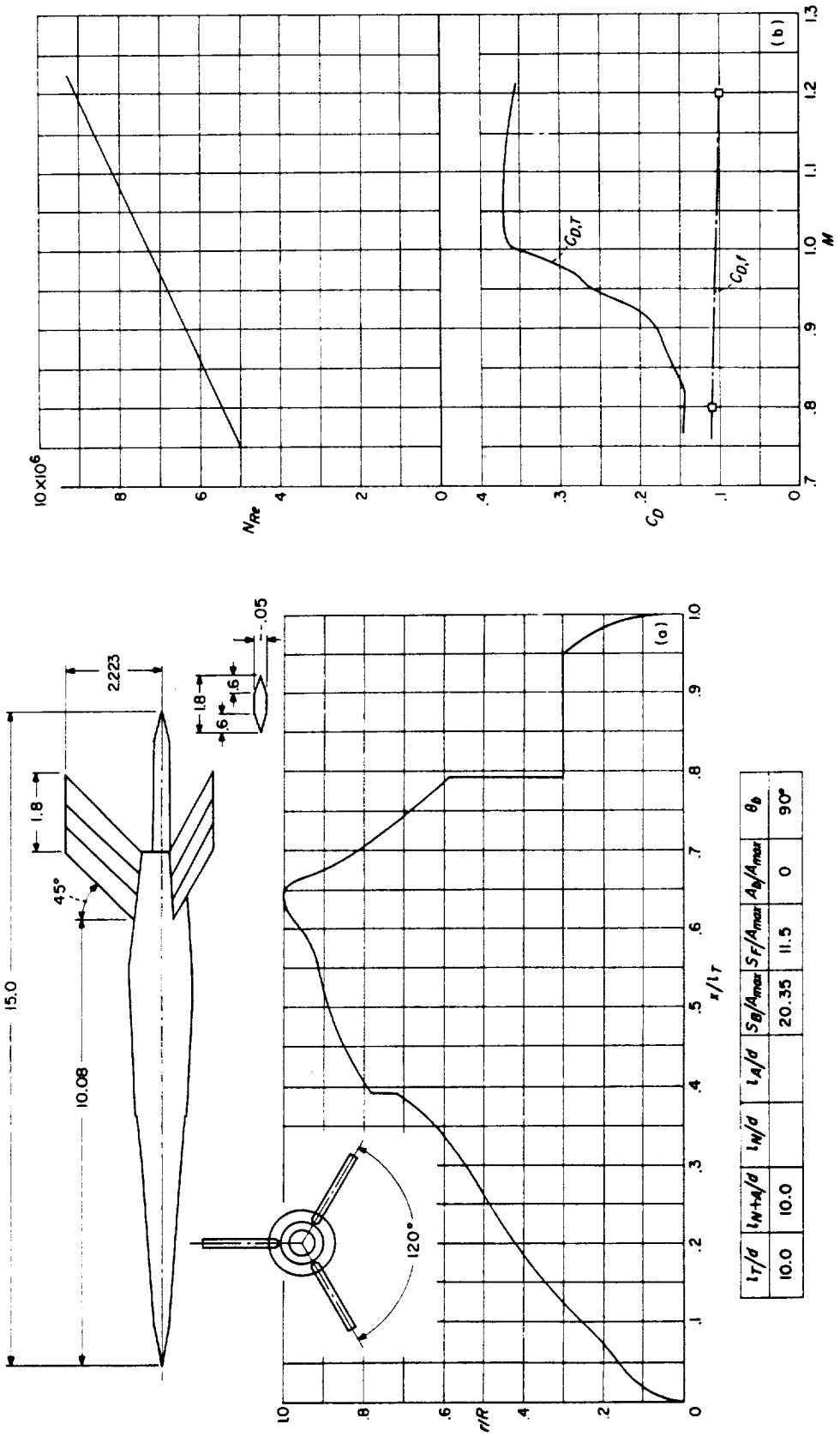

l_T/d	l_{N+A}/d	l_N/d	l_A/d	S_B/A_{max}	S_F/A_{max}	A_b/A_{max}	θ_b
10.0	10.0			20.35	11.5	0	90°

(a) Body shape. (Dimensions given are in inches.) (b) N_{Re} and C_D curves.

CONFIGURATION 169; helium-gun test.

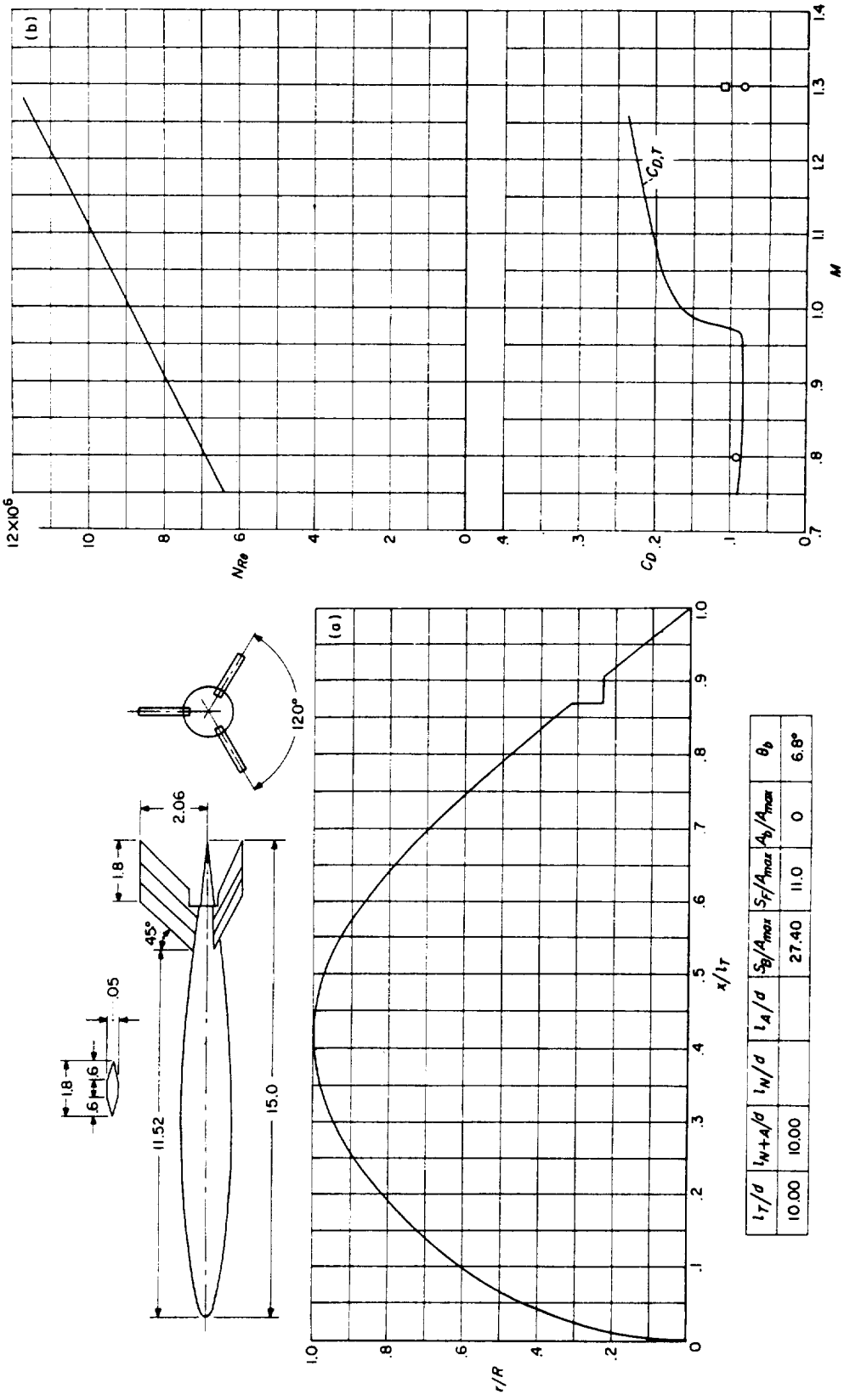

l_T/d	l_{N+A}/d	l_N/d	l_A/d	S_B/A_{max}	S_F/A_{max}	A_b/A_{max}	θ_b
10.00	10.00			27.40	11.0	0	6.8°

(a) Body shape. (Dimensions given are in inches.) (b) N_{Re} and C_D curves.

CONFIGURATION 170; helium-gun test. (Apparently there was an appreciable length of laminar flow on the body of this model.)

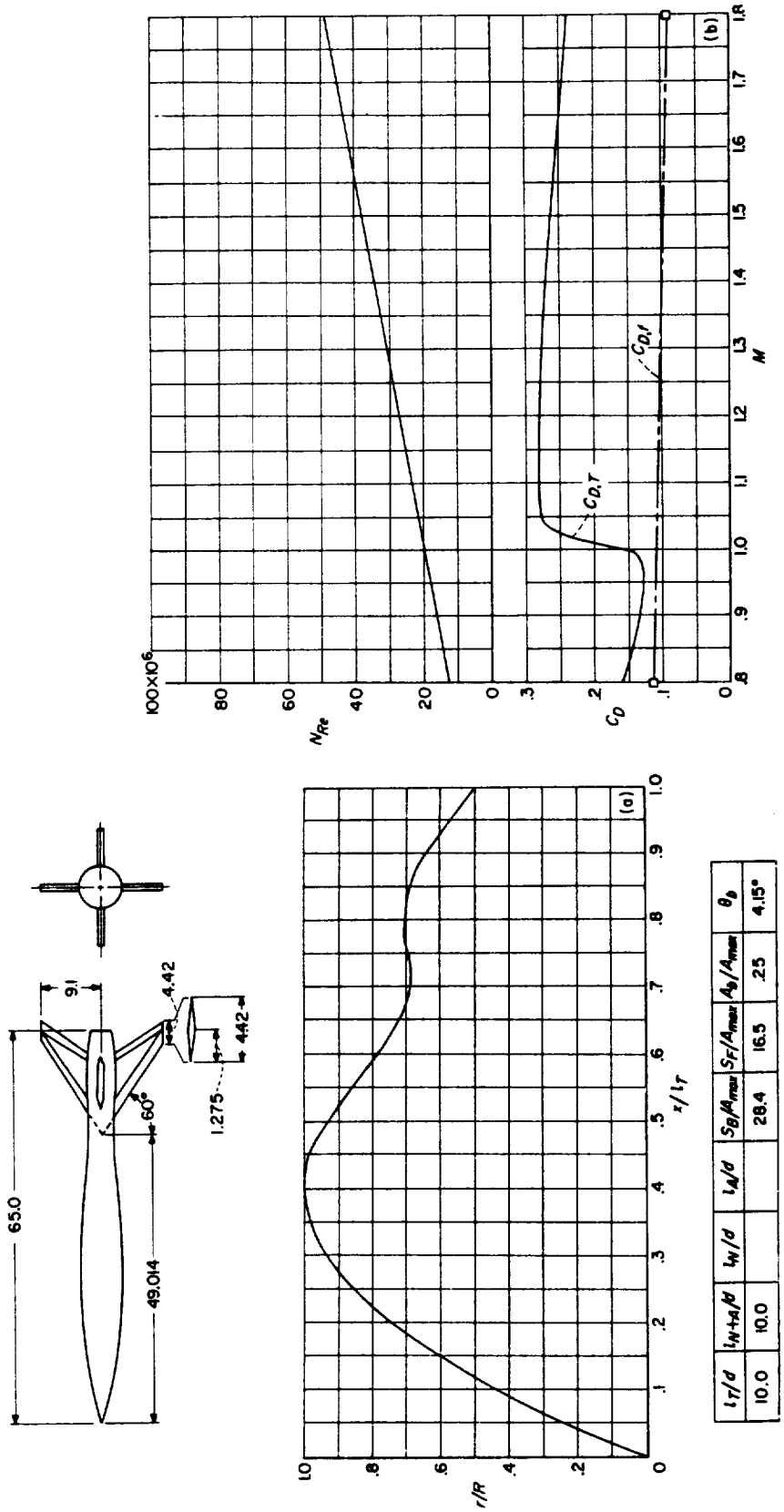

l_r/d	l_{N+A}/d	l_w/d	l_A/d	S_B/A_{max}	S_F/A_{max}	A_b/A_{max}	θ_b
10.0	10.0			28.4	16.5	.25	4.15°

(a) Body shape. (Dimensions given are in inches.) (b) N_{Re} and C_D curves.

CONFIGURATION 171; rocket test.

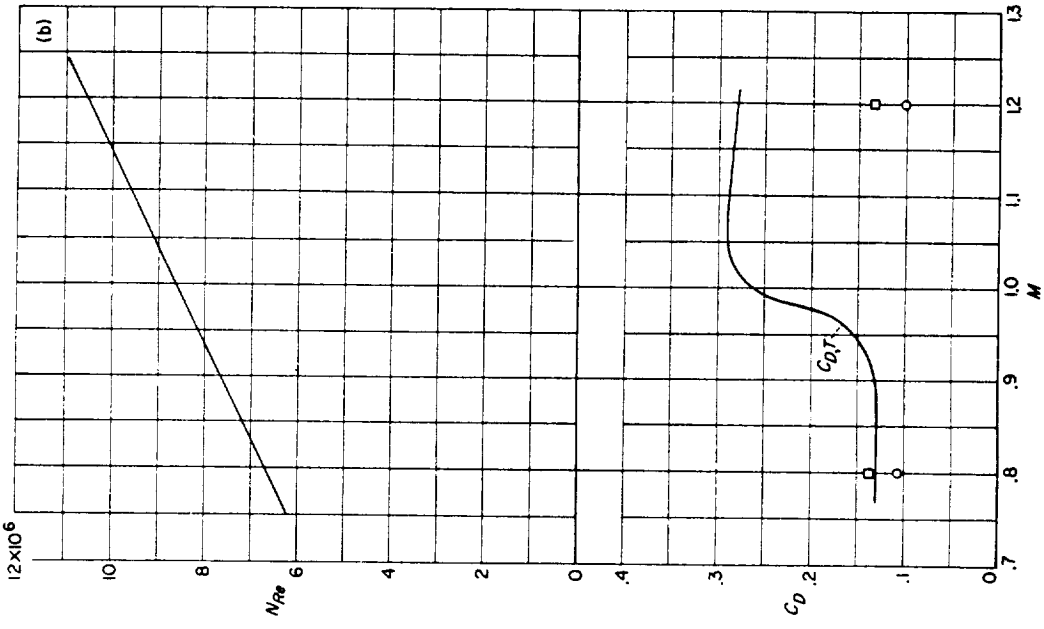

(b) N_{Re} and C_D curves.

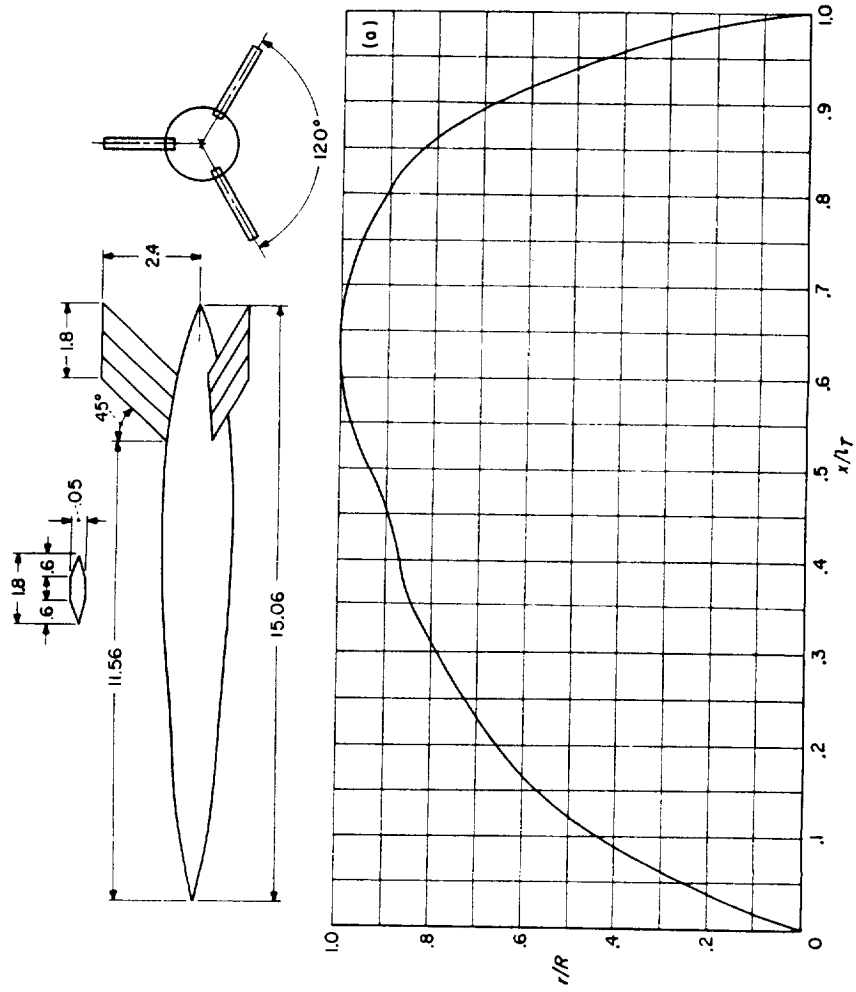

l_T/d	l_{W+A}/d	l_H/d	l_A/d	S_B/A_{max}	S_F/A_{max}	A_b/A_{max}	θ_b
10.04	10.04			30.40	11.00	0	90°

(a) Body shape. (Dimensions given are in inches.)

CONFIGURATION 172; helium-gun test.

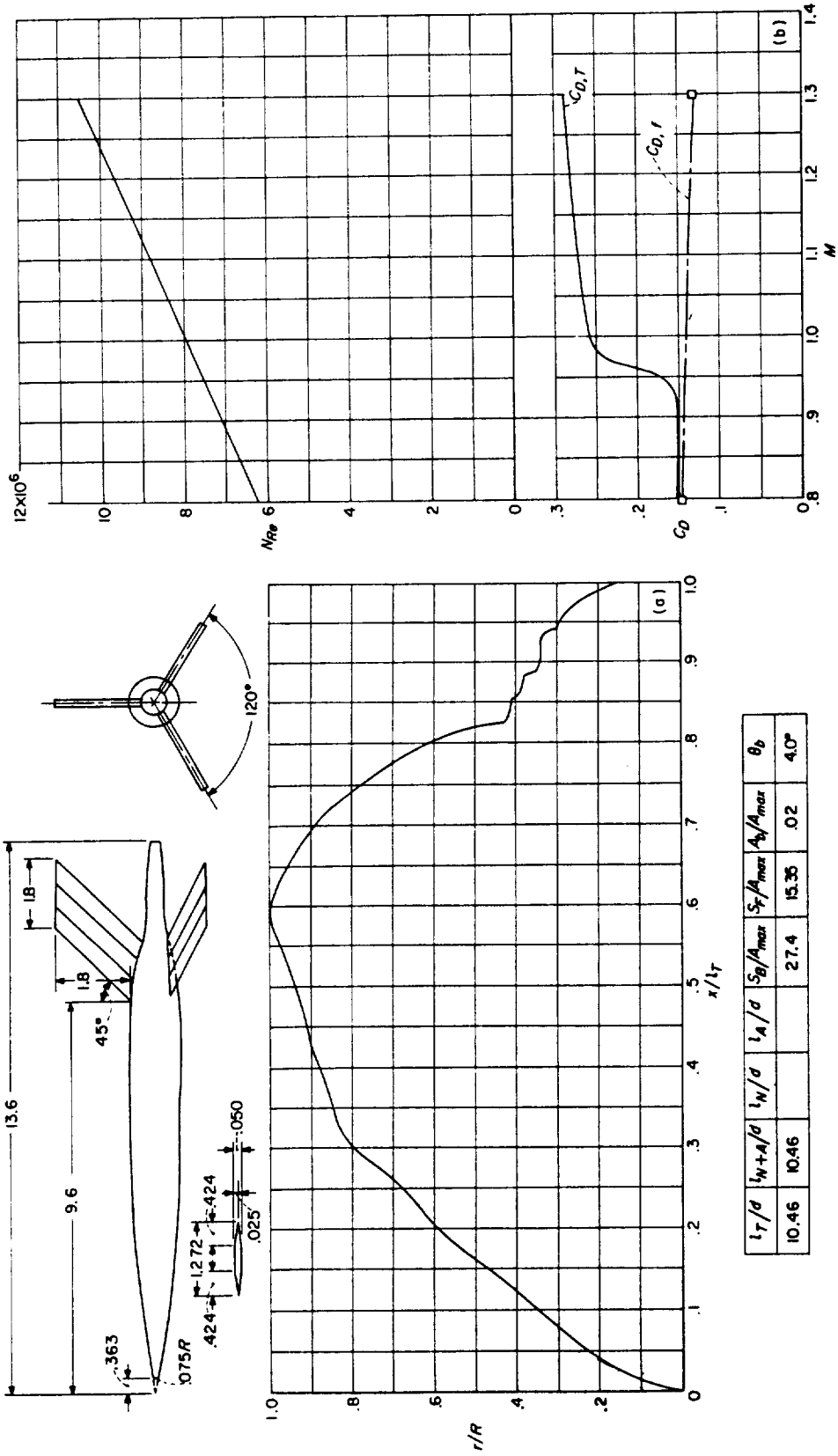

l_T/d	l_{N+A}/d	l_N/d	l_A/d	S_B/A_{max}	S_F/A_{max}	A_b/A_{max}	θ_b
10.46	10.46			27.4	15.35	.02	4.0°

(a) Body shape. (Dimensions given are in inches.) (b) N_{Re} and C_D curves.

CONFIGURATION 173; helium-gun test.

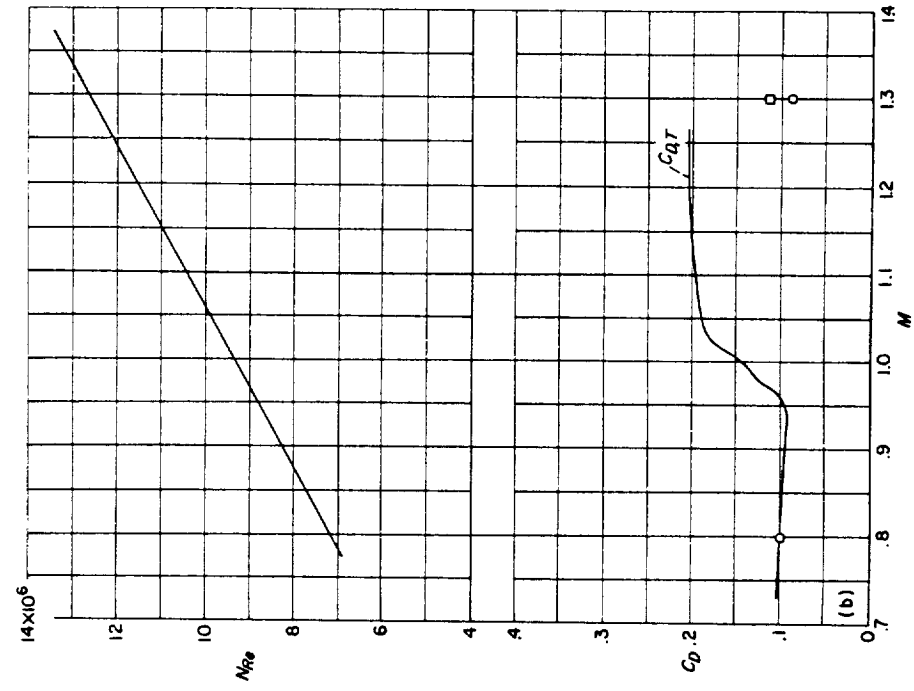

(b) N_{Re} and C_D curves.

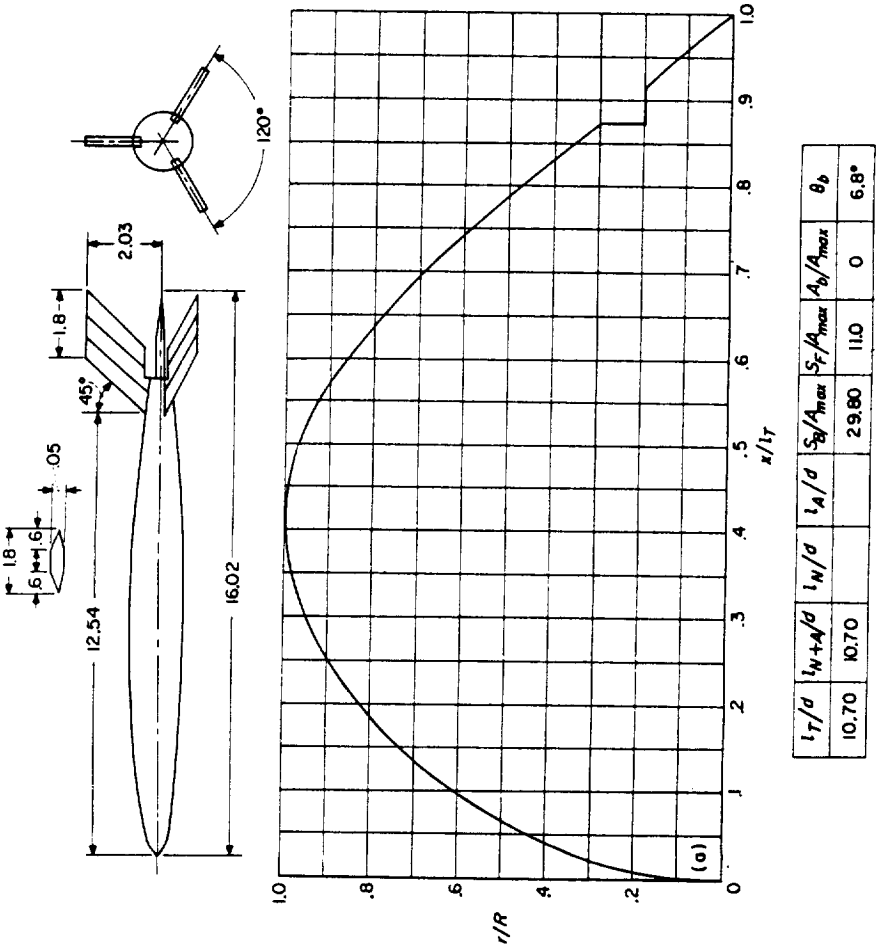

l_T/d	l_{N+A}/d	l_N/d	l_A/d	S_B/A_{max}	S_F/A_{max}	A_b/A_{max}	θ_b
10.70	10.70			29.80	11.0	0	6.8°

(a) Body shape. (Dimensions given are in inches.)

CONFIGURATION 174; helium-gun test.

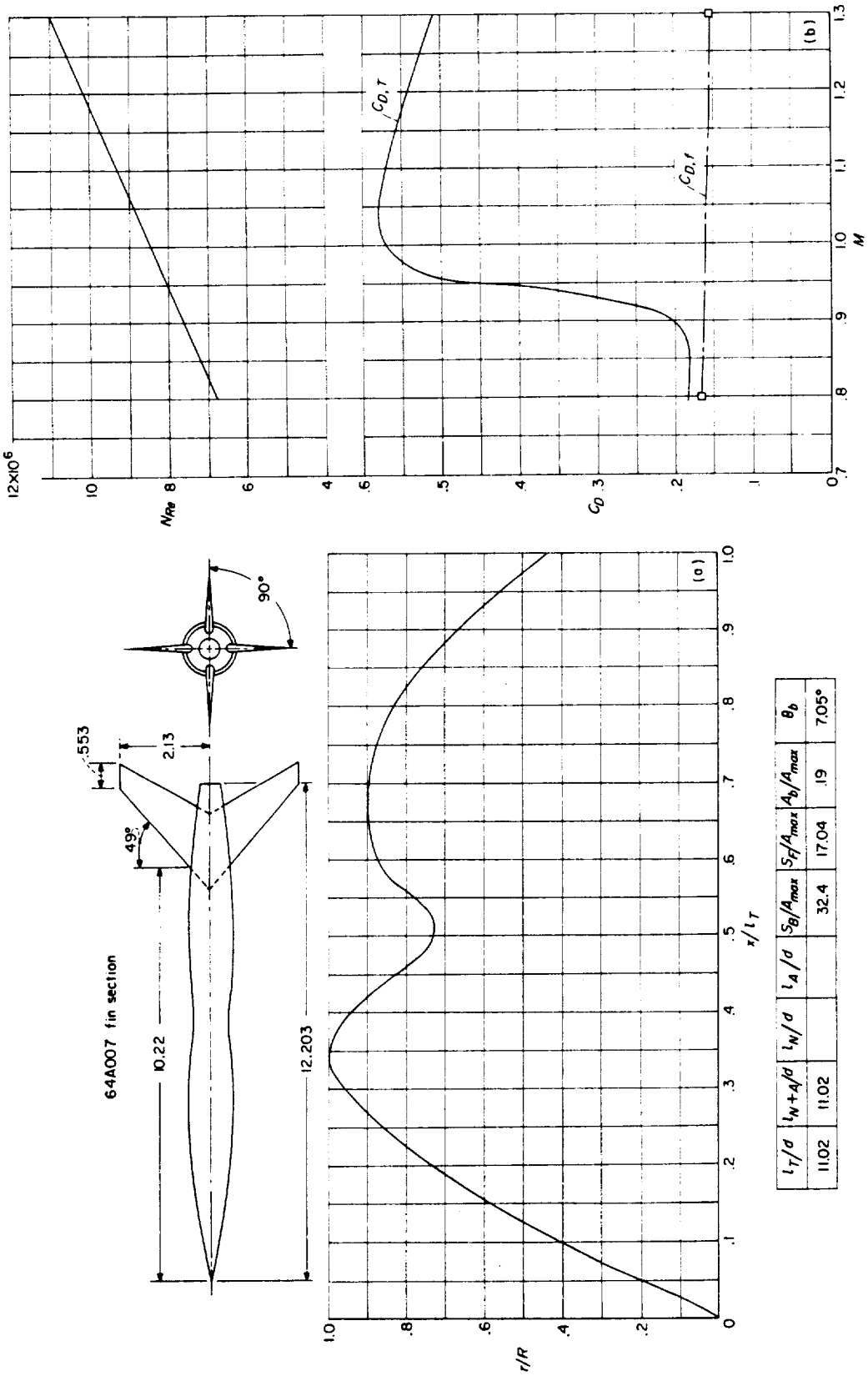

l_T/d	l_{N+A}/d	l_N/d	l_A/d	S_B/A_{max}	S_F/A_{max}	A_b/A_{max}	θ_b
11.02	11.02			32.4	17.04	.19	7.05°

(a) Body shape. (Dimensions given are in inches.) (b) N_{Re} and C_D curves.

CONFIGURATION 175; helium-gun test.

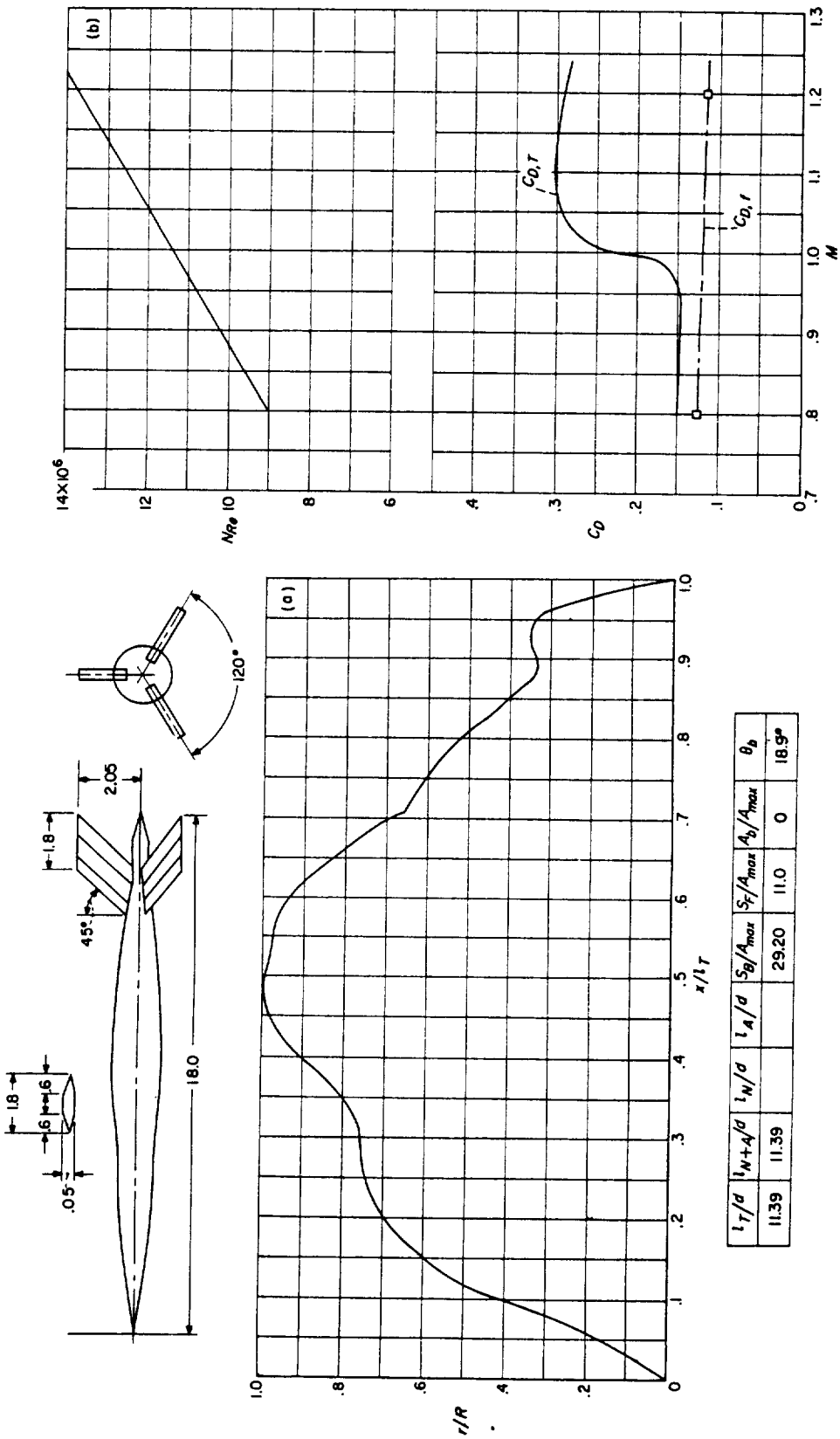

l_T/d	l_{N+A}/d	l_N/d	l_A/d	S_B/A_{max}	S_F/A_{max}	A_b/A_{max}	θ_b
11.39	11.39			29.20	11.0	0	18.9°

(a) Body shape. (Dimensions given are in inches.) (b) N_{Re} and C_D curves.

CONFIGURATION 176; helium-gun test.

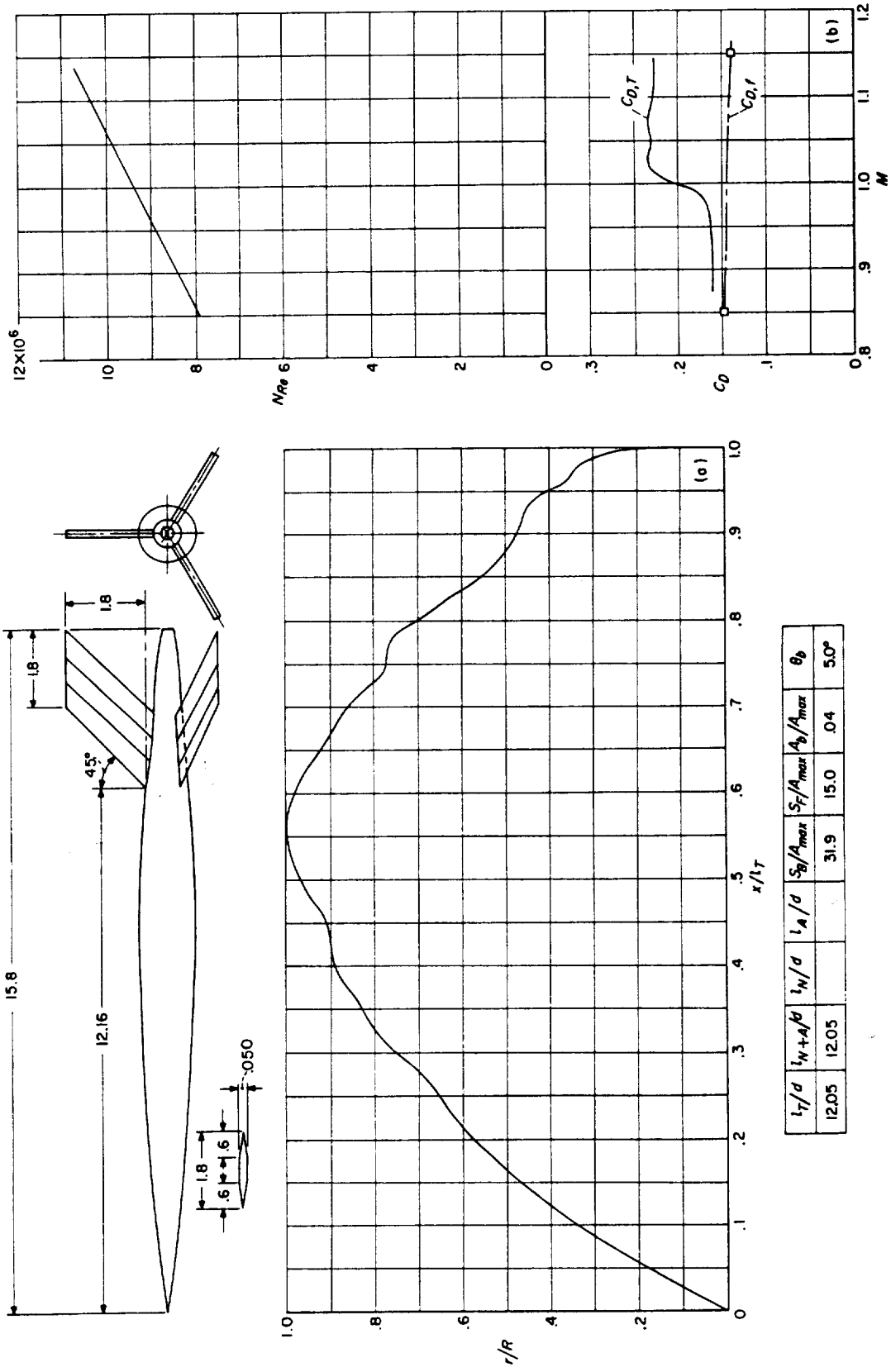

l_T/d	l_{N+A}/d	l_N/d	l_A/d	S_B/A_{max}	S_F/A_{max}	A_b/A_{max}	θ_b
12.05	12.05			31.9	15.0	.04	5.0°

(a) Body shape. (Dimensions given are in inches.) (b) N_{Re} and C_D curves.

CONFIGURATION 177; helium-gun test.

U.S. GOVERNMENT PRINTING OFFICE: 1961